

**Cell adhesion molecule close homolog of L1 regulates  
internalization of the dopamine receptor D2  
and formation of the mesolimbic dopaminergic pathway  
in mice (*Mus musculus* Linnaeus, 1758).**

Dissertation submitted to the University of Hamburg,  
with the aim of achieving a doctoral degree at the Faculty of Mathematics,  
Informatics and Natural Sciences, Department of Biology

Submitted by Agnieszka Kotarska  
from Wręczyca Wielka, Poland

Hamburg, 2019

This dissertation was prepared at the Senior Group “Biosynthesis of Neural Structures” at the Center for Molecular Neurobiology Hamburg, University Medical Center Hamburg-Eppendorf.

The following evaluators recommended the admission of the dissertation:

Prof. Dr. Melitta Schachner

Prof. Dr. Julia Kehr

Day of oral defense: 24.01.2020

**Contents:****1. Abstract 6****2. Zusammenfassung 8****3. List of abbreviations 10****4. Introduction 14****4.1. CHL1 14****4.1.1. Structure of the CHL1 molecule 14****4.1.2. CHL1 as a member of the IgSF-CAMs and L1 family of CAMs 15****4.1.3. Expression of CHL1 18****4.1.4. Functions of CHL1 in the nervous system 19****4.1.5. CHL1-related disorders in humans 21****4.1.5.1. 3p-syndrome 21****4.1.5.2. Schizophrenia 23****4.2. Dopaminergic system 24****4.2.1. Elements of the dopaminergic system 25****4.2.1.1. Dopamine 25****4.2.1.2. Dopaminergic neurons 25****4.2.1.3. Dopamine receptors 26****4.2.1.4. Dopamine transporter 28****4.2.2. Dopaminergic synapse 29****4.2.2.1. Signaling pathways triggered by DRD2 30****4.2.3. Dopaminergic pathways 31****4.2.4. Development of the dopaminergic pathways 33****4.2.5. Disorders of the dopaminergic system 34****4.3. The connection between CHL1 and the dopaminergic system 36****5. Aims of the study 39****6. Materials 40**

6.1. Antibodies	40
6.2. Plasmids	42
6.3. Oligonucleotides	42
6.3.1. Oligonucleotides used for cloning with In-Fusion Kit (Clontech)	42
6.3.2. Oligonucleotides used for genotyping of mice	43
6.4. Peptides and recombinant proteins	44
6.5. Cell lines	44
6.6. Bacteria	45
6.7. Animals	45
6.8. Buffers, solutions, chemicals and media	45
6.8.1. Cell culture	45
6.8.2. Bacteria culture	47
6.8.3. Sodium dodecyl sulfate-polyacrylamide gel electrophoresis (SDS-PAGE) and Western Blot	48
6.8.4. Fixation and staining	50
6.8.5. ELISA	51
6.8.6. Agarose gel electrophoresis	52
6.8.7. In-cell Western	53
6.9. Suppliers of the chemicals, reagents, kits and laboratory equipment	53
<b>7. Methods</b>	<b>55</b>
7.1. Molecular biology methods	55
7.1.1. PCR	55
7.1.2. PCR product clean-up	55
7.1.3. Agarose gel electrophoresis	56
7.1.4. DNA extraction from agarose gels	56
7.1.5. Plasmid constructs cloning with In-Fusion Kit (Clontech)	56
7.1.6. Transformation of E. coli	56
7.1.7. Liquid culture of bacteria	57

7.1.8. Plasmid DNA isolation from liquid cultures of bacteria	57
7.1.9. Determination of DNA concentration and purity	57
7.1.10. DNA sequencing	57
<b>7.2. Biochemical methods</b>	<b>58</b>
7.2.1. Protein sample preparation for SDS-PAGE	58
7.2.2. Determination of protein concentration	58
7.2.3. SDS-PAGE	59
7.2.4. Western Blot	59
7.2.5. Membrane stripping	59
7.2.6. Co-immunoprecipitation	60
7.2.7. ELISA	60
<b>7.3. Cell biology methods</b>	<b>61</b>
7.3.1. HEK293 cell culture maintenance	61
7.3.2. Passaging of HEK293 cells	61
7.3.3. Freezing of HEK293 cells	61
7.3.4. Transfection of cultured cells	62
7.3.5. Immunofluorescent staining of cultured cells	62
7.3.6. PLA	62
7.3.7. Antibody feeding	63
7.3.8. Cell surface biotinylation	64
7.3.9. Protein degradation assay	64
7.3.10. Ligand binding assay	64
7.3.11. In-cell Western	65
7.3.12. Trans-orientation interaction assay	65
<b>7.4. Morphological methods</b>	<b>65</b>
7.4.1. Tissue fixation	65
7.4.2. Tissue cryosectioning	66
7.4.3. Antigen retrieval	66

7.4.4. Tissue immunostaining 66

7.4.5. Stereological quantification of cells 67

7.5. Statistical analysis 67

7.6. Genotyping of mice 67

## 8. Results 69

8.1. Verification of interaction between CHL1 and DRD2 69

8.1.1. CHL1 co-localizes with DRD2 in the mouse striatum 69

8.1.2. CHL1 co-localizes with DRD2S and DRD2L in transfected cells 71

8.1.3. CHL1 binds directly to the first extracellular loop of DRD2 via its extracellular domain 75

8.1.4. CHL1 and DRD2 interact predominantly at the surface of cells 77

8.1.5. CHL1 can bind via its extracellular domain to DRD2S and DRD2L at the cell surface in trans-orientation 78

8.2. Identification of consequences of the interaction between CHL1 and DRD2 on functions of DRD2 79

8.2.1. CHL1 inhibits internalization of DRD2S upon receptor stimulation 80

8.2.2. CHL1 affects the cell surface amount of DRD2S upon receptor stimulation with the DRD2 agonist 82

8.2.3. CHL1 does not affect DRD2 degradation 83

8.2.4. Binding of an agonist to DRD2 is not affected by CHL1 87

8.2.5. CHL1 does not affect intracellular signaling pathways triggered by DRD2 stimulation with quinpirole in transfected HEK293 cells 88

8.2.6. Loss of CHL1 leads to altered levels of DRD2, pDARPP32, DARPP32 and pTH in dorsal and ventral striatum of mice 92

8.3. Characterization of dopaminergic projections running from the ventral midbrain to the striatum in CHL1<sup>-/-</sup> mice 95

8.3.1. CHL1<sup>-/-</sup> mice have more dopaminergic fibers running to the ventral striatum than CHL1<sup>+/+</sup> mice 96

8.3.2. Phospho-TH-positive dopaminergic fibers running to the ventral striatum differ in CHL1<sup>-/-</sup> and CHL1<sup>+/+</sup> mice 105

8.3.3. CHL1<sup>-/-</sup> mice have more dopaminergic fibers entering the ventral striatum compared to CHL1<sup>+/+</sup> mice 107

8.3.4. Loss of CHL1 does not affect the dopaminergic fibers density in the striatum	109
8.3.5. CHL1 <sup>-/-</sup> mice have a reduced number of dopaminergic neurons in the VTA compared to CHL1 <sup>+/+</sup> mice	112
8.4. Verification of DRD2 expression and schizophrenia-related brain morphology in CHL1 <sup>-/-</sup> mice	114
8.4.1. Thalamus size is normal in CHL1 <sup>-/-</sup> mice	114
8.4.2. Thickness of the frontal cortex is normal in CHL1 <sup>-/-</sup> mice	116
8.4.3. Expression of DRD2 in the frontal cortex is normal in CHL1 <sup>-/-</sup> mice	117
8.4.4. CHL1 <sup>-/-</sup> mice have enlarged lateral ventricles compared to CHL1 <sup>+/+</sup> mice	118
<b>9. Discussion</b>	<b>120</b>
9.1. CHL1 interacts with DRD2S and DRD2L	120
9.2. CHL1 regulates agonist-induced internalization of DRD2, but not DRD2 degradation, ligand binding to DRD2 and DRD2-regulated intracellular signaling cascades	122
9.3. CHL1 regulates the level of proteins related to DRD2 signaling in the dorsal and the ventral striatum of adult mice	125
9.4. CHL1 affects the number of dopaminergic fibers in the mesolimbic dopaminergic pathway of mice	126
9.5. CHL1 <sup>-/-</sup> mice exhibit a lower number of dopaminergic neurons in the VTA compared to CHL1 <sup>+/+</sup> mice	129
9.6. CHL1 <sup>-/-</sup> mice do not present some of the features related to schizophrenia	132
9.7. General conclusions	133
<b>10. List of figures</b>	<b>136</b>
<b>11. List of tables</b>	<b>138</b>
<b>12. Acknowledgements</b>	<b>139</b>
<b>13. References</b>	<b>140</b>

## 1. Abstract

The dopaminergic system is complex in its structure and physiology, and it is involved in many disorders with largely unknown etiology such as schizophrenia, addiction, attention deficit hyperactivity disorder (ADHD), depression, Huntington's disease and Parkinson's disease. Previous reports indicate that the cell adhesion molecule close homolog of L1 (CHL1) plays a role in the development of the dopaminergic system, is involved in schizophrenia and in the regulation of the dopamine-dependent behavior and cognitive functions. Furthermore, preliminary co-immunoprecipitation experiments done by previous coworkers showed potential binding between CHL1 and the dopamine receptor D2 (DRD2). Therefore, the aims of my thesis were to verify if CHL1 interacts directly with DRD2 and to determine the consequences of this interaction on the functions of the receptor. My further aims were to characterize the morphology of the dopaminergic system in CHL1 knock-out (CHL1<sup>-/-</sup>) mice and to analyze the DRD2 expression and morphological features related to schizophrenia in the brains of CHL1<sup>-/-</sup> mice.

In the present thesis I show with immunofluorescent stainings and proximity-ligation assay (PLA) that CHL1 co-localizes with DRD2 in the mouse striatum and in transfected cells. The co-localization of CHL1 with the two DRD2 forms – the predominantly pre-synaptic DRD2 “short” form (DRD2S) and the predominantly post-synaptic DRD2 “long” form (DRD2L) – detected with PLA occurs mostly at the surface of cells and more co-localization of CHL1 is detectable with the pre-synaptic DRD2S than with the post-synaptic DRD2L. Performing co-immunoprecipitations I show that DRD2 is co-precipitated from mouse brain homogenates by an anti-CHL1 antibody, and with the enzyme-linked immunosorbent assay (ELISA) I show a direct binding between the extracellular domain of CHL1 and the first extracellular loop of DRD2. Moreover, using a soluble recombinant extracellular domain of CHL1 conjugated with the Fc fragment of human IgG (CHL1-Fc) I found that the binding between the DRD2 forms and CHL1 can occur in *trans*-orientation.

Investigating the impact of the interaction between CHL1 and DRD2 on the functions of DRD2 I found that in “antibody feeding” experiments CHL1 reduces the agonist-induced internalization of DRD2S in transfected cells, and by cell surface biotinylation I could show that CHL1 inhibits the reduction of the DRD2S level at the surface of transfected cells upon stimulation with a DRD2 agonist. No effect of CHL1 could be shown in experiments measuring the DRD2 degradation, ligand binding to DRD2 and activation of DRD2-regulated intracellular signaling pathways in transfected cells. However, the measurement of proteins involved in DRD2 signaling showed a reduction of DRD2 and phosphorylated tyrosine hydroxylase (pTH) levels in the dorsal striatum and a reduction of phosphorylated dopamine- and cyclic adenosine monophosphate-regulated neuronal phosphoprotein 32 kDa (pDARPP32) levels and an increase of DARPP32 levels in the ventral striatum of CHL1<sup>-/-</sup> mice.

Analysis of the morphology of the dopaminergic pathways running from the ventral midbrain to the striatum using immunostained mouse brain sections showed that, in comparison to wild-type mice (CHL1+/+), adult CHL1-/- mice display morphological abnormalities in the mesolimbic dopaminergic pathway: they have less dopaminergic neurons in the ventral tegmental area (VTA), but more dopaminergic fibers running to the ventral striatum and normal dopaminergic fibers density in the ventral striatum.

Determination of features related to schizophrenia – increased DRD2 expression in the frontal cortex, reduced thalamus size, frontal cortex thinning and ventricular enlargement – showed that CHL1-/- mice differ from their CHL1+/+ littermates only in the size of the lateral ventricles, which are enlarged in the CHL1-/- mice.

These results indicate that CHL1 is a binding partner of DRD2 and that it affects the DRD2-related signaling and functions related to the DRD2 internalization in response to the stimulation with an agonist. Apart from regulating the physiology of the dopaminergic system, CHL1 has an impact on the morphology of the mesolimbic dopaminergic pathway affecting the number of dopaminergic cells and dopaminergic fibers in this pathway. Despite being considered a factor contributing to schizophrenia, CHL1 does not affect the frontal cortex DRD2 expression and the majority of schizophrenia-related morphological alterations.

The findings presented in this thesis contribute to the understanding of the dopaminergic system functioning and suggest new roles for CHL1 in this system.

## 2. Zusammenfassung

Das dopaminerge System besitzt eine komplexe Struktur und Physiologie. Bei vielen Erkrankungen mit unbekannter Ätiologie zeigen sich Veränderungen im dopaminergen System, z.B. bei Schizophrenie, Sucht, Aufmerksamkeitsdefizit-Hyperaktivitätsstörung (ADHD), Depression, Huntington-Krankheit und Parkinson-Krankheit. Frühere Berichte deuten darauf hin, dass das Zelladhäsionsmolekül „close homolog of L1“ (CHL1) eine Rolle bei der Entwicklung des dopaminergen Systems spielt, an Schizophrenie beteiligt ist und an der Regulierung des Dopamin-abhängigen Verhaltens und an kognitiven Funktionen beteiligt ist. Darüber hinaus zeigten vorangegangene Co-Immunopräzipitationsexperimente früherer Mitarbeiter eine potenzielle Bindung zwischen CHL1 und dem Dopaminrezeptor D2 (DRD2). Ziel meiner Doktorarbeit war es daher zu überprüfen, ob CHL1 direkt mit DRD2 interagiert und die Konsequenzen dieser Interaktion auf die Funktionen des Rezeptors zu ermitteln. Meine weiteren Ziele waren die Charakterisierung der Morphologie des dopaminergen Systems in CHL1-defizienten Mäusen (CHL1<sup>-/-</sup>) und die Analyse der DRD2-Expression und der mit Schizophrenie zusammenhängenden morphologischen Merkmale in Gehirnen von CHL1<sup>-/-</sup> Mäusen.

In der vorliegenden Arbeit zeige ich mit Immunfluoreszenz-Färbungen und dem „Proximity-Ligation-Assay“ (PLA), dass CHL1 mit DRD2 im Striatum von Mäusen und in transfizierten Zellen co-lokalisiert. Die Co-Lokalisation von CHL1 mit den beiden DRD2-Formen – der überwiegend präsynaptischen kurzen Form (DRD2-short; DRD2S) und der überwiegend postsynaptischen langen Form (DRD2-long; DRD2L) kann mittels PLA vor allem an der Oberfläche von Zellen nachgewiesen werden. CHL1 co-lokalisiert eher mit dem präsynaptischen DRD2S als mit dem postsynaptischen DRD2L. Immunopräzipitationsexperimente mit Maushirnhomogenaten zeigen, dass DRD2 durch einen anti-CHL1-Antikörper co-präzipitiert wird. Im „Enzyme-linked Immunosorbent Assay“ (ELISA) konnte ich eine direkte Bindung zwischen der extrazellulären Domäne von CHL1 und der ersten extrazellulären Schleife von DRD2 nachweisen. Unter Verwendung der löslichen rekombinanten extrazellulären Domäne von CHL1, die mit dem Fc-Teil von menschlichem IgG konjugiert ist (CHL1-Fc), habe ich ermittelt, dass die Bindung zwischen den DRD2-Formen und CHL1 auch in Trans-Orientierung erfolgen kann.

Bei der Untersuchung des Einflusses der Interaktion zwischen CHL1 und DRD2 auf die Funktionen von DRD2 habe ich festgestellt, dass CHL1 bei "antibody feeding"-Experimenten die Agonist-induzierte Internalisierung von DRD2S in transfizierten Zellen reduziert und bei Zelloberflächenbiotinylierungsexperimenten die Reduktion des DRD2S an den Oberfläche von transfizierten Zellen nach Stimulation mit DRD2-Agonisten inhibiert. Messungen des DRD2-Abbaus, der Ligandenbindung an DRD2 und der Aktivierung der durch DRD2 regulierten intrazellulären Signalwege in transfizierten Zellen zeigten keinen Einfluss von CHL1. Die Untersuchungen der Proteine, die an der DRD2-Signalgebung beteiligt sind, zeigten jedoch eine Reduktion der Mengen von DRD2 und phosphorylierter Tyrosinhydroxylase (pTH) im dorsalen Striatum und eine

Reduktion der Menge von phosphoryliertem „dopamine- and cyclic adenosine monophosphate-regulated neuronal phosphoprotein 32 kDa“ (pDARPP32) im ventralen Striatum von CHL1<sup>-/-</sup> Mäusen.

Die Analyse der Morphologie der vom ventralen Mittelhirn bis zum Striatum verlaufenden dopaminergen Projektionsbahnen in der Maus zeigte, dass erwachsene CHL1<sup>-/-</sup> Mäuse im Vergleich zu Wildtyp-Mäusen morphologische Abnormalitäten in den mesolimbischen dopaminergen Projektionsbahnen aufweisen: CHL1<sup>-/-</sup> Mäuse haben weniger dopaminerge Neuronen im Area tegmentalis ventralis (VTA), aber mehr dopaminerge Nervenfasern, die in das ventrale Striatum laufen, und weisen eine normale Menge von dopaminerge Nervenfasern im ventralen Striatum auf.

Überprüfung der Veränderungen, die bei Schizophrenie auftreten – erhöhte DRD2-Expression im frontaler Cortex, reduzierte Größe des Thalamus, verkleinerter frontaler Cortex und Vergrößerung der Ventrikel – in Schnitten von erwachsenen Mäusegehirnen zeigten, dass sich CHL1<sup>-/-</sup> Mäuse von ihren CHL1<sup>+/+</sup> Wurfgeschwistern nur durch vergrößerte laterale Ventrikel unterscheiden.

Die Ergebnisse zeigen, dass CHL1 ein Bindungspartner von DRD2 ist und dass CHL1 die Funktionen von DRD2 beeinflusst, die mit seiner Agonist-induzierten Internalisierung und der DRD2-abhängigen Signalübertragung zusammenhängen. Neben der Regulierung der Physiologie des dopaminergen Systems beeinflusst CHL1 die Morphologie der mesolimbischen dopaminergen Projektionsbahnen, indem CHL1 die Anzahl der dopaminergen Zellen und der dopaminergen Nervenfasern steuert. Obwohl CHL1 als ein Faktor angesehen wird, der zur Schizophrenie beiträgt, beeinflusst CHL1 die DRD2-Expression im frontaler Cortex und die Mehrheit der nachgewiesenen Schizophrenie-abhängigen morphologischen Veränderungen nicht.

Die in dieser Arbeit vorgestellten Ergebnisse tragen zum Verständnis der Funktionsweise des dopaminergen Systems bei und legen neue Rollen für CHL1 in diesem System nahe.

### 3. List of abbreviations

-/- – knock-out mice	<b>CAM</b> – cell adhesion molecule	<b>DAPI</b> – 4',6-diamidino-2-phenylindole
+/+ – wild-type mice	<b>cAMP</b> – cyclic adenosine monophosphate	<b>DARPP32</b> – dopamine- and cyclic adenosine monophosphate-regulated neuronal phosphoprotein 32 kDa
<b>3p</b> – small arm ( <i>petite</i> , p) of the third chromosome	<b>cBA</b> – chicken beta actin	<b>DAT</b> – dopamine transporter
<b>A.U.</b> – arbitrary units	<b>CC</b> – corpus callosum	<b>DCC</b> – deleted in colorectal cancer
<b>aa</b> – amino acids	<b>cDNA</b> – complementary deoxyribonucleic acid	<b>DF</b> – dopaminergic fibers
<b>AC, aco</b> – anterior commissure	<b>CHL1</b> – close homolog of L1	<b>DGEA</b> – peptide consisting of aspartic acid, glycine, glutamic acid and alanine
<b>ACy</b> – adenylyl cyclase	<b>CHL1-/-</b> – mice knock-out for close homolog of L1	<b>dH<sub>2</sub>O</b> – distilled water
<b>ADAM8</b> – a disintegrin and metalloprotease domain 8	<b>CHL1+/-</b> – mice heterozygous for close homolog of L1	<b>DJ-1-/-</b> – mice knock-out for DJ-1
<b>ADHD</b> – attention-deficit hyperactivity disorder	<b>CHL1+/+</b> – wild-type mice	<b>DMEM</b> – Dulbecco's Modified Eagle Medium
<b>AF</b> – antibody feeding	<b>CHL1-Fc</b> – extracellular domain of cell adhesion molecule close homolog of L1 conjugated with Fc fragment of human immunoglobulin G	<b>DMSO</b> – dimethyl sulfoxide
<b>Akt</b> – protein kinase B	<b>CNTN4</b> – contactin 4	<b>DNA</b> – deoxyribonucleic acid
<b>Ala</b> – alanine	<b>CNTN6</b> – contactin 6	<b>DRD1</b> – dopamine receptor D1
<b>amp</b> – ampicillin	<b>CO-IP</b> – co-immunoprecipitation	<b>DRD2</b> – dopamine receptor D2
<b>ANOVA</b> – analysis of variance	<b>CP, CPu</b> – caudate and putamen	<b>DRD2<sup>high</sup></b> – dopamine receptor D2 with high agonist binding affinity
<b>APS</b> – ammonium persulfate	<b>CRASH</b> – corpus callosum hypoplasia, retardation, adducted thumbs, spastic paraplegia and hydrocephalus	<b>DRD2L</b> – dopamine receptor D2 “long”
<b>Arg</b> – arginine	<b>CTLs</b> – C-type lectin-like domain proteins	<b>DRD2L<sup>high</sup></b> – dopamine receptor D2 “long” with high agonist binding affinity
<b>ARRIVE</b> – Animal Research: Reporting of In Vivo Experiments	<b>Cy2, 3 and 5</b> – cyanine fluorescent dyes 2, 3 and 5	<b>DRD2L<sup>low</sup></b> – dopamine receptor D2 “long” with low agonist binding affinity
<b>Asp</b> – aspartic acid	<b>DAB</b> – diaminobenzidine	
<b>BACE1</b> – $\beta$ -site amyloid precursor protein-cleaving enzyme		
<b>BCA</b> – bicinchoninic acid		
<b>BDNF</b> – brain-derived neurotrophic factor		
<b>BSA</b> – bovine serum albumin		
<b>CA1</b> – cornu Ammonis 1		
<b>CA3</b> – cornu Ammonis 3		
<b>CALL</b> – cell adhesion molecule L1 like		

<b>DRD2<sup>low</sup></b> – dopamine receptor D2 with low agonist binding affinity	<b>ERK</b> – extracellular-signal-regulated kinase	<b>HBSS</b> – Hanks' Balanced Salt Solution
<b>DRD2S</b> – dopamine receptor D2 “short”	<b>ERK1</b> – extracellular signal-regulated kinase 1	<b>HEK293</b> – human embryonic kidney 293
<b>DRD2S<sup>high</sup></b> – dopamine receptor D2 “short” with high agonist binding affinity	<b>FBS</b> – fetal bovine serum	<b>HEPES</b> – 4-(2-hydroxyethyl)-1-piperazineethanesulfonic acid
<b>DRD2S<sup>low</sup></b> – dopamine receptor D2 “short” with low agonist binding affinity	<b>Fc</b> – fragment crystallizable (of an immunoglobulin)	<b>Hp</b> – hippocampus
<b>DRD3</b> – dopamine receptor D3	<b>FC</b> – frontal cortex	<b>HpaI</b> – restriction enzyme
<b>DRD4</b> – dopamine receptor D4	<b>FIGAY</b> – peptide consisting of phenylalanine, isoleucine, glycine, alanine, tyrosine	<b>HRP</b> – horseradish peroxidase
<b>DRD5</b> – dopamine receptor D5	<b>FN-III</b> – fibronectin type III	<b>ICW</b> – in-cell Western
<b>DS</b> – dorsal striatum	<b>Foxp2</b> – forkhead box protein P2	<b>IF</b> – immunofluorescent staining
<b>DTT</b> – dithiothreitol	<b>GABA</b> – gamma-aminobutyric acid	<b>Ig</b> – immunoglobulin
<b>E</b> – embryonic day	<b>GAPDH</b> – glyceraldehyde 3-phosphate dehydrogenase	<b>IgSF-CAMs</b> – immunoglobulin superfamily of cell adhesion molecules
<b><i>E. coli</i></b> – <i>Escherichia coli</i>	<b>GASP</b> – G protein coupled receptor-associated sorting protein	<b>IHC</b> – immunohistochemistry
<b>EC</b> – extracellular cadherin repeats	<b>GDNF</b> – glial cell line-derived neurotrophic factor	<b>Ile</b> – isoleucine
<b>ECL</b> – enhanced chemiluminescence	<b>GDP</b> – guanosine diphosphate	<b>Ile184</b> – 184 <sup>th</sup> amino acid: isoleucine
<b>ECM</b> – extracellular matrix	<b>GTP</b> – guanosine triphosphate	<b>IP</b> – immunoprecipitation
<b>EcoRI</b> – restriction enzyme	<b>GFP</b> – green fluorescent protein	<b>IRDye</b> – infrared dye
<b>EcoRV</b> – restriction enzyme	<b>G<sub>i</sub></b> – G <sub>inhibitory</sub>	<b>IRES</b> – internal ribosome entry site
<b>EDTA</b> – ethylenediaminetetraacetic acid	<b>Gln</b> – glutamine	<b>ITPR1</b> – inositol 1,4,5-trisphosphate receptor type 1
<b>EGTA</b> – ethylene glycoltetraacetic acid	<b>Glu</b> – glutamic acid	<b>KpnI</b> – restriction enzyme
<b>ELISA</b> – enzyme-linked immunosorbent assay	<b>Gly</b> – glycine	<b>L1-Fc</b> – extracellular domain of cell adhesion molecule L1 conjugated with Fc fragment of human immunoglobulin G
<b>emcv</b> – encephalomyocarditis virus	<b>GPCRs</b> – G-protein-coupled receptors	<b>lac</b> – lactose
	<b>G<sub>s</sub></b> – G <sub>stimulatory</sub>	<b>LB</b> – lysogeny broth
		<b>L-DOPA</b> – levodopa/L-3,4-dihydroxyphenylalanine

<b>Leu17Phe</b> – leucine to phenylalanine substitution at the 17 <sup>th</sup> amino acid	<b>NP-40</b> – nonyl phenoxypolyethoxyethanol	<b>PCR</b> – polymerase chain reaction
<b>LV</b> – lateral ventricle	<b>NrCAM</b> – neuronal cell adhesion molecule or NgCAM (neuron-glia cell adhesion molecule)-related cell adhesion molecule	<b>pDARPP32</b> – phosphorylated dopamine- and cyclic adenosine monophosphate-regulated neuronal phosphoprotein 32 kDa
<b>Lys</b> – lysine	<b>OB</b> – olfactory bulb	<b>pDARPP32(Thr34)</b> – dopamine- and cAMP-regulated phosphoprotein 32 kDa phosphorylated at threonine 34
<b>mDA</b> – midbrain dopaminergic neurons	<b>OCT</b> – optimal cutting temperature	<b>pERK</b> – phosphorylated extracellular-signal-regulated kinase
<b>MDD</b> – major depressive disorder	<b>OPD</b> – ortho-phenylenediamine	<b>pERK1/2</b> – phosphorylated extracellular signal-regulated kinase 1/2
<b>MEK</b> – mitogen-activated protein kinase and extracellular-signal-regulated kinase kinase	<b>ORF</b> – open reading frame	<b>PFC</b> – prefrontal cortex
<b>MFBs</b> – medial forebrain bundles	<b>OT</b> – olfactory tubercle	<b>Phe</b> – phenylalanine
<b>mRNA</b> – messenger ribonucleic acid	<b>p</b> – phosphorylated	<b>PKA</b> – protein kinase A
<b>MSNs</b> – medium spiny neurons	<b>P</b> – postnatal day	<b>PLA</b> – proximity ligation assay
<b>n.s.</b> – not significant	<b>PARK7</b> – Parkinson’s disease protein 7	<b>PLL</b> – poly-L-lysine
<b>NAc</b> – nucleus accumbens	<b>pBR322</b> – “plasmid Bolivar Rodriguez 322” <i>Escherichia coli</i> expression vector	<b>Post</b> – the post-synaptic neuron
<b>NCAM</b> – neural cell adhesion molecule	<b>PBS</b> – phosphate-buffered saline	<b>PP2A</b> – serine/threonine-protein phosphatase 2A
<b>NCAM180</b> – neural cell adhesion molecule 180 kilodaltons	<b>pCAG</b> – mammalian expression vector with CAG (cytomegalovirus enhancer, promoter and first exon and first intron of chicken beta-actin, splice acceptor of rabbit beta-globin) promoter	<b>Pre</b> – the pre-synaptic neuron
<b>NCAM-Fc</b> – extracellular domain of neural cell adhesion molecule conjugated with Fc fragment of human immunoglobulin G	<b>pcDNA3.1</b> – mammalian expression vector with cytomegalovirus enhancer	<b>prom</b> – promoter
<b>NgCAM</b> – neuron-glia cell adhesion molecule		<b>Ptc1</b> – patched-1
<b>N<sup>o</sup></b> – number		<b>pTH</b> – phosphorylated tyrosine hydroxylase
<b>NotI</b> – restriction enzyme		<b>pTH(Ser40)</b> – tyrosine hydroxylase phosphorylated at serine 40

<b>px</b> – pixels	<b>Ser</b> – serine	<b>TBS-T</b> – Tris-buffered saline with Tween 20
<b>RAF</b> – rapidly accelerated fibrosarcoma kinase	<b>Ser40</b> – 40 <sup>th</sup> amino acid: serine	<b>TEMED</b> – tetramethylethylenediamine
<b>reg</b> – regulatory sequence	<b>Sfill</b> – restriction enzyme	<b>Th</b> – thalamus
<b>RGD</b> – peptide consisting of arginine, glycine and aspartic acid	<b>SN</b> – substantia nigra	<b>TH</b> – tyrosine hydroxylase
<b>RGGKYSV</b> – peptide consisting of arginine, glycine, glycine, lysine, tyrosine, serine and valine	<b>SNARE</b> – SNAP (Soluble <i>N</i> -ethylmaleimide-sensitive factor Attachment Protein) Receptor	<b>TH+</b> – tyrosine hydroxylase-positive
<b>RNase</b> – ribonuclease	<b>SNc, SNpc</b> – substantia nigra – pars compacta	<b>Thr34</b> – 34 <sup>th</sup> amino acid: threonine
<b>ROS</b> – reactive oxygen species	<b>SNP</b> – single nucleotide polymorphism	<b>Trp100</b> – 100 <sup>th</sup> amino acid: tryptophan
<b>RRF</b> – retrorubral field	<b>SNr, SNpr</b> – substantia nigra – pars reticulata	<b>Tyr</b> – tyrosine
<b>RSLE</b> – peptide consisting of arginine, serine, leucine and glutamic acid	<b>SOC</b> – super optimal catabolite repression medium	<b>v</b> – volume
<b>SDS</b> – sodium dodecyl sulfate	<b>SRY</b> – sex-determining region Y	<b>Val</b> – valine
<b>SDS-PAGE</b> – sodium dodecyl sulfate-polyacrylamide gel electrophoresis	<b>STR</b> – striatum	<b>VMAT2</b> – vesicular monoamine transporter 2
<b>SEM</b> – standard error of the mean	<b>SV40</b> – simian virus 40	<b>VS</b> – ventral striatum
	<b>TAE</b> – Tris-acetate-ethylenediaminetetraacetic acid buffer	<b>VTA</b> – ventral tegmental area
	<b>TBS</b> – Tris-buffered saline	<b>w</b> – weight
		<b>WB</b> – Western Blot
		<b>Xbal</b> – restriction enzyme
		<b>XhoI</b> – restriction enzyme

## 4. Introduction

### 4.1. CHL1

CHL1 was first described in 1996 by Holm et al. who identified this molecule while screening a cDNA library using antibodies against the cell adhesion molecule L1, and classified it as a member of the immunoglobulin superfamily (IgSF) and of the L1 family of cell adhesion molecules (CAMs). Since its discovery, CHL1 was found to be involved in development and maintenance of the nervous system of mammals and changes in the sequence of the CHL1 gene in humans (cell adhesion molecule L1 like, CALL) were linked to certain disorders of the nervous system. Although the CHL1 protein can be found in many tissues of the mammalian body, the majority of research focuses on its functions in the brain as brain tissue contains significantly more CHL1 than any other tissue.

#### 4.1.1. Structure of the CHL1 molecule

CHL1 is a transmembrane protein which passes the plasma membrane once and therefore consists of three distinct domains: an extracellular domain, a transmembrane domain and an intracellular domain. The N-terminal extracellular domain of mouse CHL1 comprises 1081 of the 1209 amino acids of the whole CHL1 protein. This domain contains two types of evolutionarily conserved protein domains: starting from the N-terminus these are 6 immunoglobulin (Ig)-like domains comprising 585 amino acids followed by 4 full and 1 partial fibronectin type III (FN-III) domains of 472 amino acids. The extracellular domain of CHL1 is followed by a transmembrane domain of 23 amino acids and an intracellular domain of 105 amino acids (Holm et al., 1996) (**Figure 1**).

Not only the full-length CHL1 protein with apparent molecular weight of 185 kDa, but also its proteolytic fragments can be found. CHL1 protein can be cleaved by a disintegrin and metalloprotease domain 8 (ADAM8) within the 5<sup>th</sup> FN-III domain and within the 2<sup>nd</sup> FN-III domain to generate a 165-kDa and a 125-kDa soluble fragment, respectively, and respective membrane-passing fragments (Holm et al., 1996; Naus et al., 2004). The CHL1 ectodomain shedding and the release of the 165-kDa and 125-kDa fragments was shown to promote cell survival and neurite outgrowth of mouse cerebellar granule neurons (Naus et al., 2004). Apart from being a substrate for ADAM8, CHL1 was shown to be cleaved also by  $\beta$ -site amyloid precursor protein-cleaving enzyme (BACE1), which has one cleavage site within mouse CHL1 between amino acids Gln1061 and Asp1062. The consequences related to CHL1 processing by BACE1 still need to be investigated (Zhou et al., 2012).

The extracellular domain of CHL1 is glycosylated. Treatment of the full-length CHL1 protein with enzymes removing N- and O-glycans results in a shift of the 185-kDa band to 145 kDa (Holm et al., 1996) (**Figure 1**).

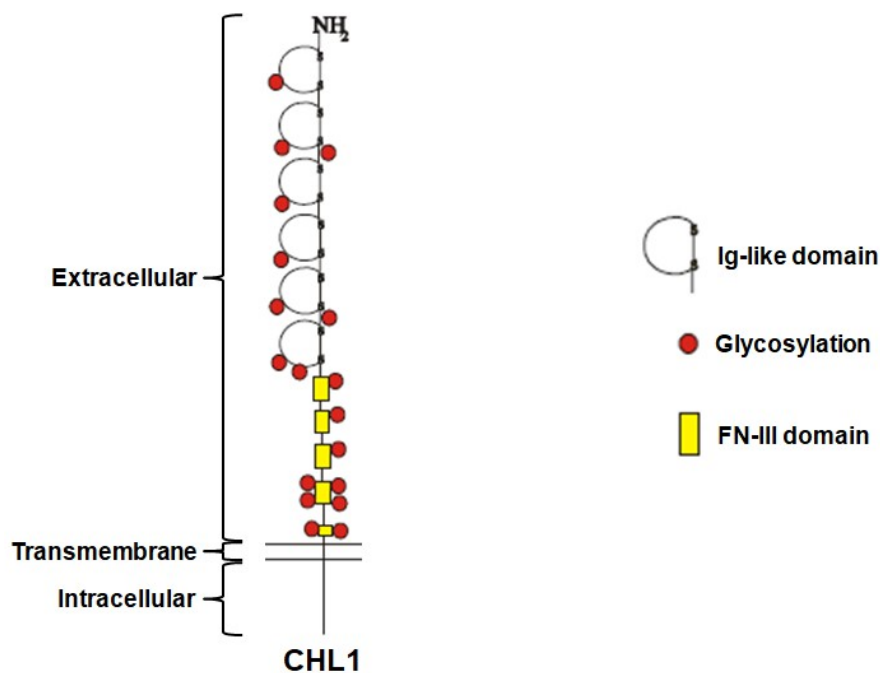


**Figure 1:**

**Schematic presentation of the CHL1 molecule.** CHL1 is a single-pass transmembrane molecule consisting of a large extracellular domain (1081 amino acids), a short transmembrane domain (23 amino acids) and an intracellular domain (105 amino acids). The extracellular domain of CHL1 contains a sequence of conserved protein domains consisting of 6 Ig-like and 4.5 FN-III domains. The figure was modified from Tian (2009). Abbreviations: CHL1 – close homolog of L1, FN-III – fibronectin type III, Ig – immunoglobulin.

Some amino acid motifs responsible for protein binding were identified in the sequence of CHL1. The Arg-Gly-Asp (RGD) motif in the second Ig-like domain and the Asp-Gly-Glu-Ala (DGEA) motif in the sixth Ig-like domain mediate interactions of CHL1 with integrins which are transmembrane proteins responsible mainly for the interaction of the cell with the extracellular matrix (ECM) (Holm et al., 1996). The intracellular domain of CHL1 contains the Phe-Ile-Gly-Ala-Tyr (FIGAY) motif responsible for the interaction of CHL1 with ankyrins and the Arg-Gly-Gly-Lys-Tyr-Ser-Val (RGGKYSV) motif mediating the interaction of CHL1 with ezrins. Both, ankyrins and ezrins link plasma membrane proteins with the cytoskeleton (Herron et al., 2009).

#### 4.1.2. CHL1 as a member of the IgSF-CAMs and L1 family of CAMs

CHL1 is classified as one of the CAMs, which are cell-surface proteins responsible for the interaction of the cell with proteins of the ECM and with proteins expressed on the surface of another cell (*trans*-interaction), as well as for the regulation of different proteins expressed at the surface of the same cell (*cis*-interaction). In the nervous system, CAMs were shown to be important for synaptic plasticity, cell migration, cell survival, cell differentiation and neurite outgrowth. Interaction of a CAM with a molecule expressed on the surface of

another cell not only results in adhesion of the two cells, but also triggers the intracellular signaling cascades resulting, for example in regulation of gene expression and reorganization of the cytoskeleton (Holm et al., 1996; Maness & Schachner, 2007; Horstkorte & Fuss, 2012).

CAMs identified so far are classified based on their structural features into four superfamilies – cadherins, integrins, superfamily of C-type lectin-like domain proteins (CTLDs) and IgSF-CAMs (**Figure 2**). The typical feature of cadherins is the presence of at least two calcium-dependent “extracellular cadherin” or EC repeats. Integrins are non-covalently linked heterodimers consisting of an  $\alpha$ - and a  $\beta$ -strand. CTLDs are characterized by the presence of carbohydrate-recognition domains. The structural feature of IgSF-CAMs is the presence of Ig-like domains (Horstkorte & Fuss, 2012). Due to the presence of the Ig-like domains CHL1 belongs to the IgSF-CAMs (Holm et al., 1996). CAMs of the IgSF can be divided into two groups: proteins containing one or more Ig-like domains and proteins containing more than one Ig-like domain followed by FN-III domains (**Figure 2**). Examples of the first group are P<sub>0</sub> and Thy-1, and examples of the second group are neural CAM (NCAM) and the L1 family of CAMs. Due to the presence of Ig-like domains and FN-III domains and the high structural homology of CHL1 and the other members of the L1 family CAMs, CHL1 was classified as a member of the L1 family CAMs (Horstkorte & Fuss, 2012).

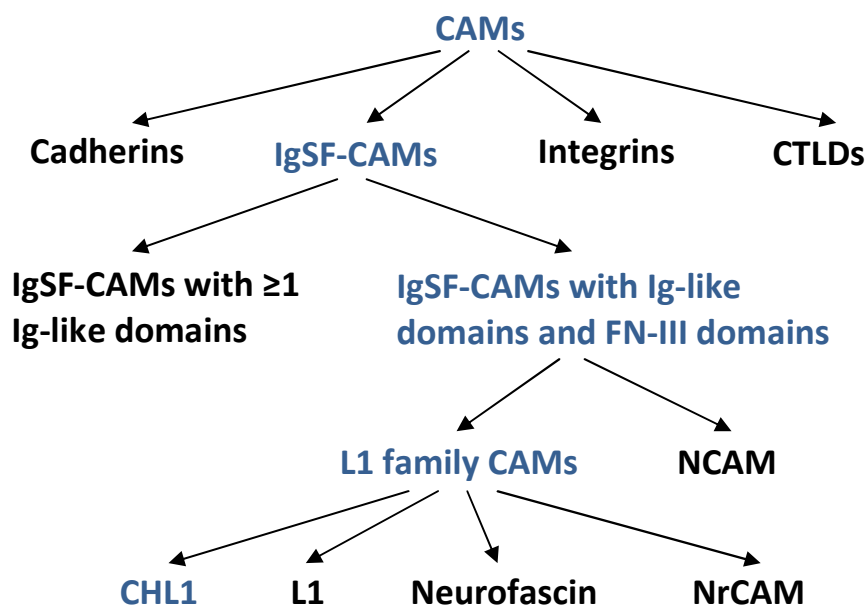


**Figure 2:**

**CHL1 is a member of the IgSF-CAMs and L1 family of CAMs.** The scheme presents the classification of CAMs, which is based predominantly on their structural features. Four superfamilies of CAMs are distinguished: cadherins, IgSF-CAMs, integrins and CTLDs. CHL1, due to the presence of Ig-like domains in its structure, belongs to IgSF-CAMs. IgSF-CAMs are further classified into two groups based on the presence of FN-III domains and CHL1 belongs to the IgSF-CAMs containing FN-III domains. Within the group of IgSF-CAMs with Ig-like and FN-III domains two groups are distinguished. One group containing 6 Ig-like domains followed by

$\geq 4$  FN-III domains (the so called “L1 family cassette”) is the L1 family of CAMs. CHL1, due to the presence of 6 Ig-like domains and 4.5 FN-III domains, is a member of the L1 family of CAMs. The figure was prepared based on: Holm et al. (1996); Maness & Schachner (2007); Herron et al. (2009); Horstkorte & Fuss (2012). Abbreviations: CAMs – cell adhesion molecules, CHL1 – close homolog of L1, CTLDs – C-type lectin-like domain proteins, FN-III – fibronectin type III, Ig-like – immunoglobulin-like, IgSF-CAMs – immunoglobulin superfamily of cell adhesion molecules, NCAM – neural cell adhesion molecule, NrCAM – neuronal cell adhesion molecule or neuron-glia cell adhesion molecule (NgCAM)-related cell adhesion molecule.

L1 family CAMs share a structural feature referred to as the “L1 family cassette” which is a sequence of evolutionarily conserved protein domains consisting of 6 Ig-like domains followed by  $\geq 4$  FN-III domains (Holm et al., 1996) (**Figure 3**). Members of the L1 family CAMs, e.g. CHL1, L1, Neurofascin, and NgCAM (neuron-glia cell adhesion molecule)-related cell adhesion molecule (NrCAM) (Maness & Schachner, 2007), share high homology especially in the intracellular domain. Structurally, the intracellular domain of CHL1 is most similar to the intracellular domain of NrCAM with which it shares 64% amino acid identity, and the extracellular domain of CHL1 is most similar to the extracellular domain of L1 sharing 37% amino acid identity. The main differences between CHL1 and the other members of the L1 family CAMs are the absence of an Arg-Ser-Leu-Glu (RSLE) motif in the intracellular domain and a partial FN-III domain in the extracellular domain (Holm et al., 1996).

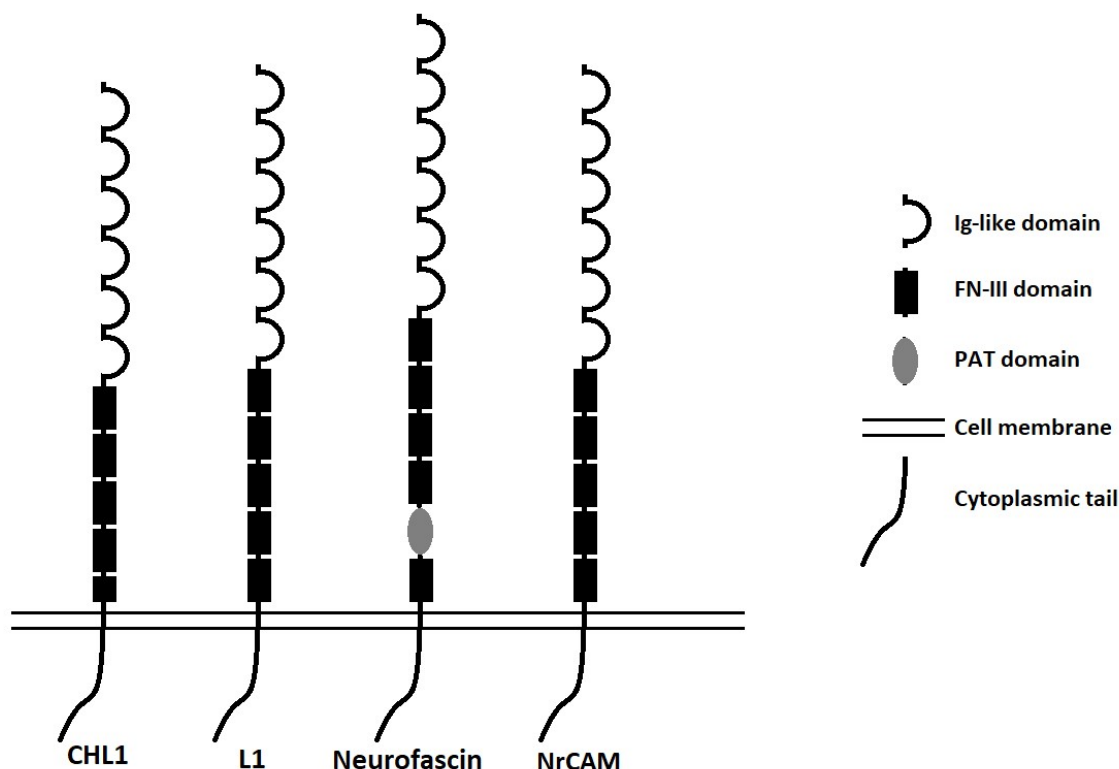


**Figure 3:**  
**CAMs of the L1 family.** Schematic presentation of the overall structures of four members of the L1 family CAMs: CHL1, L1, Neurofascin and NrCAM. Abbreviations: CHL1 – close homolog of L1, FN-III – fibronectin

type III, Ig – immunoglobulin, NrCAM – neuronal cell adhesion molecule or NgCAM (neuron-glia cell adhesion molecule)-related cell adhesion molecule, PAT domain – proline, alanine, and threonine domain.

Members of the L1 family CAMs are expressed in the nervous system predominantly by neurons, where the expression of L1 family CAMs starts late during embryonic development (Hillenbrand et al., 1999). Due to high homology of their domains, members of the L1 family CAMs share some interaction partners (Holm et al., 1996); however, although they may interact with the same proteins, the effects of these interactions may be completely different (Herron et al., 2009). Evidence for the important roles of L1 family CAMs in development and maintenance of the nervous system comes from studies performed using knock-out mice and from case reports of mutations in genes coding for these molecules in humans. For instance, mice lacking L1, CHL1, neurofascin or NrCAM show errors in axon guidance which result in behavioral deficits, such as motor coordination defects and learning deficits (Herron et al., 2009; Smigiel et al., 2018), whereas mutations within the genes coding for the L1 family CAMs in humans lead to severe phenotypes such as 3p-syndrome or schizophrenia in case of mutated CHL1 gene, CRASH syndrome (corpus callosum hypoplasia, retardation, adducted thumbs, spastic paraplegia and hydrocephalus) in case of mutations in the L1 gene, and autism in case of NrCAM mutations (Herron et al., 2009).

#### **4.1.3. Expression of CHL1**

In humans, brain and especially the cerebral cortex contain higher levels of the CHL1 protein than other organs. In addition, high amounts of CHL1 are expressed in the respiratory tract, kidneys, skin and soft tissues (Human Protein Atlas). In the mouse brain, a significant amount of the CHL1 mRNA is detected in the cerebral cortex, hippocampus, olfactory bulb, hypothalamus, striatum (pallidum) and midbrain (Allen Brain Atlas: Mouse Brain Map).

CHL1 expression in the nervous system is cell-type specific and depends on the differentiation state of the cells. CHL1 is expressed in cultures of primary hippocampal neurons, cortical neurons, mesencephalic (midbrain) neurons, spinal cord neurons, dorsal root ganglion neurons, astrocytes, Schwann cells, precursors and progenitors of oligodendrocytes, while it is not expressed in primary cultures of mature oligodendrocytes (Hillenbrand et al., 1999). The impact of the cell differentiation state on the expression of CHL1 was shown for instance for oligodendrocytes: CHL1 is expressed by 5% of oligodendrocyte precursors with unbranched processes, by 50% of developing oligodendrocyte progenitors which were stimulated with growth factors and by 0% of mature oligodendrocytes (Hillenbrand et al., 1999). Other indications for the influence of the developmental state of the cells on CHL1 expression are the finding that cerebellar granule

cells express it only after they migrate to the inner granular layer and the finding that during postnatal development CHL1 is downregulated in the thalamus and upregulated in the dentate gyrus (Hillenbrand et al., 1999). In the peripheral nervous system expression of CHL1 was confirmed not only for Schwann cells but also for femoral and sciatic nerves in 3-weeks-old mice (Hillenbrand et al., 1999).

A gene dosage effect was shown to exist for CHL1 as the studies using transgenic mice heterozygous for the CHL1 gene (CHL1<sup>+/-</sup>) showed that these mice express in the hippocampus half of the amount of CHL1 expressed by the CHL1<sup>+/+</sup> mice (Frints et al., 2003). In different analyses these mice exhibit the phenotype either similar to CHL1<sup>+/+</sup>, similar to CHL1<sup>-/-</sup> or intermediate between the CHL1<sup>-/-</sup> and CHL1<sup>+/+</sup> mice (Frints et al., 2003). An example of the importance of a correct dosage of the CHL1 gene for the normal brain function is the effect of microdeletions and microduplications within the CHL1 gene in humans, which are associated with language difficulties and different levels of mental retardation (**Table 1**) (Pohjola et al., 2010; Shoukier et al., 2013; Palumbo et al., 2015; Li et al., 2016; Bertini et al., 2017).

Like the other members of the L1 family CAMs, CHL1 is expressed in the mouse brain late during embryonic development: in homogenates of mouse forebrain CHL1 cannot be detected with immunoblotting until the embryonic day (E) 13, the highest levels of CHL1 are detected between E18 and postnatal day (P) 7, and from the second postnatal week the amount of CHL1 gradually decreases (Holm et al., 1996; Hillenbrand et al., 1999).

#### **4.1.4. Functions of CHL1 in the nervous system**

CHL1 has many binding partners and regulates their functions. Through its extracellular domain CHL1 can bind to other CHL1 molecules (Katic et al., 2014), which is called a homophilic interaction. Furthermore, it can interact heterophilically with patched-1 (Ptc1) (Katic et al., 2017), vitronectin (Katic et al., 2014), plasminogen activator inhibitor-2 (Katic et al., 2014) and integrins (Buhusi et al., 2003; Katic et al., 2014). Through the intracellular domain CHL1 interacts with serotonin receptor 2C (Kleene et al., 2015), disrupted in schizophrenia 1 (Ren et al., 2016), heat shock cognate protein 70 kDa (Leshchyn'ska et al., 2006), cysteine-string protein (Andreyeva et al., 2010),  $\beta$ II spectrin (Tian et al., 2012) and small glutamine-rich tetratricopeptide repeat-containing protein  $\alpha$  (Andreyeva et al., 2010).

CHL1 regulates neurite outgrowth in various ways. It was found that heterophilic interactions of CHL1 promote neurite outgrowth, while the homophilic interaction of CHL1 reduces neurite outgrowth of cerebellar granule cells (Jakovcevski et al., 2007). However, the effect of the type of CHL1 interaction appears to be cell-type specific as Alsanie et al. (2017) showed that CHL1-CHL1 interaction promotes the neurite outgrowth of dopaminergic neurons.

Also, regrowth of injured mature neurites in peripheral nerve cells is regulated by CHL1. CHL1 was found to guide the regenerating neurites into a proper nerve branch (Guseva et al., 2018).

Apart from having an impact on neurite outgrowth, CHL1 influences migration and differentiation of cells which was shown for instance for cerebellar neurons (Katic et al., 2014) and dopaminergic neurons (Alsanie et al., 2017). The impact of CHL1 on differentiation of cells is different depending on the type of cells: differentiation of dopaminergic neurons is enhanced (Alsanie et al., 2017) whereas differentiation of cerebellar neurons is reduced (Katic et al., 2014) in presence of CHL1.

Moreover, CHL1 was shown to have an impact on survival of neurons, which was described for instance by Katic et al. (2017) who showed that CHL1 promotes survival of cerebellar neurons, and by Bye et al. (2015) who found that CHL1 grants the transplantability of dopaminergic progenitors in trials of cell transplantation therapy for Parkinson's disease.

At the synapse, CHL1 was shown to regulate processes occurring at the pre-synaptic membrane, where it positively regulates activity of chaperones which remove clathrin from clathrin-coated vesicles, and positively regulates SNARE (SNAP (Soluble *N*-ethylmaleimide-sensitive factor Attachment Protein) Receptor) complex which is a protein complex that mediates vesicle fusion with the cell membrane (Andreyeva et al., 2010). Post-synaptically, CHL1 co-operates with Semaphorin-3B to positively regulate pruning of mouse cortical dendritic spines, which constitute the sites receiving input from other neurons (Mohan et al., 2019).

Lack of CHL1 expression in mice results in reduced reactivity to novelty (Morellini et al., 2007) and in reduced prepulse inhibition of acoustic startle response which is associated with impaired filtering of novel versus old stimuli (Irintchev et al., 2004), suggesting an involvement of CHL1 predominantly in cognitive processes. Studies showed that CHL1<sup>-/-</sup> mice have enlarged lateral ventricles (Montag-Sallaz et al., 2002), abnormal orientation of pyramidal neurons of the cortex (Demyanenko et al., 2004), altered organization of hippocampal mossy fibers (Montag-Sallaz et al., 2002), increased number of parvalbumin-expressing hippocampal interneurons during development but reduced number of these interneurons in adulthood (Schmalbach et al., 2015), enhanced basal synaptic transmission in projections running to the dentate gyrus (Morellini et al., 2007) and reduced short- and long-term potentiation at CA3-CA1 synapses (Nikonenko et al., 2006; Schmalbach et al., 2015). Behavioral studies using conditional CHL1<sup>-/-</sup> mice, which produce CHL1 during their embryonic and postnatal development until they reach adulthood, gave insight into the functions of CHL1 not related to development and showed that ablation of CHL1 in adulthood leads to working memory deficits (Kolata et al., 2008).

#### 4.1.5. CHL1-related disorders in humans

Mutations in CALL (human gene coding for CHL1) were shown to result mainly in two disorders – the 3p-syndrome (Pohjola et al., 2010; Cuoco et al., 2011; Tassano et al., 2014; Bertini et al., 2017) and schizophrenia (Sakurai et al., 2002; Chen et al., 2005; Shaltout et al., 2013), although a potential involvement of CHL1 in autism spectrum disorder (Li et al., 2016), and depression (Probst-Schendzielorz et al., 2015) were also reported.

##### 4.1.5.1. 3p-syndrome

Consequences of DNA deletions at the small arm of the third chromosome (3p), where, among other genes, CALL is located, are collectively related to as the 3p-syndrome. The deletions are variable in size, affect different genes and lead to varying phenotypes with different mental and physical problems such as growth retardation, mental retardation, microcephaly and facial dysmorphism (Pohjola et al., 2010; Cuoco et al., 2011). Considering that the deletions within 3p often affect CALL, reduced levels of functional CHL1 protein contributes to the syndrome, but the attribution of specific symptoms to CHL1 is often difficult, when the deletions affect also other genes located at 3p next to CALL, e.g. contactin 4 and 6 (CNTN4, CNTN6) (**Figure 4**) (Cuoco et al., 2011). A few reported cases including 4 familial cases of 3p syndrome in which the deletion affected only or predominantly CALL allowed to link language difficulties and different levels of mental retardation exclusively to CHL1 (**Table 1**) (Pohjola et al., 2010; Cuoco et al., 2011; Tassano et al., 2014; Bertini et al., 2017). Interestingly, reported cases of microduplications affecting only CALL were also related to language difficulties and speech delay (**Table 1**), which confirms the involvement of CHL1 in development and acquisition of language and shows that a correct dosage of the CHL1 gene is relevant for normal development (Shoukier et al., 2013; Palumbo et al., 2015; Li et al., 2016).

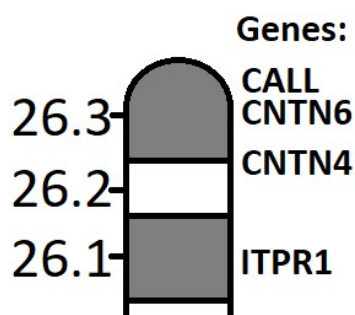


**Figure 4:**

**Localization of the human CHL1 gene (CALL) at the 3p26-pter (pter = terminus of the p arm).** CALL is located at the small (*petite*, p) arm of the 3<sup>rd</sup> chromosome making the 3<sup>rd</sup> subband of the 26<sup>th</sup> band – 3p26.3 (Tassano et al., 2014). Genes coding for two other IgSF-CAMs are located in close proximity to CALL: CNTN6 (3p26.3)

and CNTN4 (3p26.2-p26.3), and are next to ITPR1 (3p26.1) (Cuoco et al., 2011; Iwaki et al., 2015). Abbreviations: CALL – cell adhesion molecule L1-like, CNTN4 – contactin 4, CNTN6 – contactin 6, ITPR1 – inositol 1,4,5-trisphosphate receptor type 1.

**Table 1:**

**Duplications and deletions affecting CALL.** The table summarizes part of the currently available scientific literature describing cases of duplications (5,7-8) and deletions (1-4,6,9) affecting predominantly or only CALL. Abbreviations: CALL – cell adhesion molecule L1 like.

NO.	MUTATION	PATIENT	CONSEQUENCES	RELATED MUTATIONS IN THE FAMILY	REFERENCES
1.	8990 kb deletion in 3p25.3-p26.3 affected 19 genes including CALL	5-10-years-old male	mild developmental delay, writing and mathematical skills below average, difficulty coordinating limbs, short upward-turned nose, long philtrum, highly arched palate, mildly dysmorphic auricles, clubbed fingers, plantar furrows in feet	mother (healthy) and sister (relatively healthy) carrying the same mutation	Pohjola et al., 2010
2.	1100 kb deletion in 3p26.3 affected CALL	14-years-old male	severe learning disability especially in language and mathematics, microcephaly, growth retardation, slow physical development	mother (healthy) carrying the same mutation	
3.	<1000 kb deletion in 3p26.3 affected CALL, and 696 kb duplication in 1q44	8-9-years-old male	low IQ, language disorders with phonological impairment, dyslexia, dyscalculia, epichantal folds, joint hyperlaxity, strabismus at the right eye, myopia, tonic-clonic seizures at right hemi-body	father (healthy) carrying the same mutation in 3p26.3	Cuoco et al., 2011
4.		4-years-old male	difficulties in expressive and comprehensive languages – lexical and syntactic impairment		
5.	1070 kb duplication in 3p26.3 affected CALL	16-years-old female	delayed speech development, intellectual disability, generalized tonic-clonic seizures, paroxysmal eyelid myoclonia	father (healthy) carrying the same mutation	Shoukier et al., 2013
6.	956 kb deletion in 3p26.3 affected CALL, and 209.2 kb duplication in 21q22.3	6-years-old male	delayed language development, mild bilateral convergent strabismus, mild clumsiness, low IQ, microcephaly, visuo-perceptual organization deficiency	mother (healthy) carrying the same mutation	Tassano et al., 2014

7.	850 kb duplication in 3p26.3 affected CALL	2-3-years-old male	developmental delay, hyperactivity, short attention span, speech delay	-	Palumbo et al., 2015
8.	687 kb duplication in 3p26.3 affected CALL	16-months-old male	autism spectrum disorder, delayed speech, developmental delay	mother (healthy) carrying the same mutation	Li et al., 2016
9.	966 kb deletion in 3p26.3 affected CALL	6-years-old female	mild intellectual disability, language impairment, attention deficits, impaired motor skills	mother (healthy) carrying the same mutation	Bertini et al., 2017

#### 4.1.5.2. Schizophrenia

Another disorder to which CHL1 has been linked is schizophrenia. This mental disorder affects approximately 1% of the population, equally men and women, and is characterized by the general impairment of perceiving reality. The disease has no known universal cause, instead, a range of factors associated with schizophrenia has been identified with the most significant being the family history of schizophrenia: it was shown that the probability of developing schizophrenia is 50% when a monozygotic twin is affected, 17% when a dizygotic twin is affected and 6-17% when a first-degree relative is affected (Schultz et al., 2007). The occurrence of the disease was also linked to childhood trauma, residence in a city, prenatal environment including mother going through certain infections or severe stress (Patel et al., 2014), and cannabis use (Hall & Degenhardt, 2008). The diagnosis of schizophrenia is based exclusively on the behavior of the person and presence for at least 6 months of hallucinations, delusions, disorganized speech, grossly disorganized or catatonic behavior, negative symptoms such as alogia, avolition or affective flattening as well as decreased functioning regarding self-care, interpersonal relationships or work (Schultz et al., 2007; Patel et al., 2014). In addition, a high (10%) suicide risk exists for people suffering from schizophrenia (Schultz et al., 2007).

For a long time increased dopaminergic signaling related to abnormal activity of DRD2 and elevated dopamine levels were attributed to the pathophysiology of schizophrenia. Confirmations for the involvement of the dopaminergic system in schizophrenia came from the observation that recreational drugs increasing dopaminergic neurotransmission cause symptoms observed in schizophrenia as well as from the use of DRD2 antagonists in treatment of the symptoms of schizophrenia (Schultz et al., 2007; Patel et al., 2014). However, imbalances in the neurotransmission of serotonin, glutamate, glycine, gamma-aminobutyric acid (GABA) or aspartate were also found to be related to the pathophysiology of schizophrenia (Patel et al., 2014). Apart from abnormal neurotransmission people diagnosed with schizophrenia were shown to have a range of morphological alterations in the brain such as reduced size of the thalamus (Brickman et al., 2004), enlarged

brain ventricles (Vita et al., 2006), reduced thickness of the frontal cortex (Goldman et al., 2009), reduced volume of the hippocampus (Vita et al., 2006) and reduced overall brain volume (Vita et al., 2006).

Members of IgSF-CAMs were shown to be involved in schizophrenia. An indication for the important role of IgSF-CAMs in schizophrenia came from the result of the measurement of L1 and NCAM levels in the cerebrospinal fluid of people diagnosed with this disease, showing that in schizophrenia the level of soluble NCAM increases and the level of soluble L1 decreases (Poltorak et al., 1995). Although other IgSF-CAMs were not analyzed, the results obtained for L1 and NCAM suggest an involvement of these molecules in the disease.

The involvement of CHL1 in the etiology of schizophrenia has not been reported by genome-wide investigations of schizophrenia-susceptibility genes (Shaw et al., 1998); however, some of the single nucleotide polymorphisms (SNPs) in CALL were linked in several studies to schizophrenia (Sakurai et al., 2002; Chen et al., 2005; Shaltout et al., 2013). A study by Sakurai et al. (2002) performed among the Japanese population showed that a missense polymorphism resulting in Leu to Phe substitution at the 17<sup>th</sup> amino acid of CHL1 (Leu17Phe) occurred significantly more often among patients diagnosed with schizophrenia versus healthy controls. Three years later, Chen et al. (2005) reported a very strong correlation of the same SNP with schizophrenia in the Han Chinese population ( $P < 0.000001$ ). The results of Sakurai and Chen were further confirmed with the result obtained by Shaltout et al. (2013) who investigated the correlation of the same Leu17Phe polymorphism with schizophrenia in the Qatari population.

#### **4.2. Dopaminergic system**

Neurons releasing the neurotransmitter dopamine, dopamine transporters on dopamine-releasing neurons and receptors for dopamine on target cells are elements of the dopaminergic system. Dopamine released into the synapse binds to different types of presynaptic and postsynaptic dopamine receptors leading to modifications in the intracellular signaling cascades, reduction in dopamine production and internalization of the receptors. In the brain, groups of dopaminergic neurons that innervate different brain structures and have different functions form the dopaminergic pathways. The final shape of the dopaminergic pathways is formed during embryonic and early postnatal development. Abnormal dopaminergic signaling constitutes the pathophysiology of many psychiatric and neurological disorders.

#### 4.2.1. Elements of the dopaminergic system

##### 4.2.1.1. Dopamine

Dopamine (3,4-dihydroxyphenethylamine) is a monoamine, which, together with the neurotransmitters epinephrine and norepinephrine (for which dopamine is a precursor), belongs to the catecholamine family of molecules that consist of a catechol group (benzene ring with two hydroxyl groups) and an amine group (Drozak & Bryła, 2005).

Dopamine is synthesized predominantly in the dopaminergic neurons and the metabolic pathway of dopamine synthesis starts with the conversion of amino acids phenylalanine (Phe) or tyrosine (Tyr) and continues as follows: Phe → Tyr → levodopa (L-DOPA) → dopamine, where the first reaction of Phe into Tyr conversion is catalyzed by phenylalanine hydroxylase, then tyrosine hydroxylase (TH) converts Tyr to L-DOPA, and L-DOPA is converted to dopamine by a decarboxylase of aromatic amino acids (Daubner et al., 2011). Dopamine then can serve as neurotransmitter and precursor for norepinephrine and epinephrine.

Catabolism of dopamine is mediated by a monoamine oxidase in the dopaminergic neurons and glial cells, followed by a catechol-*O*-methyl transferase in the glial cells and aldehyde dehydrogenase in the dopaminergic neurons, which act to eventually produce homovanillic acid in the glial cells and 3,4-dihydroxyphenylacetic acid in the dopaminergic neurons. The oxidation of dopamine, which is a step in dopamine degradation, often leads to production of toxic quinones and reactive oxygen species (ROS), which can accumulate and are then responsible for degeneration of the dopaminergic neurons e.g. in Parkinson's disease (Meiser, 2013).

Apart from being a neurotransmitter, dopamine is a paracrine/autocrine agent in kidneys, pancreas, pulmonary alveoli and blood vessels (Drozak & Bryła, 2005).

##### 4.2.1.2. Dopaminergic neurons

Dopaminergic neurons constitute less than 1% of all brain neurons (Arias-Carrión et al., 2010). The highest number of dopaminergic neurons is found in the ventral midbrain (sometimes called the ventral mesencephalon), where they form three structures: VTA, substantia nigra (SN) and retrorubralfield (RRF) (Van den Heuvel & Pasterkamp, 2008). Bilaterally, the midbrain of an adult mouse contains 20,000-30,000 dopaminergic neurons, in an adult rat the midbrain contains about 40,000 dopaminergic neurons (Van den Heuvel & Pasterkamp, 2008), whereas the midbrain of a human in the 40s contains 590,000 dopaminergic neurons and their number drops to 350,000 by the time humans reach their 60s (Chinta et al., 2005). A

substantial amount of dopaminergic cell bodies is concentrated also in the diencephalon where they are located mostly in the arcuate nucleus of the hypothalamus (Drozak & Bryła, 2005; Lyons et al., 2012).

Dopaminergic neurons of the SN send their axons to the dorsal striatum consisting of caudate and putamen (CP, CPu) to form the so called nigrostriatal dopaminergic pathway (Van den Heuvel & Pasterkamp, 2008). The SN is functionally and morphologically divided into two parts: pars compacta (SNc, SNpc) containing the dopaminergic cell bodies and pars reticulata (SNr, SNpr) containing the dopaminergic fibers (van Domburg & tenDonkelaar, 1991). The SN received its name due to presence of neuromelanin in its neurons, which gives this brain structure a darker color relatively to the tissue surrounding it (Zecca et al., 2001). Dopaminergic neurons of the VTA project predominantly to the ventral striatum consisting of the nucleus accumbens (NAc) and of the olfactory tubercle (OT) and to the frontal cortex forming the mesolimbic and the mesocortical dopaminergic pathways, respectively. Dopaminergic neurons located in the hypothalamus project from the arcuate nucleus to the median eminence forming the tuberoinfundibular pathway (Lyons et al., 2012).

Dopaminergic neurons forming the VTA and the SN have different functions. Moreover, within each of these structures there are subpopulations of dopaminergic neurons, which have distinct properties and can be regulated by separate mechanisms. For instance, in the ventral SN a subpopulation of dopaminergic neurons expressing deleted in colorectal cancer (DCC) protein was identified, whereas in the VTA two subpopulations of dopaminergic neurons have been identified based on their response to certain opioids and these two subpopulations of the VTA dopaminergic neurons were later identified to project to different brain structures – the frontal cortex and the ventral striatum (Van den Heuvel & Pasterkamp, 2008).

#### 4.2.1.3. Dopamine receptors

Dopamine released from the presynaptic terminal activates 5 types of pre- and post-synaptic dopamine receptors named DRD1 (dopamine receptor D1), DRD2, DRD3 (dopamine receptor D3), DRD4 (dopamine receptor D4) and DRD5 (dopamine receptor D5). All dopamine receptors are G-protein-coupled receptors (GPCRs) which pass the plasma membrane 7 times. They are metabotropic receptors, which influence the activity of the cell via secondary messengers. One of the secondary messengers regulated by the dopamine receptors is cyclic adenosine monophosphate (cAMP). Depending on the influence on the level of cAMP, the five types of dopamine receptors were divided into two classes: D1-like receptors (DRD1 and DRD5) which increase the amount of cAMP and D2-like receptors (DRD2, DRD3 and DRD4) which decrease the level of cAMP upon dopamine binding (**Figure 5**). The difference in the impact of D1-like and D2-like receptors on the cAMP level is due to the different types of G-proteins with which the receptors are coupled. D1-like receptors are  $G_s$  ( $G_{stimulatory}$ )-coupled and activate the enzyme adenylyl cyclase (ACy) which produces cAMP,

whereas D2-like receptors are coupled with  $G_i$  ( $G_{\text{inhibitory}}$ ) protein and inhibit the ACy activity leading to a drop in cAMP (Beaulieu & Gainetdinov, 2011).

Apart from being coupled with different G-proteins, D1-like and D2-like receptors differ also in their coding sequence which only in the case of D2-like receptors contains introns. Moreover, unlike D1-like receptors, D2-like receptors have splice variants and can be expressed (in case of DRD2 and DRD3) both pre- and post-synaptically (Beaulieu & Gainetdinov, 2011).

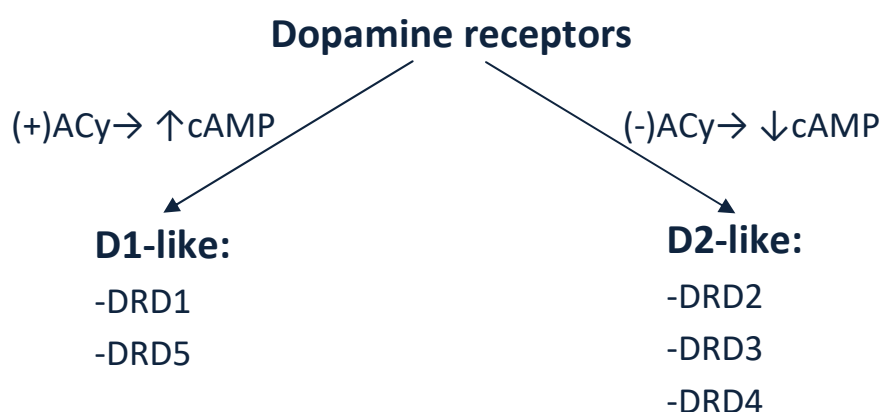


**Figure 5:**

**Types of dopamine receptors.** Five different types of dopamine receptors are classified into two groups – D1-like receptors (to which DRD1 and DRD5 belong), and D2-like receptors (to which DRD2, DRD3 and DRD4 belong). The classification is based on the impact of agonist binding on the activity of the enzyme ACy, which produces cAMP. D1-like receptors activate ACy and increase the cAMP level while D2-like receptors inhibit ACy and lead to a reduction in the cAMP amount. The figure was prepared based on Beaulieu & Gainetdinov (2011). **Abbreviations:** ACy – adenylyl cyclase, cAMP – cyclic adenosine monophosphate, DRD1 – dopamine receptor D1, DRD2 – dopamine receptor D2, DRD3 – dopamine receptor D3, DRD4 – dopamine receptor D4, DRD5 – dopamine receptor D5.

Presynaptic receptors for dopamine are referred to as autoreceptors and play a major role in regulation of the amount of dopamine in the synapse via the negative feedback loop: upon binding of dopamine to the autoreceptor a signaling cascade is activated leading to inhibition of the dopamine-producing enzyme TH (Ford, 2014). Although two dopamine receptor types can function as autoreceptors, DRD2 and DRD3, the majority of the autoreceptor function in the brain is mediated by DRD2. DRD2 has two splice variants that differ by 87 nucleotides coding for 29 additional amino acids in the third intracellular loop and therefore are called “long” (DRD2L) and “short” (DRD2S) form (**Figure 6**). DRD2S is the predominant DRD2 autoreceptor form while DRD2L is expressed mostly postsynaptically (Beaulieu & Gainetdinov, 2011).

Dopamine receptors are expressed in the nervous system as well as in the blood vessels, heart, kidneys, adrenal glands, pancreas, lungs and gastrointestinal tract (Drozak & Bryła, 2005; Beaulieu & Gainetdinov, 2011). In the brain the highest levels of DRD1 are expressed in striatum, frontal cortex, SN, amygdala, olfactory bulb, hippocampus, cerebellum, thalamus and hypothalamus. DRD2 is expressed in high levels in striatum and OT, but substantial amounts of DRD2 are also expressed in SN, VTA, hypothalamus, amygdala, hippocampus, pituitary gland and certain cortical areas. Highest levels of DRD3 are expressed in striatum, SN, VTA, hippocampus, septum and cortex. DRD4 and DRD5 have low expression in the brain, but can be detected in cortex, hypothalamus and hippocampus (Beaulieu & Gainetdinov, 2011).

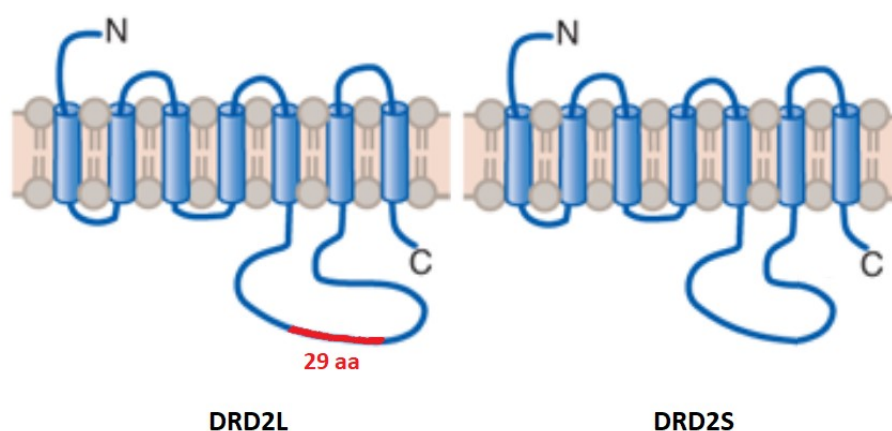


**Figure 6:**

**Forms of DRD2.** The scheme presents the two forms of the DRD2: DRD2L and DRD2S. The two DRD2 forms differ by additional 29 aa in the third intracellular loop of DRD2L. The figure was modified from Sanders-Bush & Hazelwood (2011). Abbreviations: aa – amino acids, DRD2L – dopamine receptor D2 “long”, DRD2S – dopamine receptor D2 “short”.

#### 4.2.1.4. Dopamine transporter

Dopamine can be pulled back from the synapse by the neuron that released it. The process of dopamine reuptake is mediated by the dopamine transporter (DAT) which is a 12-transmembrane pre-synaptic protein with C- and N-tails located in the cytoplasm and which symports dopamine into the cell together with sodium ions. DAT is a target for ADHD medications and for addictive drugs such as amphetamine, methamphetamine and cocaine which increase the level of dopamine in the synapse by either blocking its reuptake (in case of cocaine) or by competing with dopamine for the reuptake and by causing a dopamine efflux (in case of amphetamine and methamphetamine) (Vaughan & Foster, 2013).

#### 4.2.2. Dopaminergic synapse

Dopamine synthesized in the cytoplasm at the synaptic terminals of dopaminergic neurons is transported into synaptic vesicles via vesicular monoamine transporter 2 (VMAT2) and stored at the synaptic terminals. When the action potential transmitted along the axon of the dopaminergic neuron reaches the synaptic terminal, influx of calcium ions and activation of calcium-dependent proteins occur. One of the activated proteins is synaptotagmin 1, which mediates the fusion of dopamine-carrying synaptic vesicles with the plasma membrane resulting in dopamine release into the synaptic cleft via exocytosis. The dopamine released into the synaptic cleft binds to its receptors at the postsynaptic membrane and activates intracellular signaling cascades leading to activation or inhibition of the postsynaptic neuron (Lodish et al., 2000). Dopamine binds also to its autoreceptors located at the presynaptic neuron, which initiates the intracellular signaling cascade resulting in inhibition of dopamine production (Beaulieu & Gainetdinov, 2011). Unbound dopamine is removed from the synaptic cleft and pulled back to the dopaminergic neuron via the DAT, then transported again to the synaptic vesicles by VMAT2 or degraded (Meiser et al., 2013).

As a consequence of dopamine binding to the receptors the neurons desensitize to dopamine by reducing the amount of receptors at the plasma membrane. This occurs via internalization of the receptors (**Figure 7**). The internalized receptors are enclosed in endosomes and can later be restored back to the plasma membrane or the endosomes can fuse with lysosomes and the receptors are degraded. The fate of different types of the internalized receptors depends on the type of the receptor, as it was shown that DRD2 is predominantly destined to be degraded whereas DRD1 is usually restored back to the plasma membrane, which in case of cells expressing both DRD1 and DRD2 results in a shift from the activation of both types of receptors during the initial dopamine release to the activation of mostly DRD1 during the next dopamine release (Bartlett et al., 2005).

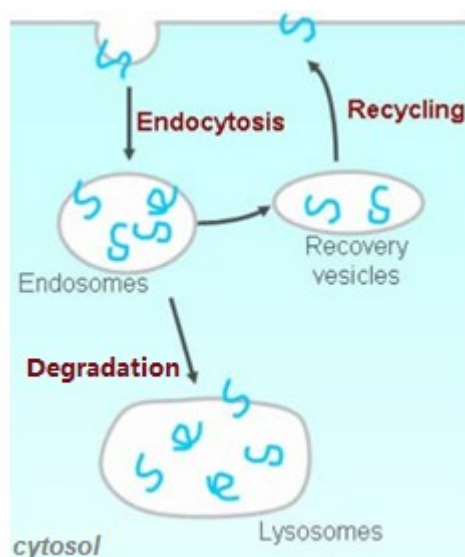


**Figure 7:**

**Dopamine receptor trafficking.** Upon dopamine binding, the dopamine receptors (presented as blue patterns) are internalized through endocytosis and enclosed in vesicles which turn into endosomes. The internalized receptors can further be degraded if the endosomes fuse with lysosomes or become recycled and restored back to the plasma membrane (Bartlett et al., 2005). The figure was modified from: Xiao (2009).

**4.2.2.1. Signaling pathways triggered by DRD2**

Due to the high homology of DRD2S and DRD2L the two receptor forms regulate similar signaling cascades upon ligand binding. Stimulation of DRD2 leads to a conformational change of the receptor and dissociation of the  $\alpha$  subunit of the G protein, which regulates the activity of AC $\gamma$  that produces cAMP which in turn affects the activity of protein kinase A (PKA). Also, the  $\beta\gamma$  subunits complex of the G protein regulates signaling cascades; for instance, it affects the activity of phospholipase C which is an enzyme producing diacylglycerol and inositol trisphosphate, which in turn regulate protein kinase C activity and calcium homeostasis, respectively. Longer stimulation of the receptors leads to recruitment of  $\beta$ -arrestin2, serine/threonine-protein phosphatase 2A (PP2A) and protein kinase B (Akt), deactivation of Akt by PP2A and activation of glycogen synthase kinase 3 signaling (Beaulieu & Gainetdinov, 2011).

Internalization of DRD2 is also mediated by the intracellular signaling: G-protein-coupled receptor kinases (GRKs) phosphorylate the receptors, which leads to recruitment of  $\beta$ -arrestins and internalization of the receptors in a clathrin-dependent pathway (Beaulieu & Gainetdinov, 2011).

However, as DRD2S and DRD2L are located in different cells (for example in the striatum the autoreceptor DRD2S is expressed in high levels by dopaminergic neurons whereas DRD2L is located predominantly at striatal medium spiny neurons (MSNs)) and regulate the activity of different intracellular proteins expressed by these cells (Chen et al., 2012). Binding of agonists to DRD2S triggers the intracellular signaling pathway inhibiting the phosphorylation and thus the activity of TH by PKA (Dunkley et al., 2004; Chen et al., 2012). Agonists binding to DRD2L negatively affect the phosphorylation of DARPP32 by PKA (**Figure 8**) (Beaulieu & Gainetdinov, 2011). Moreover, DRD2S and DRD2L activate extracellular-signal-regulated kinase (ERK) through rapidly accelerated fibrosarcoma (RAF) kinase / mitogen-activated protein kinase and ERK kinase (MEK) / ERK signaling pathways with DRD2S-dependent ERK activation being more associated with  $\beta$ -arrestins recruitment and receptor internalization (Chen et al., 2012).

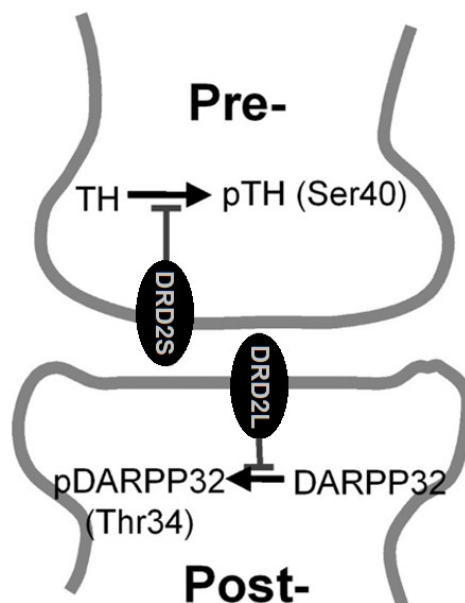


**Figure 8:**

**Targets of DRD2S and DRD2L signaling.** Agonist binding to pre-synaptic DRD2S leads to inhibition of TH phosphorylation at Ser40, whereas agonist binding to post-synaptic DRD2L causes inhibition of phosphorylation of DARPP32 at Thr34. The figure was modified from Xiao et al. (2009). Abbreviations: DARPP32 – dopamine- and cyclic adenosine monophosphate-regulated neuronal phosphoprotein 32 kDa, DRD2L – dopamine receptor D2 “long”, DRD2S – dopamine receptor D2 “short”, p – phosphorylated, Pre- – the pre-synaptic neuron, Post- – the post-synaptic neuron, Ser40 – 40<sup>th</sup> amino acid: serine, TH – tyrosine hydroxylase, Thr34 – 34<sup>th</sup> amino acid: threonine.

#### 4.2.3. Dopaminergic pathways

In the brain, groups of dopaminergic neurons projecting to different structures form different dopaminergic pathways. The most prominent dopaminergic pathways are the nigrostriatal, the mesolimbic, the mesocortical and the tuberoinfundibular pathways (**Figure 9**) (Beaulieu & Gainetdinov, 2011).

Dopaminergic neurons of the nigrostriatal pathway are located in the SN in the ventral midbrain and send their axons to the dorsal striatum, where they form synapses predominantly on two populations of the GABA-ergic MSNs expressing either DRD1 or DRD2. The DRD1-expressing MSNs send information to the SNr/SNpr directly and the DRD2-expressing MSNs send information to the SNr/SNpr indirectly through additional brain structures leading to the initiation or inhibition of movements, respectively. The nigrostriatal dopaminergic pathway is mostly involved in regulation of voluntary movements and goal-directed behaviors and degeneration of dopaminergic neurons in the SN is associated with Parkinson’s disease (Money & Stanwood, 2013).

The mesolimbic dopaminergic pathway runs from the VTA to the ventral striatum. The main functions of this pathway are regulation of goal-directed behavior, regulation of emotions, consolidation of memory for

salient events, experience of novelty, aversion, motivation and reward, while malfunctions of this pathway are associated with addiction, schizophrenia and depression (Goodman, 2008; Van den Heuvel & Pasterkamp, 2008; Money & Stanwood, 2013; Luo & Huang, 2016).

Apart from projecting to the ventral striatum, the VTA sends projections also to the prefrontal cortex forming the mesocortical dopaminergic pathway. This pathway plays major roles in learning and memory (Drozak & Bryła, 2005; Van den Heuvel & Pasterkamp, 2008).

The fourth most prominent dopaminergic pathway of the brain, the tuberoinfundibular pathway, unlike the other three, does not start in the midbrain and does not project to the telencephalon, but it projects within the diencephalon: the dopaminergic neurons located in the arcuate nucleus of the hypothalamus project to the median eminence of the hypothalamus. This dopaminergic pathway regulates prolactin secretion by the pituitary gland (Lyons et al., 2012).

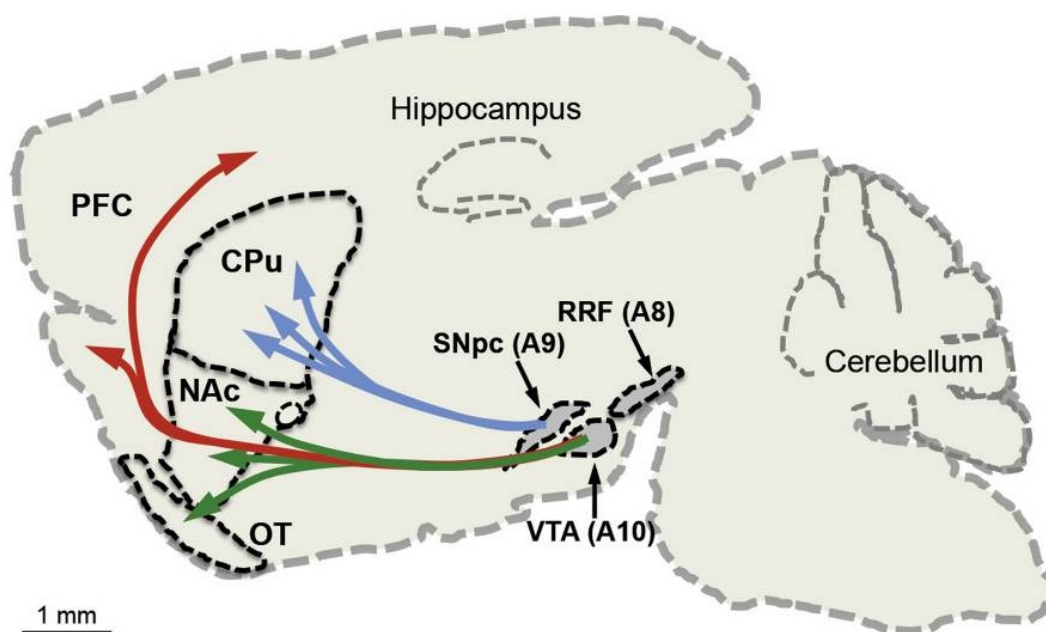


**Figure 9:**

**Brain dopaminergic pathways.** In the scheme of a sagittal mouse brain section three out of four main dopaminergic pathways are presented: the nigrostriatal pathway (blue) runs from the SNpc (A9) to the dorsal striatum consisting of CPu, the mesolimbic pathway (green) runs from the VTA (A10) to the ventral striatum consisting of NAc and OT and the mesocortical pathway (red) runs from the VTA to the PFC (Luo & Huang, 2016). The dopaminergic pathway not shown in the scheme is the tuberoinfundibular pathway which projects from the arcuate nucleus to the median eminence of the hypothalamus (Lyons et al., 2012). The RRF (A8) constitutes the third ventral midbrain group of dopaminergic neurons (Van den Heuvel & Pasterkamp, 2008). The figure is derived from: Luo & Huang (2016). Abbreviations: CPu – caudate and putamen, NAc – nucleus accumbens, OT – olfactory tubercle, PFC – prefrontal cortex, RRF – retro-rubral field, SNpc – substantia nigra-pars compacta, VTA – ventral tegmental area.

#### 4.2.4. Development of the dopaminergic pathways

Early embryonic stages of the ventral midbrain dopaminergic system development include radial migration of proliferating dopaminergic progenitors from the ventricular surface (the most medial surface of the midbrain vesicle) to the intermediate zone of the developing midbrain, where the progenitors differentiate into post-mitotic neuroblasts which then migrate radially to the marginal zone. In the marginal zone a group of the neuroblasts becomes TH-positive dopaminergic neurons forming the early VTA, whereas the rest of the neuroblasts migrates tangentially in the direction of the basal plate to form the TH-positive dopaminergic neurons of the SN. In the developing mouse brain, this process of dopaminergic precursor migration and differentiation continues until E14.5 while the first TH-positive neurons are detected in the marginal zone at E10.5 (Alsanie et al., 2017).

Upon their terminal differentiation, the dopaminergic neurons begin to develop axons which initially grow dorsally within the midbrain and then, upon leaving the midbrain, follow the rostral trajectory to form the two axon bundles called the medial forebrain bundles (MFBs). The MFBs follow the ventrorostral path through the diencephalon and then the ventrolateral path through the telencephalon to finally reach the developing striatum. First the dopaminergic axons reach the ventromedial part of the striatum which will give rise to the NAc, then the dorsolateral part of the striatum which develops into the CP/CPu, and finally the cortex (Van den Heuvel & Pasterkamp, 2008; Alsanie et al., 2017). Within the target structures, the dopaminergic fibers follow different paths to fully innervate the structures. The process of the striatum innervation in rats continues at least until the third postnatal week, while the final pattern of the dopaminergic innervations of the rat cerebral cortex is mostly reached within the first postnatal week (Van den Heuvel & Pasterkamp, 2008).

Many of the dopaminergic fibers innervating the telencephalon are withdrawn during late embryonic and early postnatal stages of the dopaminergic pathways development. This process of eliminating the dopaminergic synapses and withdrawing the fibers is not associated with dopaminergic cells death and is called the synaptic pruning. In the process of synaptic pruning fibers sent earlier from the VTA to the dorsal striatum and fibers sent from the SN to the ventral striatum get eliminated. As a consequence innervations by the VTA dopaminergic neurons are restricted to the ventral striatum and the SN innervates specifically the dorsal striatum in the adult brain (**Figure 10**). The signals regulating the synaptic pruning in the dopaminergic system remain to be identified (Van den Heuvel & Pasterkamp, 2008).

Further events that shape the adult mouse dopaminergic pathways are the two episodes of programmed cell death eliminating part of the midbrain dopaminergic neurons directly after birth and during the second postnatal week. The signals regulating this process largely remain to be identified, nevertheless, it is likely that apoptosis of dopaminergic neurons is regulated by the target structures of the dopaminergic projections

as the experimental lesions of the striatum or disruptions of the interaction of the dopaminergic neurons with the striatum lead to death of dopaminergic neurons (Oo et al., 2003).

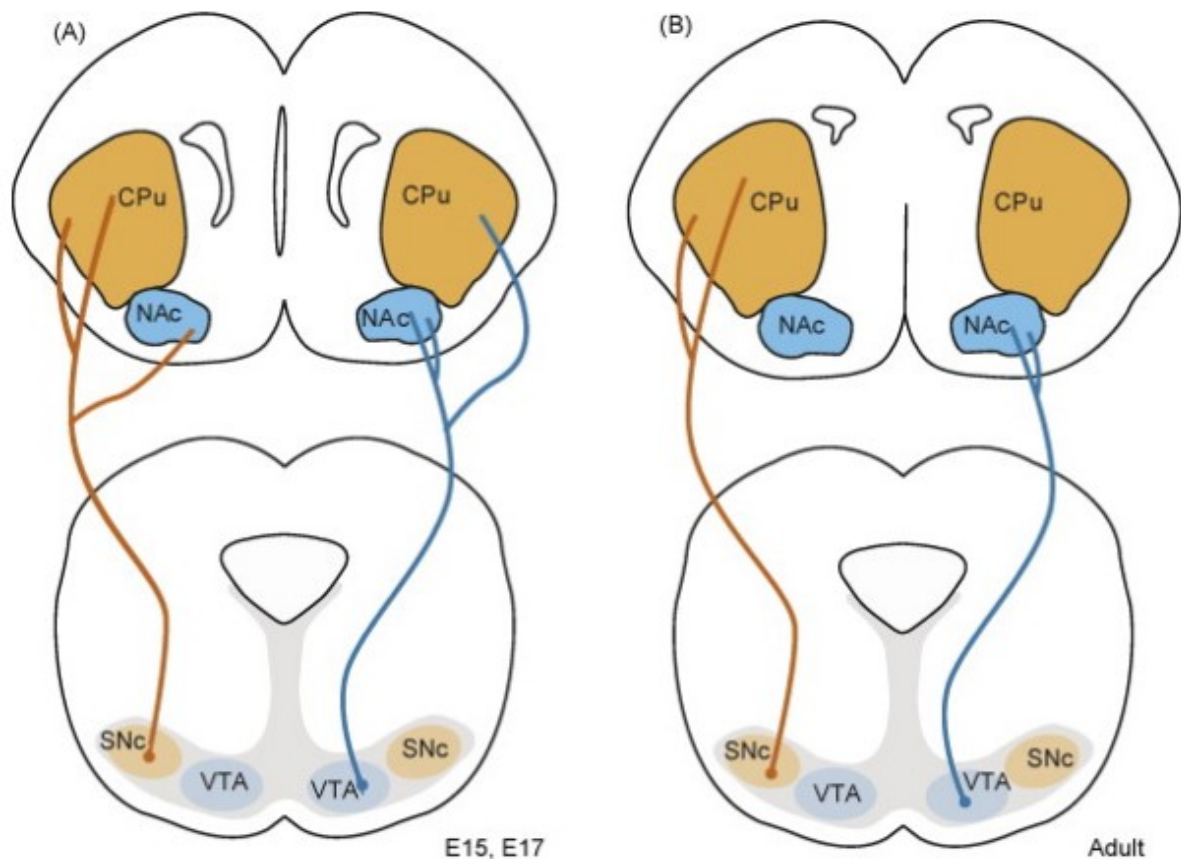


**Figure 10:**

**Synaptic pruning in the developing dopaminergic pathways.** Schemes of coronal mouse brain sections containing striatum (upper sections) and midbrain (lower sections) and schemes of dopaminergic axons (brown and blue lines) running from the midbrain to the striatum are shown. **A)** During development of the dopaminergic projections, neurons of the SNc and the VTA in the ventral midbrain send axons to both the dorsal striatum (CPu) and the ventral striatum (NAc). **B)** During late embryonic and early postnatal development the SNc fibers innervating the NAc and the VTA fibers innervating the CPu are withdrawn. The figure is derived from: Van den Heuvel & Pasterkamp (2008). Abbreviations: CPu – caudate and putamen, E – embryonic day, NAc – nucleus accumbens, SNc – substantia nigra-pars compacta, VTA – ventral tegmental area.

#### 4.2.5. Disorders of the dopaminergic system

Abnormal dopaminergic system functioning was related to many psychiatric and neurological disorders. One of the disorders directly linked to the dopaminergic system is the Parkinson's disease. This

neurodegenerative disease affects 7-10 million people worldwide with men being affected 1.5 times more often than women, and leads to different motor and non-motor dysfunctions such as stooping posture, rest tremor, bradykinesia (slow movement), rigidity (stiffness), dementia, mood disorders and autonomic dysfunctions. The cause of the disease is loss of the SN dopaminergic neurons that innervate the dorsal striatum and development of Lewy Bodies (intracellular aggregates of  $\alpha$ -synuclein, ubiquitin and other proteins) in the dopaminergic neurons. What contributes to this dopaminergic cell loss is largely unknown, with few factors such as family history, aging (average age of disease onset is 50-60 years), mitochondrial dysfunctions, generation of ROS and exposure to environmental chemicals such as pesticides and synthetic heroin being often reported. For treatment of the symptoms of Parkinson's disease a blood-brain-barrier-crossing dopamine precursor L-DOPA is used (Beitz, 2014).

Another disorder related to the abnormal function of the dopaminergic system is schizophrenia. Among many factors associated with schizophrenia a missense nucleotide polymorphism in a gene coding for CHL1 is mentioned (Sakurai et al., 2002; Chen et al., 2005; Shaltout et al., 2013).

ADHD is another example of a disorder with a strong dopamine component. It affects up to 5% of primary school children with 3:1 male to female ratio, and manifests itself through hyperactivity, impulsivity and inattention. In the etiology of ADHD both environmental and genetic factors play a role. Factors associated with ADHD include mutations in genes coding for DAT and DRD4, abnormal dopamine and noradrenalin metabolism, family history of ADHD, prenatal stress and smoking during pregnancy. For treatment of ADHD, medication affecting the DAT and medication increasing the amount of ligands for dopamine and noradrenalin receptors are used (Ougrin et al., 2010).

A disorder associated with abnormal dopaminergic signaling is also addiction. Addiction is a complex disorder manifested by an inability to control the use of certain substances (such as psychoactive recreational drugs, psychoactive prescription medication, alcohol, nicotine and food) or repeating certain activities (such as gambling, shopping and sex) regardless of their negative and harmful consequences. Use of the addictive substance and engagement in the addictive behavior lead to activation of the mesolimbic dopaminergic pathway and release of dopamine in the NAc and, if practiced regularly, eventually lead to reduction of the DRD2 level in the NAc. The role of the DRD2 in addiction is crucial as the level of DRD2 expression directly correlates with the experience of "intoxication", whereas a particular allele of the DRD2 gene identified to be associated with low DRD2 density in the striatum was shown to increase the susceptibility to addiction. Reduction in DRD2 predisposes an addict to use more of the psychoactive substance in order to compensate for the low DRD2 level. Activation of DRD1 by the addictive factor is associated with reward-related learning due to induction of the glutamate receptors expression, long-term potentiation and remodeling of the synapses in the NAc (Goodman, 2008).

Dopamine signaling deficit is one of the features of major depressive disorder (MDD). MDD is a complex disorder with largely unknown etiology which affects 8-12% of the general population and manifests itself through a variety of symptoms, to which belong anhedonia, depressed mood, fatigue, suicidality, problems with sleep and changes in activity such as psychomotor retardation. In major depression, dopamine was shown to contribute to anhedonia which is an inability to experience pleasure. Anhedonia was linked to the dysfunction of the mesolimbic and mesocortical dopaminergic pathways which constitute a significant part of the brain reward system. Most common medications used in the treatment of the MDD increase the level of serotonin and noradrenalin in the synapse, but some of the medications positively affect also the dopamine signaling (Belujon&Grace, 2017).

A disorder associated with dopaminergic system abnormalities is also Huntington's disease. Huntington's disease is an autosomal dominantly inheritable neurodegenerative disorder caused by the mutated version of the protein huntingtin. Expression of the mutated allele of the huntingtin gene leads to production of huntingtin protein with abnormally long fragment of polyglutamine repeats. The mutated huntingtin forms aggregates and causes neurodegeneration through different mechanisms, e.g. through disruption of mitochondrial activity and disruption of gene expression. Neurodegeneration in Huntington's disease affects different parts of the nervous system with the first signs observed in the dorsal striatum (the target of the nigrostriatal dopaminergic pathway) followed by cortex, thalamus, subthalamic nuclei and cerebellum. The degeneration of the striatal MSNs was shown to have two stages with DRD2-expressing MSNs of the indirect pathway being affected earlier than DRD1-expressing MSNs of the direct pathway, which results in a hyperkinetic phenotype (with chorea) at the earlier stages of the disease followed by a hypokinetic phenotype (with bradykinesia, dystonia and disturbed balance) at the later stages. Cognitive and neuropsychiatric impairment manifested by problems with recognizing emotions, impaired visuospatial and executive functioning, apathy, anxiety, obsessive-compulsive behavior, irritability and psychosis usually precede the motoric symptoms by a few years. The disease affects less than 1% of the general population (McColgan & Tabrizi, 2018).

#### **4.3. The connection between CHL1 and the dopaminergic system**

In a couple of studies an involvement of CHL1 in the development and functioning of the dopaminergic system was indicated.

During mouse embryonic development, the mRNA coding for CHL1 was detected in the cells of the developing ventral midbrain starting from E10.5, which overlaps with the early differentiation of the dopaminergic neurons. Peak of CHL1 mRNA expression in the ventral midbrain occurs at E14.5 which overlaps with dopaminergic axons reaching their targets in the forebrain, with termination of migration and

with termination of the dopaminergic neurons differentiation. Subsequently, the level of CHL1 mRNA decreases. This temporal overlap between CHL1 expression and dopaminergic progenitor migration and differentiation suggested an involvement of CHL1 in the development of the dopaminergic system (Alsanie et al., 2017).

The analysis of the spatial CHL1 mRNA expression showed that it is mainly found in early dopaminergic neurons in the ventral midline of the developing midbrain vesicle at E10.5. At E12.5 the amount of CHL1 mRNA increases in the basal plate, the intermediate zone and the marginal zone, and declines at the ventricular zone. Two days later (at E14.5), CHL1 is expressed predominantly in the lateral basal plate. This pattern of spatial CHL1 mRNA expression indicated that CHL1 may play a role in guidance of the dopaminergic cells migration, which was later confirmed with the analysis of dopaminergic cells distribution in the developing ventral midbrain showing that the distribution of dopaminergic cells in CHL1<sup>-/-</sup> mice is abnormal. Moreover, chemoattractive properties of CHL1 for the dopaminergic neuroblasts were found in an *in vitro* study (Alsanie et al., 2017).

Although CHL1 is expressed by the differentiating dopaminergic neurons, the impact of CHL1 on dopaminergic neurons differentiation in the developing mouse brain is insignificant. However, CHL1 increases the proportion of dopaminergic neurons in *in vitro* cultures of ventral midbrain cells (Alsanie et al., 2017).

The impact of CHL1 on the outgrowth of dopaminergic fibers was also shown in studies performed by Alsanie et al. (2017). The authors found that CHL1 does not affect the amount of dopaminergic fibers but it positively affects branching of the fibers, particularly the main fiber, in cultures of E12.5 ventral midbrain neurons. This impact of CHL1 was found to be most likely triggered by its homophilic interactions. The homophilic CHL1 interactions were also shown to promote the length of the dopaminergic axon. This result is not in line with previous reports indicating that homophilic CHL1 interaction inhibits and heterophilic CHL1 interactions promote neurite outgrowth (Alsanie et al., 2017).

Moreover, chemorepellent properties of CHL1 on developing dopaminergic neurites were shown in cultures of ventral midbrain explants from 12.5-days-old mouse embryos. Due to the chemorepellent properties, spatial distribution of CHL1 in the developing brain, with high expression in the marginal zone and the hindbrain and very low expression in the ventricular zone and the basal forebrain, may contribute to proper development of dopaminergic projections which grow from the ventral midbrain first dorsally and then frontally towards the forebrain. However, the contribution of CHL1 to proper guidance of dopaminergic neurites is insignificant as CHL1-deficient mice develop proper dopaminergic connections to the forebrain, as assessed for embryos from E12.5, E14.5 and E18.5 mice (Alsanie et al., 2017).

Further indications for the important role of CHL1 in the dopaminergic system development and functioning were obtained by Bye et al. (2015). The authors showed that CHL1 expression at the surface of dopaminergic progenitors used for trial transplantation therapy in Parkinson's disease is an indicator for their survival and leads to generation of a higher proportion of dopaminergic neurons in the transplanted ventral midbrain progenitors.

Although not considered as one of the factors strongly associated with the development of schizophrenia, an SNP in the CHL1 gene was shown to correlate with the development of schizophrenia in studied Japanese, Chinese and Qatari populations (Sakurai et al., 2002; Chen et al., 2005; Shaltout et al., 2013).

Mice lacking CHL1 present certain behavioral features related to abnormal dopaminergic system functioning. CHL1 deficient mice show, among other behavioral abnormalities, reduced reactivity to novelty (Morellini et al., 2007) and reduced pre-pulse inhibition of an acoustic startle response (Irintchev et al., 2004) which are controlled by the dopaminergic system. The exposure to novelty is associated with activation of the mesolimbic dopaminergic pathway which results in increased exploration of the novel stimulus by the animal (Wittmann et al., 2007), whereas the pre-pulse inhibition is associated with dopaminergic activation of the medial prefrontal cortex (Ellenbroek et al., 1996).

A link between CHL1 and the dopaminergic system can also be drawn from the only common consequence of deletions and duplications of and within the CHL1 gene in humans, which is the delayed speech development (**Table 1**) (Pohjola et al., 2010; Cuoco et al., 2011; Tassano et al., 2014; Bertini et al., 2017). Acquisition of the ability to speak is strongly dependent on proper functioning and proper morphological structure of the striatum (De Diego-Balaguer et al., 2008) and proper protein expression in the striatum (Takahashi et al., 2002), which is an element of the dopaminergic system.

## 5. Aims of the study

The aims of my study are based on results of co-immunoprecipitation experiments previously performed in the group, which showed a potential interaction between CHL1 and DRD2 (data not published), as well as on the available literature showing that CHL1 promotes outgrowth and branching of dopaminergic neurites (Alsanie et al., 2017), contributes to development of schizophrenia (Sakurai et al., 2002; Chen et al., 2005; Shaltout et al., 2013) and to development of cognitive problems associated with impaired dopaminergic system functioning such as delayed speech development (Pohjola et al., 2010; Cuoco et al., 2011; Tassano et al., 2014; Bertini et al., 2017), reduced anxiety (Morellini et al., 2007) and reduced pre-pulse inhibition (Irintchev et al., 2004).

**The first aim of my study was to verify if CHL1 interacts with the two DRD2 splice variants: DRD2S and DRD2L.** This aim was addressed with immunostainings analyzing the co-localization of the proteins, with co-immunoprecipitations showing that the proteins are present in a complex, and with ELISA by which direct binding between the proteins was determined and the specific DRD2 domain responsible for CHL1 binding could be identified.

**Secondly, I investigated the consequences of the interaction between DRD2 and CHL1 on the functioning of the receptor.** In order to address this aim, I performed experiments measuring receptor internalization, receptor degradation, binding of ligands to the receptor and activation of receptor-induced intracellular signaling pathways in presence and absence of CHL1. Using Western Blot I analyzed the expression of DRD2 and protein targets of the pre-synaptic and the post-synaptic DRD2 signaling in the mouse striatum.

**The third aim of the study was to characterize the impact of CHL1 on the morphology of the dopaminergic projections running from the ventral midbrain to the striatum.** To address this aim, I performed immunostainings on CHL1<sup>-/-</sup> and CHL1<sup>+/+</sup> mouse brain sections and quantified dopaminergic fibers running to the striatum, the density of dopaminergic fibers in the striatum and the number of midbrain dopaminergic neurons.

**Lastly, I determined if lack of CHL1 leads to development of brain morphology and DRD2 expression associated with schizophrenia.** This aim was addressed with immunostainings performed on CHL1<sup>-/-</sup> and CHL1<sup>+/+</sup> mouse brain sections and measurements of DRD2 level in the frontal cortex and of the size of brain structures known to be affected in schizophrenia: frontal cortex, thalamus and lateral ventricles.

## 6. Materials

### 6.1. Antibodies

The primary antibodies used in the study are listed in **Table 2** and the secondary antibodies used in the study are listed in **Table 3**. In both tables dilutions of the antibodies used in the indicated experiments are given.

**Table 2:**

**Primary antibodies used in the study.** Abbreviations: CHL1 – close homolog of L1, DARPP32 – dopamine- and cAMP-regulated phosphoprotein 32 kDa, pDARPP32(Thr34) – dopamine- and cAMP-regulated phosphoprotein 32 kDa phosphorylated at threonine 34, DRD2 – dopamine receptor D2, ERK1 – extracellular signal-regulated kinase 1, pERK1/2 – phosphorylated extracellular signal-regulated kinase 1/2, GAPDH – glyceraldehyde 3-phosphate dehydrogenase, TH – tyrosine hydroxylase, pTH(Ser40) – tyrosine hydroxylase phosphorylated at serine 40, AF – antibody feeding, CO-IP – co-immunoprecipitation, ICW – in-cell Western, IF – immunofluorescent staining, IHC – immunohistochemistry, PLA – proximity ligation assay, WB – Western Blot.

ANTIBODY	DILUTION
Goat anti-CHL1 (AF2147, R&D Systems)	IF 1:100
	PLA 1:100
	WB 1:1000
Goat anti-CHL1 (C-18, Santa Cruz Biotechnology)	CO-IP 4 µg/ml
Rabbit anti-DARPP32 (19A3, Cell Signaling Technology)	WB 1:1000
Rabbit anti-pDARPP32(Thr34) (AHP897, Bio-Rad)	WB 1:200
Mouse anti-DRD2 (B-10, Santa Cruz Biotechnology)	AF 1:500
	ICW 1:200
	IF 1:100
	PLA 1:100
	WB 1:200
Rabbit anti-ERK1 (C-16, Santa Cruz Biotechnology)	WB 1:1000
Rabbit anti-pERK1/2 (p44/42, Thr202/Tyr204) (9101S, Cell Signaling Technology)	WB 1:1000

Rabbit anti-GAPDH (FL-335, Santa Cruz Biotechnology)	ICW 1:200 WB 1:1000
Rabbit anti-TH (AB152, Millipore)	ICW 1:200 IF 1:100 IHC 1:1000 WB 1:1000
Mouse anti-TH (F-11, Santa Cruz Biotechnology)	ICW 1:200
Rabbit anti-pTH (Ser40) (AHP912, Bio-Rad)	ICW 1:200 IF 1:100 WB 1:500
Mouse anti- $\beta$ III-tubulin (TU-20, Santa Cruz Biotechnology)	WB 1:500

**Table 3:**

**Secondary antibodies used in the study.** Abbreviations: AF – antibody feeding, Cy2, 3 and 5 – cyanine fluorescent dyes 2, 3 and 5, HRP – horseradish peroxidase, IRDye – infrared dye, ELISA – enzyme-linked immunosorbent assay, ICW – in-cell Western, IF – immunofluorescent staining, WB – Western Blot.

ANTIBODY	DILUTION
Cy2-conjugated donkey anti-mouse (Dianova)	AF 1:500 IF 1:200
Cy2-conjugated donkey anti-rabbit (Dianova)	IF 1:200
Cy2-conjugated donkey anti-goat (Dianova)	IF 1:200
Cy3-conjugated donkey anti-mouse (Dianova)	AF 1:500 IF 1:200
Cy3-conjugated donkey anti-rabbit (Dianova)	IF 1:200
Cy3-conjugated donkey anti-goat (Dianova)	IF 1:200
Cy5-conjugated donkey anti-mouse (Dianova)	IF 1:200
Cy5-conjugated donkey anti-rabbit (Dianova)	IF 1:200
Cy5-conjugated donkey anti-goat (Dianova)	IF 1:200
IRDye800CW goat anti-rabbit (LI-COR)	ICW 1:800

IRDye680RD goat anti-mouse (LI-COR)	ICW 1:800
HRP-conjugated donkey anti-goat (Dianova)	WB 1:10000
HRP-conjugatedgoat anti-rabbit (Dianova)	WB 1:10000
HRP-conjugatedgoat anti-mouse (Dianova)	WB 1:10000
HRP-conjugated donkey anti-human (Dianova)	ELISA 1:2500

## 6.2. Plasmids

The plasmids listed below were used in the study. Abbreviations: CHL1 – close homolog of L1, DARPP32 – dopamine- and cAMP-regulated phosphoprotein 32 kDa, DRD2L – dopamine receptor D2 “long”, DRD2S – dopamine receptor D2 “short”, GFP – green fluorescent protein, pCAG – mammalian expression vector with CAG (cytomegalovirus enhancer, promoter and first exon and first intron of chicken beta-actin, splice acceptor of rabbit beta-globin) promoter, pcDNA3.1 – mammalian expression vector with cytomegalovirus enhancer, TH – tyrosine hydroxylase.

- pCAG-GFP (Addgene)
- CHL1-coding plasmid (Holm et al., 1996)
- pcDNA3.1 carrying DRD2L (OHu23461, GenScript)
- pcDNA3.1 carrying DRD2S (OHu23557, GenScript)
- pcDNA3.1 carrying DARPP32 (OHu18812, GenScript)
- pcDNA3.1 carrying TH (OHu25815D, GenScript)

## 6.3. Oligonucleotides

All the oligonucleotides used in the study are listed below. The oligonucleotides were always obtained from Metabion International.

### 6.3.1. Oligonucleotides used for cloning with In-Fusion Kit (Clontech)

The oligonucleotides listed below were used for cloning with In-Fusion (Clontech). Abbreviations: CHL1 – close homolog of L1, DRD2L – dopamine receptor D2 “long”, DRD2S – dopamine receptor D2 “short”, GFP – green fluorescent protein, IRES – internal ribosome entry site, pCAG – mammalian expression vector with CAG (cytomegalovirus enhancer, promoter and first exon and first intron of chicken beta-actin, splice

acceptor of rabbit beta-globin) promoter, pcDNA3.1 – mammalian expression vector with cytomegalovirus enhancer, PCR – polymerase chain reaction.

**Amplification of DRD2L and DRD2S sequences:**

- annealing temperature in PCR: 58°C
  - template: pcDNA3.1 carrying human DRD2L (OHu23461, GenScript) and pcDNA3.1 carrying human DRD2S (OHu23557, GenScript)
- 5'-GTTGCCTTCGCCCGATGGATCCACTGAATCTGTC-3'
- 5'-TCGCACGATTACCATTACAGCAGTGGAGGATCTTCAG-3'

**Amplification of the CHL1 sequence:**

- annealing temperature in PCR: 52°C
  - template: mouse CHL1-coding plasmid (Holm et al., 1996)
- 5'-ATGATGGAATTGCCATTATGT-3'
- 5'-TGGCGGCCGCGCCGCTTCATGCCCGGAGTGGGAA-3'

**Amplification of pCAG backbone sequence:**

- annealing temperature in PCR: 58°C
  - template: pCAG-GFP, Addgene
- 5'-AGCGGCCGCGCCAGCACAGTGG-3'
- 5'-CGGGCGAAGGCAACGCAGCGACT-3'

**Amplification of IRES sequence:**

- annealing temperature in PCR: 58°C
  - template: pCAG-GFP, Addgene
- 5'-ATGGTAATCGTGCGAGAGG-3'
- 5'-TGGCAATTCCATCATGGTTGTGGCCATATTATCAT-3' or
- 5'-TGGCGGCCGCGCCGCTGGTTGTGGCCATATTATCAT-3'

**6.3.2. Oligonucleotides used for genotyping of mice**

The following oligonucleotides were used for genotyping of mice:

5'-AATTGATCGAGGCAGCACTACTTTCTG-3'

5'-CATTCCCAGAAAGGAGGCAACGTG-3'

5'-CTAAAGCGCATGCTCCAGACTGCC-3'

#### 6.4. Peptides and recombinant proteins

The following peptides and recombinant proteins were used in the study:

N-terminal extracellular fragment of DRD2 biotinylated at the N-terminus (Schafer-N):

Biotin-MDPLNLSWYDDDLERQNWSRPFNGSEGKPDPRPHYNY-OH

1<sup>st</sup> extracellular loop of DRD2 biotinylated at the N-terminus (Schafer-N):

Biotin-LEVVGWKFVSRHCD-OH

2<sup>nd</sup> extracellular loop of DRD2 biotinylated at the N-terminus (Schafer-N):

Biotin-GLNNTDQNECIANPA-OH

3<sup>rd</sup> extracellular loop of DRD2 biotinylated at the N-terminus (Schafer-N):

Biotin-NIHCDNIPPVLYS-OH

CHL1-Fc – extracellular domain of murine cell adhesion molecule close homolog of L1 conjugated with Fc fragment of human IgG (InVivo BioTech Services; custom made)

L1-Fc – extracellular domain of murine cell adhesion molecule L1 conjugated with Fc fragment of human IgG (InVivo BioTech Services; custom made)

NCAM-Fc – extracellular domain of murine neural cell adhesion molecule conjugated with Fc fragment of human IgG (InVivo BioTech Services; custom made)

#### 6.5. Cell lines

The following cell line was used in the study:

Human embryonic kidney 293 (HEK293) (CRL-1573, American Type Culture Collection)

## 6.6. Bacteria

The following bacteria strains were used in the study:

Stellar competent *Escherichia coli* (*E. coli*) (Clontech)

One Shot TOP10 Chemically Competent *E. coli* (Invitrogen)

## 6.7. Animals

CHL1<sup>-/-</sup> mice were created by replacing the first exon and part of the first intron of the CHL1 gene with a different sequence (Montag-Sallaz et al., 2002). The mice were back-crossed onto the C57BL/6J background for more than eight generations. CHL1<sup>-/-</sup> and C57BL/6J mice were maintained at the animal facility of the Universitätsklinikum Hamburg-Eppendorf and housed on a 12-h light-dark cycle at 25°C with food and water provided *ad libitum*. Adult (3-5-month-old) male and female CHL1<sup>-/-</sup> mice and their CHL1<sup>+/+</sup> littermates were used in the experiments. All animal experiments were approved by the local authorities of the State of Hamburg (animal permits ORG 679 and TVA 6/14), conform to the guidelines set by the European Union and adhere to the ARRIVE guidelines.

## 6.8. Buffers, solutions, chemicals and media

In the study, the following buffers, solutions, chemicals and media were used:

### 6.8.1. Cell culture

Buffers, solutions and media used for cell culture are listed and described in **Table 4**.

#### Table 4:

**List of buffers, solutions and media used for maintenance and experimental treatment of living HEK293 cells.** Abbreviations: AF – antibody feeding, dH<sub>2</sub>O – distilled water, BSA – bovine serum albumin, DMEM – Dulbecco's Modified Eagle Medium, DMSO – dimethyl sulfoxide, DRD2 – dopamine receptor D2, EDTA – ethylenediaminetetraacetic acid, FBS – fetal bovine serum, HBSS – Hanks' Balanced Salt Solution, HEPES –4-(2-hydroxyethyl)-1-piperazineethanesulfonic acid, PBS – phosphate-buffered saline, v – volume, w – weight.

#### BUFFER, SOLUTION OR MEDIUM

Maintenance medium

#### INGREDIENTS

DMEM, high glucose (PAN Biotech)

	10% (v/v) FBS (PAN Biotech)
	2% (v/v) Penicillin/Streptomycin (PAN Biotech)
HBSS	without calcium and magnesium ions (PAN Biotech)
Trypsin-EDTA	0.05% trypsin and 0.02% EDTA (PAN Biotech)
Freezing solution	70% (v/v) DMEM, high glucose (PAN Biotech) 20% (v/v) FBS (PAN Biotech) 10% (v/v) DMSO (Sigma-Aldrich)
Medium without supplements	DMEM, high glucose (PAN Biotech)
AF incubation medium	0.5% (w/v) BSA fatty acids-free (PAA Laboratories) 1:500 mouse anti-DRD2 antibody (B-10, Santa Cruz Biotechnology) DMEM (PAN Biotech)
Ligand binding buffer	5 mM Tris 7.5 mM HEPES 120 mM NaCl 5.4 mM KCl 1.2 mM CaCl <sub>2</sub> 1.2 mM MgSO <sub>4</sub> 1 mM ascorbic acid 5 mM glucose pH 7.1
Quinpirole	stock: 1 mM in dH <sub>2</sub> O (Sigma Aldrich); 10 μM used for stimulation of cells
Cycloheximide	stock: 10 mg/ml in dH <sub>2</sub> O (Tocris)
DnsylD1	stock: 1 mg/ml in DMSO (FIVEPhotonBiochemicals)

PBS++	PBS without calcium ions and magnesium ions (PAN Biotech) 0.5 mM CaCl <sub>2</sub> 2 mM MgCl <sub>2</sub>
Quenching solution	20 mM glycine PBS++
Biotin	0.5 mg/ml Sulfo-NHS-LC-Biotin (ThermoFisher Scientific) PBS++

### 6.8.2. Bacteria culture

Media and solutions used for bacteria culture are listed and described in **Table 5**.

**Table 5:**

**List of solutions and media used for bacteria cultures.** Abbreviations: LB – lysogeny broth.

SOLUTION OR MEDIUM	INGREDIENTS
LB medium	10 g/l bacto-tryptone pH 7.4 10 g/l NaCl 5 g/l yeast extract
LB medium with ampicillin	100 mg/l ampicillin LB medium
Agar plates with ampicillin	20 g/l agar 100 mg/l ampicillin LB medium

### 6.8.3. Sodium dodecyl sulfate-polyacrylamide gel electrophoresis (SDS-PAGE) and Western Blot

Buffers, solutions and chemicals used for SDS-PAGE and Western Blot are listed and described in **Table 6**.

**Table 6:**

**Buffers and solutions used for SDS-PAGE and Western Blot analyses.** Abbreviations: APS – ammonium persulfate, dH<sub>2</sub>O – distilled water, DTT – dithiothreitol, EDTA – ethylenediaminetetraacetic acid, EGTA – ethylene glycoltetraacetic acid, NP-40 – nonyl phenoxypolyethoxylethanol, SDS – sodium dodecyl sulfate, TBS – Tris-buffered saline, TBS-T – Tris-buffered saline with Tween 20, TEMED – tetramethylethylenediamine, v – volume, w – weight, WB – Western Blot.

BUFFER, CHEMICAL OR SOLUTION	INGREDIENTS
Separating gel (for a 12%-gel)	0.9 ml dH <sub>2</sub> O 1.6 ml 30% acrylamide 1.5 ml 1M Tris-HCl pH 8.8 40 µl 10% SDS 10 µl 10% APS 4 µl TEMED
Stacking gel (for a 5%-gel)	1.05 ml dH <sub>2</sub> O 0.25 ml 30% acrylamide 0.2 ml 1M Tris-HCl pH 6.8 20 µl 10% SDS 10 µl 10% APS 4 µl TEMED
Lysis buffer	20 mM Tris 150 mM NaCl 1 mM EDTA 1 mM EGTA 1% NP-40 1% sodium deoxycholate 2.5 mM sodium pyrophosphate 1 mM β-glycerophosphate 1 mM sodium orthovanadate adjust to pH 7.5 with HCl

## MATERIALS

Protease inhibitors	stock (in dH <sub>2</sub> O) and working solution (in lysis buffer) prepared according to the manufacturer's protocol (cOmplete EDTA-free Protease Inhibitor Cocktail, 04693132001, Roche)
Phosphatase inhibitors	stock (in dH <sub>2</sub> O) and working solution (in lysis buffer) prepared according to the manufacturer's protocol (PhosSTOP, 04906845001, Roche)
5x sample buffer	0.4 M Tris-HCl 10% (w/v) SDS 50% (v/v) glycerol 0.5 mg/ml bromophenol blue 0.5% (w/v) DTT adjust to pH 6.8
Running buffer	0.19 M glycine 0.025 M Tris 0.1% (w/v) SDS
Protein ladder	Precision Plus Dual Color (161-037-4, Bio-Rad) or PageRuler Plus Prestained Protein Ladder (26619, ThermoFisher Scientific)
Transfer buffer	20% (v/v) methanol 0.19 M glycine 0.025 M Tris
TBS	10 mM Tris 0.15 M NaCl adjust to pH 7.5 with HCl
TBS-T	50 µl/l Tween 20 TBS

WB blocking buffer	5% (w/v) nonfat milk powder (Carl Roth) or 5% (w/v) BSA with fatty acids (PAA Laboratories) TBS-T
Stripping solution	0.5 M NaCl 0.5 M acetic acid
Neutralization solution	1 M Tris adjust to pH 8.0 with HCl

#### 6.8.4. Fixation and staining

Buffers and solutions used for fixation and staining are listed and described in **Table 7**.

##### Table 7:

**List of solutions and buffers used for fixation and staining of mouse tissue and HEK293 cells.** Abbreviations: AF – antibody feeding, BSA – bovine serum albumin, PBS – phosphate-buffered saline, v – volume, w – weight.

SOLUTION OR BUFFER	INGREDIENTS
Cacodylate buffer	0.2 M sodium cacodylate (Carl Roth) adjust to pH 7.3 with HCl
Homemade PBS	13.7 mM NaCl 0.27 mM KCl 0.8 mM Na <sub>2</sub> HPO <sub>4</sub> 0.15 mM KH <sub>2</sub> PO <sub>4</sub> pH 7.4
Antigen retrieval buffer	2.94 mg/ml tri-sodium citrate dihydrate (Merck Chemicals) adjust to pH 9.0 with NaOH
Blocking serum	0.2% (v/v) TritonX-100 0.02% (w/v) sodium azide

	5% (v/v) normal donkey serum (Dianova) homemade PBS
Carrageenan buffer	5 mg/ml lambda-carrageenan (Sigma-Aldrich) 0.2 mg/ml NaN <sub>3</sub> (Sigma-Aldrich) homemade PBS
Non-permeabilizing AF blocking buffer	5% (w/v) BSA with fatty acids (PAA Laboratories) homemade PBS
Permeabilizing AF blocking buffer	5% (w/v) BSA with fatty acids (PAA Laboratories) 0.1% (v/v) Triton X-100 homemade PBS
8% Fixating solution	8% (w/v) paraformaldehyde (Carl Roth) homemade PBS adjust to pH 7.5 with NaOH
4% Formaldehyde in cacodylate byffer	0.1 M sodium cacodylate (Carl Roth) 4% (w/v) paraformaldehyde (Carl Roth) 0.1% CaCl <sub>2</sub> adjust to pH 7.3 with NaOH
Dehydrating solution	15% (w/v) sucrose (Carl Roth) 0.1 M cacodylate buffer
Section storage buffer	PBS with calcium and magnesium ions (PAN Biotech) 0.01% (w/v) sodium azide

### 6.8.5. ELISA

Buffers and solutions used for ELISA are listed and described in **Table 8**.

**Table 8:**

**List of solutions and buffers used for ELISA.** Abbreviations: BSA – bovine serum albumin, ELISA – enzyme-linked immunosorbent assay, OPD – ortho-phenylenediamine, PBS – phosphate-buffered saline, v – volume, w – weight.

<b>SOLUTION OR BUFFER</b>	<b>INGREDIENTS</b>
ELISA blocking buffer	2% (w/v) BSA fatty acids-free (PAA Laboratories) PBS with calcium ions and magnesium ions (PAN Biotech)
ELISA washing buffer	0.05% (v/v) Tween 20 PBS with calcium ions and magnesium ions (PAN Biotech)
OPD solution	0.5 mg/ml OPD (ThermoFisher Scientific) Stable peroxidase buffer (10x, ThermoFisher Scientific)
Stopping solution	2.4 M H <sub>2</sub> SO <sub>4</sub>

### 6.8.6. Agarose gel electrophoresis

Buffers, solutions and chemicals used for agarose gel electrophoresis are listed and described in **Table 9**.

**Table 9:**

**List of buffers, solutions and chemicals used for agarose gel electrophoresis.** Abbreviations: EDTA – ethylenediaminetetraacetic acid, TAE – Tris-acetate-EDTA buffer.

<b>BUFFER, SOLUTION OR CHEMICAL</b>	<b>INGREDIENTS</b>
50xTAE	2 M Tris 1 M acetic acid 50 mM EDTA adjust pH 8.0
Agarose gel with Roti-GelStain	agarose powder (Carl Roth)

	1xTAE
	0.05 µl/ml Roti-GelStain (Carl Roth)
DNA Ladder	1 kb Plus DNA Ladder (ThermoFisher Scientific)

### 6.8.7. In-cell Western

Buffers used for in-cell Western are listed and described in **Table 10**.

#### Table 10:

**Buffers used for the in-cell Western experiment.** Abbreviations: BSA – bovine serum albumin, ICW – in-cell Western, PBS – phosphate-buffered saline, v – volume, w – weight.

BUFFER	INGREDIENTS
ICW blocking buffer	3% (w/v) BSA fatty acids-free (PAA Laboratories) 0.1% (v/v) Triton X-100 homemade PBS
ICW antibody dilution buffer	0.1% (v/v) Triton X-100 homemade PBS

### 6.9. Suppliers of the chemicals, reagents, kits and laboratory equipment

Chemicals, reagents, kits and laboratory equipment used in the study were purchased from the following companies: Addgene (Watertown, Massachusetts, USA), American Type Culture Collection (Manassas, Virginia, USA), Amersham/GE Healthcare via Sigma-Aldrich (Braunschweig, Germany), Bio-Rad Laboratories (Munich, Germany), Bio-Tek Instruments (Bad Friedrichshall, Germany), Biozym (Hessisch Oldendorf, Germany), Carl Roth (Karlsruhe, Germany), Clontech (Heidelberg, Germany), Corning (Wiesbaden, Germany), Cell Signaling Technology via New England BioLabs (Frankfurt am Main, Germany), Dianova (Hamburg, Germany), Eppendorf (Hamburg, Germany), FIVEPhoton Biochemicals (San Diego, California, USA), GE Healthcare (Braunschweig, Germany), GeneTex (Irvine, CA, USA), GenScript (Piscataway, New Jersey, USA), Greiner Bio-One (Solingen, Germany), Herolab (Wiesloch, Germany), Invitrogen via ThermoFisher Scientific (Ulm, Germany), InVivo BioTech Services (Hennigsdorf, Germany), Leica (Wetzlar, Germany), LI-COR (Lincoln,

Nebraska, USA), Life Technologies (Darmstadt, Germany), Macherey-Nagel (Düren, Germany), Marienfeld (Lauda-Königshofen, Germany), Merck Chemicals (Darmstadt, Germany), Metabion (Munich, Germany), Millipore (Schwalbach, Germany), New England BioLabs (Frankfurt am Main, Germany), Olympus (Hamburg, Germany), PAA Laboratories (Cölbe, Germany), PAN Biotech (Aidenbach, Germany), Promega (Mannheim, Germany), Qiagen (Hilden, Germany), R&D Systems (Wiesbaden, Germany), Roche Diagnostics (Mannheim, Germany), Sakura Finetek (Staufen, Germany), Santa Cruz Biotechnology (Dallas, Texas, USA), Sarstedt (Nümbrecht, Germany), Schafer-N (Copenhagen, Denmark), Sigma-Aldrich (Deisenhofen, Germany), Tecan (Mannedorf, Switzerland), ThermoFisher Scientific (Ulm, Germany), Tocris (Bristol, UK), VWR International GmbH (Darmstadt, Germany).

## 7. Methods

### 7.1. Molecular biology methods

#### 7.1.1. PCR

The amplification of DNA fragments was performed in thin-walled 0.2-ml tubes (Biozym) using the SimpliAmp Thermal Cycler (Life Technologies). The PCR reactions were prepared combining the 2x CloneAmpHiFi DNA Polymerase (Clontech) (half of the reaction volume), primers forward and reverse (10 pM each), DNA template (less than 1 ng per reaction) and the reaction was filled-up to the final volume of 25  $\mu$ l with RNase-free water (Qiagen). The cycling conditions described in **Table 11** were used.

**Table 11:**  
Cycling conditions – Amplification of fragments used for cloning with InFusion Kit (Clontech).

Number of cycles	Step	Temperature	Time
1	Initial denaturation	98°C	3 minutes
35	Denaturation	98°C	10 seconds
	Primer annealing	indicated in point <b>6.3.1</b>	15 seconds
	Extension	72°C	5 seconds/1 kb of template
1	Final extension	72°C	10 minutes
1	Storage	4°C	hold

#### 7.1.2. PCR product clean-up

DNA amplified in the PCR was cleaned from the ingredients of the PCR reaction with a NucleoSpin Gel and PCR Clean-up Kit (Macherey-Nagel) following the manufacturer's protocol. The cleaned DNA was stored at -20°C until use.

### 7.1.3. Agarose gel electrophoresis

The 0.8-2.5% agarose gels were prepared combining all the ingredients of the agarose gel and pouring the solution into a horizontal gel form with inserted combs (Bio-Rad). Once the gel solidified, it was placed in an electrophoresis chamber (Bio-Rad) filled up with 1xTAE buffer. DNA mixed with 6x Loading Dye (ThermoFisher Scientific) in a proportion 5:1 and a DNA ladder (Thermo Fisher Scientific) was loaded on the gel and electric current was applied. After the DNA separated on the gel, the DNA bands were visualized at the E.A.S.Y. UV-light documentation system (Herolab, Germany).

### 7.1.4. DNA extraction from agarose gels

DNA bands cut out from the agarose gel were extracted with a NucleoSpin Gel and PCR Clean-up Kit (Macherey-Nagel) following the manufacturer's protocol. The extracted DNA was stored at -20°C until use.

### 7.1.5. Plasmid constructs cloning with In-Fusion Kit (Clontech)

DNA fragments coding the pCAG backbone, DRD2S, DRD2L, IRES and CHL1 were amplified in PCR reactions using primers that contained additional 15 nucleotides overlapping with the DNA fragments next to which the amplified fragments were supposed to be located in the final plasmid constructs, according to the protocol of the In-Fusion Kit (Clontech) manufacturer.

The appropriate DNA fragments were combined in a ligation reaction (Clontech) prepared according to the manufacturer's protocol, followed by the transformation of Stellar competent *E. coli* (Clontech). Colonies of bacteria growing on the agar plate were then screened for the expression of the final construct through inoculation of the bacteria colonies in small (5 ml) liquid cultures followed by plasmid DNA isolation and sequencing.

### 7.1.6. Transformation of *E. coli*

Chemically competent *E. coli* were incubated on ice and an appropriate amount of DNA (indicated in the instructions of the provider of the bacteria) was added to them. The bacteria with added DNA underwent a heat shock in a water bath pre-warmed to 42°C, in which they were incubated for 45-90 seconds, followed by a 1-minute incubation on ice and a 60-minutes incubation with 450 µl super optimal catabolite (SOC) repression medium on a shaker set at 220 rpm at 37°C. Next, 100 µl of bacteria in SOC medium were seeded

on a warm agar plate containing an appropriate antibiotic, incubated overnight at 37°C and then stored at 4°C.

#### **7.1.7. Liquid culture of bacteria**

Single colonies of bacteria were collected from agar plates and transferred to warm LB medium containing the appropriate antibiotic and incubated overnight at 37°C on a shaker set at 220 rpm.

#### **7.1.8. Plasmid DNA isolation from liquid cultures of bacteria**

**Small scale** – Liquid culture of a bacterial colony was prepared in 5 ml LB medium and plasmid DNA was isolated from the bacteria with a MiniPrep Kit (Qiagen) according to the manufacturer's protocol. The isolated DNA was stored at -20°C.

**Large scale** – Liquid culture of a bacterial colony was prepared in 300 ml LB medium and plasmid DNA was isolated from the bacteria with a MaxiPrep Kit (Qiagen) according to the manufacturer's protocol. In the last step of the protocol the plasmid DNA was dissolved in 400 µl of RNase-free water (Qiagen). The isolated DNA was stored at -20°C.

#### **7.1.9. Determination of DNA concentration and purity**

Concentration of the DNA was measured in a 1.5-µl sample aliquot at the NanoDrop 1000 spectrophotometer (ThermoFisher Scientific), which measures the DNA concentration via reading the absorbance of light at 260 nm. The NanoDrop also measured the purity of the DNA sample by determining the absorbance of light at 280 nm and 230 nm. The accepted 260/280 and 260/230 ratios for the DNA sample were approximately 1.8 and 2.0, respectively.

#### **7.1.10. DNA sequencing**

The sequencing of DNA probes was performed at the service group of the ZMNH (UKE, Hamburg, Germany) using Step-by-Step protocols for DNA-sequencing with Sequenase Version 2.0 (5th ed., 1990). A sample sent for sequencing always contained the DNA which was supposed to be sequenced and a specific primer.

## 7.2. Biochemical methods

### 7.2.1. Protein sample preparation for SDS-PAGE

**From tissue** – Mice were killed in a CO<sub>2</sub>-chamber, then decapitated and their brains were dissected out and placed on ice. If necessary, from the brains specific structures were dissected out on a cold acrylic matrix (Leica) allowing to cut 1 mm-thick coronal sections. The tissue was homogenized in cold lysis buffer containing protease inhibitors (Roche) and phosphatase inhibitors (Roche) in a potter, then transferred to 1.5-ml Eppendorf tubes and sonicated 8 times for 30 seconds at >20 kHz using Micro Ultrasonic Cell Disruptor KT 50 (Kontes). Next, the lysed tissue was centrifuged at 4°C for 10 minutes at 1000 g and the supernatant was collected. Protein concentration in the supernatant was determined using the bicinchinonic acid (BCA) protein assay and an appropriate amount of the supernatant was boiled with 5x sample buffer for 7 minutes at 98°C then applied to the SDS-acrylamide gel or stored at -20°C.

**From cultured cells** – Plates with cells were placed on ice and rinsed with cold PBS containing calcium and magnesium (PAN Biotech); then an appropriate amount of cold lysis buffer containing protease inhibitors (Roche) and phosphatase inhibitors (Roche) was added to the cells. The cells were incubated with lysis buffer for 15 minutes on ice, collected in Eppendorf tubes followed by centrifugation at 4°C for 10 minutes at 1000 g and collection of the supernatant. Next, protein concentration in the supernatant was determined using the bicinchinonic acid (BCA) protein assay and an appropriate amount of the supernatant was boiled with 5x sample buffer for 7 minutes at 98°C then applied to the SDS-acrylamide gel or stored at -20°C.

### 7.2.2. Determination of protein concentration

Different dilutions of the obtained homogenates in distilled water were prepared and transferred into 96-well Immuno LockWell Module Plates (Nunc; ThermoFisher Scientific) in a volume of 10 µl/well and on the same plate a protein standard consisting of known concentrations of BSA (ThermoFisher Scientific) was pipetted in a volume of 10 µl/well. Next, to each well 200 µl of a mixture of solutions A and B of the BCA Protein Assay Kit (ThermoFisher Scientific) prepared according to the manufacturer's protocol was added. After 30 minutes incubation at 37°C the concentration of proteins in the wells was determined by measuring the absorbance of light at 562 nm by the mixture in the wells using the µQuant™ microplate spectrophotometer (Bio-Tek Instruments).

### 7.2.3. SDS-PAGE

For the SDS-PAGE pre-cast 4-20% gels (Bio-Rad) or homemade gels were used. The homemade gels were prepared mixing the ingredients for the separating gel and pouring the mixture into a glass form for the mini gels (Bio-Rad), and then pouring on the top of the gel some isopropanol to even out the separating gel. After the gel polymerized and the isopropanol was removed, the ingredients of the stacking gel were combined and the mixture was poured on top of the separating gel. Next, a comb was inserted into the stacking gel and the gel was left to polymerize.

The gel was inserted into an SDS-PAGE Mini Cassette (Bio-Rad) filled up with a running buffer, the samples and a protein ladder were loaded on the gel and an electric current was applied. The electrophoresis was running at 90 V until the bromphenol blue in the samples reached the bottom of the gel.

### 7.2.4. Western Blot

Proteins separated in the SDS-PAGE were transferred from the gel to a nitrocellulose membrane (Amersham, GE Healthcare). Membranes with a pore diameter of 0.2  $\mu\text{m}$  were used for the transfer of proteins smaller than 50 kDa and membranes with 0.45  $\mu\text{m}$  pore diameter were used for proteins larger than 50 kDa. The transfer was performed in a Bio-Rad transfer apparatus filled up with transfer buffer and lasted 90 minutes when the applied electric potential was 90 V.

Upon the transfer, the membrane was washed shortly in TBST-T then blocked with gentle shaking with the WB blocking buffer for 1 hour at room temperature followed by an overnight incubation with gentle shaking at 4°C with primary antibody diluted in the WB blocking buffer. The membrane was then washed three times for 5 minutes with TBS-T at room temperature and the HRP-conjugated secondary antibody diluted in the WB blocking buffer was applied for 1 hour at room temperature. The unbound secondary antibody was washed away from the membrane with three 5 minutes-long washes with TBS-T at room temperature and gentle shaking and the proteins labeled with the HRP-coupled antibodies were visualized at the LAS 4000 Mini camera (GE Healthcare) upon application on the membrane of the mixture of ECL (enhanced chemiluminescence) solutions (Amersham, GE Healthcare) prepared according to the manufacturer's protocol.

### 7.2.5. Membrane stripping

The membrane incubated with the first set of primary and secondary antibodies was sometimes incubated additionally with a different set of primary and secondary antibodies. For this, antibodies were removed

from the membrane by stripping. Stripping of the membrane was performed by incubation with stripping solution for 5 minutes with gentle shaking at room temperature followed by a 5 minutes-long incubation with neutralization solution with gentle shaking at room temperature. Next, the membrane was rinsed twice with distilled water followed by a 1 hour-long blocking at room temperature with WB blocking buffer. On the blocked membrane the next primary antibody could be applied.

#### **7.2.6. Co-immunoprecipitation**

HEK293 cells grown on culture plates (Greiner Bio-One) were placed on ice, washed with ice-cold PBS containing calcium and magnesium ions (PAN Biotech) and then lysis buffer containing protease inhibitors (Roche) and phosphatase inhibitors (Roche) was added to them. Upon 10 minutes of incubation with the lysis buffer, the cells were collected in Eppendorf tubes and centrifuged at 4°C for 10 minutes at 10000 g. The obtained supernatant was collected and an aliquot of the supernatant was kept as input. The remaining supernatant was pre-cleared with agarose beads with conjugated protein A and protein G (Santa Cruz Biotechnologies) for 30 minutes at 4°C with gentle rotation, then the beads were spun down for 5 minutes at 1000 g and 4°C and the supernatant was transferred to new Eppendorf tubes. Next, primary antibody was added to the supernatant and samples were incubated with gentle rotation for 1 hour at 4°C followed by addition of agarose beads with conjugated protein A and protein G (Santa Cruz Biotechnologies) and an overnight incubation with rotation at 4°C. The following day the samples were centrifuged at 1000 g for 5 minutes at 4°C, the supernatant was removed and the beads were washed twice with ice-cold lysis buffer and once with ice-cold PBS with calcium and magnesium ions (PAN Biotech). Beads were centrifuged at 1000 g for 5 minutes at 4°C and the supernatant was removed after every wash. Afterwards, 5x sample buffer was added to the beads and to the input sample and all samples were boiled for 5 minutes at 98°C. Before being loaded on the SDS-acrylamide gel, the samples containing beads were centrifuged at 1000 g for 5 minutes and the beads were removed from the samples.

#### **7.2.7. ELISA**

A 384-well polystyrene high-binding plate (Corning) was coated with 25 µl/well equal molar concentrations of peptides coding for four different extracellular domains of DRD2 (N-terminal extracellular fragment (12 µg/ml), 1<sup>st</sup> extracellular loop (4.73 µg/ml), 2<sup>nd</sup> extracellular loop (4.73 µg/ml) and 3<sup>rd</sup> extracellular loop (4.73 µg/ml) (all from Schafer-N)) and incubated overnight at 4°C with gentle shaking. The following day non-bound peptides were removed and the plate was washed once for 5 minutes at room temperature with PBS containing calcium and magnesium ions (PAN Biotech), blocked with ELISA blocking buffer for 1.5 hours at

room temperature and gentle shaking and then washed again once for 5 minutes with PBS containing calcium and magnesium ions. Next, different concentrations of ligands, namely CHL1-Fc (InVivo BioTech Services) and NCAM-Fc (InVivoBioTech Services) in PBS with calcium and magnesium ions were applied into the wells and incubated for 2 hours at room temperature with gentle shaking. Afterwards, wells were washed three times for 5 minutes at room temperature with ELISA washing buffer, incubated for 1 hour at room temperature and gentle shaking with an HRP-conjugated anti-human Fc antibody diluted in PBS with calcium and magnesium ions and washed three times for 5 minutes with ELISA washing buffer at room temperature. Next, OPD solution was added to the wells. Once the liquid in the wells changed its color, stopping solution was added to the wells to stop the HRP-reaction and the absorbance was measured at 492 nm using an ELISA reader ( $\mu$ Quant<sup>TM</sup> microplate spectrophotometer, Bio-Tek Instruments).

### **7.3. Cell biology methods**

#### **7.3.1. HEK293 cell culture maintenance**

HEK293 cells were grown in maintenance medium in flat-bottom cell culture flasks (Greiner Bio-One) at 37°C, 5% CO<sub>2</sub> and high humidity. The cells were passaged when reaching at least 80% confluency and never maintained for more than 25 passages.

#### **7.3.2. Passaging of HEK293 cells**

Cells were gently rinsed with HBSS without calcium and magnesium ions (PAN Biotech) followed by incubation with Trypsin-EDTA (PAN Biotech) for up to 4 minutes at room temperature. The trypsinized cells were collected from the flask with medium without supplements (PAN Biotech) and centrifuged for 5 minutes at 1000 g at room temperature. The obtained pellet of cells was resuspended in fresh maintenance medium (PAN Biotech) and an appropriate amount of cells was seeded in new flasks.

#### **7.3.3. Freezing of HEK293 cells**

Cells were rinsed with HBSS without calcium and magnesium ions (PAN Biotech) and incubated with Trypsin-EDTA (PAN Biotech) for up to 4 minutes at room temperature. Upon trypsinization, cells were resuspended in medium without supplements and centrifuged for 5 minutes at 1000 g at room temperature, followed by resuspension of the obtained cell pellet in freezing solution. Cells were then transferred to cryotubes (VWR), frozen at -80°C in an isopropanol box and three days later placed in a liquid nitrogen tank.

#### 7.3.4. Transfection of cultured cells

HEK293 cells were seeded in maintenance medium on sterile cell culture plates (Greiner Bio-One or Corning), poly-L-lysine (PLL)-coated glass coverslips (Sarstedt) or PLL-coated glass slides (Millicell EZ Slides, Millipore) in a dilution ensuring 70-80% confluency of cells at the following day. The following day, transfection of cells with plasmid constructs was performed using Lipofectamine LTX with Plus Reagent (Invitrogen) according to the manufacturer's protocol. Two days after transfection cells were used for experiments.

#### 7.3.5. Immunofluorescent staining of cultured cells

HEK293 growing on PLL-coated glass coverslips (Sarstedt) were fixed for 30 minutes at room temperature with 8% fixating solution added to the maintenance medium in the proportion of 1:1, washed 3 times for 5 minutes with homemade PBS followed by permeabilization and blocking with blocking serum for 1 hour at room temperature. Primary antibodies diluted in carrageenan buffer were then applied and samples were incubated at 4°C overnight. The following day cells were washed three times for 5 minutes with homemade PBS and incubated for 2 hours at room temperature with secondary antibodies diluted in carrageenan buffer. Unbound secondary antibodies were washed away from the cells with three 15 minutes-long washes with homemade PBS performed at room temperature. Next, coverslips were mounted on glass slides (Marienfeld) using mounting medium with 4',6-diamidino-2-phenylindole (DAPI) (Roti-Mount; Carl Roth). Pictures of the stained cells were taken at a confocal microscope (Olympus).

#### 7.3.6. PLA

**Cultured cells** – Transfected HEK293 cells grown on PLL-coated glass slides (Millicell EZ Slides, Millipore) were fixed for 30 minutes at room temperature with 8% fixating solution added to the maintenance medium in a proportion of 1:1 and washed with homemade PBS 3 times for 5 minutes at room temperature. Afterwards, PLA was performed according to the manufacturer's (Sigma-Aldrich) protocol. Briefly: cells were blocked at 37°C using Duolink Blocking Solution, then incubated overnight at 4°C with primary antibodies diluted in Duolink Antibody Diluent, followed by washing at room temperature with Duolink Washing buffer A and incubation with Duolink PLA Probes diluted in Duolink Antibody Diluent at 37°C. Next, cells were washed at room temperature with Duolink Washing buffer A after which Duolink Ligase diluted in Duolink Ligation Buffer and RNase-free water (Qiagen) was applied and incubated at 37°C. Cells were washed again with Duolink Washing buffer A at room temperature and Duolink Polymerase diluted in Duolink Amplification Buffer and RNase-free water (Qiagen) was applied and incubated at 37°C. Afterwards, cells were washed

with 1x Duolink Washing buffer B and with 0.01x Duolink Washing buffer B, then mounted using Duolink In Situ Mounting Medium with DAPI.

**Brain tissue** – Mouse brain cryosections mounted on glass slides (Superfrost Plus, ThermoFisher Scientific) were subjected to antigen retrieval, then PLA was performed on them according to the manufacturer's protocol with the primary antibodies incubation step lasting for 3 days.

Images of HEK293 cells and mouse brain sections on which the PLA was performed were taken at a confocal microscope (Olympus) using a 60x objective.

### 7.3.7. Antibody feeding

Two days after transfection HEK293 cells grown on PLL-coated glass coverslips (Sarstedt) were removed from the cell culture incubator, their maintenance medium was changed to AF incubation medium and cells were incubated for 60 minutes at 4°C. The AF incubation medium was removed from the wells, the cells were rinsed with medium without supplements and fresh medium without supplements was added to the cells. The cells were stimulated with 10 µM quinpirole for 30 minutes during which time they were kept at 37°C in the cell culture incubator. After incubation with quinpirole, cells were placed on ice, washed quickly with ice-cold homemade PBS, fixed for 5 minutes at room temperature with 8% fixating solution mixed 1:1 with homemade PBS and then rinsed 3 times with homemade PBS. Next, cells were blocked with the non-permeabilizing AF blocking buffer for 1 hour at room temperature followed by a 5 hours-long incubation with Cy3-conjugated secondary antibody diluted in the non-permeabilizing AF blocking buffer at room temperature. The unbound secondary antibody was washed away from the wells with two 5 minutes-long washes with homemade PBS and then cells were fixed again with the 8% fixating solution mixed 1:1 with homemade PBS for 5 minutes at room temperature. After the second fixation, cells were blocked and permeabilized with permeabilizing AF blocking buffer for 30 minutes at room temperature followed by an overnight incubation with Cy2-conjugated secondary antibody diluted in the permeabilizing AF blocking buffer at 4°C. The unbound antibody was washed away from the cells with 3 5-minutes-long washes with homemade PBS at room temperature and coverslips with cells were mounted on glass slides (Marienfeld) using mounting medium with DAPI (Carl Roth). Once the mounting medium hardened, pictures of the cells were taken at a confocal microscope (Olympus).

### 7.3.8. Cell surface biotinylation

Cells grown on 6-well cell culture plates (Greiner Bio-One) were placed on ice and rinsed twice with ice-cold PBS++. Afterwards, biotin was added to the cells and cells were incubated on ice for 15 minutes, washed shortly with ice-cold quenching buffer and incubated for 5 minutes with quenching buffer on ice. Next, the cells were rinsed twice with cold PBS++ and lysis buffer containing protease inhibitors (Roche) and phosphatase inhibitors (Roche) was added to the cells. After 15 minutes incubation with lysis buffer on ice cells were collected in Eppendorf tubes and centrifuged for 10 minutes at 4°C and 1000 g. The supernatants were collected and aliquots saved for input analysis. To the rest of the supernatants magnetic beads conjugated with streptavidin (Invitrogen) were added and incubated overnight at 4°C with gentle rotation. The following day, the supernatant was removed from the beads on a magnetic rack and the beads were washed once with lysis buffer and three times with PBS++. The beads were then resuspended in PBS++ and in 5x sample buffer and the input samples were mixed with 5x sample buffer. All samples were boiled for 5 minutes at 95°C then loaded on the SDS-acrylamide gels or stored at -20°C.

### 7.3.9. Protein degradation assay

Transfected HEK293 cells grown on 6-well cell culture plates (Greiner Bio-One) were treated with 100 µg/ml cycloheximide at 37°C for 30 minutes and stimulated with 10 µM quinpirole for 0-180 min at 37°C. Next, the plates with cells were removed from the cell culture incubator and placed on ice after which cell lysates were prepared for an SDS-PAGE analysis.

### 7.3.10. Ligand binding assay

HEK293 cells grown on sterile 96-well black polystyrene cell culture microplates (Corning) had their maintenance medium removed and ligand binding buffer containing 30 µM DnsyID1 was added to the cells. Upon 0-30 min-long incubation with DnsyID1, which was performed in the cell culture incubator, the cells were fixed for 20 minutes at room temperature with 8% fixating solution diluted 1:1 with the buffer present in the wells. Once the fixing solution was removed, the cells were washed twice for 5 minutes with homemade PBS and, with 100 µl homemade PBS left in the wells, the fluorescence intensity of bound DnsyID1 was measured at the microplate reader Spark (Tecan), setting the excitation wavelength at 320 nm, excitation bandwidth at 25 nm, emission wavelength at 520 nm and emission bandwidth at 10 nm.

### **7.3.11. In-cell Western**

HEK293 cells grown on sterile 96-well black polystyrene cell culture microplates (Corning) were fixed for 30 minutes at room temperature with 8% fixating solution added to the culture media in proportion 1:1. The fixing solution was removed and the cells were washed twice for 5 minutes with homemade PBS, then blocked and permeabilized for 1 hour at room temperature with ICW blocking buffer. Next, the cells were incubated overnight at 4°C with primary antibodies diluted in ICW antibody dilution buffer and washed 4 times for 5 minutes with ICW antibody dilution buffer. Secondary antibodies diluted in ICW antibody dilution buffer were applied on the cells and incubated for 1 hour at room temperature, after which the cells were washed 4 times for 5 minutes with ICW antibody dilution buffer and the immunostaining was analyzed using the Odyssey CLx reader (LI-COR).

### **7.3.12. *Trans*-orientation interaction assay**

HEK293 cells grown on PLL-coated glass slides (Millicell EZ Slides, Millipore) were incubated at 37°C for 15 min with 50 µg/ml CHL1-Fc in PBS containing calcium and magnesium ions added to the culture medium without supplements, washed two times for 2 minutes with PBS containing calcium and magnesium ions at room temperature then fixed with 8% fixating solution added to the PBS containing calcium and magnesium ions in proportion 1:1 for 30 minutes at room temperature. Next, cells were subjected to immunofluorescent staining.

## **7.4. Morphological methods**

### **7.4.1. Tissue fixation**

Living mice were intraperitoneally injected with 100 mg/kg pentobarbital (Sigma-Aldrich). Once the animals became unresponsive, transcardial perfusion with 4% formaldehyde in cacodylate buffer was performed by injecting the buffer through the left ventricle of the heart and at the same time disrupting the right atrium of the heart. 40-50 ml of the 4% formaldehyde in cacodylate buffer was pumped through the body of an adult mouse manually using a syringe. The brains of perfused mice were then dissected out and post-fixed for two days in 4% formaldehyde in cacodylate buffer at 4°C.

#### 7.4.2. Tissue cryosectioning

Formaldehyde-fixed brains were dehydrated for 3 days at 4°C in dehydrating solution, then shock-frozen in -80°C-cold isopentan (Sigma-Aldrich) for 2 minutes. The frozen brains were removed from the isopentan and stored dry at -80°C.

Prior to cryosectioning, the chamber of the cryostat (Leica) was cooled down to -21°C and the tissue holder of the cryostat was cooled down to -19°C. Brains were attached to the cold stage with a solution of Tissue-Tek OCT (optimal cutting temperature) Compound (Sakura Finetek) and covered with the same solution. Once the Tissue-Tek OCT Compound covering the brain froze (after about 1 hour), the brain was cut into 20 µm-thick sagittal sections or 30 µm-thick coronal sections. Depending on the experiment, the sections were either directly attached to the glass (Superfrost Plus, ThermoFisher Scientific) and stored dry at -20°C, or collected in section storage buffer and stored at 4°C.

#### 7.4.3. Antigen retrieval

Glass slides (Superfrost Plus, ThermoFisher Scientific) with mouse brain cryosections mounted on them were removed from -20°C and dried out completely at room temperature. Next, sections were placed in pre-warmed antigen retrieval buffer and incubated at 80°C for 30 minutes and then cooled down to room temperature without removing them from the buffer.

#### 7.4.4. Tissue immunostaining

**Immunofluorescent staining** – Free-floating cryosections or cryosections mounted on glass slides (Superfrost Plus, ThermoFisher Scientific) were permeabilized and blocked with blocking serum for 1 hour at room temperature and then incubated for 3 days at 4°C with primary antibodies diluted in carrageenan solution. Sections were washed with homemade PBS 3 times for 5 minutes at room temperature and incubated with Cy-conjugated secondary antibodies diluted in carrageenan solution for 2 hours at room temperature. The unbound secondary antibody was washed away with 3 15-minute washes with homemade PBS at room temperature followed by application of mounting medium containing DAPI (Carl Roth) and covering the sections with a cover glass. The images of the sections were taken at a confocal microscope (Olympus).

**Immunohistochemical staining** – This staining was performed by Professor Rosario Moratalla and Dr. Noelia Granado at the Cajal Institute in Madrid. Description of the protocol can be found in Granado et al. (2011) and Granado et al. (2011a). Shortly, free-floating cryosections were incubated for 10 minutes in 3% H<sub>2</sub>O<sub>2</sub> to inhibit endogenous peroxidase activity, then blocked with normal goat serum (Vector Laboratories, USA) for

1 hour followed by an overnight incubation at 4°C with primary antibody diluted in PBS containing Tween20 and normal goat serum. The following day the primary antibody was removed, the sections were washed and incubated at room temperature with biotinylated secondary antibody (Vector Laboratories). Next, the sections were washed and developed using diaminobenzidine (DAB). The reaction and change of the color by the sections was monitored every 5 minutes under a light microscope (Leica). Next, the reaction mixture was removed from the sections, the sections were washed, mounted on gelatin-coated glass slides, dehydrated in increasing concentrations of ethanol and cleared using xylene then covered with a cover glass using Permount.

#### **7.4.5. Stereological quantification of cells**

Stereological quantification of cells was performed on immunohistochemically stained brain sections by Professor Rosario Moratalla and Dr. Noelia Granado at the Cajal Institute in Madrid. Description of the protocol can be found in Granado et al. (2008) or Granado et al. (2011a). Shortly, the cells were quantified using an optical fractionator, where first the brain structure in which cells were to be quantified was outlined at small magnification (10x objective), then the cells that occupied the set focal point in the structure were quantified at a higher magnification (100x objective).

#### **7.5. Statistical analysis**

Statistical analysis was performed in SigmaPlot v12 or v13. First, the normality of data distribution and equality of variances were verified with Shapiro test and Levene test (p-value in both tests  $\leq 0.05$ ), respectively. For the data with normal distribution and equal variances, Student's *t*-test was performed for comparison of two groups and ANOVA followed by a *post-hoc* test was performed to compare more than two groups. If the Shapiro test and/or Levene test were not passed, Mann-Whitney U-test was performed to compare two groups and ANOVA on ranks followed by a *post-hoc* test was performed to compare more than two groups. The types of tests used are indicated in the graph legends. The p-value for acceptance of differences between groups was always 0.05, which is indicated with one star in the graph. Lower p-values are also marked in the graphs with  $p \leq 0.01$  and  $p \leq 0.001$  indicated with two and three stars, respectively.

#### **7.6. Genotyping of mice**

Tissue from the tip of the tail of each newborn mouse was lysed for 5-10 minutes at room temperature in a mixture of Dilution Buffer (20  $\mu$ l/tail cut, ThermoFisher Scientific) and DNA Release solution (0.5  $\mu$ l/tail cut,

ThermoFisher Scientific), then the reaction was stopped by a 5 min incubation at 98°C using the SimpliAmp Thermal Cycler (Life Technologies). Next, a PCR reaction was prepared combining 2x Phire Tissue Buffer (10 µl/reaction, ThermoFisher Scientific), DNA from a tail cut (2 µl/reaction), primers (one forward primer – 2.5 pM and both reverse primers – 1.25 pM each) and RNase-free water (to fill up to the final volume of 20 µl, Qiagen). The cycling conditions described in **Table 12** were set at the SimpliAmp Thermal Cycler (Life Technologies).

**Table 12:**  
**Cycling conditions – genotyping of mice.**

Number of cycles	Step	Temperature	Time
1	Initial denaturation	98°C	5 minutes
35	Denaturation	98°C	5 seconds
	Primer annealing	68°C	1 minute
	Extension	72°C	1 minute
1	Final extension	72°C	10 minutes
1	Storage	4°C	hold

The PCR products were analyzed with agarose gel electrophoresis on a 2.5% gel. A single band at 450 kb indicated the CHL1+/+ genotype, a single band at 380 kb indicated the CHL1-/- genotype, and two bands with one at 450 kb and the other at 380 kb indicated the CHL1+/- genotype.

## 8. Results

### 8.1. Verification of interaction between CHL1 and DRD2

Studies of Sakurai et al. (2002), Chen et al. (2005) and Shaltout et al. (2013) linked the CHL1 gene (CALL) to schizophrenia – a psychiatric disorder in which DRD2 plays a role. Moreover, behavioral studies using CHL1<sup>-/-</sup> mice showed that these mice display certain dopamine-dependent and schizophrenia-related features, like reduced reactivity to novelty (Morellini et al., 2007) and impaired filtering of novel and old stimuli (Irintchev et al., 2004), further linking CHL1 to schizophrenia and to the dopaminergic system. Since DRD2 and possibly CHL1 are involved in schizophrenia, CHL1 and DRD2 might interact with each other or influence one another. Therefore, the first aim of my study was to investigate whether CHL1 and DRD2 interact.

#### 8.1.1. CHL1 co-localizes with DRD2 in the mouse striatum

To analyze if CHL1 and DRD2 are localized in the mouse brain in close proximity, which is a prerequisite for a direct interaction, I performed immunostainings on brain sections from CHL1<sup>-/-</sup> and CHL1<sup>+/+</sup> adult mouse littermates using primary antibodies directed against DRD2 and CHL1 followed by fluorescently-labeled secondary antibodies. The brain sections in which I analyzed the co-localization of DRD2 and CHL1 contained the striatum which is one of the main targets of the dopaminergic signaling and contains a high density of dopamine receptors (Beaulieu & Gainetdinov, 2011). I detected the co-localization of DRD2 and CHL1 as yellow spots appearing as a result of overlapping of the signals labeling DRD2 (red) and CHL1 (green) in the striatum of CHL1<sup>+/+</sup> mice, but not CHL1<sup>-/-</sup> mice (**Figure 11**).

An assay verifying a close co-localizations of DRD2 and CHL1 – PLA – was performed to confirm the result obtained with the immunostaining. In this assay, upon incubation of adult CHL1<sup>-/-</sup> and CHL1<sup>+/+</sup> mouse brain sections with primary antibodies directed against DRD2 and CHL1, the sections were incubated with PLA probes conjugated with oligonucleotides. The oligonucleotides were connected through applied connector oligos when the distance between DRD2 and CHL1 was less than 40 nm and a rolling circle was amplified from the oligonucleotides using DNA polymerase. Hybridization of detection probes (fluorescently-labeled oligonucleotides) to the rolling circles allowed detection of an interaction at the confocal microscope as red dots. Many red dots, which indicate the close proximity of CHL1 with DRD2, were detected in sections of CHL1<sup>+/+</sup> mice striatum, while only few, possibly unspecific, dots were detected in sections of CHL1<sup>-/-</sup> mice striatum (**Figure 12**). The result showed that DRD2 and CHL1 are present in striatal cells in close proximity, which potentially enables physical interaction between them.

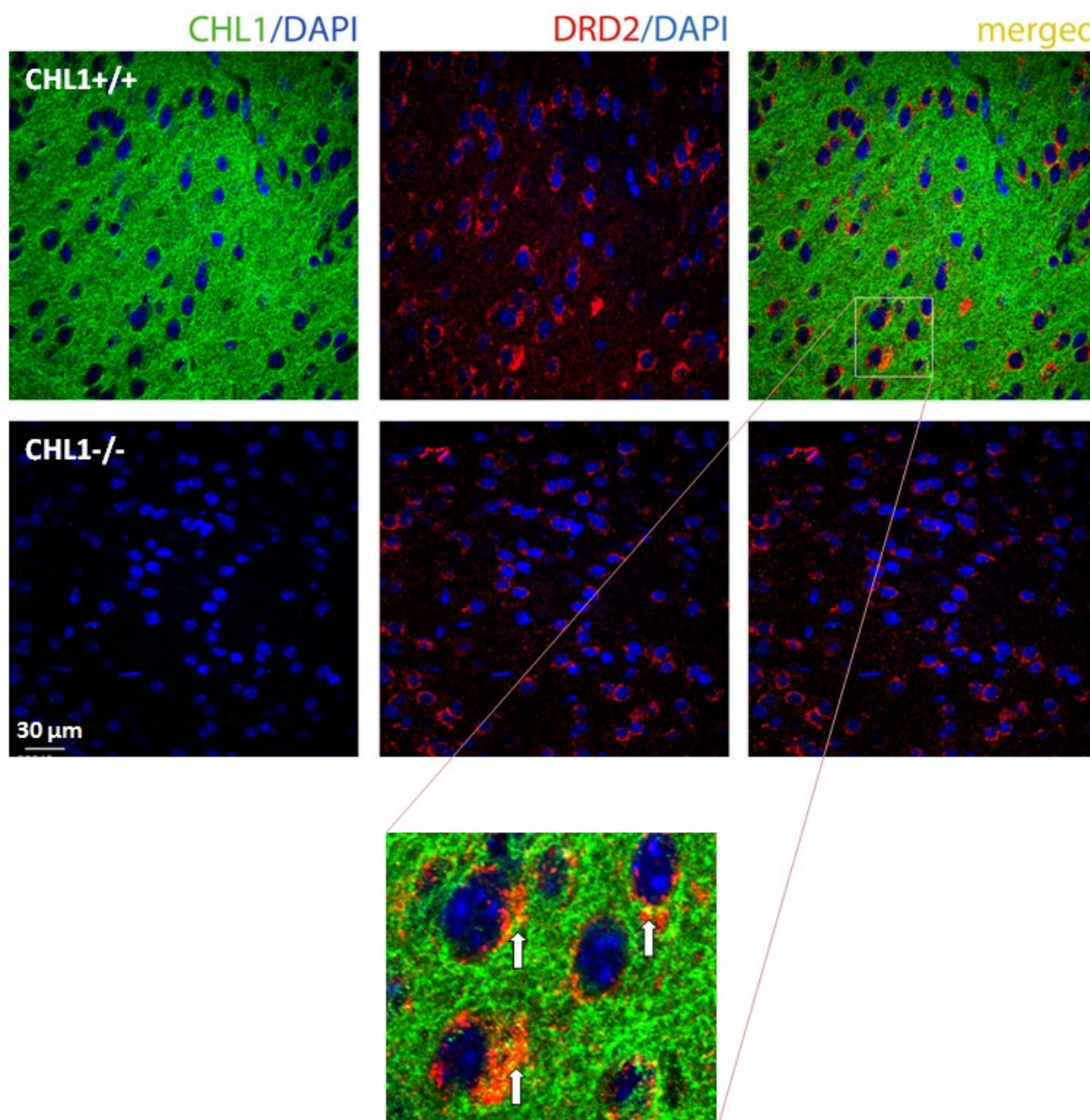


**Figure 11:**

**CHL1 and DRD2 co-localize in the adult mouse striatum.** Representative confocal images of anti-DRD2 and anti-CHL1 immunofluorescently stained 20  $\mu\text{m}$ -thick sagittal sections from brains of 3-4.5 months old female CHL1<sup>-/-</sup> and CHL1<sup>+/+</sup> mice are shown. The sections used for the staining were collected between 1200 – 1400  $\mu\text{m}$  laterally off the midsagittal plane and contained the striatum. Nuclei were stained with DAPI (blue). Co-localization of DRD2 (red) and CHL1 (green) resulted in overlapping of the signals and appeared as yellow spots. The yellow spots are visible only in the merged image of the CHL1<sup>+/+</sup> striatum and are indicated with arrows. The experiment was performed three times every time using a different set of animals. Abbreviations: CHL1 – close homolog of L1, CHL1<sup>-/-</sup> – mice knock-out for close homolog of L1, CHL1<sup>+/+</sup> – wild-type mice, DAPI – 4',6-diamidino-2-phenylindole, DRD2 – dopamine receptor D2.

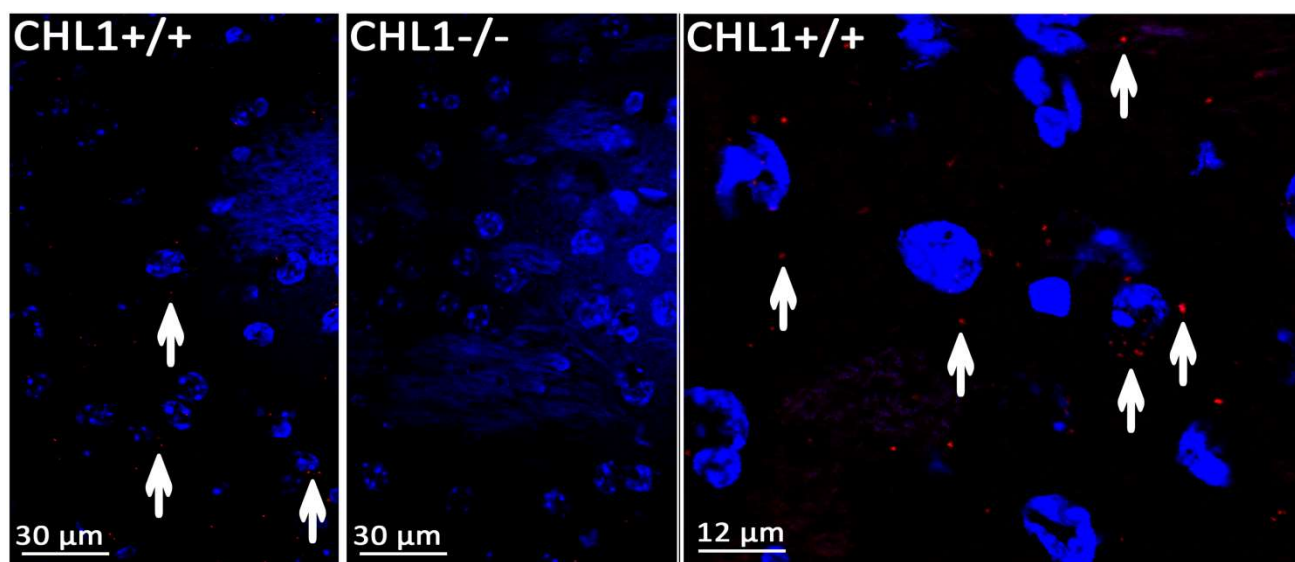


**Figure 12:**

**CHL1 and DRD2 are in a close proximity in the adult mouse striatum.** Shown are representative confocal images of PLA performed on corresponding 20  $\mu\text{m}$ -thick sagittal striatal sections collected between 1200 – 1400  $\mu\text{m}$  laterally off the midsagittal plane. The sections were derived from 3-4.5 months old female CHL1 $^{-/-}$  and CHL1 $^{+/+}$  mice. The assay was performed using primary DRD2 and CHL1 antibodies directed against the extracellular domains; nuclei were stained with DAPI (blue). Red dots indicating the close proximity of DRD2 and CHL1 are visible in images of CHL1 $^{+/+}$  mouse striatum (left and right panel) and are marked with white arrows. The experiment was performed two times, every time using a different set of animals. Abbreviations: CHL1 $^{-/-}$  – mice knock-out for close homolog of L1, CHL1 $^{+/+}$  – wild-type mice.

In summary, co-localization of DRD2 and CHL1 was observed predominantly around the nuclei of the striatal cells suggesting that the potential interaction between DRD2 and CHL1 takes place at the cell membrane or in the cytoplasm of these cells.

### 8.1.2. CHL1 co-localizes with DRD2S and DRD2L in transfected cells

To investigate whether CHL1 interacts with both splice variants of DRD2 – the predominantly pre-synaptic DRD2S and the predominantly post-synaptic DRD2L – I cloned plasmid constructs carrying DRD2S alone, DRD2S with CHL1, DRD2L alone and DRD2L with CHL1 (**Figure 13**). The sequences of the two DRD2 forms and CHL1 were cloned into a the high-copy mammalian expression vector pCAG-GFP. The GFP sequence was removed from the pCAG-GFP vector during the cloning to reduce its size and thus to increase the efficiency of transfection with the constructs.

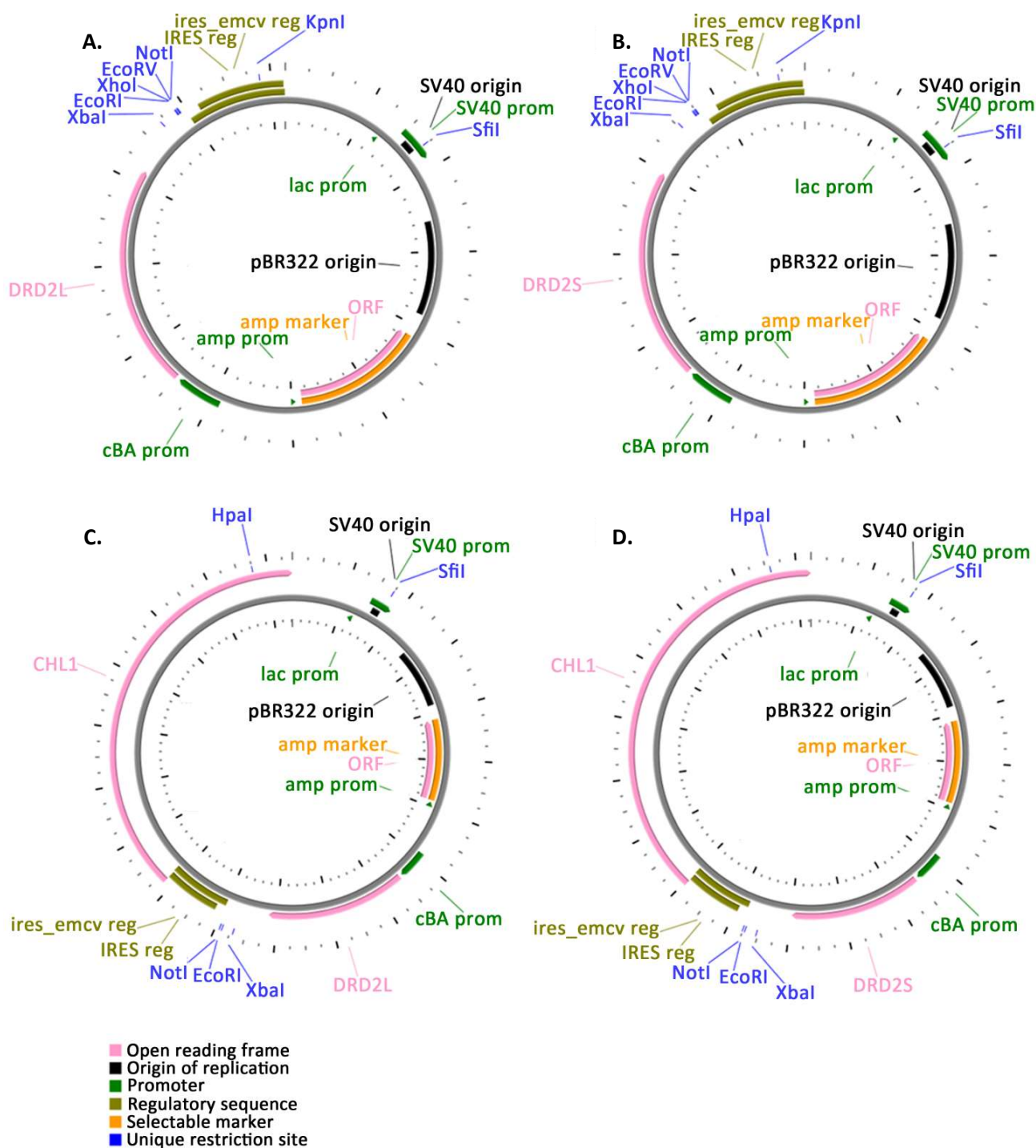


**Figure 13:**

**Cloned plasmid constructs carrying DRD2S or DRD2L in presence and absence of CHL1.** Presented are maps of constructs carrying DRD2L (pCAG-DRD2L, **A**), DRD2S (pCAG-DRD2S, **B**), DRD2L and CHL1 (pCAG-DRD2L-CHL1, **C**), DRD2S and CHL1 (pCAG-DRD2S-CHL1, **D**). Major ticks mark every 500 bp. Abbreviations: amp – ampicillin, cBA – chicken beta actin, CHL1 – close homolog of L1, DRD2L – dopamine receptor D2 “long”, DRD2S – dopamine receptor D2 “short”, EcoRI / EcoRV / HpaI / KpnI / NotI / SfiI / XbaI / XhoI – restriction enzymes, emcv – encephalomyocarditis virus, GFP – green fluorescent protein, IRES – internal ribosome entry site, lac – lactose, ORF – open reading frame, pBR322 – “plasmid Bolivar Rodriguez 322” *Escherichia coli* expression vector, pCAG – mammalian expression vector with CAG (cytomegalovirus enhancer, promoter and first exon and first intron of chicken beta-actin, splice acceptor of rabbit beta-globin) promoter, prom – promoter, reg – regulatory sequence, SV40 – simian virus 40.

To investigate if CHL1 co-localizes closely with both DRD2 forms, I performed PLA on HEK293 cells transfected with the cloned plasmid constructs carrying DRD2S alone, DRD2S with CHL1, DRD2L alone and DRD2L with CHL1, as well as on HEK293 cells transfected with pCAG-GFP plasmid as control and on not transfected cells. Mouse anti-DRD2 and goat anti-CHL1 primary antibodies directed against the extracellular domains of DRD2 and CHL1 were used in this experiment. Red dots indicating close proximity of DRD2 and CHL1 were detected in cells co-expressing DRD2S and CHL1 and in cells co-expressing DRD2L and CHL1. Cells expressing DRD2S or DRD2L alone, non-transfected control cells and cells transfected with the GFP-carrying control plasmid showed almost no red dots proving the specificity of the signal detected in cells expressing the two DRD2 forms together with CHL1 (**Figure 14.A**). This result showed that both pre- and post-synaptic forms of DRD2 are in close proximity to CHL1 and thus may directly interact with CHL1.

To determine if both DRD2 forms co-localize with CHL1 to the same extent, I quantified the number of red dots per cell in confocal images of transfected HEK293 cells expressing DRD2S with CHL1 and DRD2L with CHL1 subjected to the PLA using anti-DRD2 and anti-CHL1 antibodies. I found that the numbers of red dots per cell are about three times higher in cells co-expressing DRD2S and CHL1 than in cells co-expressing DRD2L and CHL1 (**Figure 14.B**). This result indicated that more CHL1 interacts with the pre-synaptic DRD2S than with the post-synaptic DRD2L.

In order to exclude the possibility that the observed differences in close proximity assay for CHL1 with DRD2S and CHL1 with DRD2L are caused by different levels of expression of the two receptor forms in HEK293 cells, the expression of both DRD2 forms in transfected HEK293 cells co-expressing DRD2S or DRD2L with CHL1 was quantified. In the confocal images of transfected cells immunofluorescently stained for DRD2, cells expressing DRD2 were manually delineated and the values for integrated density and area of the cells as well as mean grey value of the background readings were measured. Using the obtained values, for every analyzed cell its fluorescence intensity was calculated as described by McCloy et al. (2014). In brief: integrated density of a selected cell was reduced by the multiplication of area of the selected cell and mean grey value of a background. I did not observe a statistically significant difference in the level of DRD2L and DRD2S expression (**Figure 15**), which means that the different amount of co-localization of CHL1 with the two DRD2 forms found in PLA was not caused by different levels of expression of different DRD2 forms.

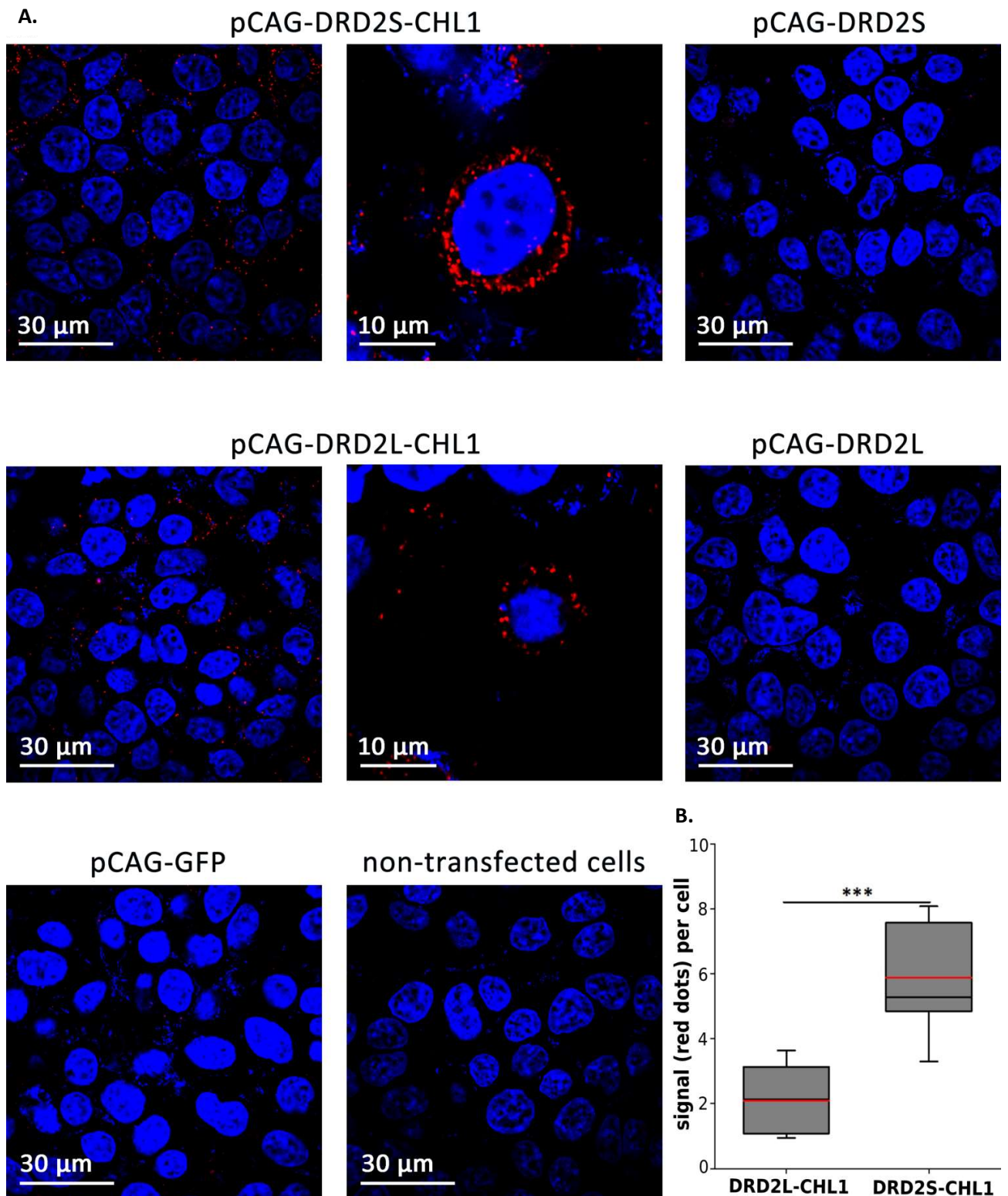


**Figure 14:**

**CHL1 co-localizes closely with DRD2S and DRD2L in transfected HEK293 cells and the co-localization of DRD2S with CHL1 is more pronounced than the co-localization of DRD2L with CHL1. A)** Shown are representative confocal images of transfected HEK293 cells expressing DRD2S with CHL1 (pCAG-DRD2S-CHL1), DRD2L with CHL1 (pCAG-DRD2L-CHL1), DRD2S alone (pCAG-DRD2S), DRD2L alone (pCAG-DRD2L), GFP (pCAG-GFP) as control and of non-transfected cells. PLA was performed on the cells using antibodies against extracellular domains of DRD2 and CHL1; nuclei were stained with DAPI (blue). Red dots indicating the close proximity of DRD2 and CHL1 were detected in cells co-expressing DRD2S with CHL1 and in cells co-expressing DRD2L with CHL1. No red dots or only few unspecific red dots could be detected in cells expressing DRD2S

alone, DRD2L alone or GFP and in non-transfected cells. The experiment was performed two times in duplicates. **B)** Box plots represent the number of positive signal (red dots) per cell quantified from the confocal images of transfected HEK293 cells co-expressing DRD2L and CHL1 (DRD2L-CHL1) or DRD2S and CHL1 (DRD2S-CHL1). Using ImageJ, the numbers of nuclei in each picture were quantified manually and the numbers of red dots in each picture were quantified automatically using a macro. At least seven pictures per condition from two independent experiments were analyzed. Red line represents the mean. Result of two-tailed Student's *t*-test:  $p < 0.001^{***}$ . **Abbreviations:** CHL1 – close homolog of L1, DRD2L – dopamine receptor D2 “long”, DRD2S – dopamine receptor D2 “short”, GFP – green fluorescent protein, pCAG – mammalian expression vector with CAG (cytomegalovirus enhancer, promoter and first exon and first intron of chicken beta-actin, splice acceptor of rabbit beta-globin) promoter.

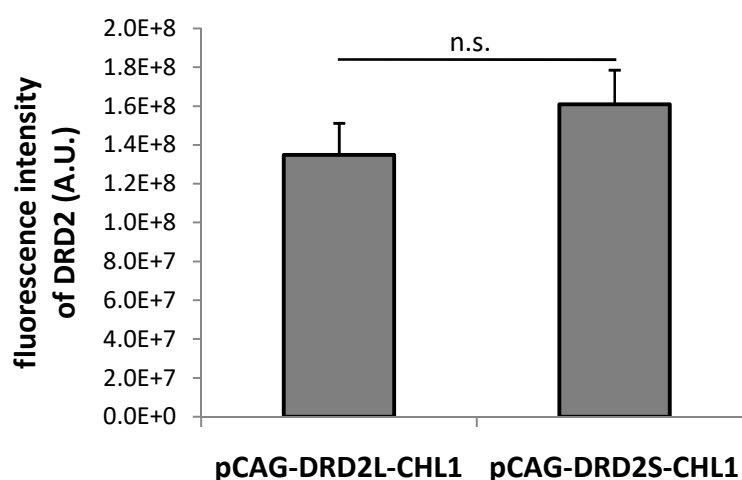


**Figure 15:**

**Similar expression of DRD2S and DRD2L in transfected HEK293 cells.** The graph presents expression of DRD2 forms in the presence of CHL1 measured in HEK293 cells transfected with pCAG-DRD2S-CHL1 and with pCAG-DRD2L-CHL1. The cells were immunofluorescently stained for DRD2 and as a measure of DRD2 expression the fluorescence intensity of stained cells was determined. Presented are means +SEM from one experiment performed in duplicate in which at least 50 cells per condition were analyzed. The experiment was repeated and a similar result was obtained. Result of two-tailed Student's *t*-test:  $p > 0.05$  n.s. (not significant). **Abbreviations:** A.U. – arbitrary units, CHL1 – close homolog of L1, DRD2 – dopamine receptor D2, DRD2L – dopamine receptor D2 “long”, DRD2S – dopamine receptor D2 “short”, n.s. – not significant, pCAG – mammalian expression vector with CAG (cytomegalovirus enhancer, promoter and first exon and first intron of chicken beta-actin, splice acceptor of rabbit beta-globin) promoter.

### 8.1.3. CHL1 binds directly to the first extracellular loop of DRD2 via its extracellular domain

After having shown that CHL1 and DRD2 co-localize closely in the mouse brain and in transfected cells, it was analyzed whether the two proteins bind to each other. I performed a co-immunoprecipitation experiment using adult CHL1<sup>-/-</sup> and CHL1<sup>+/+</sup> mouse brain homogenates and anti-CHL1 antibody directed against the intracellular fragment of CHL1. The precipitated proteins and the input controls (= brain homogenates not

subjected to the immunoprecipitation) were subjected to Western Blot analysis using anti-DRD2 antibody. An approximately 60 kDa DRD2 band was detected in the immunoprecipitates from the CHL1+/+ mouse brain homogenate, while only a very weak band was detectable in the immunoprecipitates from the CHL1-/- mouse brain homogenate (**Figure 16**). The obtained result suggested that DRD2 and CHL1 are present in a complex and may bind to each other.



**Figure 16:**

**DRD2 is co-precipitated with CHL1.** A representative immunoblot from a co-immunoprecipitation experiment performed on brain homogenates of adult female CHL1-/- and CHL1+/+ mice is shown. Proteins were precipitated using anti-CHL1 antibody and agarose beads. The proteins eluted from the beads (IP: CHL1) and the whole brain homogenates not subjected to immunoprecipitation (Input) were analyzed on Western Blot using anti-DRD2 antibody. Note: an approximately 60 kDa DRD2 band was detected in the eluate from the IP using CHL1+/+ brain homogenate but was only barely detectable in the eluate from the IP using control CHL1-/- brain. The experiment was repeated two times showing similar results. Abbreviations: CHL1 – close homolog of L1, DRD2 – dopamine receptor D2, IP – immunoprecipitation, -/- – mice knock-out for close homolog of L1, +/+ – wild-type mice.

Since the ability to precipitate DRD2 using CHL1 antibodies does not prove that the two proteins bind directly to each other, I analyzed by ELISA if a direct binding of CHL1 to DRD2 can occur. Previous study on an interaction of DRD2 with the intracellular domain of the cell adhesion molecule NCAM showed that DRD2 does not interact with the intracellular domain of CHL1 (Xiao, 2009). Therefore, I analyzed the binding of the extracellular domain of CHL1 to the extracellular parts of DRD2.

Equimolar concentrations of short synthetic peptides coding for the four different extracellular domains of DRD2, namely N-terminus, first loop, second loop and third loop, were immobilized. As ligands I used different concentrations of CHL1-Fc or NCAM-Fc (control) comprising the extracellular domains of CHL1 or NCAM conjugated with the Fc fragment of human IgG. Bound CHL1-Fc and NCAM-Fc were detected with HRP-conjugated anti-human IgG antibody. CHL1-Fc showed a concentration-dependent and saturable binding to the first extracellular loop of DRD2, but not to the other DRD2 peptides, while NCAM-Fc showed

no binding to any of the DRD2 peptides (**Figure 17**). This result shows that the extracellular domain of CHL1 directly binds to the first extracellular loop of DRD2.

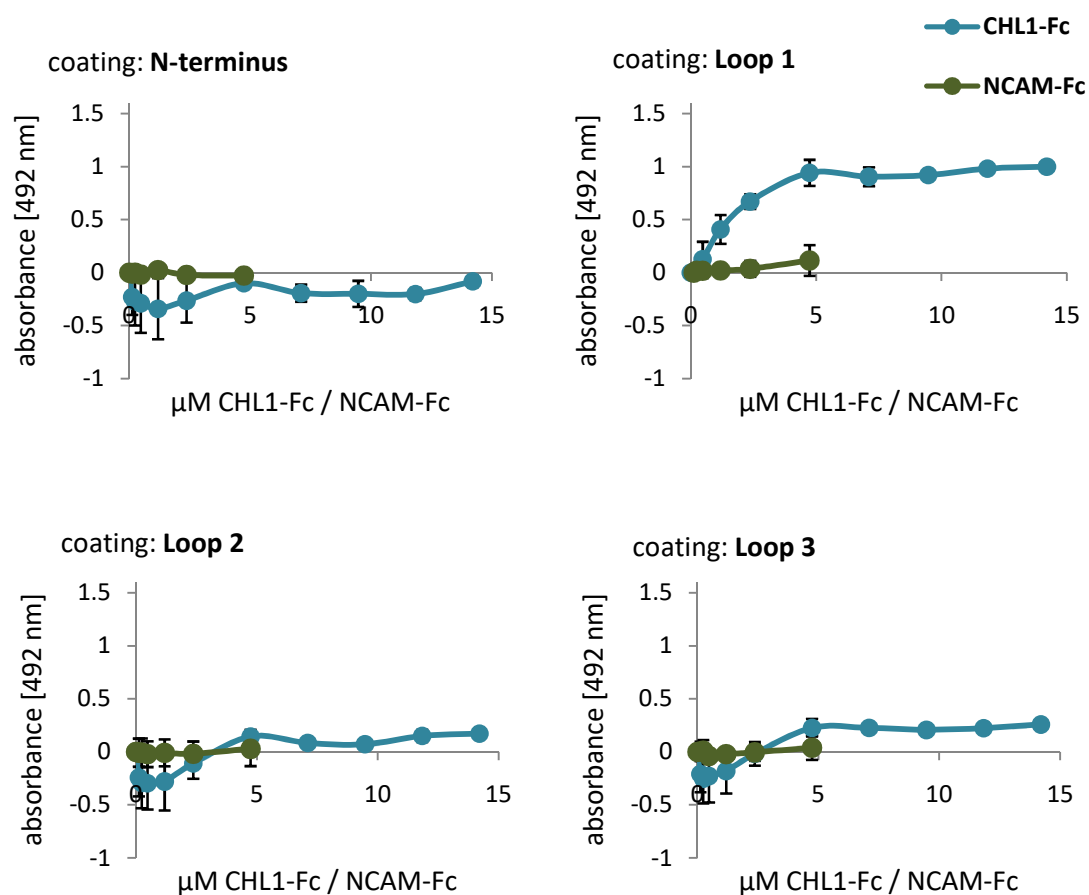


**Figure 17:**

**The extracellular domain of CHL1 binds directly to the first extracellular loop of DRD2.** Graphs present the results of ELISA performed immobilizing equimolar concentrations of synthetic peptides coding for four extracellular domains of DRD2 (N-terminus, loop 1, loop 2 and loop 3) and incubating them with different concentrations of extracellular domain of CHL1 and NCAM conjugated to the Fc fragment of human IgG (CHL1-Fc and NCAM-Fc). A concentration-dependent and saturable binding curve was obtained only upon application of CHL1-Fc on the first extracellular loop of DRD2, but not on loop 2, loop 3 or the N-terminus of DRD2. The extracellular domain of NCAM showed no binding to any of the DRD2 fragments. Presented are means  $\pm$ SEM from three independent experiments performed in triplicates. **Abbreviations:** CHL1-Fc – extracellular domain of cell adhesion molecule close homolog of L1 conjugated with Fc part of human immunoglobulin G, NCAM-Fc – extracellular domain of neural cell adhesion molecule conjugated with Fc part of human immunoglobulin G.

#### 8.1.4. CHL1 and DRD2 interact predominantly at the surface of cells

To narrow down the cellular compartment where the interaction of DRD2 and CHL1 takes place, I performed PLA on transfected HEK293 cells expressing DRD2S with CHL1 and DRD2L with CHL1 using primary antibodies

against the extracellular domains of DRD2 and CHL1 and took images of the cells at the confocal microscope using phase-contrast, which allowed to visualize shapes of the cells. Relative to the phase-contrast, the majority of red dots indicating the close co-localization of DRD2 and CHL1 were detectable at the surface of the transfected cells in both cells expressing DRD2S with CHL1 and in cells expressing DRD2L with CHL1 (Figure 18).

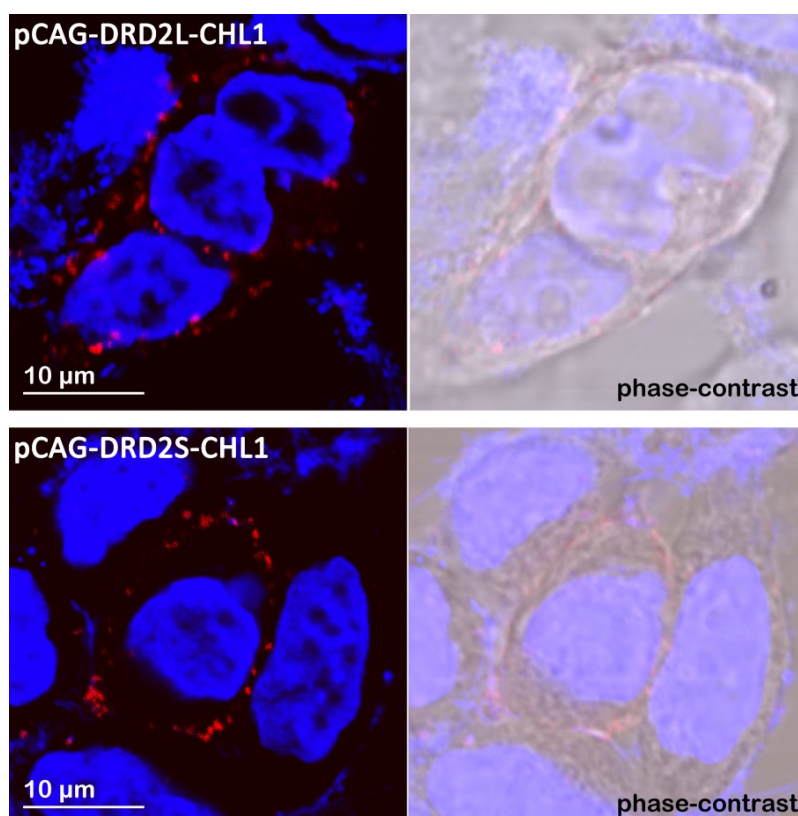


**Figure 18:**

**CHL1 co-localizes closely with DRD2S and DRD2L predominantly at the surface of transfected HEK293 cells.** Presented are representative confocal images of HEK293 cells transfected with plasmid constructs carrying either DRD2L with CHL1 (pCAG-DRD2L-CHL1) or DRD2S with CHL1 (pCAG-DRD2S-CHL1) on which PLA using anti-DRD2 and anti-CHL1 antibodies was performed; nuclei were stained with DAPI (blue). Red dots indicate close co-localization of CHL1 and DRD2. The use of phase-contrast allowed to visualize membranes of the cells and to narrow down the localization of the red dots to, mostly, the cell surface. The experiment was performed two times in duplicates yielding similar results.

#### **8.1.5. CHL1 can bind via its extracellular domain to DRD2S and DRD2L at the cell surface in *trans*-orientation**

Since CHL1 and DRD2 interact via their extracellular domains, binding in *cis*-and/or *trans*-orientation is possible. To determine if the binding between the two DRD2 forms and CHL1 can occur in *trans*-orientation,

HEK293 cells transfected to express either DRD2S or DRD2L alone were incubated with the extracellular domain of CHL1 (CHL1-Fc). Next, cells were fixed and stained using primary antibodies against extracellular domains of DRD2 and CHL1 followed by fluorescently-labeled secondary antibodies. Signals from the stained CHL1-Fc were detectable only in cells expressing DRD2L or DRD2S but not in non-transfected cells which do not express the receptor (**Figure 19**). This result indicates that CHL1 and DRD2 can interact in *trans*-orientation and strengthens the notion that CHL1 and DRD2 interact at the surface of cells.

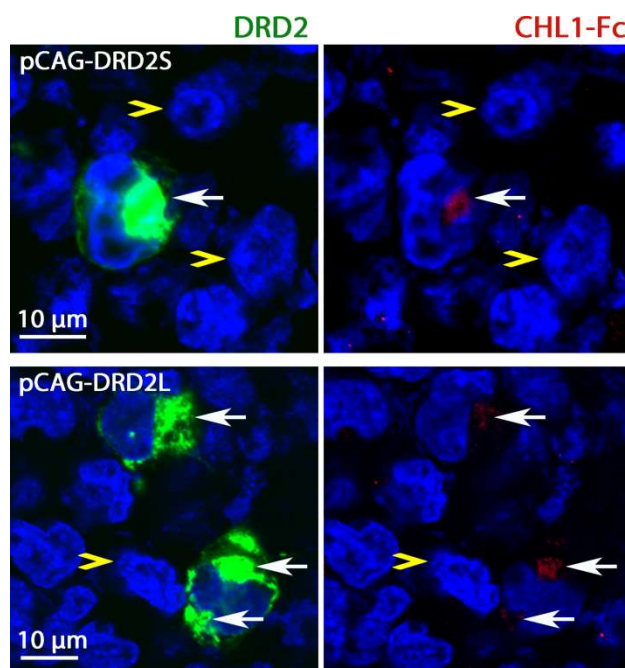


**Figure 19:**

**CHL1 interacts with DRD2S and DRD2L in *trans*-orientation via its extracellular domain.** Shown are representative confocal images of transfected HEK293 cells expressing DRD2S (pCAG-DRD2S) and DRD2L (pCAG-DRD2L) incubated with CHL1-Fc, which were immunofluorescently stained against DRD2 (labeled with green) and against the extracellular domain of CHL1 (labeled with red); nuclei were stained with DAPI (blue). Signal from CHL1-Fc was detected on cells expressing DRD2S or DRD2L (spots of DRD2 and CHL1 detected on the same cells are indicated with white arrows). Control cells not expressing DRD2 forms are indicated with yellow arrowheads. The experiment was performed independently two times. **Abbreviations:** CHL1-Fc – extracellular domain of cell adhesion molecule close homolog of L1 conjugated with Fc fragment of human immunoglobulin G, DRD2 – dopamine receptor D2, DRD2L – dopamine receptor D2 “long”, DRD2S – dopamine receptor D2 “short”, pCAG – mammalian expression vector with CAG (cytomegalovirus enhancer, promoter and first exon and first intron of chicken beta-actin, splice acceptor of rabbit beta-globin) promoter.

## 8.2. Identification of consequences of the interaction between CHL1 and DRD2 on functions of DRD2

Knowing that CHL1 binds to the DRD2, I investigated the consequences of this interaction on the functions of DRD2. Thus, the impact of CHL1 on agonist-induced internalization of the receptor, on degradation of the

receptor, on binding of a ligand to the receptor and on activation of the intracellular signaling pathways triggered by stimulation of the receptor were analyzed in transfected cells. Additionally, the DRD2-dependent intracellular signaling pathways in the striata of adult CHL1+/+ and CHL1-/- mice were analyzed.

### 8.2.1. CHL1 inhibits internalization of DRD2S upon receptor stimulation

The previous experiments showed that CHL1 binds directly to the two DRD2 forms and that the binding occurs predominantly at the surface of cells. Presence of DRD2L at the membrane of post-synaptic neurons and of DRD2S at the membrane of pre-synaptic neurons allows the receptors to bind their agonists present in the extracellular environment and thus to evoke a response of the neurons followed by the internalization of the receptors (Guo et al., 2010). To investigate whether CHL1 influences the internalization of DRD2S and DRD2L an “antibody feeding” experiment was performed measuring DRD2 internalization upon receptor stimulation with an agonist quinpirole. Living HEK293 cells transfected to express DRD2 forms alone or with CHL1 were incubated with anti-DRD2 antibody directed against the extracellular N-terminal domain of DRD2. Afterwards, the unbound antibody was washed away, and cells were stimulated with quinpirole and fixed. Then, without permeabilization, cells were incubated with the first fluorescently-labeled secondary antibody to label only the anti-DRD2 antibody-bound receptor located at the cell membrane. In order to label the internalized anti-DRD2 antibody-bound receptor, the cells were shortly fixed again then permeabilized, blocked and incubated with the second fluorescently-labeled secondary antibody. The first secondary antibody labeling cell surface DRD2 and the second secondary antibody labeling internalized DRD2 were conjugated with two different fluorescent dyes (**Figure 20.A**). Fluorescence intensities of internalized DRD2 and surface DRD2 were calculated from the confocal images as described by McCloy et al. (2014) and the fluorescence intensities of internalized DRD2 were calculated relative to the sum of fluorescence intensities of internalized and surface DRD2. Statistical analysis showed that quinpirole-induced internalization of DRD2S occurred in presence and absence of CHL1; however, internalization of DRD2S was significantly weaker when CHL1 was co-expressed than when DRD2S was expressed without CHL1 (**Figure 20.B**).

Additionally, the impact of CHL1 on the internalization of DRD2L was analyzed using the same method; however, inconsistent results were obtained (data not shown) making a final conclusion about the influence of CHL1 on the agonist-induced internalization of DRD2L impossible.

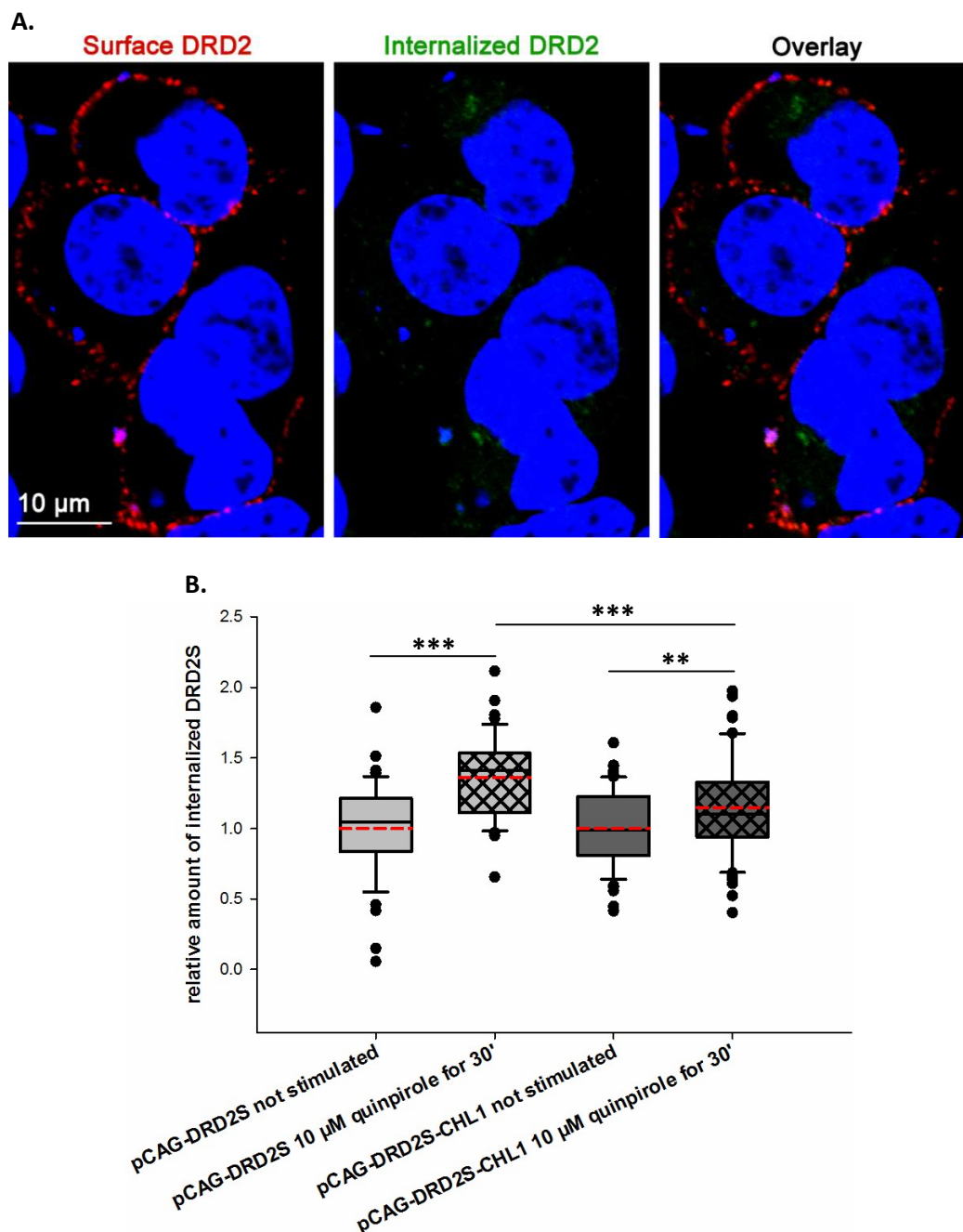


**Figure 20:**

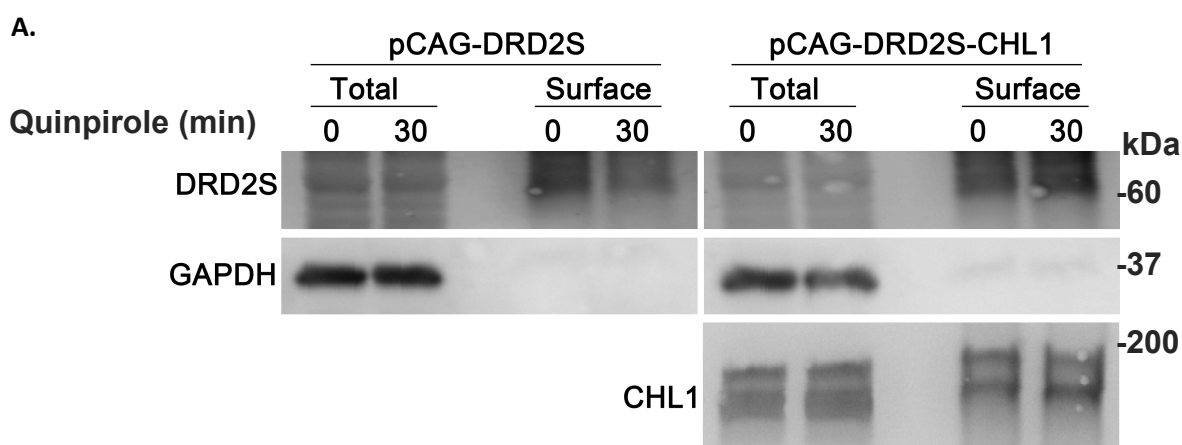
**CHL1 affects internalization of DRD2S upon stimulation with the DRD2 agonist quinpirole.** **A)** Presented are representative confocal images of transfected HEK293 cells on which the “antibody feeding” experiment was performed. HEK293 cells transfected to express DRD2S (pCAG-DRD2S) or to co-express DRD2S and CHL1 (pCAG-DRD2S-CHL1) were incubated with anti-DRD2 antibody directed against its N-terminus; next, the cells were stimulated with quinpirole followed by fixation with formaldehyde. The “Surface DRD2” was then labeled with the first secondary antibody. After permeabilization of the cells “Internalized DRD2” was labeled with the second secondary antibody. The overlay shows labeling of the “Surface DRD2” (red) at the cell membrane and “Internalized DRD2” (green) in the cytosol and the DAPI-stained nuclei (blue). **B)** Box plots present the result of analysis performed on the confocal images of transfected HEK293 cells expressing DRD2S alone (pCAG-DRD2S) or DRD2S with CHL1 (pCAG-DRD2S-CHL1) subjected to the “antibody feeding” experiment using anti-DRD2 antibody. As a measure of “Surface DRD2” and “Internalized DRD2” amounts their fluorescence intensities were determined and the values obtained for “Internalized DRD2” were calculated relative to the sums of “Internalized DRD2” and “Surface DRD2”. Results of two-way ANOVA followed by *post-hoc* Student Newman-Keul’s:  $p < 0.01^{**}$ ,  $0.001^{***}$ . The experiment was performed two times in duplicates and from every experiment at least 17 cells were analyzed. Abbreviations: CHL1 – close

homolog of L1, DRD2 – dopamine receptor D2, DRD2L – dopamine receptor D2 “long”, DRD2S – dopamine receptor D2 “short”, pCAG – mammalian expression vector with CAG (cytomegalovirus enhancer, promoter and first exon and first intron of chicken beta-actin, splice acceptor of rabbit beta-globin) promoter.

### 8.2.2. CHL1 affects the cell surface amount of DRD2S upon receptor stimulation with the DRD2 agonist

To confirm the “antibody feeding” experiment, cell-surface biotinylation, which allows to measure the amount of cell-surface receptor, was performed. In this experiment, HEK293 cells transfected with plasmids carrying DRD2S alone and DRD2S with CHL1 were stimulated with quinpirole and then incubated with Sulfo-NHS-LC-Biotin, which is not cell-permeable and thus only couples to surface proteins. The unbound biotin was quenched and washed away and the cells were lysed. The cell surface proteins to which biotin covalently attached were precipitated using streptavidin beads, then eluted from the beads and analyzed on Western Blot using anti-DRD2 antibody. Together with the precipitated proteins, samples of cell lysates not subjected to protein precipitation were analyzed on Western Blot. Intensities of bands representing cell-surface DRD2S were visibly weaker upon 30-minutes incubation with quinpirole than in non-stimulated cells when cells were not co-expressing CHL1, but not when CHL1 was co-expressed in the cells (**Figure 21.A**). In cells co-expressing DRD2S and CHL1 treatment with quinpirole for 30 minutes did not reduce the intensity of bands representing cell-surface DRD2S. This result is consistent with the “antibody feeding” result and further confirms that CHL1 affects cell surface levels of the DRD2S upon receptor stimulation with an agonist.

Considering that no detectable change in the amount of cell-surface DRD2S upon stimulation with quinpirole for 30 minutes was seen when DRD2S was co-expressed with CHL1, I determined if longer stimulation times cause detectable changes in the cell-surface amount of DRD2S. For this purpose cell surface biotinylation was performed as described before except for the stimulation times which this time were 0, 30, 90 and 180 minutes. Still, the amount of the biotinylated (surface) DRD2S detected with Western Blot decreased with time of stimulation in cells expressing DRD2S alone, but not in cells co-expressing CHL1 (**Figure 21.B**).



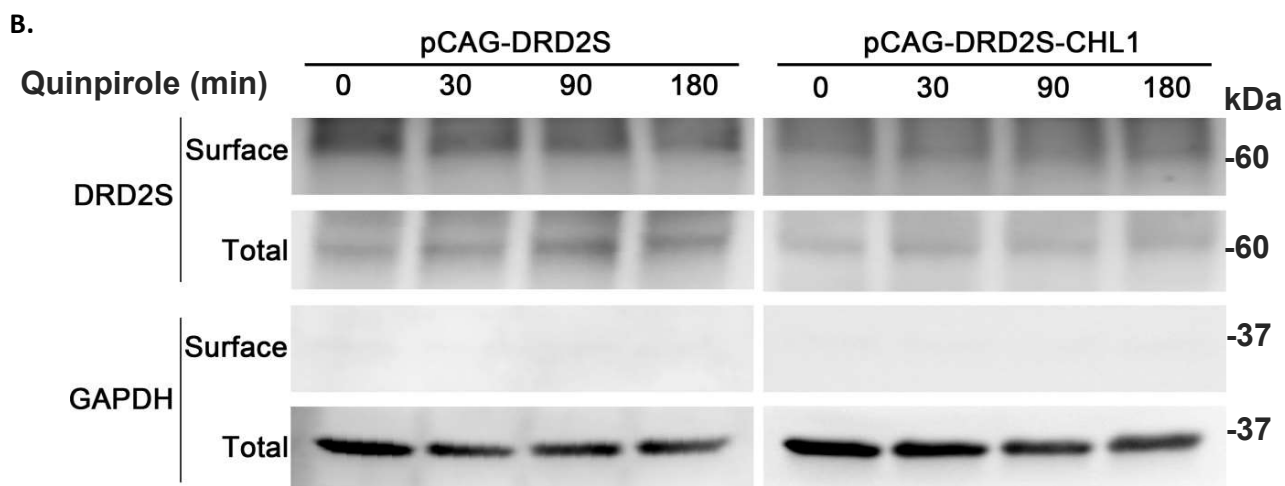


**Figure 21:**

**CHL1 affects the cell surface amount of DRD2S upon receptor stimulation with its agonist quinpirole.** Representative blots from the cell surface biotinylation experiments performed on HEK293 cells expressing DRD2S alone (pCAG-DRD2S) and DRD2S with CHL1 (pCAG-DRD2S-CHL1) stimulated with quinpirole for 0 and 30 minutes (**A**) or for 0, 30, 90 and 180 minutes (**B**) are shown. Upon precipitation of the biotinylated proteins from the whole-cell lysates of the stimulated cells, the precipitated proteins (“Surface”) as well as the whole-cell lysate proteins (“Total”) were subjected to Western Blot analysis using anti-DRD2 antibody as well as anti-GAPDH and anti-CHL1 antibodies to control loading. The experiment was performed independently three times yielding similar results. Abbreviations: CHL1 – close homolog of L1, DRD2S – dopamine receptor D2 “short”, GAPDH – glyceraldehyde 3-phosphate dehydrogenase, pCAG – mammalian expression vector with CAG (cytomegalovirus enhancer, promoter and first exon and first intron of chicken beta-actin, splice acceptor of rabbit beta-globin) promoter.

Cell-surface biotinylation experiments were performed also to analyze the impact of CHL1 on the cell-surface amount of DRD2L, however, similarly as in the “antibody feeding” experiment performed with DRD2L, inconsistent results were obtained (data not shown), again allowing no final conclusion about the impact of CHL1 on DRD2L surface expression.

### 8.2.3. CHL1 does not affect DRD2 degradation

Previous studies showed that DRD2 is internalized after stimulation with its agonist and then mostly degraded in lysosomes and rarely recycled back to the plasma membrane (Bartlett et al., 2005). Therefore, I determined the impact of CHL1 on DRD2 degradation using transfected HEK293 cells expressing DRD2S alone, DRD2S with CHL1, DRD2L alone and DRD2L with CHL1. The transfected cells were pre-treated with the protein synthesis inhibitor cycloheximide, followed by stimulation with the DRD2 agonist quinpirole for 0, 30, 60, 90, 120 and 180 minutes. Next, the cells were lysed and the amounts of non-degraded DRD2 in the

lysates were analyzed by Western Blot using anti-DRD2 antibody. The Western Blot membranes were further incubated with anti-CHL1 antibody in order to verify possible co-degradation of DRD2 with its newly discovered binding partner CHL1, as well as with anti-GAPDH antibody to control loading. Western Blot results were analyzed by measuring the intensities of obtained bands representing DRD2, CHL1 and GAPDH, and the intensities of DRD2 and CHL1 bands relative to the intensities of GAPDH bands were calculated. At least 50% of the initial amount of DRD2L expressed without CHL1, of DRD2L co-expressed with CHL1 and of DRD2S co-expressed with CHL1 degraded within 90-150 minutes of quinpirole stimulation (**Figure 22**, **Figure 23**), while in case of DRD2S expressed without CHL1 even after 180 minutes of quinpirole stimulation less than 50% of receptor was degraded (**Figure 22**). The difference in the rate of degradation of DRD2S expressed alone and co-expressed with CHL1 was statistically analyzed, however no significant differences were found. Interestingly, cells co-expressing DRD2 and CHL1 that were treated with quinpirole also showed a time-dependent degradation of CHL1 (**Figure 24**), which could mean that agonist-induced degradation of DRD2 is associated with degradation of its binding partner CHL1. Of note, the rate of degradation of CHL1 was not different in cells expressing DRD2S and DRD2L and reached 50% between 90-120 minutes after stimulation.

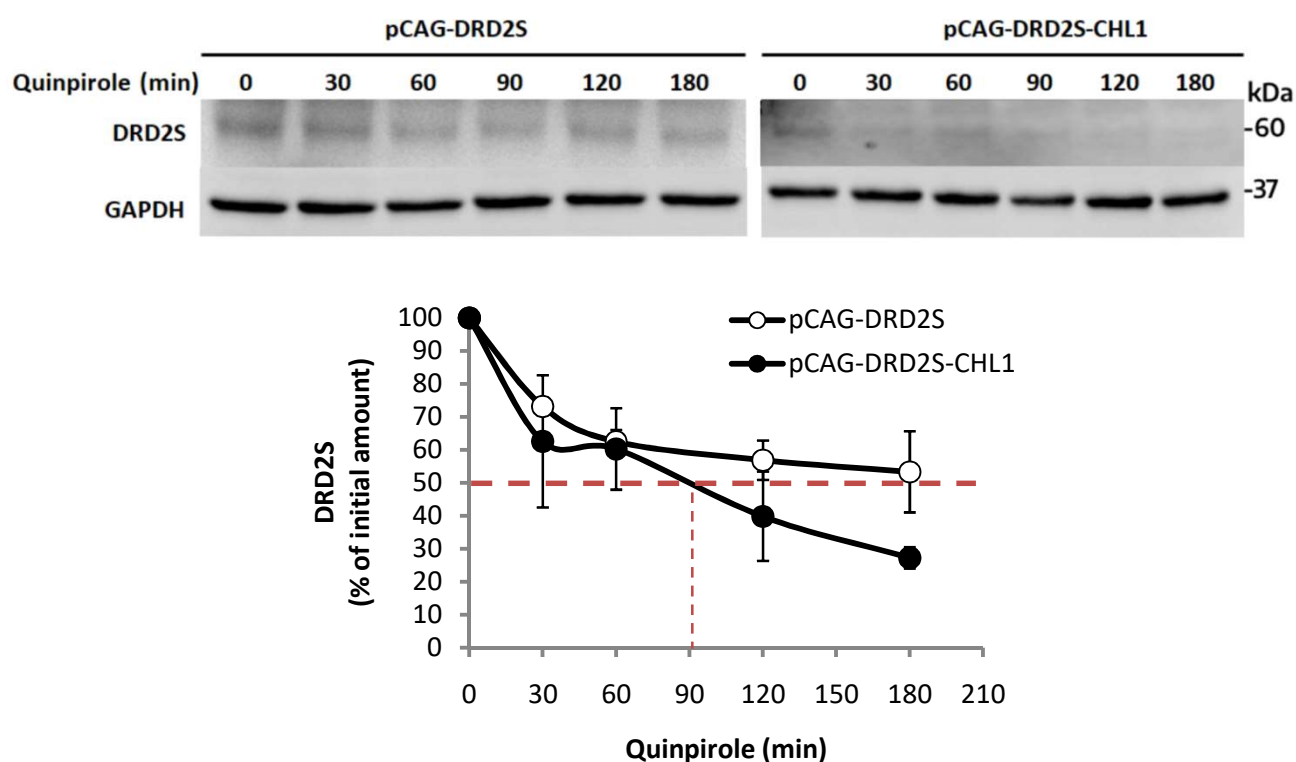


**Figure 22:** CHL1 does not influence DRD2S degradation upon receptor stimulation with quinpirole. Shown are representative blots (upper panel) and a graph (lower panel) from experiments in which the influence of

CHL1 on agonist-induced DRD2S degradation was measured. HEK293 cells expressing DRD2S alone (pCAG-DRD2S) and DRD2S with CHL1 (pCAG-DRD2S-CHL1) were pre-treated with protein synthesis inhibitor cycloheximide and then stimulated with quinpirole for 0, 30, 60, 90, 120 and 180 minutes. Lysates of the cells were analyzed on Western Blot using anti-DRD2 and anti-GAPDH antibodies and intensities of bands representing the amounts of DRD2 were calculated relative to the amounts of GAPDH, with the relative DRD2 amount in cells stimulated with quinpirole for 0 minutes set to 100%. No statistically significant differences between cells expressing DRD2S alone and with CHL1 were found with one-way ANOVA ( $p > 0.05$ ). The dashed lines indicate degradation of 50% of the initial DRD2S. In graphs presented are means  $\pm$  SEM from three independent experiments. **Abbreviations:** CHL1 – close homolog of L1, DRD2S – dopamine receptor D2 “short”, GAPDH – glyceraldehyde 3-phosphate dehydrogenase, pCAG – mammalian expression vector with CAG (cytomegalovirus enhancer, promoter and first exon and first intron of chicken beta-actin, splice acceptor of rabbit beta-globin) promoter.

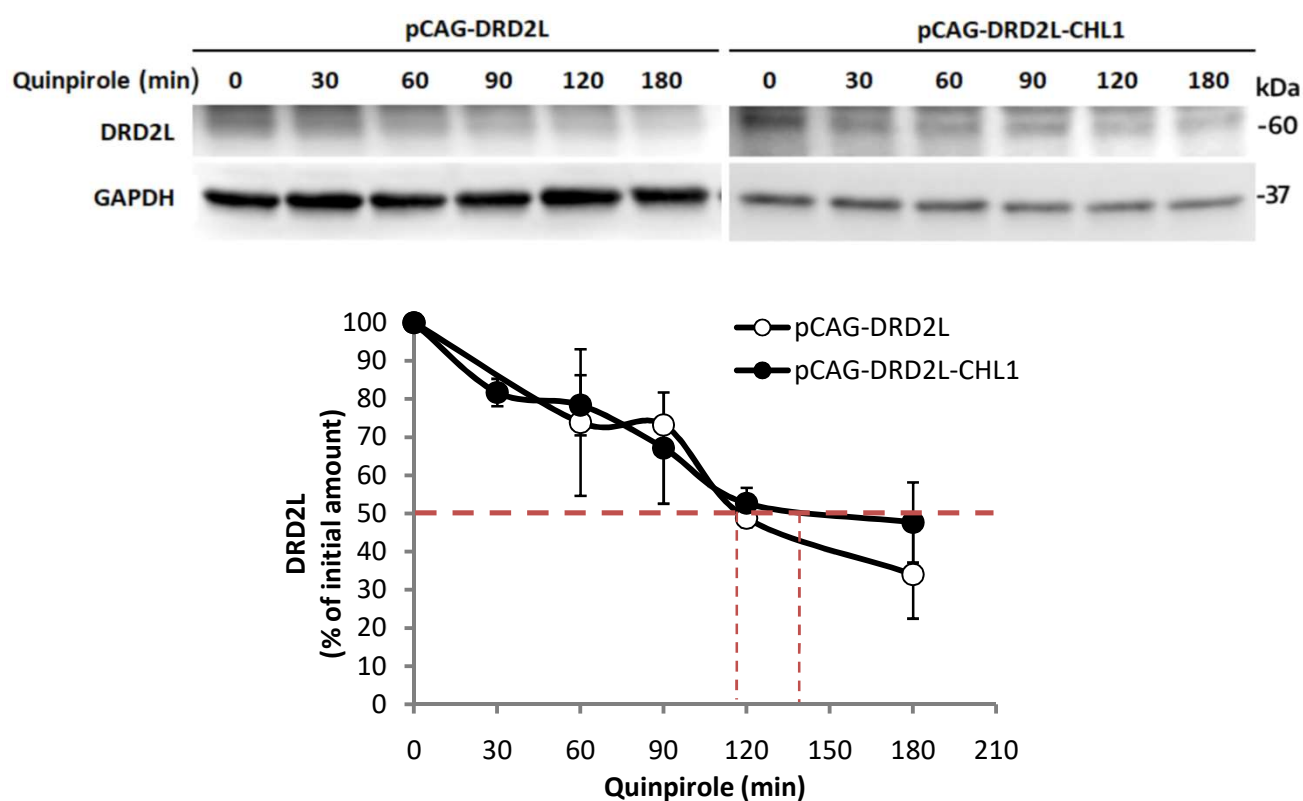


**Figure 23:**

**CHL1 does not influence DRD2L degradation upon receptor stimulation with quinpirole.** Representative blots (upper panel) and a graph (lower panel) from DRD2L degradation assay are shown. HEK293 cells expressing DRD2L alone (pCAG-DRD2L) and DRD2L with CHL1 (pCAG-DRD2L-CHL1) were pre-treated with cycloheximide and then stimulated with quinpirole for 0, 30, 60, 90, 120 and 180 minutes. Cell lysates were analyzed by Western Blot using anti-DRD2 and anti-GAPDH antibodies. Intensities of bands representing non-degraded DRD2L were calculated relative to intensities of bands representing GAPDH. Relative DRD2L level in cells stimulated for 0 minutes was set to 100%. No statistically significant differences between cells expressing DRD2L alone and with CHL1 were found with one-way ANOVA ( $p > 0.05$ ). The dashed lines indicate degradation of 50% of the initial DRD2L. Means  $\pm$  SEM from three independent experiments are presented in

graphs. **Abbreviations:** CHL1 – close homolog of L1, DRD2L – dopamine receptor D2 “long”, GAPDH – glyceraldehyde 3-phosphate dehydrogenase, pCAG – mammalian expression vector with CAG (cytomegalovirus enhancer, promoter and first exon and first intron of chicken beta-actin, splice acceptor of rabbit beta-globin) promoter.

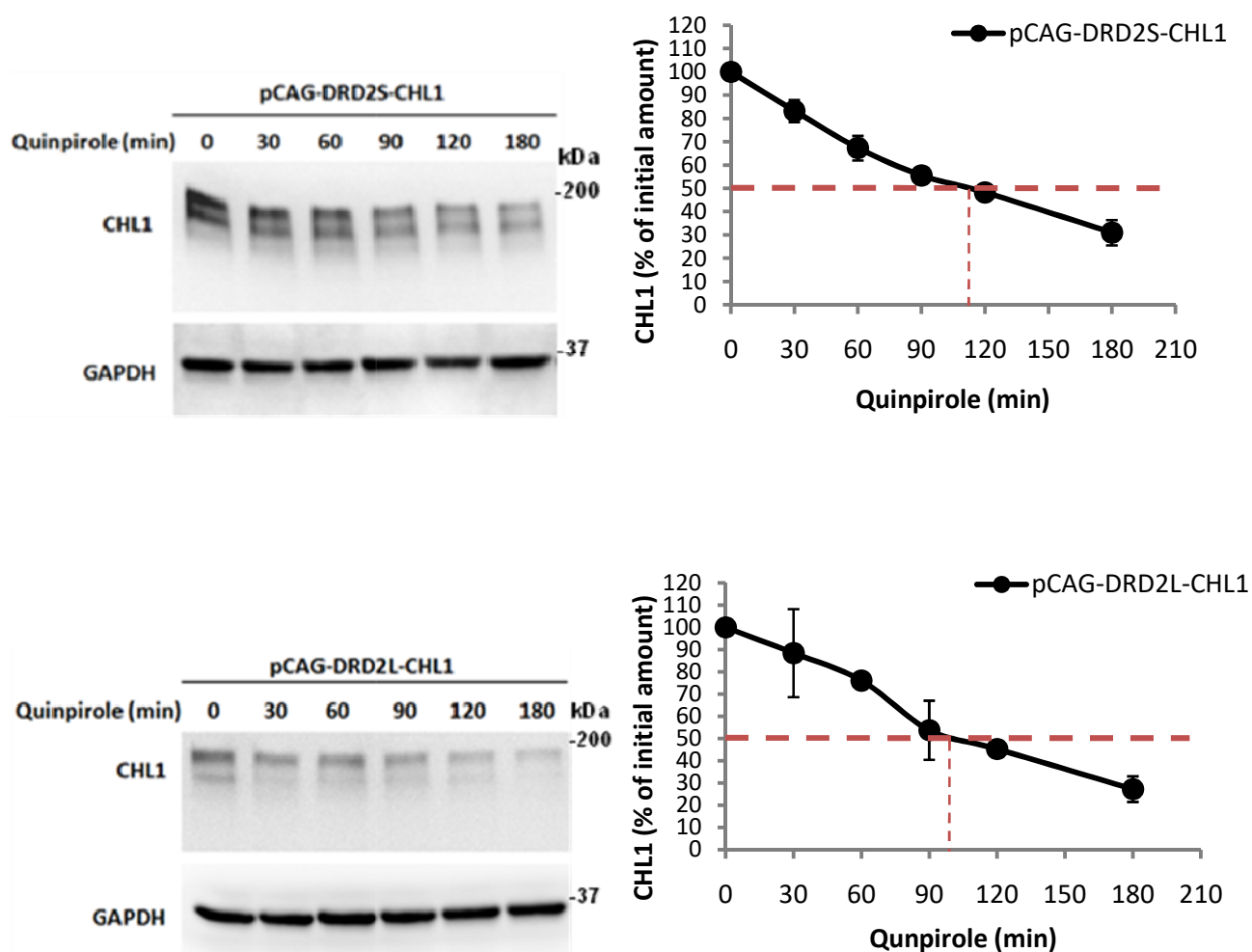


**Figure 24:**

**Degradation of CHL1 induced by DRD2 agonist quinpirole is similar in cells expressing DRD2S and DRD2L.** Representative blots (left) and graphs (right) present the results of the receptor protein degradation assay performed on HEK293 cells expressing DRD2S with CHL1 (pCAG-DRD2S-CHL1) and DRD2L with CHL1 (pCAG-DRD2L-CHL1) pre-treated with protein synthesis inhibitor cycloheximide and stimulated for 0, 30, 60, 90, 120 and 180 minutes with DRD2 agonist quinpirole. Lysates of the stimulated cells were analyzed on Western Blot using antibodies against CHL1 and GAPDH and intensities of bands representing CHL1 were calculated relative to intensities of GAPDH bands, with the relative CHL1 amount in cells stimulated with quinpirole for 0 minutes set to 100%. The dashed lines indicate degradation of 50% of the initial CHL1. Presented are means  $\pm$ SEM from three independent experiments. Result of one-way ANOVA performed to compare CHL1 degradation between cells expressing DRD2S and DRD2L:  $p > 0.05$ . **Abbreviations:** CHL1 – close homolog of L1, DRD2L – dopamine receptor D2 “long”, DRD2S – dopamine receptor D2 “short”, GAPDH – glyceraldehyde 3-phosphate dehydrogenase, pCAG – mammalian expression vector with CAG (cytomegalovirus enhancer,

promoter and first exon and first intron of chicken beta-actin, splice acceptor of rabbit beta-globin) promoter.

#### 8.2.4. Binding of an agonist to DRD2 is not affected by CHL1

Next, I investigated if CHL1 affects binding of agonists to DRD2L and DRD2S. For this purpose, HEK293 cells were transfected with plasmid constructs carrying DRD2S alone, DRD2S with CHL1, DRD2L alone and DRD2L with CHL1 and incubated with a fluorescent dopamine analog DnsyID1 for 0, 2.5, 10 and 30 minutes. After the incubation, unbound fluorescent ligand was washed away from the cells and the fluorescence of the ligand bound to the receptors was measured. In order to control for the effect of potential differential expression of the two DRD2 forms, an in-cell Western analysis of DRD2 expression was performed on the cells following the measurement of DnsyID1 binding. In the in-cell Western, cells were incubated with anti-DRD2 and anti-GAPDH (control) primary antibodies followed by fluorescently-labeled secondary antibodies. As a measure of DRD2 and GAPDH expression intensities of fluorescence of the secondary antibodies labeling DRD2 and GAPDH were determined. The values for detected DRD2 expression were normalized to the expression of GAPDH, and the data obtained from the analysis of DnsyID1 binding to the DRD2 were further normalized to the normalized expression of the DRD2. Results of this experiment show that with longer times of incubation with DnsyID1 increasing amount of receptor-bound DnsyID1 is detected, however, no effect of CHL1 on DnsyID1 binding to both DRD2L and DRD2S was found (**Figure 25**).

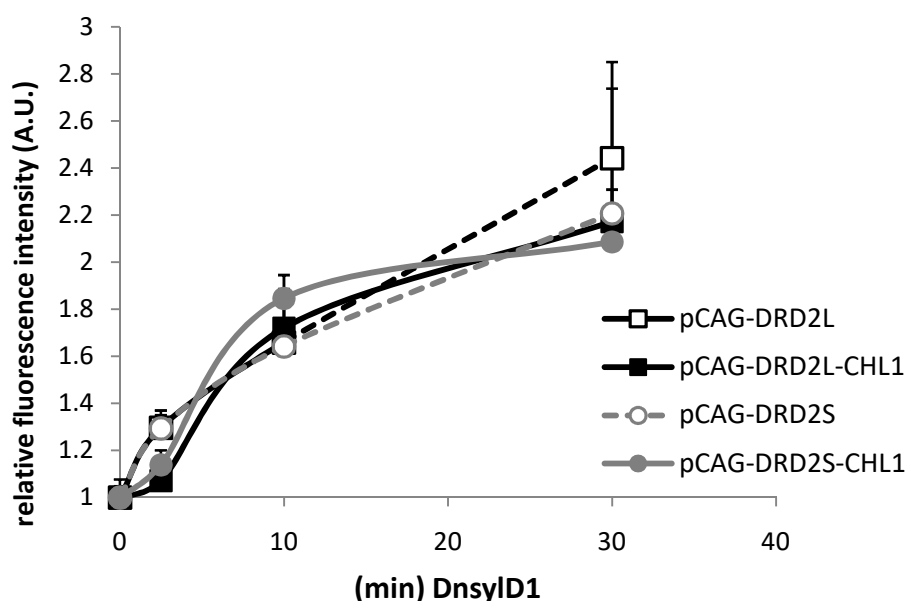


**Figure 25:**

**CHL1 does not influence dopamine analog binding to DRD2S and DRD2L.** Graph presents the result of dopamine binding assay performed on transfected HEK293 cells expressing DRD2L alone (pCAG-DRD2L),

DRD2L with CHL1 (pCAG-DRD2L-CHL1), DRD2S alone (pCAG-DRD2S) and DRD2S with CHL1 (pCAG-DRD2S-CHL1). Cells were treated with the fluorescent dopamine analog DnsyID1 for 0, 2.5, 10 and 30 minutes, bound DnsyID1 was measured and the cells were subjected to in-cell Western using anti-DRD2 and anti-GAPDH primary antibodies followed by fluorescently-labeled secondary antibodies. The fluorescence intensity of DRD2 was calculated relative to the fluorescence intensity of GAPDH and the obtained values were used to normalize the results of DnsyID1 binding. Presented are means  $\pm$ SEM from two independent experiments performed in duplicates. Abbreviations: A.U. – arbitrary units, CHL1 – close homolog of L1, DRD2L – dopamine receptor D2 “long”, DRD2S – dopamine receptor D2 “short”, pCAG – mammalian expression vector with CAG (cytomegalovirus enhancer, promoter and first exon and first intron of chicken beta-actin, splice acceptor of rabbit beta-globin) promoter.

#### **8.2.5. CHL1 does not affect intracellular signaling pathways triggered by DRD2 stimulation with quinpirole in transfected HEK293 cells**

Stimulation of DRD2 causes dissociation of bound G-proteins from the receptor and subsequent modulation of different intracellular signaling pathways, components of which, among many others, are: ERK, DARPP32 and TH. Regulation of phosphorylation of these proteins controls their activity and down-stream signaling (Lindgren et al., 2003).

Since CHL1 binds to DRD2 and affects its cell surface levels, it was interesting to analyze if CHL1 can affect the activation of intracellular signaling pathways triggered by agonist binding to DRD2. DRD2L, the predominantly post-synaptic DRD2 form, is expressed in the striatum, where ligands binding to DRD2L cause changes in the phosphorylation of DARPP32 and ERK (Beaulieu & Gainetdinov, 2011; Chen et al., 2012). Knowing that HEK293 cells do not express DARPP32, I introduced this protein into the cells via co-transfection with a plasmid construct carrying DARPP32 and a plasmid construct carrying DRD2L alone or DRD2L with CHL1. As control, cells were co-transfected with a plasmid construct carrying DARPP32 and a control pCAG-GFP plasmid. Two days after transfection cells were stimulated with quinpirole for 0, 5, 10, 15, 30 and 60 minutes and lysates of the stimulated cells were analyzed on Western Blots using antibodies against phosphorylated ERK (pERK), ERK, pDARPP32 and DARPP32. Pictures of the blots were analyzed using ImageJ where intensities of bands were measured and then the intensities of bands representing levels of phosphorylated (pERK and pDARPP32) proteins were calculated relative to intensities of bands representing total (ERK and DARPP32) proteins. Interestingly, in this experiment no statistically significant impact of CHL1 on phosphorylation of DARPP32 (**Figure 26**) and ERK (**Figure 27**) upon DRD2L stimulation with quinpirole was observed.

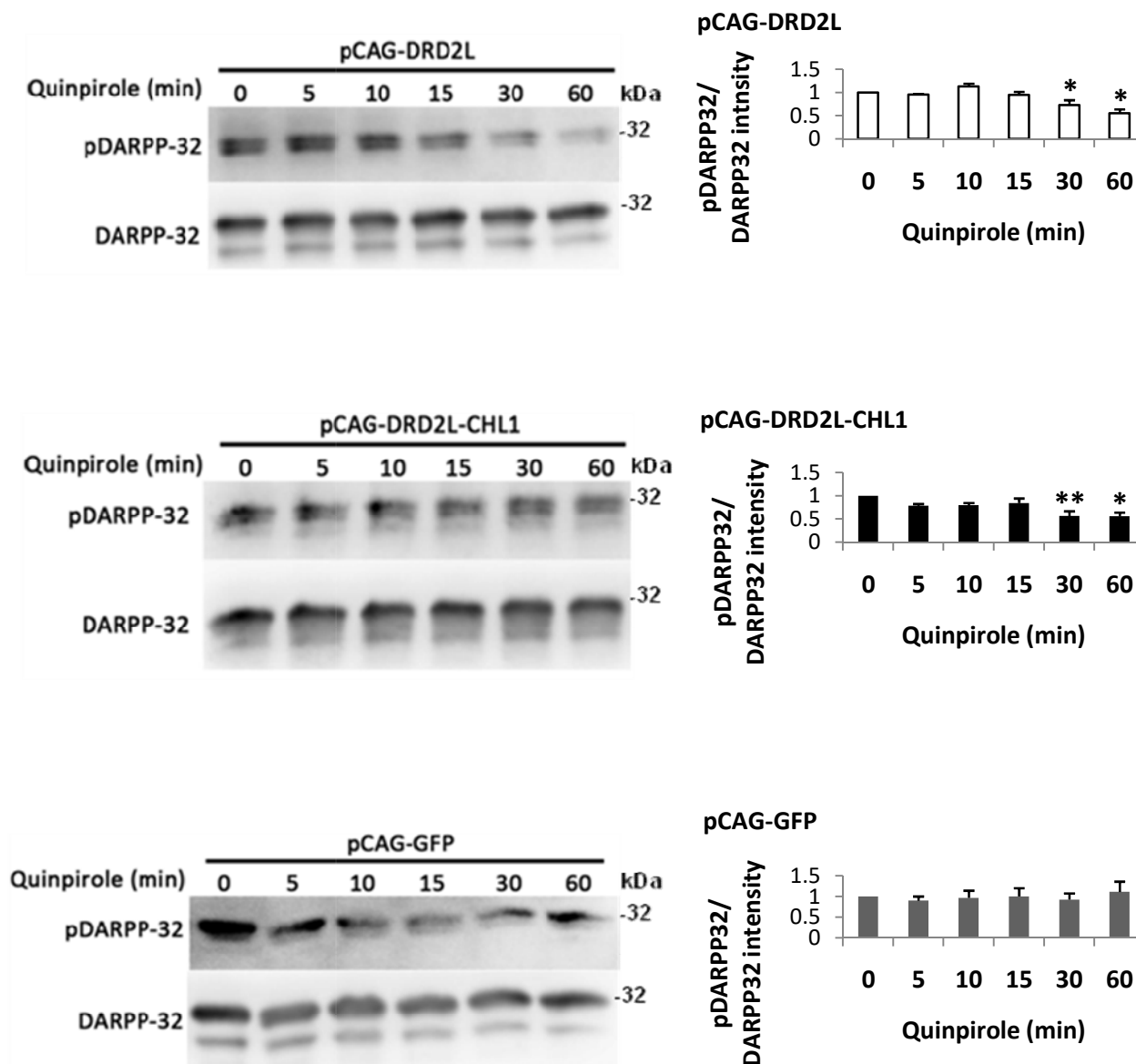


**Figure 26:**

**CHL1 does not affect DARPP32 phosphorylation upon DRD2L stimulation with quinpirole.** Representative blots (left) and graphs (right) present levels of pDARPP32 in HEK293 cells co-expressing DARPP32 and DRD2L (pCAG-DRD2L), DARPP32 and DRD2L with CHL1 (pCAG-DRD2L-CHL1) or DARPP32 and the control plasmid (pCAG-GFP) stimulated with quinpirole for 0, 5, 10, 15, 30 and 60 minutes. The whole cell lysates of the cells were analyzed on Western Blots using antibodies against pDARPP32(Thr34) and DARPP32, the intensity of the bands were measured and the values obtained for phosphorylated proteins were normalized to total proteins, with the relative pDARPP32 amounts in cells stimulated with quinpirole for 0 minutes set to 1. In graphs presented are means +SEM from 3-6 independent experiments. Statistical comparison of cells expressing pCAG-DRD2L and cells expressing pCAG-DRD2L-CHL1 regarding DARPP32 phosphorylation showed no impact of CHL1. Results of one-way ANOVA followed by *post-hoc* Holm-Bonferroni performed within construct vs. 0 min quinpirole:  $p < 0.05^*$ ,  $0.01^{**}$ . **Abbreviations:** CHL1 – close homolog of L1, DARPP32 – dopamine- and cyclic adenosine monophosphate-regulated neuronal phosphoprotein 32 kDa, DRD2L – dopamine receptor D2 “long”, GFP – green fluorescent protein, pCAG – mammalian expression vector with CAG (cytomegalovirus enhancer, promoter and first exon and first intron of chicken beta-actin, splice acceptor of rabbit beta-globin) promoter, pDARPP32 – phosphorylated dopamine- and cyclic adenosine monophosphate-regulated neuronal phosphoprotein 32 kDa.

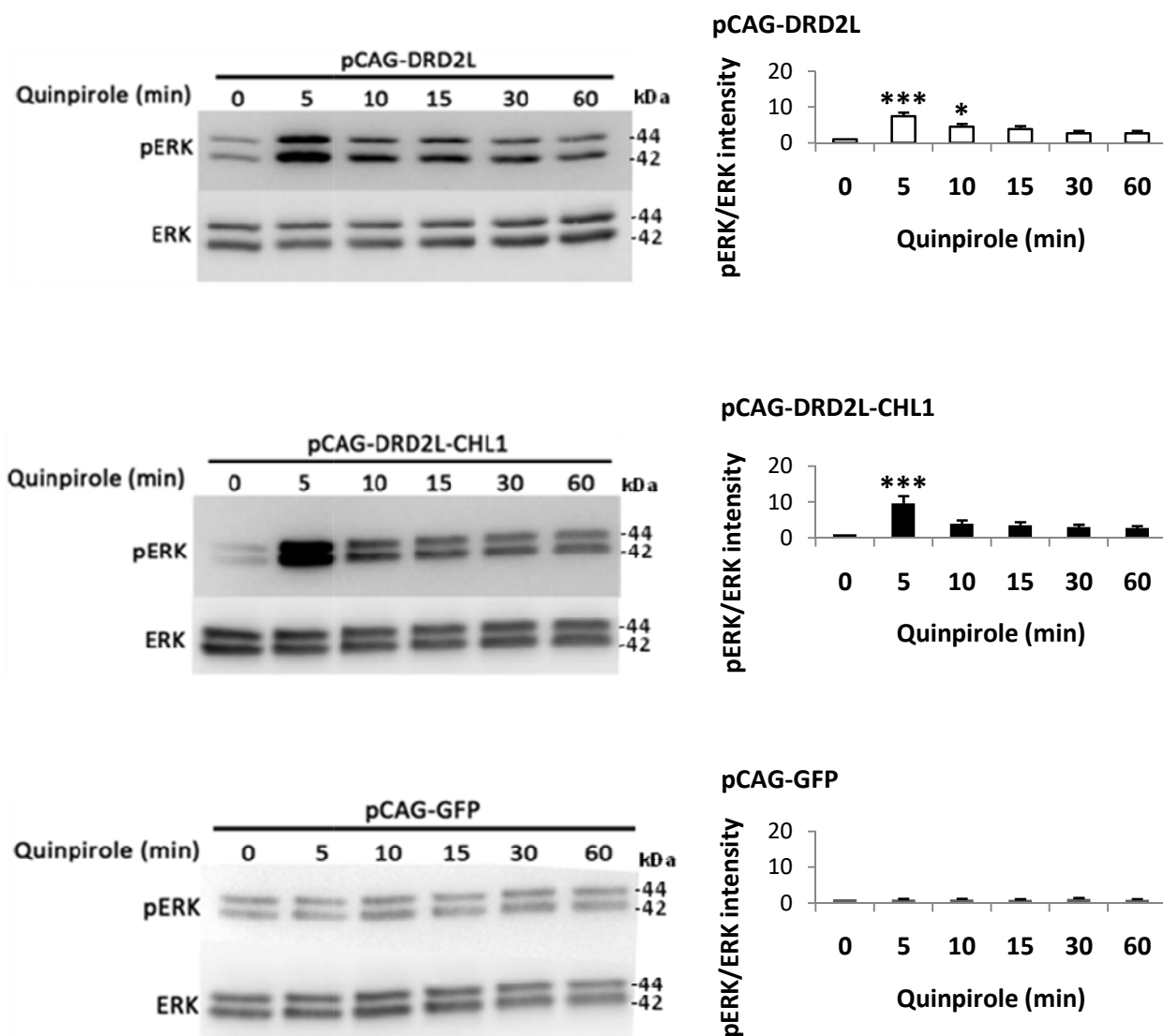
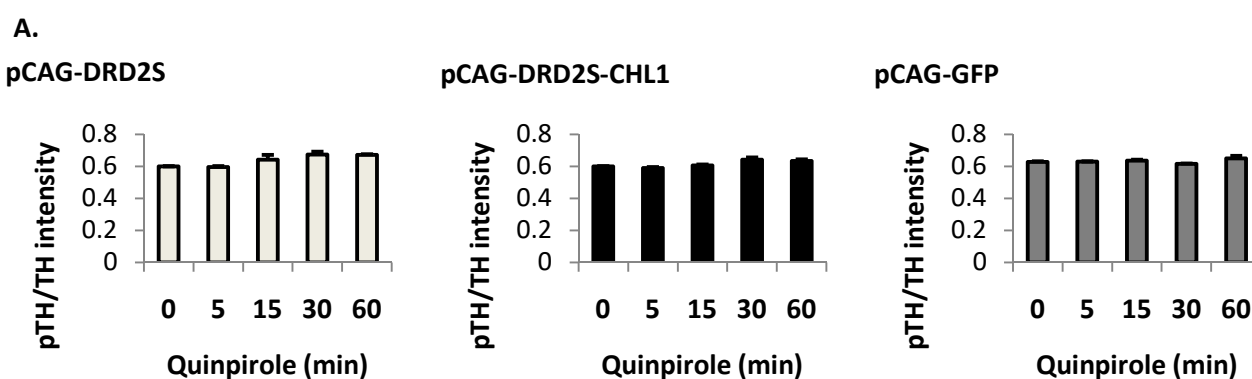


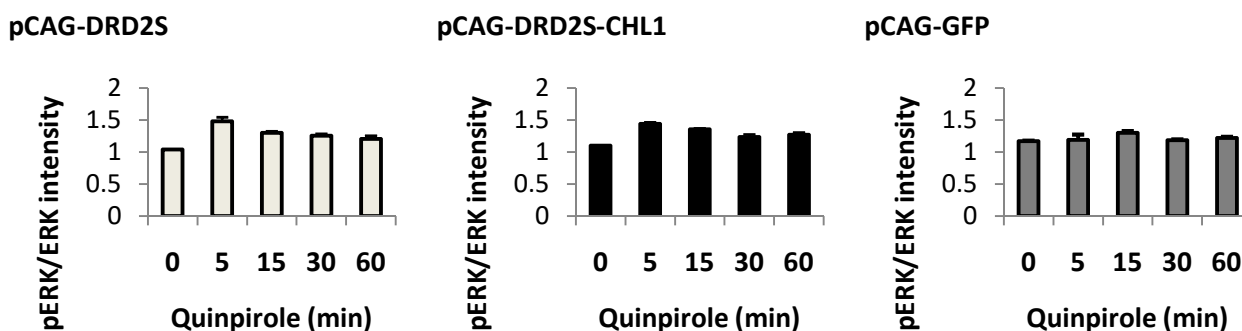
**Figure 27:**

**CHL1 does not affect the level of phosphorylated ERK upon DRD2L stimulation with quinpirole.** Shown are representative blots (left) and graphs (right) presenting levels of pERK in HEK293 cells co-expressing DARPP32 and DRD2L (pCAG-DRD2L), DARPP32 and DRD2L with CHL1 (pCAG-DRD2L-CHL1) or DARPP32 and the control plasmid (pCAG-GFP) stimulated with quinpirole for 0, 5, 10, 15, 30 and 60 minutes. Cell homogenates were analyzed on Western Blots using antibodies against pERK and ERK, and the intensities of the bands were measured. Intensities of bands representing phosphorylated proteins were calculated relative to total proteins, with the relative pERK amounts in cells stimulated with quinpirole for 0 minutes set to 1. Graphs present means +SEM from 3-6 independent experiments. Statistical comparison of cells expressing pCAG-DRD2L and cells expressing pCAG-DRD2L-CHL1 regarding ERK phosphorylation showed no impact of CHL1. Results of one-way ANOVA followed by *post-hoc* Holm-Bonferroni performed within construct vs. 0 min quinpirole:  $p < 0.05^*$ ,  $0.001^{***}$ . Abbreviations: CHL1 – close homolog of L1, DRD2L – dopamine receptor D2 “long”, ERK – extracellular-signal-regulated kinase, GFP – green fluorescent protein, pCAG – mammalian expression vector with CAG (cytomegalovirus enhancer, promoter and first exon and first intron of chicken beta-actin, splice acceptor of rabbit beta-globin) promoter, pERK – phosphorylated extracellular-signal-regulated kinase.

DRD2S is the mainly pre-synaptic form of DRD2 and it is expressed by dopaminergic neurons, where it functions as an autoreceptor that regulates the amount of dopamine in the synapse by regulating the activity (phosphorylation) of TH – the rate-limiting enzyme in dopamine production. Phosphorylation of TH is influenced by ligands binding to DRD2S (Lindgren et al., 2003). Apart from TH, activation of presynaptic ERK is also regulated by DRD2S ligands (Chen et al., 2012). In order to determine the impact of CHL1 on the phosphorylation of TH induced by quinpirole binding to DRD2S, HEK293 cells were co-transfected with a plasmid construct carrying TH and either a plasmid construct carrying DRD2S alone or DRD2S with CHL1. As control, cells were co-transfected with a plasmid construct carrying TH and a pCAG-GFP plasmid. Cells were stimulated with the DRD2 agonist quinpirole for 0, 15, 30, 45 and 60 minutes, then fixed and in-cell Western was performed on the cells using a combination of anti-pERK with anti-ERK or anti-pTH with anti-TH antibodies followed by a combination of two different fluorescently-labeled secondary antibodies. Intensities of fluorescence of the stained proteins were measured using a fluorescent plate reader and the values for the phosphorylated proteins were calculated relative to the total proteins. Interestingly, no impact of CHL1 on phosphorylation of TH (**Figure 28.A**) and ERK (**Figure 28.B**) after stimulation of DRD2S with quinpirole was found. Of note, stimulation of DRD2S with its agonist quinpirole did not induce any changes in phosphorylation of TH as the normalized values for the pTH were similar in cells expressing DRD2S alone, DRD2S with CHL1 and in cells expressing the control plasmid. This result indicates that quinpirole stimulation of DRD2S expressed by HEK293 cells does not lead to activation of the same down-stream signaling pathways that are triggered in dopaminergic neurons after stimulation of DRD2S.



B.

**Figure 28:**

**CHL1 does not affect TH and ERK phosphorylation upon DRD2S stimulation with quinpirole.** Graphs present the result of in-cell Western performed on HEK293 cells co-expressing a construct carrying TH with a construct carrying DRD2S alone (pCAG-DRD2S), DRD2S with CHL1 (pCAG-DRD2S-CHL1) or control plasmid (pCAG-GFP). Cells were stimulated with DRD2 agonist quinpirole for 0, 5, 15, 30 and 60 minutes. The in-cell Western was performed using anti-pTH(Ser40) and anti-TH primary antibodies (A) or anti-pERK and anti-ERK primary antibodies (B) followed by fluorescently labeled secondary antibodies. Intensities of fluorescence of the stained proteins were measured and the values obtained for phosphorylated proteins were calculated relative to total proteins. Presented are means +SEM from one experiment performed in duplicate. **Abbreviations:** CHL1 – close homolog of L1, DRD2S – dopamine receptor D2 “short”, ERK – extracellular-signal-regulated kinase, GFP – green fluorescent protein, pCAG – mammalian expression vector with CAG (cytomegalovirus enhancer, promoter and first exon and first intron of chicken beta-actin, splice acceptor of rabbit beta-globin) promoter, pERK – phosphorylated extracellular-signal-regulated kinase, pTH – phosphorylated tyrosine hydroxylase, TH – tyrosine hydroxylase.

### 8.2.6. Loss of CHL1 leads to altered levels of DRD2, pDARPP32, DARPP32 and pTH in dorsal and ventral striatum of mice

Since DRD2 and CHL1 co-localize in the striatum and CHL1 affects the internalization of DRD2 in response to the DRD2 agonist quinpirole, I analyzed if the striatal expression of DRD2 and of proteins involved in the intracellular signaling triggered by DRD2 are affected by lack of CHL1 in mice. For this aim, dorsal and ventral striata of adult CHL1<sup>-/-</sup> and CHL1<sup>+/+</sup> mice were subjected to Western Blot analysis using antibodies against CHL1, DRD2 and against the phosphorylated and not phosphorylated (total) pre- and post-synaptic targets of the DRD2 signaling pathways, which are TH and DARPP32, respectively. Intensities of the obtained bands were measured in ImageJ and the values for the total proteins were calculated relative to GAPDH or  $\beta$ -tubulin whereas the values for the phosphorylated proteins were calculated relative to total proteins upon the values of total protein levels were calculated relative to GAPDH or  $\beta$ -tubulin. Statistical analysis showed that CHL1<sup>-/-</sup> mice have less DRD2 (Figure 31) and pTH (Figure 30) in their dorsal striatum and less pDARPP32 (Figure 29) but more DARPP32 (Figure 29) in their ventral striatum. Interestingly, the analysis showed also that the dorsal and the ventral striatum of CHL1<sup>+/+</sup> mice differ regarding expression of all the analyzed proteins while in case of CHL1<sup>-/-</sup> mice the dorsal and the ventral striatum differ only regarding the expression of TH (Figure 30).

These results show that lack of CHL1 affects expression and phosphorylation of proteins in the dorsal striatum and the ventral striatum of adult mice.

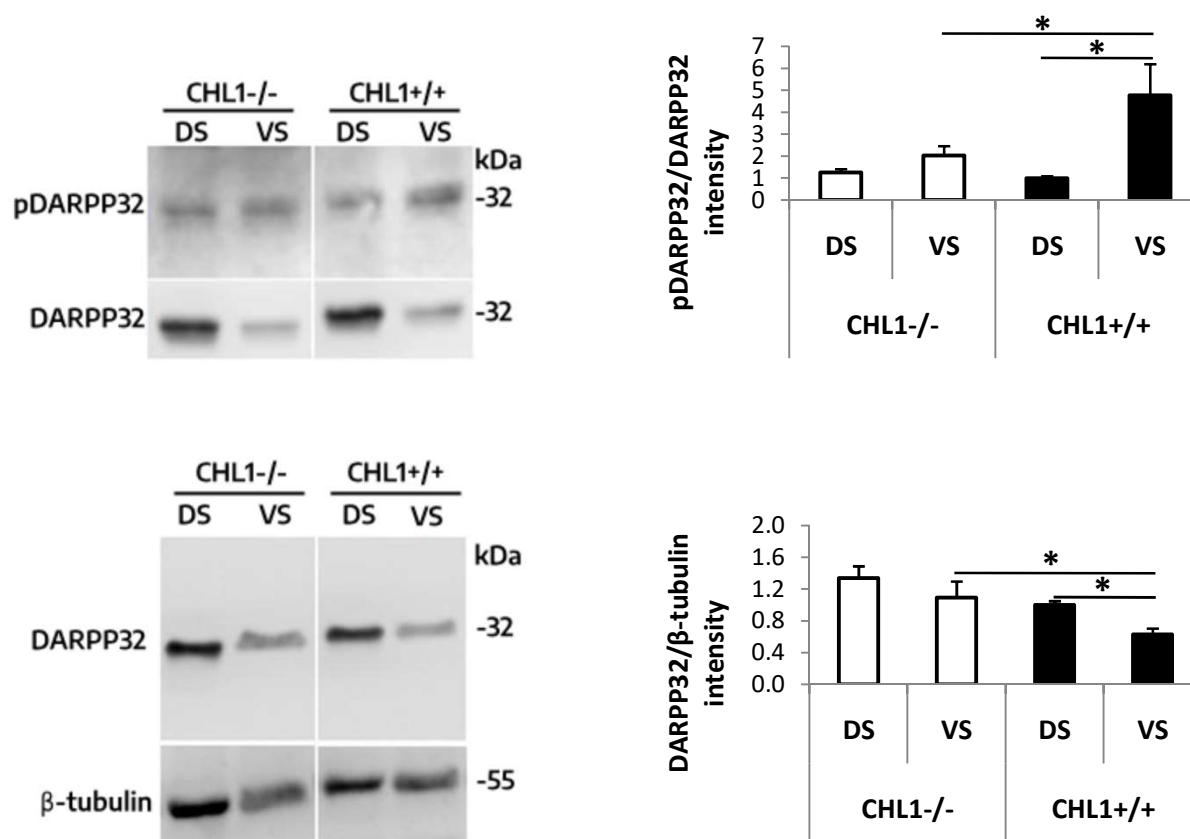


**Figure 29:**

**CHL1 affects the level of pDARPP32 and DARPP32 in the ventral striatum of adult mice.** Left: presented are representative blots of lysates of dorsal (DS) and ventral striata (VS) of 3-5-months old CHL1<sup>-/-</sup> and CHL1<sup>+/+</sup> mice subjected to Western Blot analysis using antibodies against pDARPP32(Thr34), DARPP32 and  $\beta$ -tubulin. Right: graphs represent the results of the Western Blot analysis of the amounts of pDARPP32 and DARPP32 in dorsal and ventral striata of CHL1<sup>-/-</sup> (n=8) and CHL1<sup>+/+</sup> (n=11) mice of mixed genders. The intensities of Western Blot bands representing DARPP32 were calculated relative to  $\beta$ -tubulin and the values for pDARPP32 were calculated relative to intensities of bands representing DARPP32 upon the intensities of bands representing  $\beta$ -tubulin. One-way ANOVA followed by *post-hoc* Student Newman-Keul's test were performed. Presented are means +SEM.  $p < 0.05^*$ . Abbreviations: CHL1<sup>-/-</sup> – mice knock-out for close homolog of L1, CHL1<sup>+/+</sup> – wild-type mice, DARPP32 – dopamine- and cyclic adenosine monophosphate-regulated neuronal phosphoprotein 32 kDa, DS – dorsal striatum, pDARPP32 – phosphorylated dopamine- and cyclic adenosine monophosphate-regulated neuronal phosphoprotein 32 kDa, VS – ventral striatum.

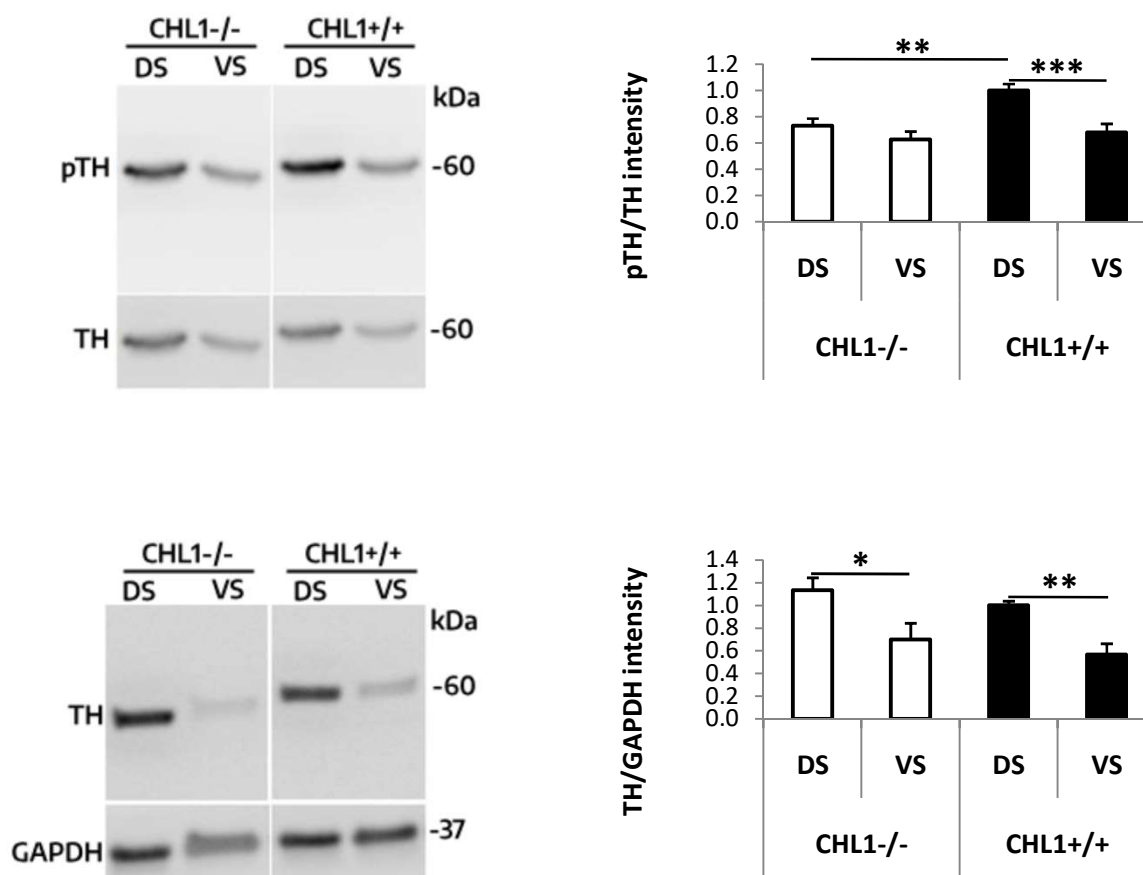


**Figure 30:**

**CHL1 influences pTH level in the dorsal striatum of adult mice.** Representative blots (left) of lysates of dorsal and ventral striata of 3-5-months old CHL1<sup>-/-</sup> and CHL1<sup>+/+</sup> mice subjected to Western Blot analysis using antibodies against pTH(Ser40), TH and GAPDH are shown. Intensities of Western Blot bands were measured and intensities of bands representing TH were calculated relative to GAPDH whereas intensities of pTH were calculated relative to TH upon the intensities of bands representing TH were calculated relative to GAPDH. Graphs (right) represent the results of the Western Blot analysis of the amounts of pTH and TH in dorsal and ventral striata of CHL1<sup>-/-</sup> (n=8) and CHL1<sup>+/+</sup> (n=11) mice of mixed genders. One-way ANOVA followed by *post-hoc* Student Newman-Keul's test were performed. Presented are means +SEM.  $p < 0.05^*$ ,  $0.01^{**}$ ,  $0.001^{***}$ . **Abbreviations:** CHL1<sup>-/-</sup> – mice knock-out for close homolog of L1, CHL1<sup>+/+</sup> – wild-type mice, DS – dorsal striatum, GAPDH – glyceraldehyde 3-phosphate dehydrogenase, pTH – phosphorylated tyrosine hydroxylase, TH – tyrosine hydroxylase, VS – ventral striatum.

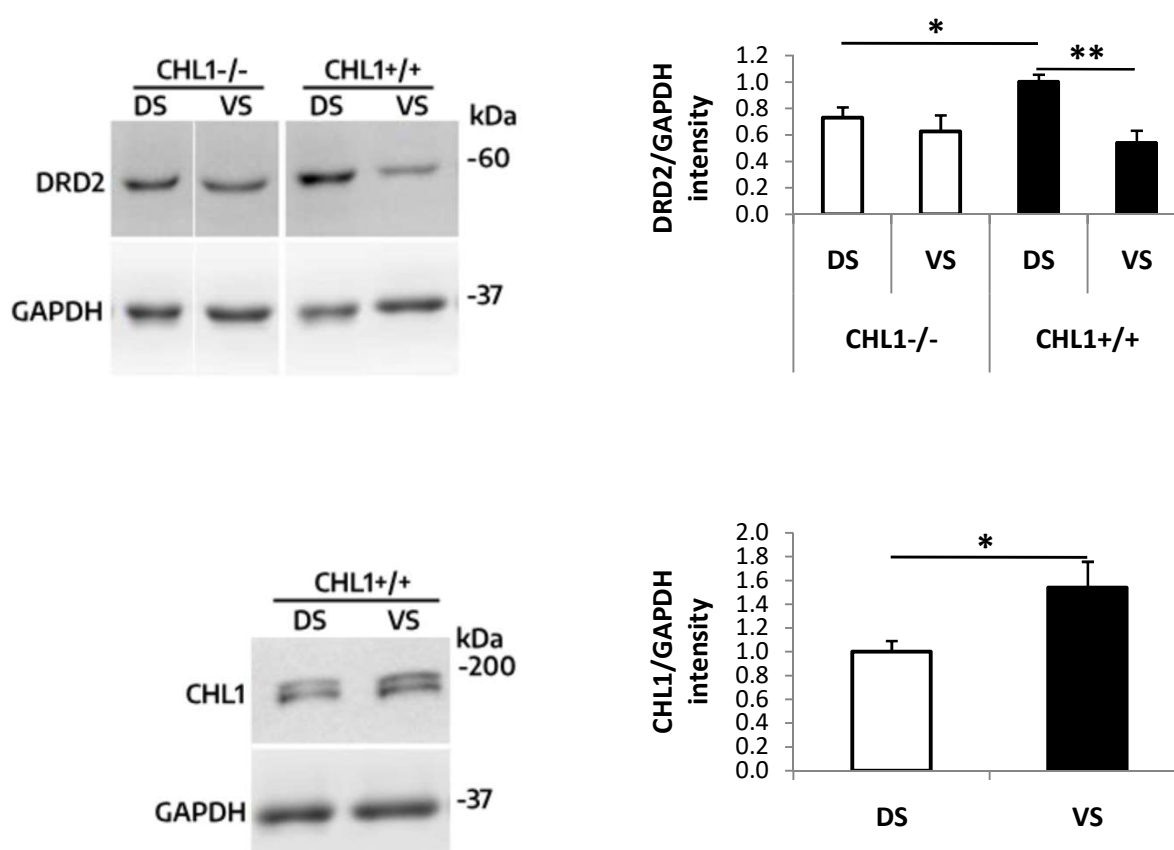


**Figure 31:**

**Mice lacking CHL1 present reduced level of DRD2 in the dorsal striatum.** Shown are representative blots (left) of lysates of dorsal and ventral striata of 3-5-months old CHL1<sup>-/-</sup> and CHL1<sup>+/+</sup> mice subjected to Western Blot analysis using antibodies against DRD2, CHL1 and GAPDH. Graphs (right) represent the results of the analysis of DRD2 and CHL1 levels in dorsal and ventral striata of CHL1<sup>-/-</sup> (n=8) and CHL1<sup>+/+</sup> (n=11) mice of mixed genders: intensities of DRD2 and CHL1 bands were calculated relative to intensities of GAPDH bands. To compare CHL1 levels in dorsal and ventral striata of CHL1<sup>+/+</sup> mice two-tailed Student's *t*-test was performed. To compare amounts of DRD2 in dorsal and ventral striata of CHL1<sup>-/-</sup> and CHL1<sup>+/+</sup> mice one-way ANOVA followed by *post-hoc* Student Newman-Keul's test were performed. Presented are means +SEM.  $p < 0.05^*$ ,  $0.01^{**}$ . **Abbreviations:** CHL1 – close homolog of L1, CHL1<sup>-/-</sup> – mice knock-out for close homolog of L1, CHL1<sup>+/+</sup> – wild-type mice, DRD2 – dopamine receptor D2, DS – dorsal striatum, GAPDH – glyceraldehyde 3-phosphate dehydrogenase, VS – ventral striatum.

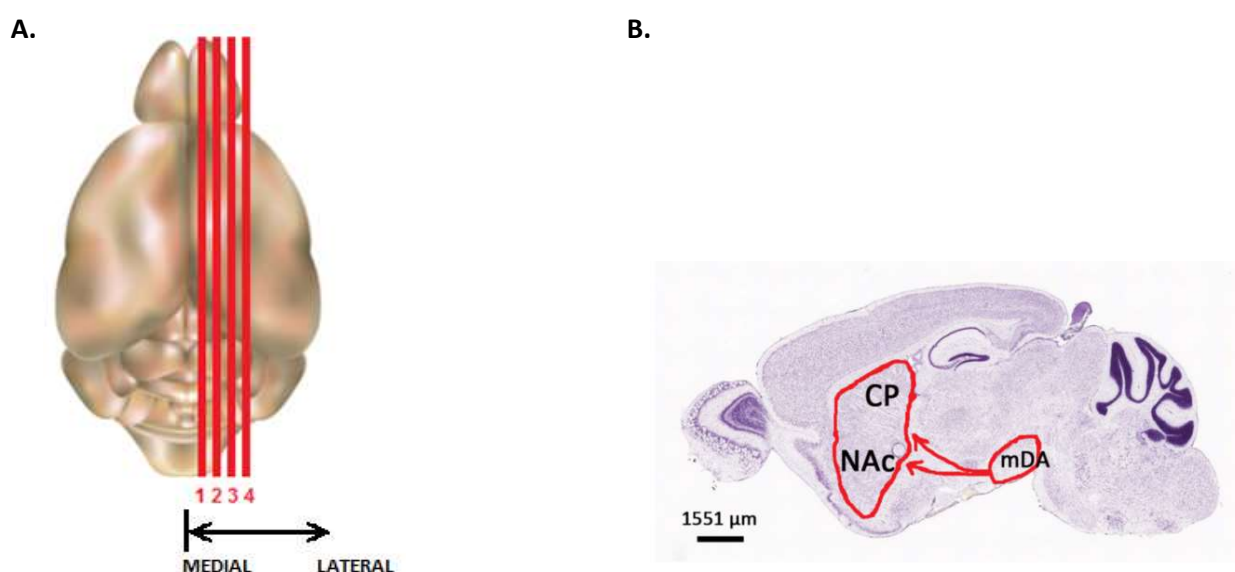
### 8.3. Characterization of dopaminergic projections running from the ventral midbrain to the striatum in CHL1<sup>-/-</sup> mice

Recent reports show that CHL1 is involved in development of the dopaminergic system and important for survival of dopaminergic neurons, e.g. it was reported that CHL1 affects differentiation and migration of dopaminergic progenitors (Alsanie et al., 2017), outgrowth and branching of dopaminergic neurites (Alsanie et al., 2017) and survival of transplanted dopaminergic progenitors (Bye et al., 2015). Moreover, the CHL1-related disorders in humans strongly rely on the morphology of the brain: schizophrenia (Sakurai et al.,

2002; Chen et al., 2005; Shaltout et al., 2013) is associated with abnormal morphology of multiple brain structures (Brickman et al., 2004; Vita et al., 2006; Goldman et al., 2009) and 3p-syndrome is associated with impaired language development (Pohjola et al., 2010; Cuoco et al., 2011; Tassano et al., 2014; Bertini et al., 2017) that strongly relies on the proper morphology of the striatum (De Diego-Balaguer et al., 2008). In summary, these results suggest that CHL1 expression might influence the shape and the formation of dopaminergic projections. Therefore, my next aim was to characterize the impact of CHL1 on the formation of the dopaminergic projections running from the ventral midbrain (SN and VTA) to the dorsal and the ventral striatum. Thus I analyzed the dopaminergic fibers running to the striatum and entering the striatum, the dopaminergic fibers density in the striatum and the amount of the dopaminergic neurons in the midbrain of CHL1<sup>-/-</sup> mice and their CHL1<sup>+/+</sup> littermates.

### 8.3.1. CHL1<sup>-/-</sup> mice have more dopaminergic fibers running to the ventral striatum than CHL1<sup>+/+</sup> mice

To characterize the morphology of the dopaminergic system in the CHL1<sup>-/-</sup> mouse brain, first the fibers of the nigrostriatal and of the mesolimbic dopaminergic projections, which start in the ventral midbrain and run to the dorsal striatum (the nigrostriatal projection) and to the ventral striatum (the mesolimbic projection), were analyzed. For that purpose, sagittal sections of adult CHL1<sup>-/-</sup> and CHL1<sup>+/+</sup> mouse brains were immunofluorescently stained for TH, which is a marker for dopaminergic neurons. Pictures of stained sections (**Figure 32.C, Figure 33**) were taken at a fluorescence microscope.



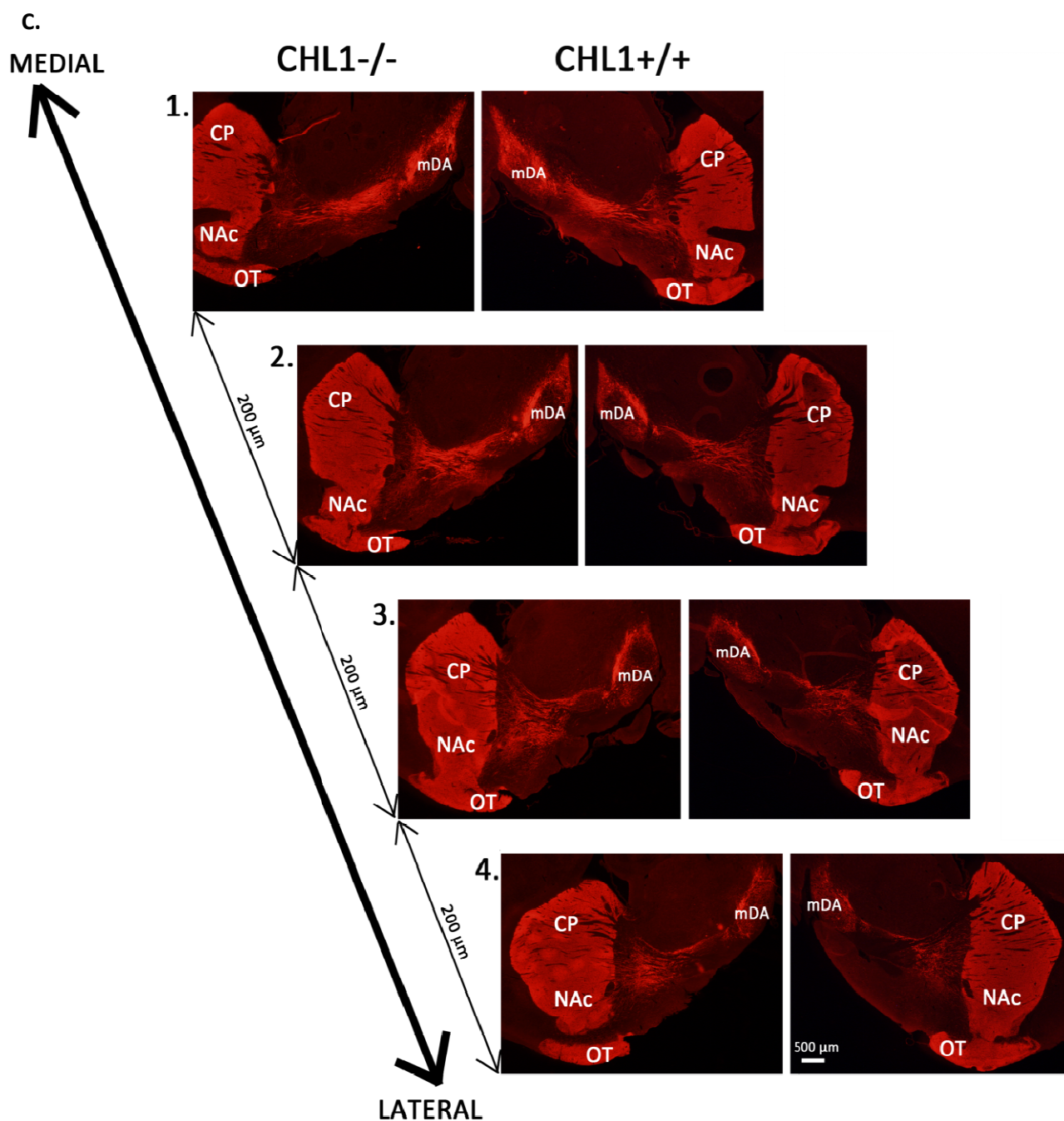


**Figure 32:**

**Method for the collection of sagittal sections for the analysis of the dopaminergic fibers running from the ventral midbrain to the striatum.** **A)** Presentation of the levels from which the sagittal sections were chosen. Number 1 marks the level from which the most medial sections were collected (about 1000 μm laterally off the intrahemispheric fissure) and number 4 marks the level for the most lateral sections (about 1800 μm laterally off the intrahemispheric fissure). Between levels is always a 200-μm distance. **B)** Picture of a sagittal mouse brain section stained with Nissl method. mDA project to dorsal striatum (CP) and ventral striatum (NAc). The picture was modified from: Allen Brain Atlas: Mouse Brain Map. **C)** Representative fluorescence microscope images from the right hemisphere of 3-4.5 months old CHL1<sup>-/-</sup> and CHL1<sup>+/+</sup> mouse brains. Every tenth 20 μm-thick sagittal section was immunofluorescently stained against TH (red). 1. represents the most medial and 4. represents the most lateral sections. mDA projecting to the CP and to the NAc can be seen. Scale bar: 500 μm. **Abbreviations:** CHL1<sup>-/-</sup> – mice knock-out for close homolog of L1, CHL1<sup>+/+</sup> – wild-type mice, CP – caudate and putamen, mDA – midbrain dopaminergic neurons, NAc – nucleus accumbens, OT – olfactory tubercle.

The area covered by the dopaminergic fibers and the fluorescence intensity of the dopaminergic fibers were analyzed in ImageJ. For an objective analysis of the projections, an arbitrary line connecting the anterior commissure (AC), which was considered as a border between the dorsal and the ventral striatum, with the bottom of the midbrain dopaminergic neurons (mDA) was drawn (**Figure 33**).

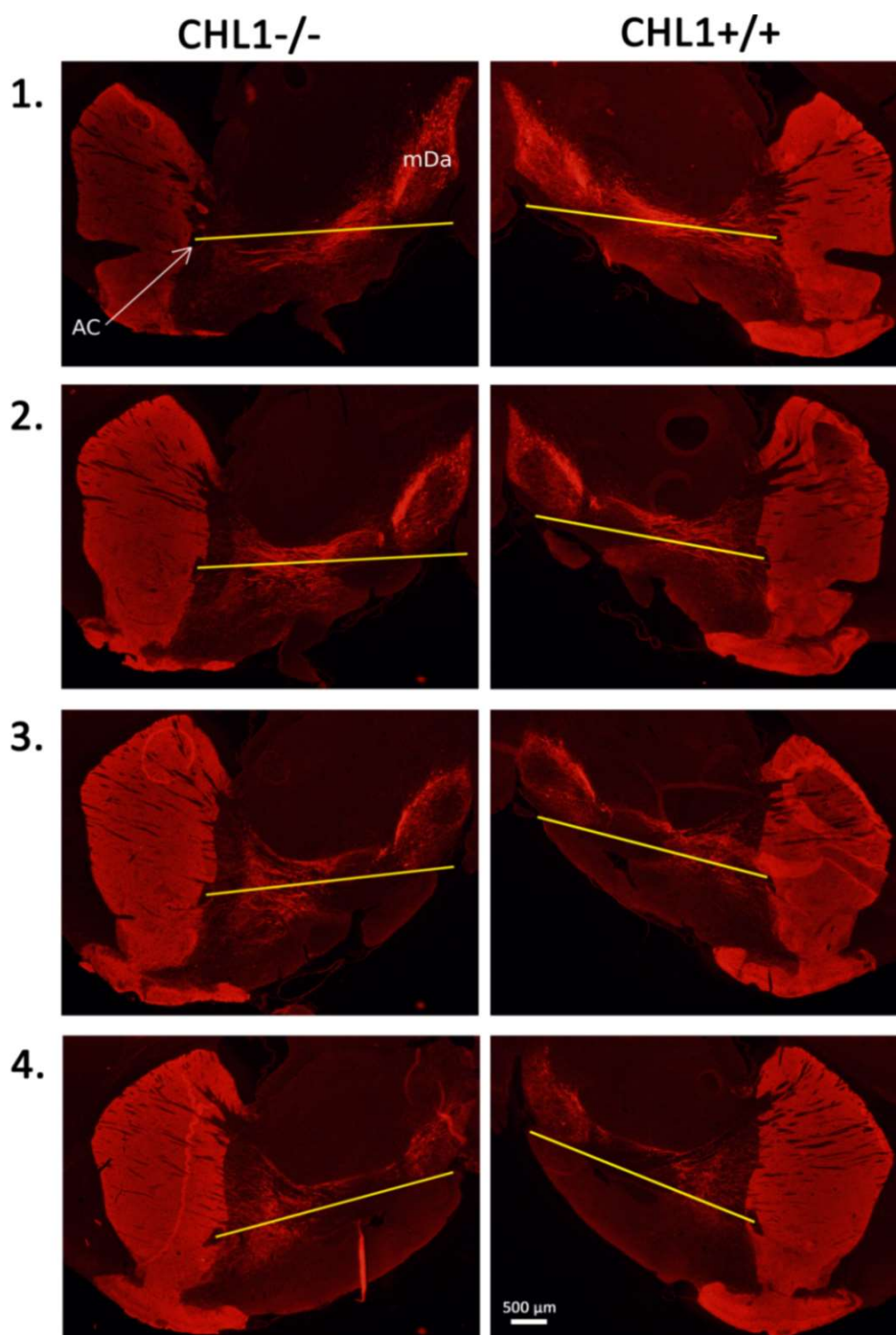


**Figure 33:** Separation of the dopaminergic fibers running from the ventral midbrain to the striatum into two portions. Representative fluorescence microscopic images of 20 µm-thick sagittal sections from brains of 3-4.5 months old female CHL1<sup>-/-</sup> and CHL1<sup>+/+</sup> mice are shown. The sections were collected 1000 to 1800 µm laterally off

the intrahemispheric fissure and every tenth section was stained using a primary antibody against TH followed by a fluorescently-labeled secondary antibody (red). Presented sections are separated by 200  $\mu\text{m}$  and organized in order 1.-4., where 1. is the most medial and 4. is the most lateral section. Yellow lines connecting the structure considered as border between dorsal and ventral striatum (AC) with the bottom of the mDA were drawn for objective quantification as well as better presentation of dopamine projections. Scale bar: 500  $\mu\text{m}$ . Abbreviations: AC – anterior commissure, CHL1<sup>-/-</sup> – mice knock-out for close homolog of L1, CHL1<sup>+/+</sup> – wild-type mice, mDA – midbrain dopaminergic neurons.

The fluorescence intensity (integrated density of the delineated projection reduced by background fluorescence measured on the thalamus, calculated as described by McCloy et al. (2014)) and the area covered by the dopaminergic fibers above and below the line were measured. Statistical analysis showed that the TH-stained projections below the arbitrary line cover larger area and show stronger fluorescence intensity in CHL1<sup>-/-</sup> mice than in CHL1<sup>+/+</sup> mice, while projections above the arbitrary line are similar in CHL1<sup>-/-</sup> mice and CHL1<sup>+/+</sup> mice (**Figure 34**, **Figure 36**). This result indicates that CHL1<sup>-/-</sup> mice have more dopaminergic fibers running to the ventral striatum and/or higher TH expression by these fibers, therefore lack of CHL1 may affect the mesolimbic dopaminergic pathway. When the intensity of fluorescence and the area of the dopaminergic projections were analyzed separately in males and females no gender-related differences were found (**Figure 35**, **Figure 37**).

In order to verify the result obtained from the analysis of the dopaminergic projections running from the ventral midbrain to the striatum using the sagittal sections of CHL1<sup>-/-</sup> and CHL1<sup>+/+</sup> mice brains, those dopaminergic projections were also looked at in horizontal sections stained for TH. Pictures of the stained sections were taken at a fluorescence microscope. In the pictures of the most ventral sections more dopaminergic fibers running to the striatum were detected in CHL1<sup>-/-</sup> mice than in CHL1<sup>+/+</sup> mice (**Figure 38**). This result confirms that CHL1<sup>-/-</sup> mice have more dopaminergic fibers running to the ventral striatum than CHL1<sup>+/+</sup> mice.

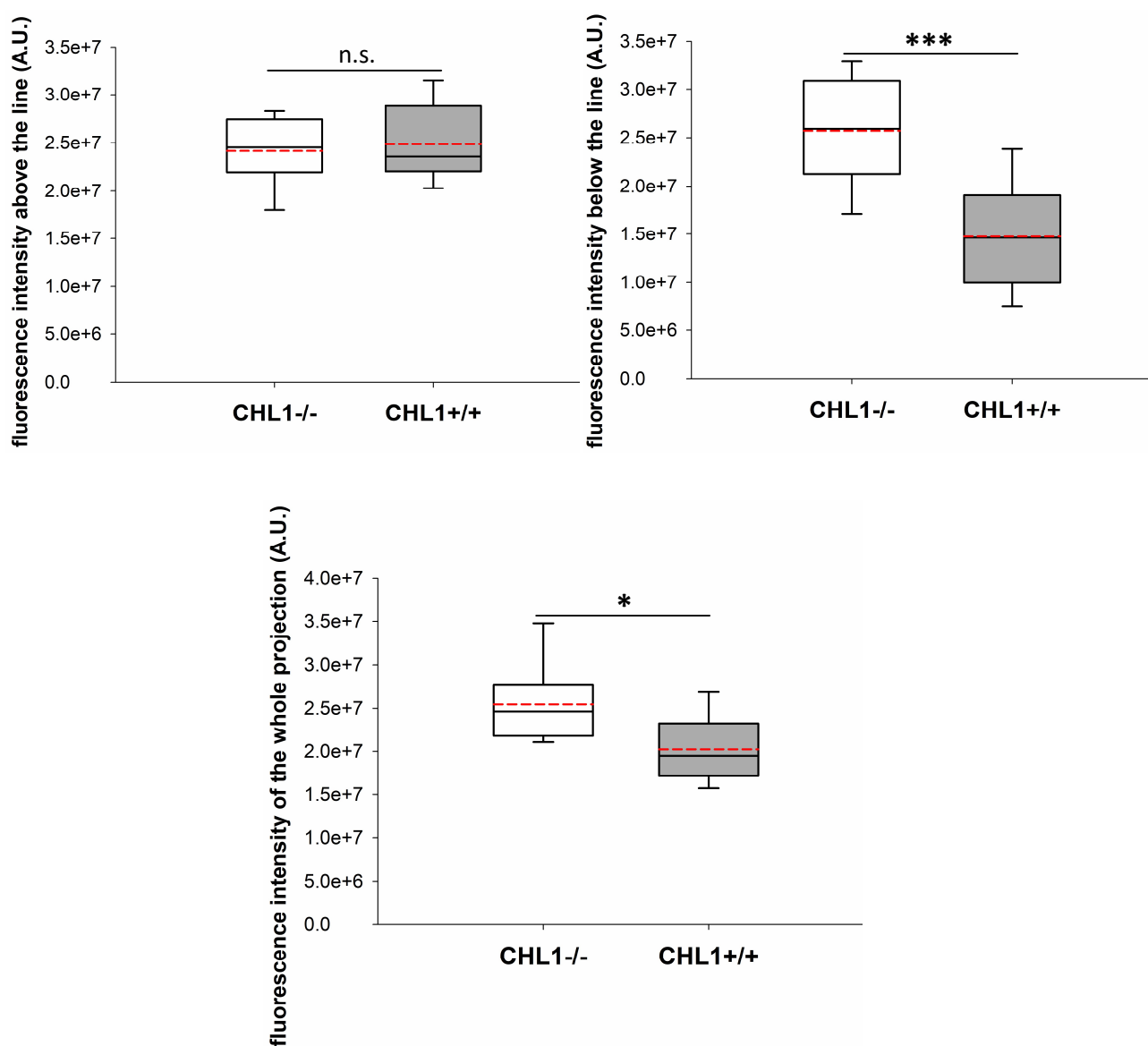


**Figure 34:**

**Dopaminergic fibers running to the ventral striatum in CHL1<sup>-/-</sup> mice show stronger fluorescence intensity.** The box plots represent fluorescence intensity of the fibers above and below the line (Figure 33) connecting AC with the bottom of mDA and of the whole projection for 8-9 animals per group of mixed genders. The fluorescence intensity of the dopaminergic fibers was measured in anti-TH immunofluorescently stained 20  $\mu$ m-thick sagittal sections of brains of 3-4.5-months old CHL1<sup>-/-</sup> and CHL1<sup>+/+</sup> mice of both genders. Red dotted line represents the mean. Results of the two-tailed Student's *t*-test or Mann-Whitney U-test:  $p < 0.05$ \*, 0.001\*\*\*. **Abbreviations:** A.U. – arbitrary units, CHL1<sup>-/-</sup> – mice knock-out for close homolog of L1, CHL1<sup>+/+</sup> – wild-type mice, mDA – midbrain dopaminergic neurons, n.s. – not significant.

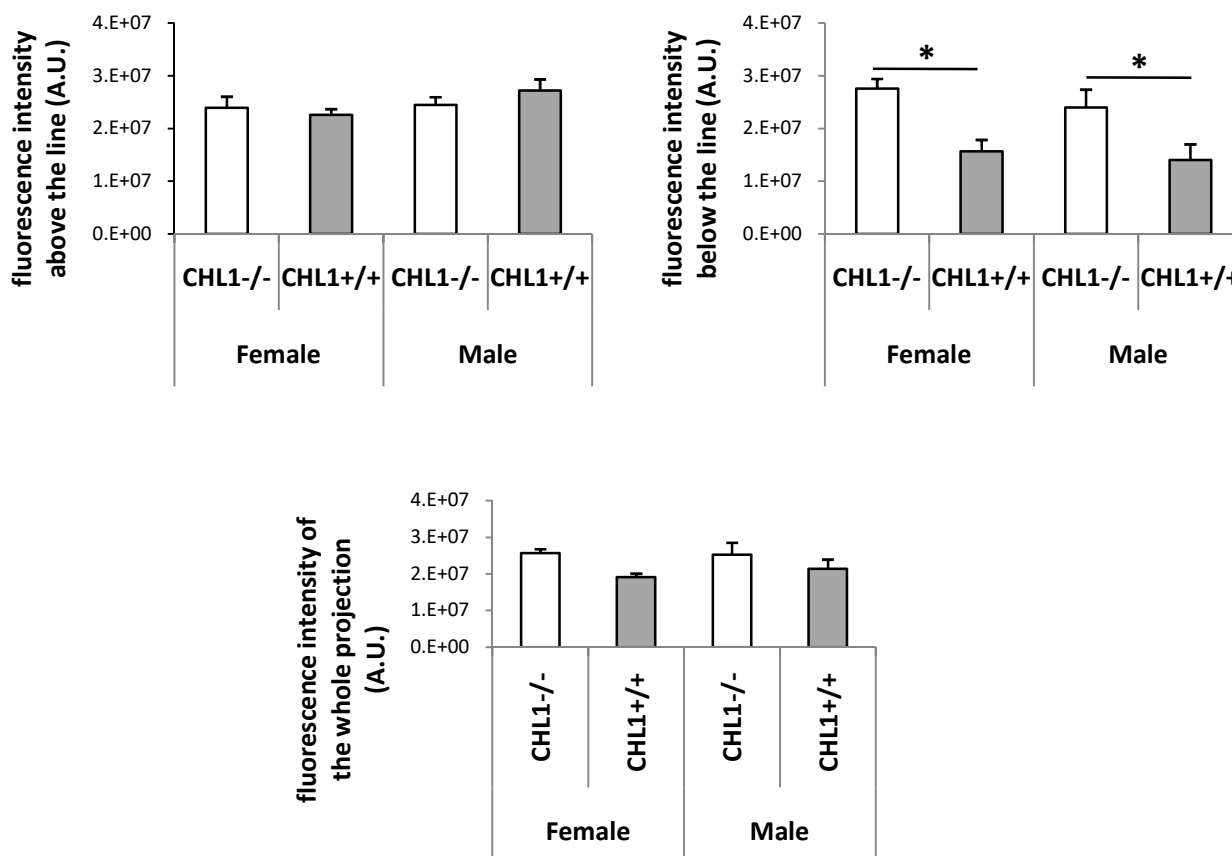


**Figure 35:**

**Dopaminergic fibers running from the ventral midbrain to the striatum have similar fluorescence intensity in male and female mice.** The bar graphs represent fluorescence intensity of the dopaminergic fibers running from the ventral midbrain to the striatum above the line connecting AC with bottom of mDA (**Figure 33**), below the line and of the whole projection measured in 20  $\mu$ m-thick anti-TH immunofluorescently stained sagittal sections of brains of 3-4.5-months old CHL1<sup>-/-</sup> and CHL1<sup>+/+</sup> mice. Presented are means +SEM for 4-5 animals per group of each gender. Results of one-way ANOVA followed by *post-hoc* Student Newman-Keul's test:  $p < 0.05^*$  are shown. Abbreviations: A.U. – arbitrary units, CHL1<sup>-/-</sup> – mice knock-out for close homolog of L1, CHL1<sup>+/+</sup> – wild-type mice.

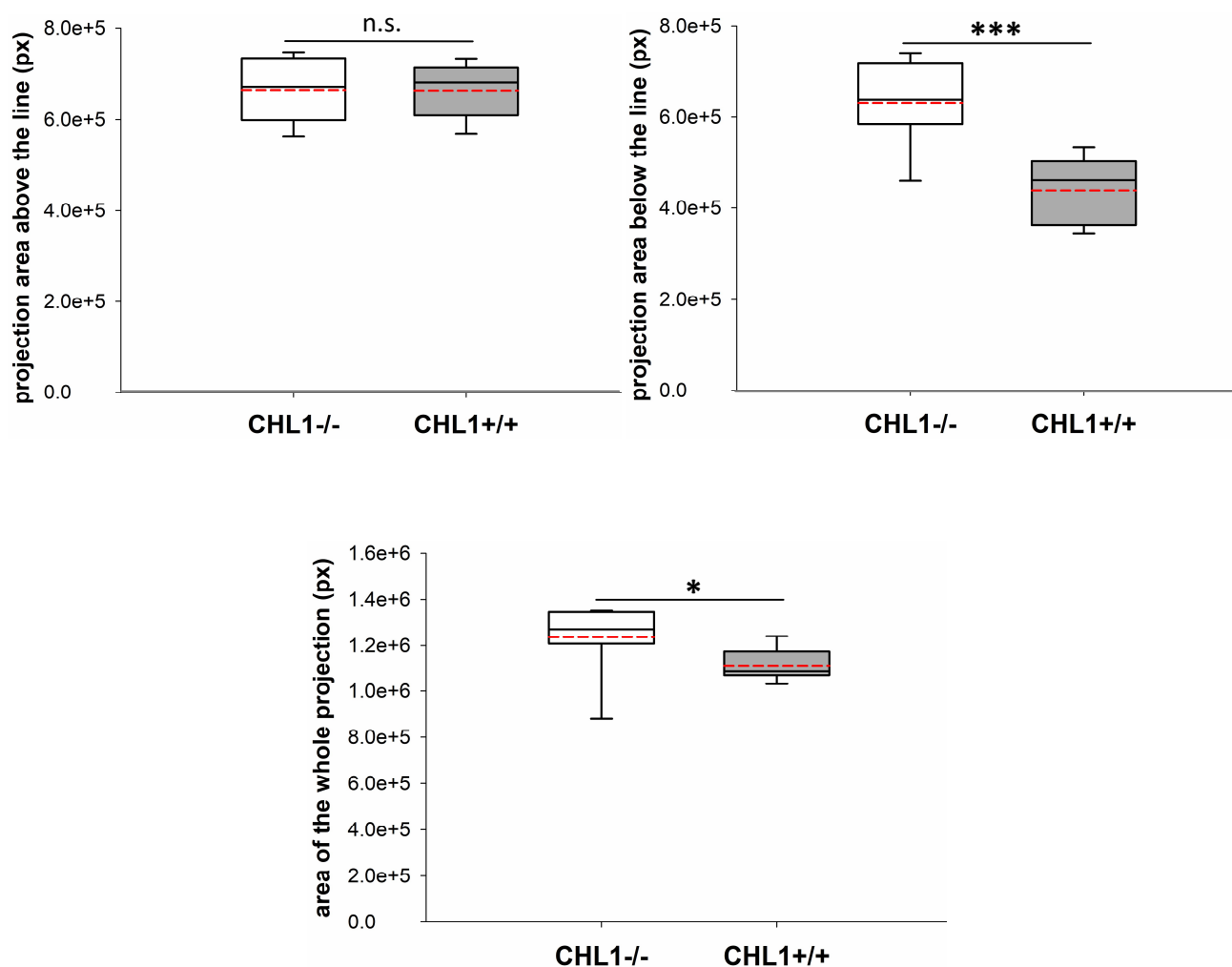


**Figure 36:**

**Dopaminergic fibers running to the ventral striatum in CHL1<sup>-/-</sup> mice cover a larger area.** The box plots represent the area covered by the dopaminergic fibers running from the ventral midbrain to the striatum in brains of 3-4.5-months old CHL1<sup>-/-</sup> and CHL1<sup>+/+</sup> mice (8-9 per group of mixed genders). The area was measured above and below the line connecting AC with bottom of mDA (**Figure 33**) and of the whole projection in anti-TH immunofluorescently stained 20  $\mu$ m-thick sagittal sections of the mouse brains. Red dotted line represents the mean. Results of the two-tailed Student's *t*-test or Mann-Whitney U-test:  $p < 0.05^*$ ,  $0.001^{***}$  are shown. Abbreviations: CHL1<sup>-/-</sup> – mice knock-out for close homolog of L1, CHL1<sup>+/+</sup> – wild-type mice, n.s. – not significant, px – pixels.

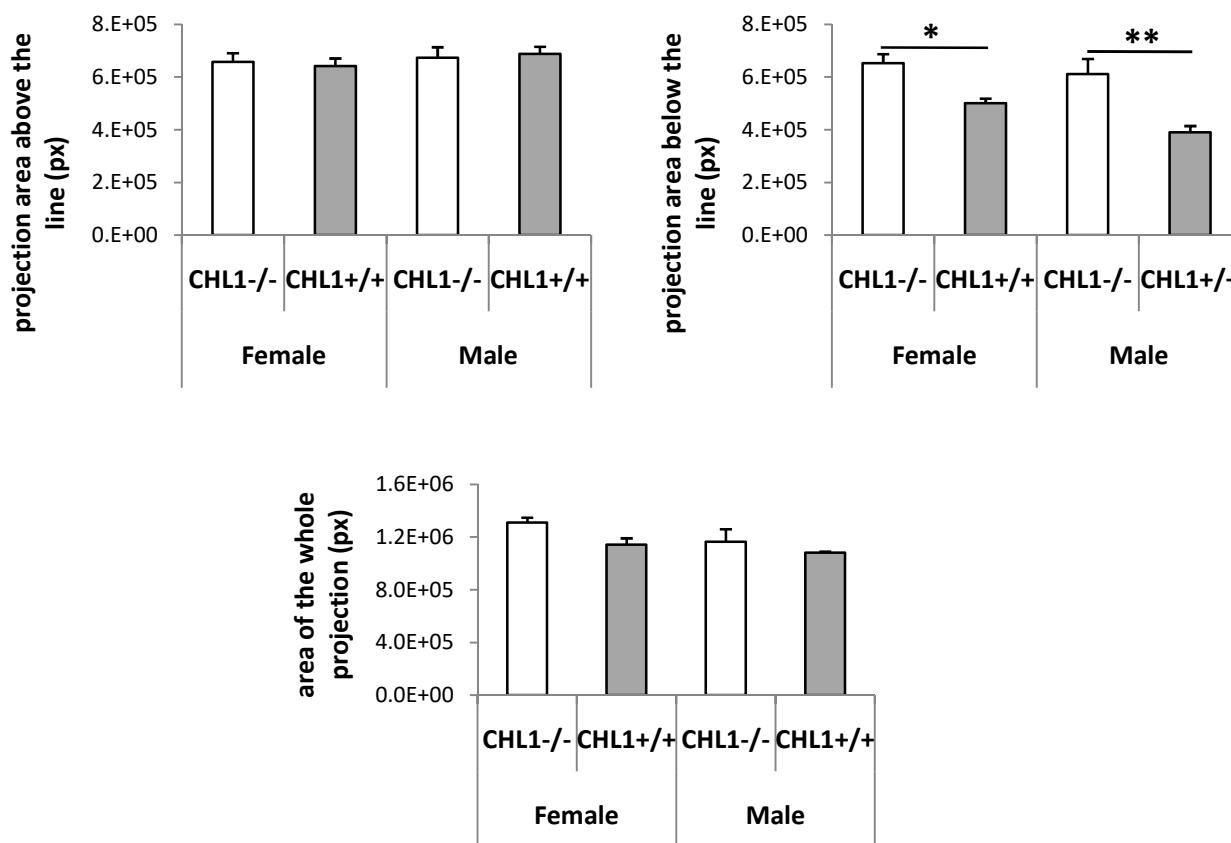


**Figure 37:**

**Dopaminergic fibers running from the ventral midbrain to the striatum cover a similar area in male and female mice.** The bar graphs represent the area covered by the dopaminergic fibers running from the ventral midbrain to the striatum above the line connecting AC with bottom of mDA (**Figure 33**), below the line and of the whole projection measured in 20  $\mu$ m-thick anti-TH immunofluorescently stained sagittal sections of brains of 3-4.5-months old CHL1-/- and CHL1+/+ mice. Presented are means +SEM for 4-5 animals per group of each gender. Results of one-way ANOVA followed by *post-hoc* Student Newman-Keul's test:  $p < 0.05^*$ ,  $0.01^{**}$  are shown. Abbreviations: CHL1-/- – mice knock-out for close homolog of L1, CHL1+/+ – wild-type mice, px – pixels.

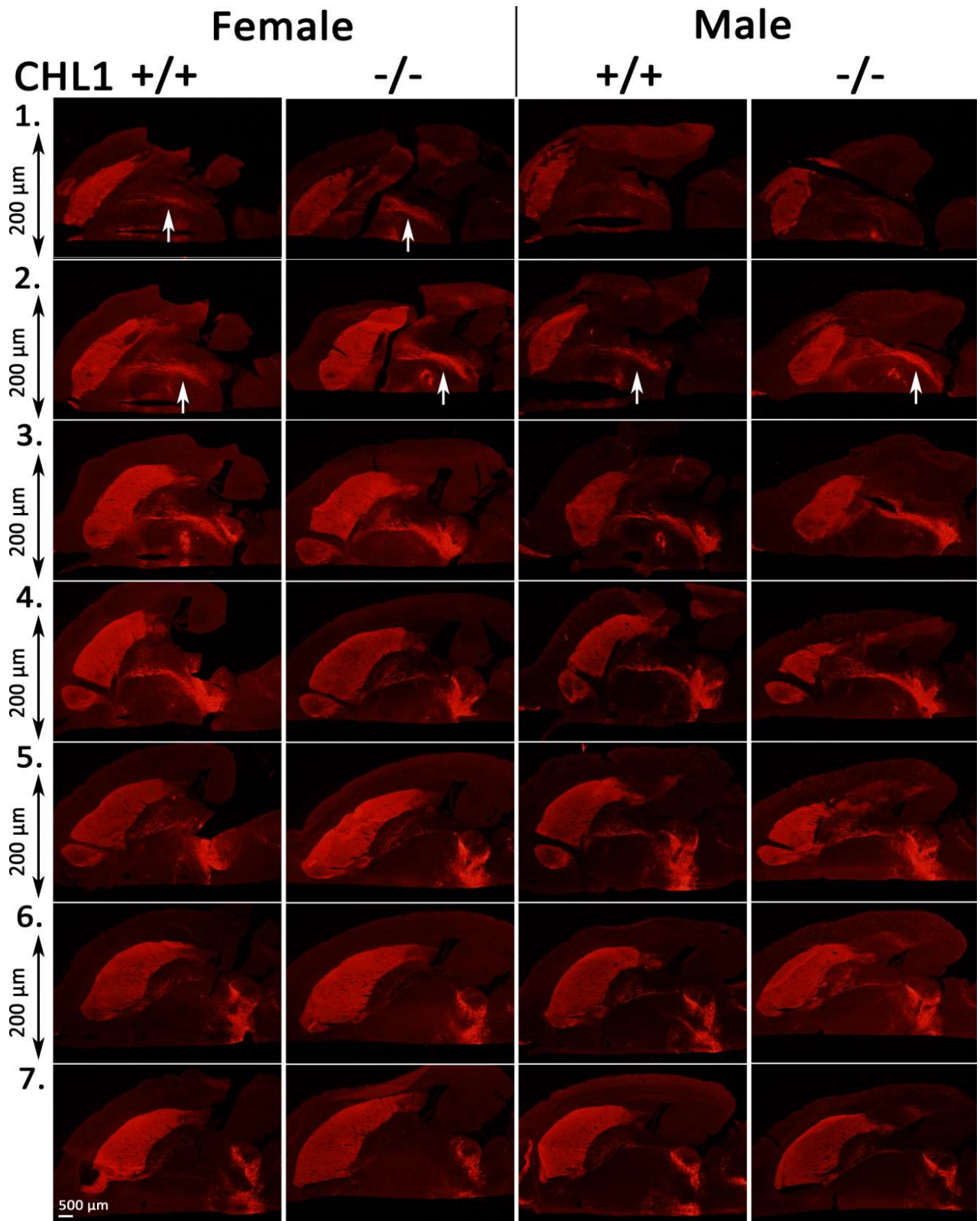


**Figure 38:**

**CHL1<sup>-/-</sup> mice have more dopaminergic fibers running to the ventral portion of the striatum than CHL1<sup>+/+</sup> mice.** Fluorescence microscope images of anti-TH immunofluorescently stained 20 μm-thick horizontal cryosections collected from 3-4.5 months old CHL1<sup>-/-</sup> and CHL1<sup>+/+</sup> male and female mouse brains are shown. Presented images of the sections are organized in order 1.-7. where 1. is the most ventral and 7. the most dorsal section. The sections are separated by 200 μm. In the sections representing the most ventral parts of

the brains fluorescence of the dopaminergic fibers is stronger in CHL1<sup>-/-</sup> than in CHL1<sup>+/+</sup> mice. The result was similar for males and females. White arrows indicate the ventral portion of the dopaminergic projections with the different fluorescence intensity in CHL1<sup>-/-</sup> and CHL1<sup>+/+</sup> mice. The staining was performed on 2-3 animals per genotype. Abbreviations: <sup>-/-</sup> – mice knock-out for close homolog of L1, <sup>+/+</sup> – wild-type mice, CHL1 – close homolog of L1.

### **8.3.2. Phospho-TH-positive dopaminergic fibers running to the ventral striatum differ in CHL1<sup>-/-</sup> and CHL1<sup>+/+</sup> mice**

In the previous experiment I found that adult CHL1<sup>-/-</sup> mice have more dopaminergic fibers running below the line connecting the AC with the bottom of mDA than CHL1<sup>+/+</sup> mice. To determine if the observed abnormal distribution of the dopaminergic fibers in CHL1<sup>-/-</sup> mice is the same for the dopaminergic fibers containing the active form of the TH – pTH – as the next step sagittal sections of adult CHL1<sup>-/-</sup> and CHL1<sup>+/+</sup> mouse brains were immunofluorescently stained against pTH. In the images of the stained sections taken at a fluorescence microscope, similarly as in the analysis of the anti-TH-stained sagittal sections, a line connecting the AC (considered as the border between the dorsal and the ventral striatum) with the bottom of the mDA was drawn (**Figure 39**). More pTH-containing fibers projecting below the arbitrary line were detected in CHL1<sup>-/-</sup> mice than in CHL1<sup>+/+</sup> mice. This is comparable to the staining observed in the experiment measuring TH-positive dopaminergic fibers.

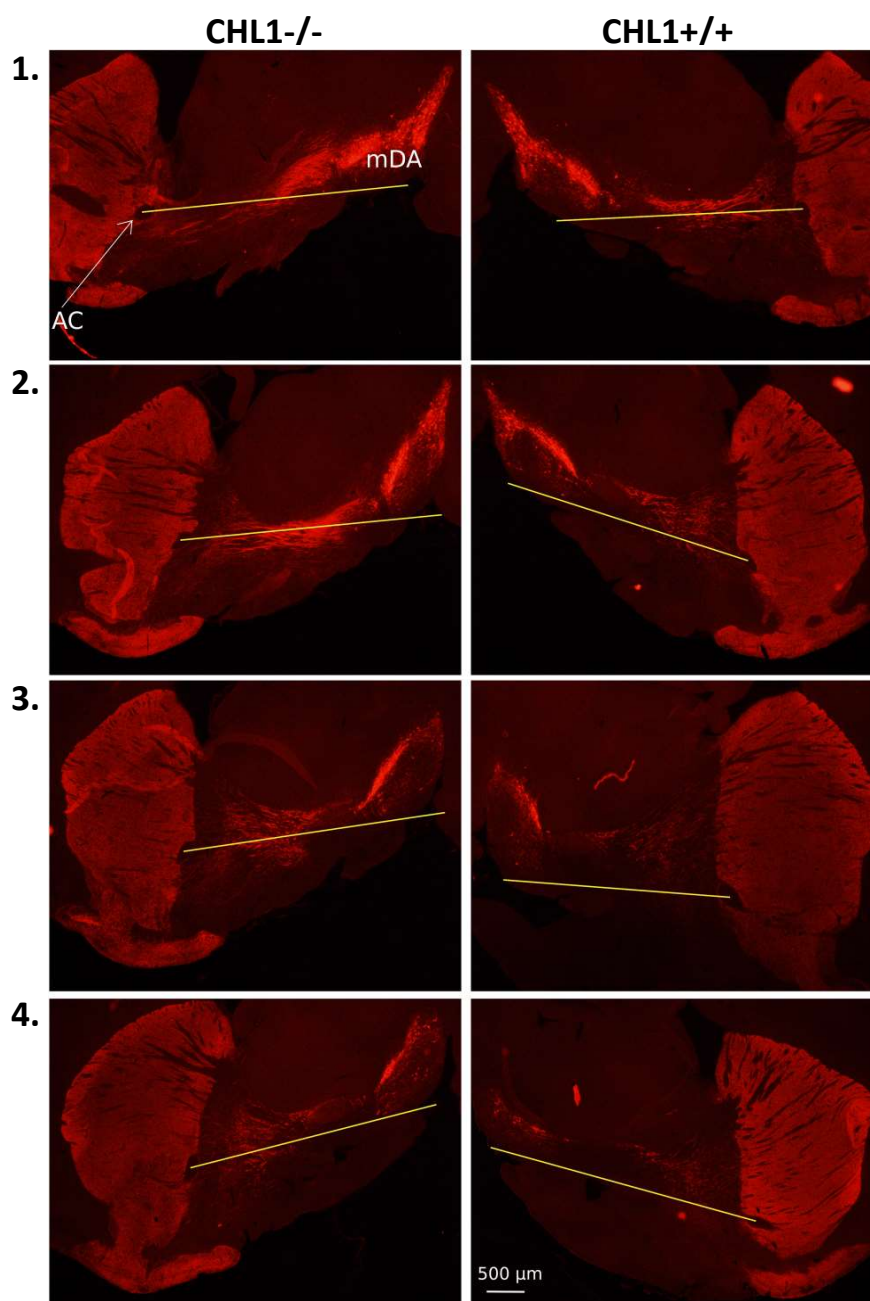
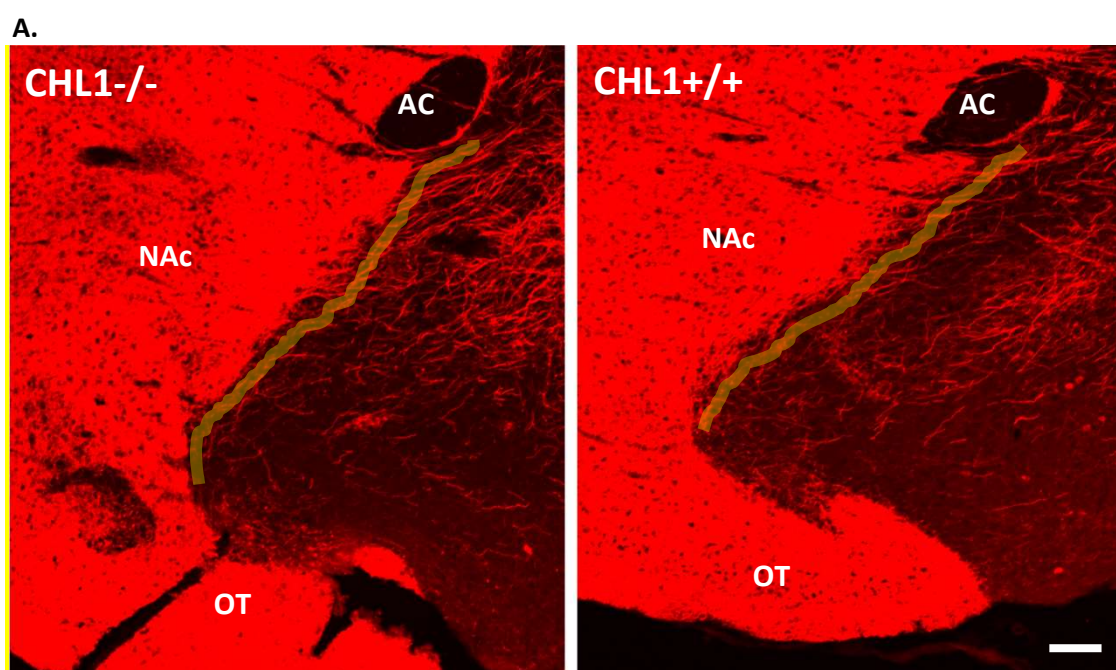


**Figure 39:**

**CHL1<sup>-/-</sup> mice have more pTH-expressing dopaminergic fibers running to the ventral striatum than CHL1<sup>+/+</sup> mice.** Presented are representative fluorescence microscopic images of the anti-pTH(Ser40) immunofluorescently stained sections from the right hemispheres of 3-4.5 months old female CHL1<sup>-/-</sup> and CHL1<sup>+/+</sup> mouse brains. Every tenth 20  $\mu$ m-thick section collected between 1000 and 1800  $\mu$ m laterally off the intrahemispheric fissure are presented above in order 1.-4., where 1. are the most medial and 4. are the most lateral sections. Yellow lines connecting the AC with the bottom of the visible mDA were drawn to roughly separate the pTH-positive dopaminergic fibers running to the dorsal and to the ventral striatum. More pTH-positive fibers running to the ventral striatum (below the yellow line) were detected in CHL1<sup>-/-</sup> sections than in CHL1<sup>+/+</sup> sections. The staining was performed on one animal per group. **Abbreviations:** AC – anterior commissure, CHL1<sup>-/-</sup> – mice knock-out for close homolog of L1, CHL1<sup>+/+</sup> – wild-type mice, mDA – midbrain dopaminergic neurons.

### 8.3.3. CHL1<sup>-/-</sup> mice have more dopaminergic fibers entering the ventral striatum compared to CHL1<sup>+/+</sup> mice

After showing that dopaminergic fibers running to the ventral striatum (below the line connecting the AC with the bottom of the mDA (**Figure 33**)) have a stronger intensity of TH-fluorescence and cover a larger area in CHL1<sup>-/-</sup> mice compared to CHL1<sup>+/+</sup> mice, it was relevant to analyze whether the amount of the dopaminergic fibers entering/innervating the ventral striatum is higher in CHL1<sup>-/-</sup> mice than in CHL1<sup>+/+</sup> mice. The number of dopaminergic fibers entering the dorsal and the ventral striatum was quantified in the microscopic images of sagittal sections from adult CHL1<sup>-/-</sup> and CHL1<sup>+/+</sup> mouse brains immunofluorescently stained for TH. In ImageJ, a thick line at the edge of the striatum was drawn in each picture, then the area of fibers crossing the line was determined and calculated relative to the area of the line (**Figure 40.A**). The AC was taken as a border between the dorsal and the ventral striatum and the dopaminergic fibers entering the part of the striatum above the AC were considered as fibers innervating the dorsal striatum while the dopaminergic fibers entering the part of the striatum below the AC were considered as fibers innervating the ventral striatum. Statistical comparison of the relative area of dopaminergic fibers crossing the line and entering the striatum in CHL1<sup>-/-</sup> and CHL1<sup>+/+</sup> mice showed that CHL1<sup>-/-</sup> mice have more dopaminergic fibers entering the ventral striatum compared to CHL1<sup>+/+</sup> mice while the amount of dopaminergic fibers entering the dorsal striatum is similar in CHL1<sup>-/-</sup> and CHL1<sup>+/+</sup> mice (**Figure 40.B**). Comparison of the dopaminergic innervation of the striatum in CHL1<sup>-/-</sup> and CHL1<sup>+/+</sup> males and females showed no differences between genders (**Figure 40.B**). The results obtained in this analysis show that in the absence of CHL1 increased amounts of dopaminergic fibers running from the ventral midbrain reach the ventral striatum in adult mouse brains.



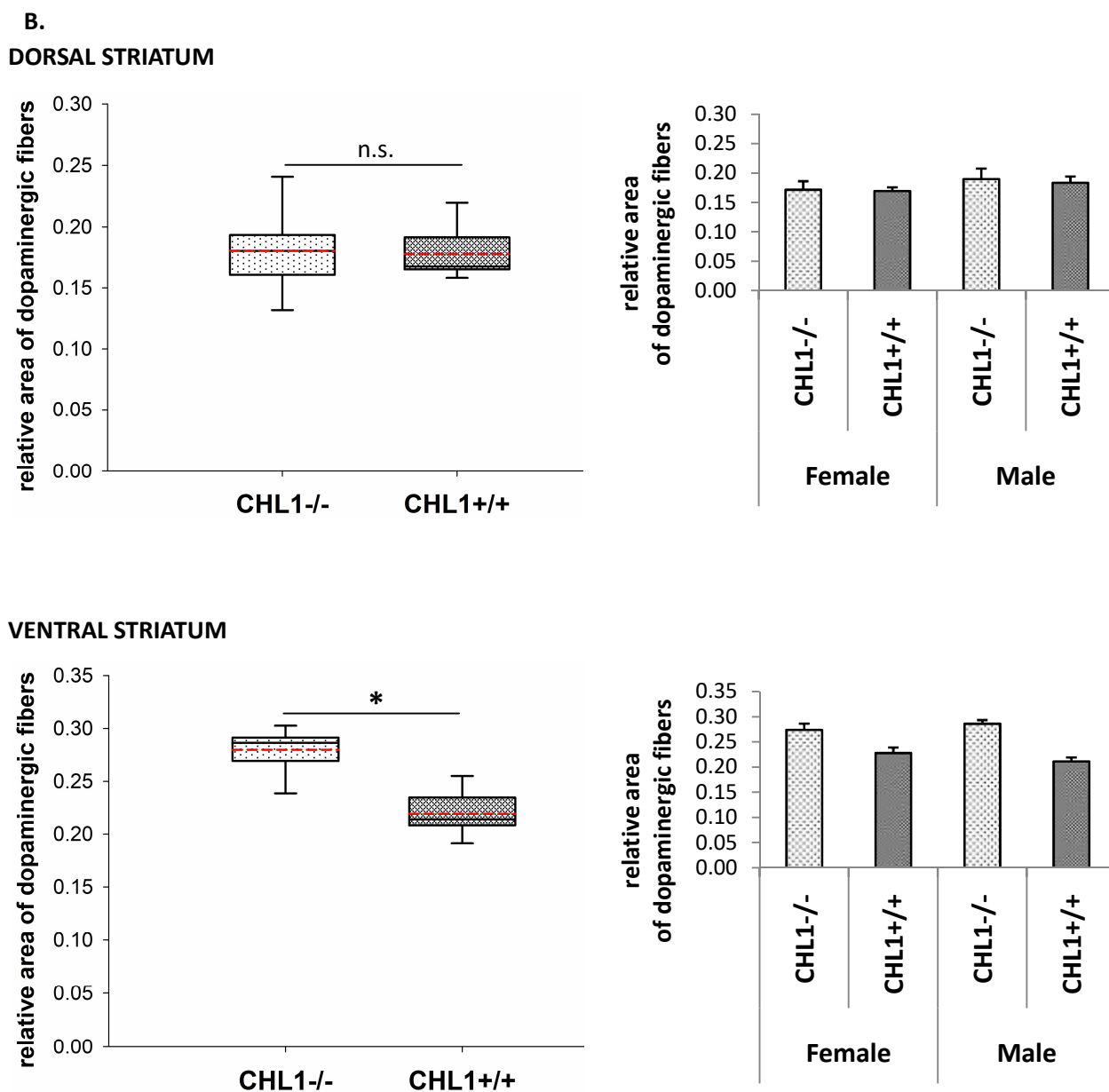


**Figure 40:**

**More dopaminergic fibers enter the ventral striatum in CHL1<sup>-/-</sup> mice.** **A)** Presentation of the method of the analysis of the dopaminergic fibers entering the striatum in sagittal sections of brains of 3-4.5 months old CHL1<sup>-/-</sup> and CHL1<sup>+/+</sup> mice. The sections were immunofluorescently stained against TH (red). A line (here: yellow, partially transparent) was drawn at the edge of the striatum in confocal images of the sections and the area of fibers crossing the line was measured and calculated relative to the area of the line. The AC was considered as a border between the dorsal and the ventral (NAc) striatum. For the analysis every tenth 20  $\mu$ m-thick section collected from 1000 and 1800  $\mu$ m laterally off the intrahemispheric fissure was used. Corresponding sections from CHL1<sup>-/-</sup> and CHL1<sup>+/+</sup> mice are shown. Scale bar: 120  $\mu$ m. **B)** Graphs present the results of the quantification of dopaminergic fibers innervating the dorsal striatum (entering the striatum above the AC) and of dopaminergic fibers innervating the ventral striatum (entering the striatum below the AC). Box plots represent 8-9 animals per group of mixed genders; red dotted line represents the mean. Bar graphs present means +SEM for 4-5 animals per group of single gender. Results of the two-tailed Student's *t*-test performed to compare two groups or one-way ANOVA performed to compare more than two groups:  $p < 0.05^*$ . **Abbreviations:** AC – anterior commissure, CHL1<sup>-/-</sup> – mice knock-out for close homolog of L1, CHL1<sup>+/+</sup> – wild-type mice, CP – caudate and putamen, NAc – nucleus accumbens, n.s. – not significant, OT – olfactory tubercle.

### 8.3.4. Loss of CHL1 does not affect the dopaminergic fibers density in the striatum

Since the analysis of the amount of dopaminergic fibers entering the dorsal and the ventral striatum showed that more fibers enter the ventral striatum in adult CHL1<sup>-/-</sup> mice compared to CHL1<sup>+/+</sup> mice, I analyzed whether the density of dopaminergic fibers in the ventral striatum is also higher in CHL1<sup>-/-</sup> mice than in CHL1<sup>+/+</sup> mice. For that purpose coronal sections of adult CHL1<sup>-/-</sup> and CHL1<sup>+/+</sup> mouse brains were collected and immunostained for TH. In microscopic images of the dorsal striatum, the ventral striatum and the total striatum area of the immunolabeled dopaminergic fibers was measured and calculated relative to the area of the analyzed part of the striatum. Statistical analysis showed no significant difference in the proportional stained area of the dorsal striatum (**Figure 41**), the ventral striatum (**Figure 42**) and the total striatum (**Figure 43**) between CHL1<sup>-/-</sup> and CHL1<sup>+/+</sup> mice. The same result was obtained when CHL1<sup>-/-</sup> and CHL1<sup>+/+</sup> males and females were analyzed separately. This result indicates that although more dopaminergic fibers run to the ventral striatum and enter the ventral striatum in CHL1<sup>-/-</sup> mice than in CHL1<sup>+/+</sup> mice (shown in **8.3.1.**, **8.3.2.** and **8.3.3.**), the density of the dopaminergic fibers in the ventral striatum of CHL1<sup>-/-</sup> mice is normal.

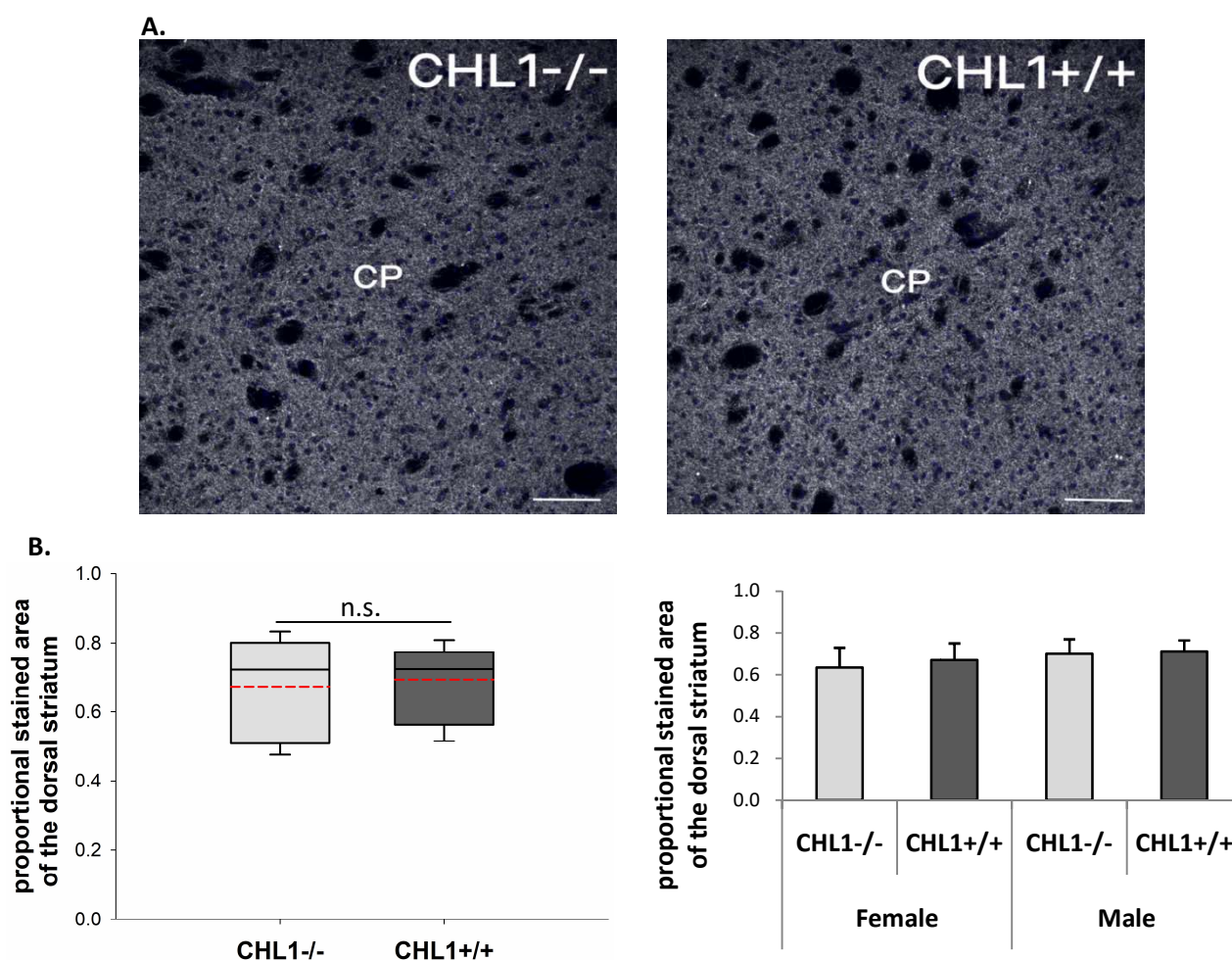


**Figure 41:**

**Lack of CHL1 does not affect the dopaminergic fibers density in the dorsal striatum.** **A)** Representative confocal images from the anti-TH immunofluorescently stained dorsal striatum (CP) of brains of 3-4.5

months old CHL1<sup>-/-</sup> and CHL1<sup>+/+</sup> mice are presented. Dopaminergic fibers are labeled in white; nuclei are stained with DAPI. Scale bars: 0.1 mm. **B)** Proportional stained area (the area of dopaminergic fibers calculated relative to the area of the striatum) of the dorsal striatum was measured in every 6<sup>th</sup> 30  $\mu$ m-thick coronal section of the striatum collected between Bregma +1.1 and -0.1 (5-7 sections per animal). 8 confocal images per section were analyzed. Box plots represent values from 7 animals per group of mixed genders; red dotted line represents the mean. Bar graphs represent means  $\pm$ SEM from 3-4 animals per group of single gender. Result of two-tailed Student's *t*-test performed to compare two groups or one-way ANOVA performed to compare more than two groups:  $p > 0.05$ . Abbreviations: CHL1<sup>-/-</sup> – mice knock-out for close homolog of L1, CHL1<sup>+/+</sup> – wild-type mice, CP – caudate and putamen, n.s. – not significant.

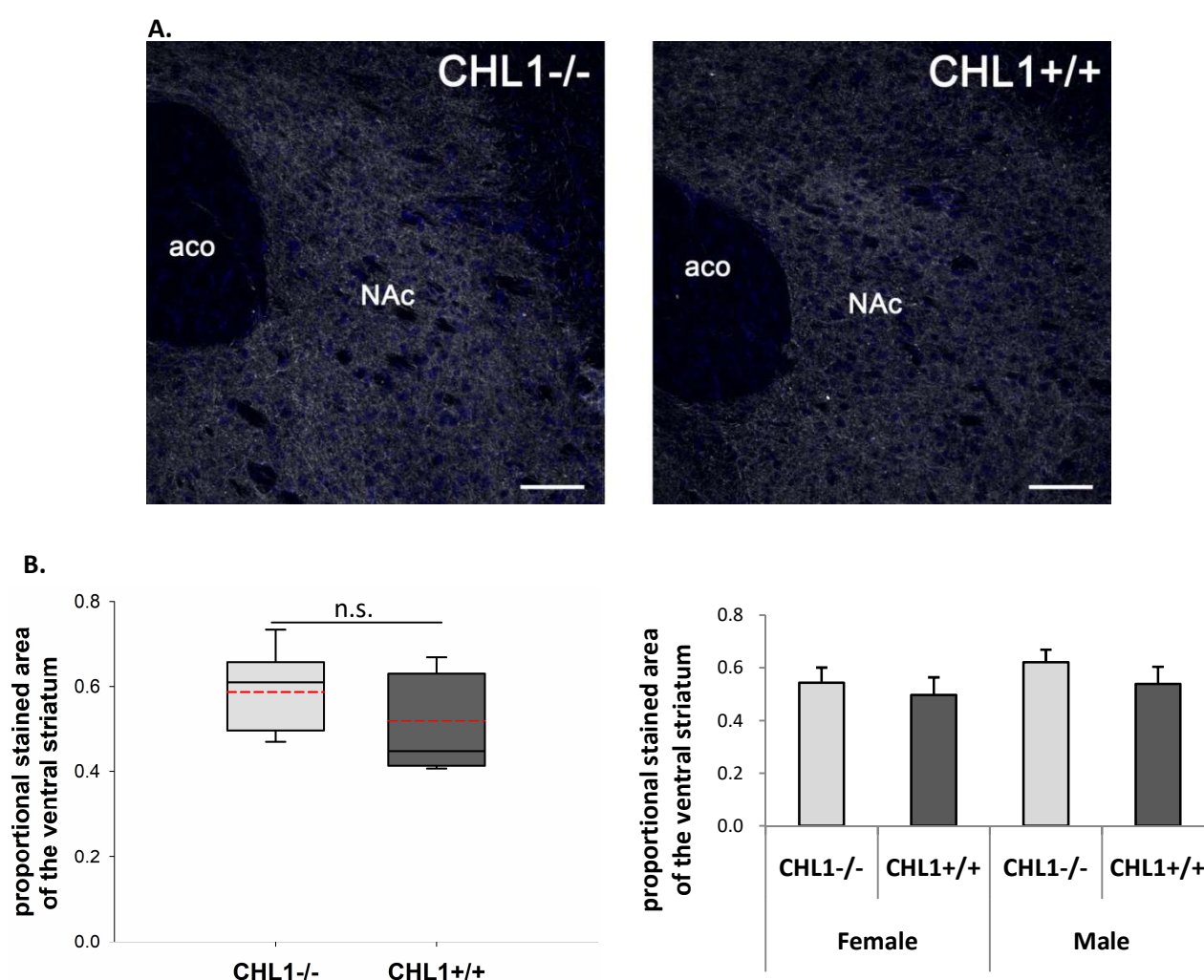


**Figure 42:**

**Lack of CHL1 does not affect the dopaminergic fibers density in the ventral striatum.** **A)** Shown are representative confocal images of the anti-TH (white) immunofluorescently stained ventral striatum (NAc) of brains of adult CHL1<sup>-/-</sup> and CHL1<sup>+/+</sup> mice. Nuclei are stained with DAPI (blue). The structure not covered by the dopaminergic fibers is the AC. Scale bars: 0.1 mm. **B)** Proportional stained area (area of dopaminergic fibers calculated relative to the area of the ventral striatum) was analyzed in every 6<sup>th</sup> 30  $\mu$ m-thick coronal section containing the ventral striatum collected between Bregma +1.1 and -0.1 (5-7 sections per animal) of

3-4.5 months old CHL1<sup>-/-</sup> and CHL1<sup>+/+</sup> mice. 7-8 confocal images per section were analyzed. Box plots represent 7 animals per group of mixed genders; red dotted line represents the mean. Bar graphs present means +SEM from 3-4 animals per group of single gender. Result of Mann-Whitney U-test performed to compare two groups or one-way ANOVA performed to compare more than two groups:  $p > 0.05$ . **Abbreviations:** aco – anterior commissure, CHL1<sup>-/-</sup> – mice knock-out for close homolog of L1, CHL1<sup>+/+</sup> – wild-type mice, NAc – nucleus accumbens, n.s. – not significant.

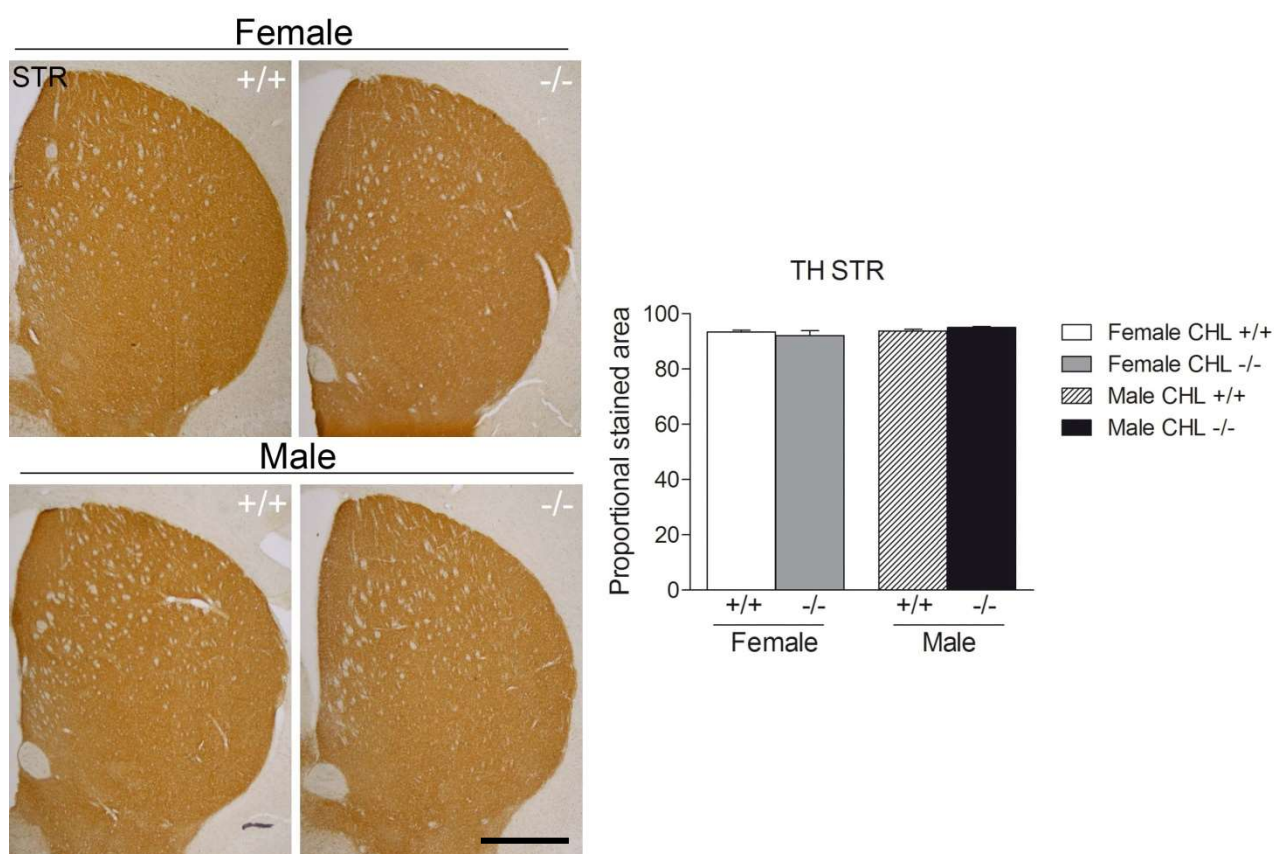
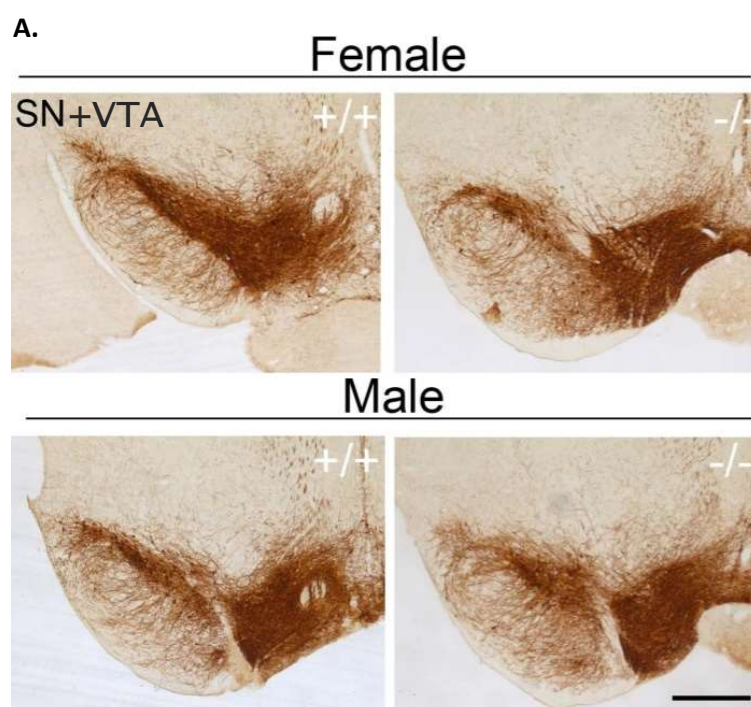


**Figure 43:**

**Lack of CHL1 does not affect the dopaminergic fibers density in the whole striatum.** Images present the matching sections of the striatal (STR) 30  $\mu\text{m}$ -thick cryosections of brains of 3-4.5 months old male and female CHL1<sup>-/-</sup> and CHL1<sup>+/+</sup> mice. Every 6<sup>th</sup> coronal section collected between Bregma +1.1 and -0.1 (5-7 sections per animal) was stained using primary antibody against the marker for the dopaminergic neurons – TH, followed by avidin-biotin immunocytochemical staining resulting in labeling of the TH-positive fibers with brown color. Images of the whole striatum were taken at the light microscope. The area of the fibers in the whole striatum was measured and calculated relative to the area of the striatum. Scale bar: 500  $\mu\text{m}$ . Graphs present means +SEM from 3-4 animals per group of single gender. Result of two-way ANOVA:  $p > 0.05$ . The staining, the imaging and the analysis in this experiment were performed by Dr. Noelia Granado and Prof. Rosario Moratalla at the Cajal Institute in Madrid. **Abbreviations:** <sup>-/-</sup> – mice knock-out for close homolog of L1, <sup>+/+</sup> – wild-type mice, CHL1<sup>-/-</sup> – mice knock-out for close homolog of L1, CHL1<sup>+/+</sup> – wild-type mice, STR – striatum, TH – tyrosine hydroxylase.

### 8.3.5. CHL1<sup>-/-</sup> mice have a reduced number of dopaminergic neurons in the VTA compared to CHL1<sup>+/+</sup> mice

From my previous experiments I had indications that the amount of the dopaminergic fibers running to the ventral striatum is different in adult CHL1<sup>-/-</sup> versus CHL1<sup>+/+</sup> mice. To determine a possible cause for the observed difference in the amount of dopaminergic fibers, which could be a different amount of ventral midbrain dopaminergic neurons that send their axons to the striatum in CHL1<sup>+/+</sup> and CHL1<sup>-/-</sup> mice, the numbers of dopaminergic neurons of the SN and the VTA were quantified. In order to quantify the dopaminergic cells, coronal sections from brains of adult CHL1<sup>-/-</sup> and CHL1<sup>+/+</sup> mice were collected and stained using the primary antibody against TH followed by avidin-biotin staining (**Figure 44.A**). Dopaminergic neurons of the SN and of the VTA were then stereologically quantified as described in Granado et al. (2011). Statistical comparison of the number of the dopaminergic cells in the SN of CHL1<sup>-/-</sup> and CHL1<sup>+/+</sup> mice showed no significant differences, also when males and females were analyzed separately. However, the analysis of the TH-positive cells in the VTA and in the VTA together with the SN showed that CHL1<sup>-/-</sup> mice have less dopaminergic neurons in the VTA and in the VTA and the SN summed up. Interestingly, statistical comparison of TH-positive neurons in the VTA and the VTA+SN separately in males and females showed significant differences only between CHL1<sup>-/-</sup> and CHL1<sup>+/+</sup> males (**Figure 44.B**).



B.

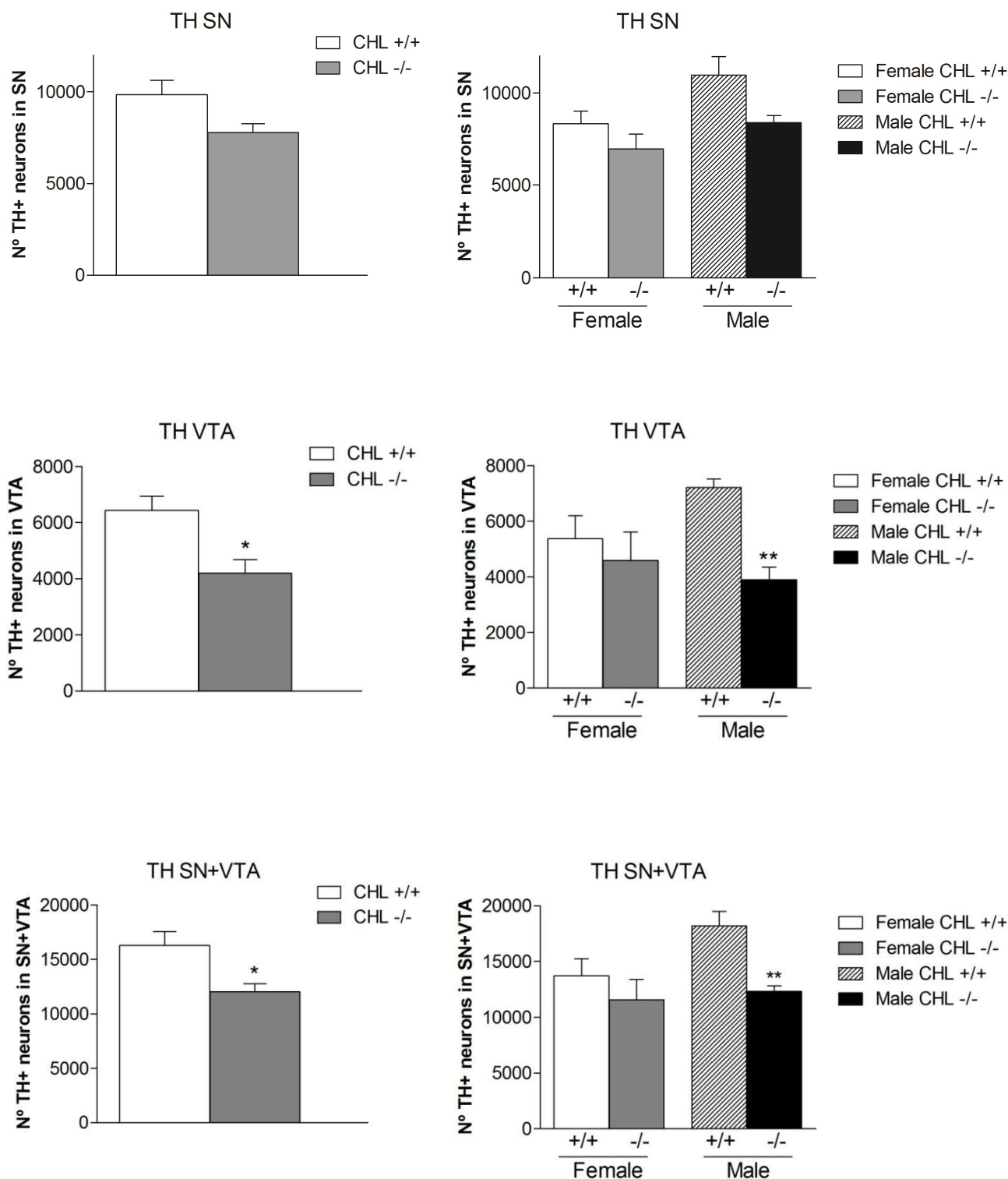


Figure 44:

**Adult CHL1<sup>-/-</sup> mice have less dopaminergic neurons in the VTA compared to CHL1<sup>+/+</sup> mice.** A) Representative images of matching coronal cryosections containing SN and VTA of 3-4.5-months old female and male CHL1<sup>-/-</sup> and CHL1<sup>+/+</sup> mice are shown. Every 4<sup>th</sup> 30  $\mu$ m-thick brain section containing the midbrain was immunohistochemically stained using anti-TH primary antibody followed by avidin-biotin staining, which labeled the TH-positive cells with brown color. Scale bar: 500  $\mu$ m. B) Graphs present means +SEM from the stereological quantification of TH-positive cells in the SN (top), the VTA (middle) and in both structures (SN+VTA; bottom) of CHL1<sup>-/-</sup> and CHL1<sup>+/+</sup> mice. In the experiment 7 mice per group of mixed genders and 3-

4 mice per group of single gender were analyzed. Result of Student's *t*-test performed to compare two groups or two-way ANOVA followed by Tukey's test performed to compare more than two groups:  $p < 0.05^*$ ,  $0.01^{**}$ . The staining, the imaging and the analysis were performed by Dr. Noelia Granada and Prof. Rosario Moratalla at the Cajal Institute in Madrid. Abbreviations: -/- – mice knock-out for close homolog of L1, +/+ – wild-type mice, CHL1-/- – mice knock-out for close homolog of L1, CHL1+/+ – wild-type mice, N° – number, SN – substantia nigra, TH – tyrosine hydroxylase, TH+ – tyrosine hydroxylase-positive, VTA – ventral tegmental area.

#### **8.4. Verification of DRD2 expression and schizophrenia-related brain morphology in CHL1-/- mice**

Taking into consideration the reports from genetic studies showing that CHL1 is related to the development of schizophrenia in humans (Sakurai et al., 2002; Chen et al., 2005; Shaltout et al., 2013), and the reports from behavioral studies showing that CHL1 is associated with schizophrenia-related behavior such as reduced reactivity to novelty (Morellini et al., 2007) and reduced pre-pulse inhibition (Irintchev et al., 2004) in mice, my next aim was to investigate if lack of CHL1 leads to development of certain brain features that were associated with schizophrenia: decreased size of the thalamus (Andreasen et al., 1994; Brickman et al., 2004), reduced thickness of the frontal cortex (Rimol et al., 2010; Asmal et al., 2016), increased expression of the DRD2 in the frontal cortex (Tallerico et al., 2001) and enlarged lateral ventricles (Andreasen et al., 1994; Gaser et al., 2004; Kempton et al., 2010).

##### **8.4.1. Thalamus size is normal in CHL1-/- mice**

The size of the thalamus was determined using anti-TH immunofluorescently stained sagittal brain sections from adult CHL1-/- and CHL1+/+ mice. The staining with anti-TH antibody allowed to visualize the thalamus and structures surrounding the thalamus (**Figure 45.A**). Fluorescence microscopic images of the stained sections were analyzed in ImageJ, where the thalamus was delineated and its area was measured. Statistical comparison of the thalamus size in CHL1-/- and CHL1+/+ mice showed no significant difference and the same result was obtained when the thalamus size in CHL1-/- and CHL1+/+ males and females was compared (**Figure 45.B**). This result shows that lack of CHL1 does not lead to a reduction of the thalamus size.

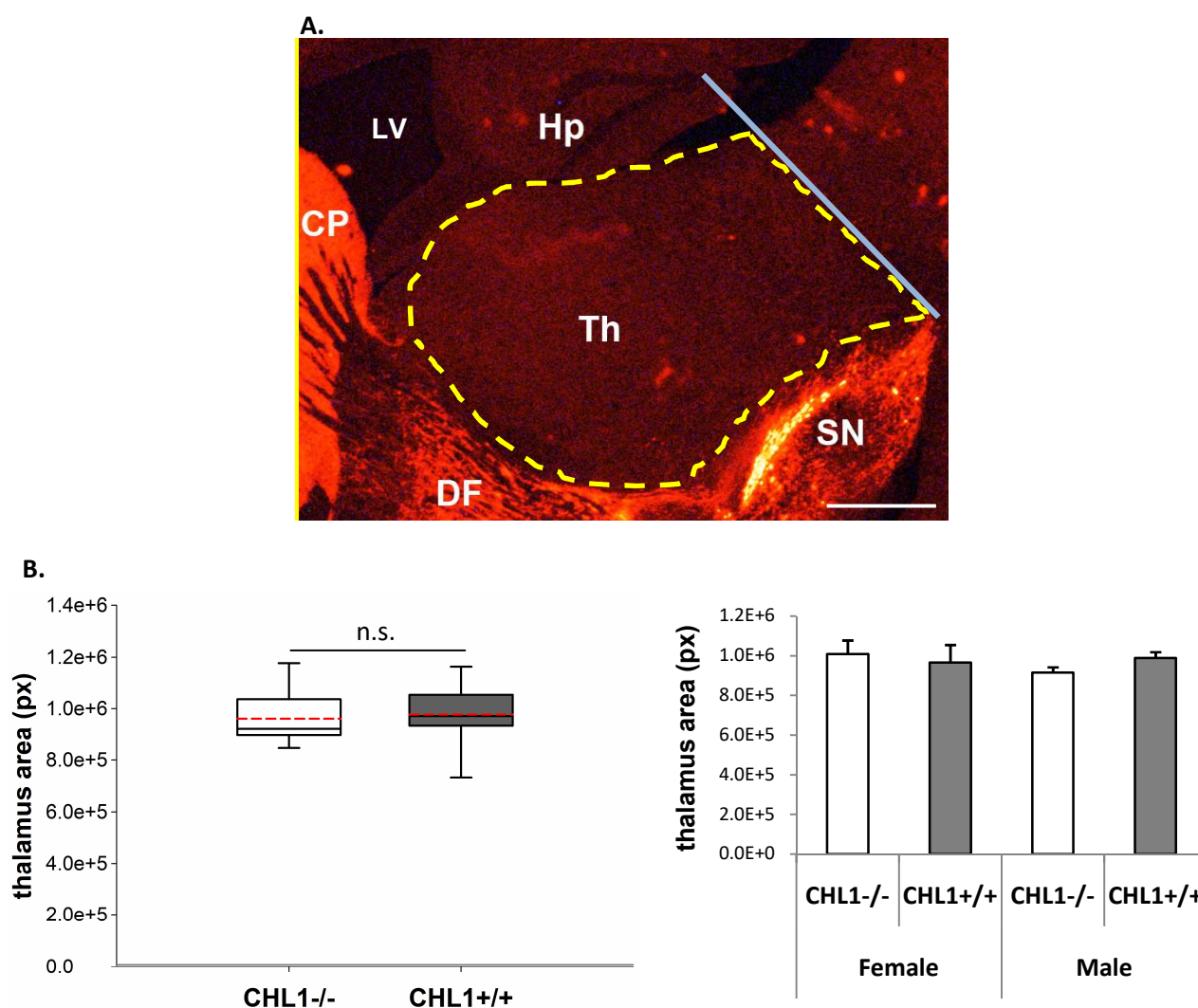


**Figure 45:**

**Thalamus size is similar in CHL1<sup>-/-</sup> and CHL1<sup>+/+</sup> mice.** **A)** Representative picture of anti-TH immunofluorescently stained 20  $\mu\text{m}$ -thick sagittal section of an adult CHL1<sup>-/-</sup> mouse brain is shown. The yellow dotted line delineates the thalamus; borders of the thalamus: ventrally – dopaminergic neurons of the SN and dopaminergic fibers (DF) running to the striatum, rostrally – edge of the dorsal striatum (CP) and lateral ventricle (LV), dorsally – hippocampus (Hp), caudally – a line (blue line in the image) connecting the dentate gyrus of the hippocampus with the caudal part of the SN. Scale bar: 0.7 mm. **B)** Graphs present the results of the thalamus size measurement in sagittal sections collected between 1000  $\mu\text{m}$  and 1800  $\mu\text{m}$  laterally off the intrahemispheric fissure of brains of 3-4.5 months old CHL1<sup>-/-</sup> and CHL1<sup>+/+</sup> mice (every tenth section was used for the analysis – this made 4 sections per hemisphere). Box plots represent 8-9 mice per group of mixed genders; red dotted line represents the mean. Bar graphs present means +SEM from 4-5 mice per group of a single gender. Result of two-tailed Student *t*-test performed to compare two groups or one-way ANOVA performed to compare more than 2 groups:  $p > 0.05$ . **Abbreviations:** CHL1<sup>-/-</sup> – mice knock-out for close homolog of L1, CHL1<sup>+/+</sup> – wild-type mice, CP – caudate and putamen, DF – dopaminergic fibers, Hp – hippocampus, LV – lateral ventricle, n.s. – not significant, px – pixels, SN – substantia nigra, Th – thalamus.

#### 8.4.2. Thickness of the frontal cortex is normal in CHL1<sup>-/-</sup> mice

To measure the thickness of the frontal cortex in adult CHL1<sup>-/-</sup> and CHL1<sup>+/+</sup> mice, immunofluorescence staining of TH was performed on sagittal sections of CHL1<sup>-/-</sup> and CHL1<sup>+/+</sup> mouse brains. TH staining allowed a good visualization of the corpus callosum which constitutes the inner border of the frontal cortex. Frontal cortex thickness was measured in pictures of the stained sections obtained at the fluorescence microscope. In each picture a line connecting the corpus callosum with the external edge of the frontal cortex was drawn (**Figure 46.A**) and its length was measured in ImageJ. Statistical analysis of the obtained values representing the frontal cortex thickness showed no significant differences between CHL1<sup>-/-</sup> and CHL1<sup>+/+</sup> mice also when males and females were analyzed separately (**Figure 46.B**). The obtained result indicates that CHL1<sup>-/-</sup> mice do not present the verified morphological brain feature related to schizophrenia – the reduced thickness of the frontal cortex.

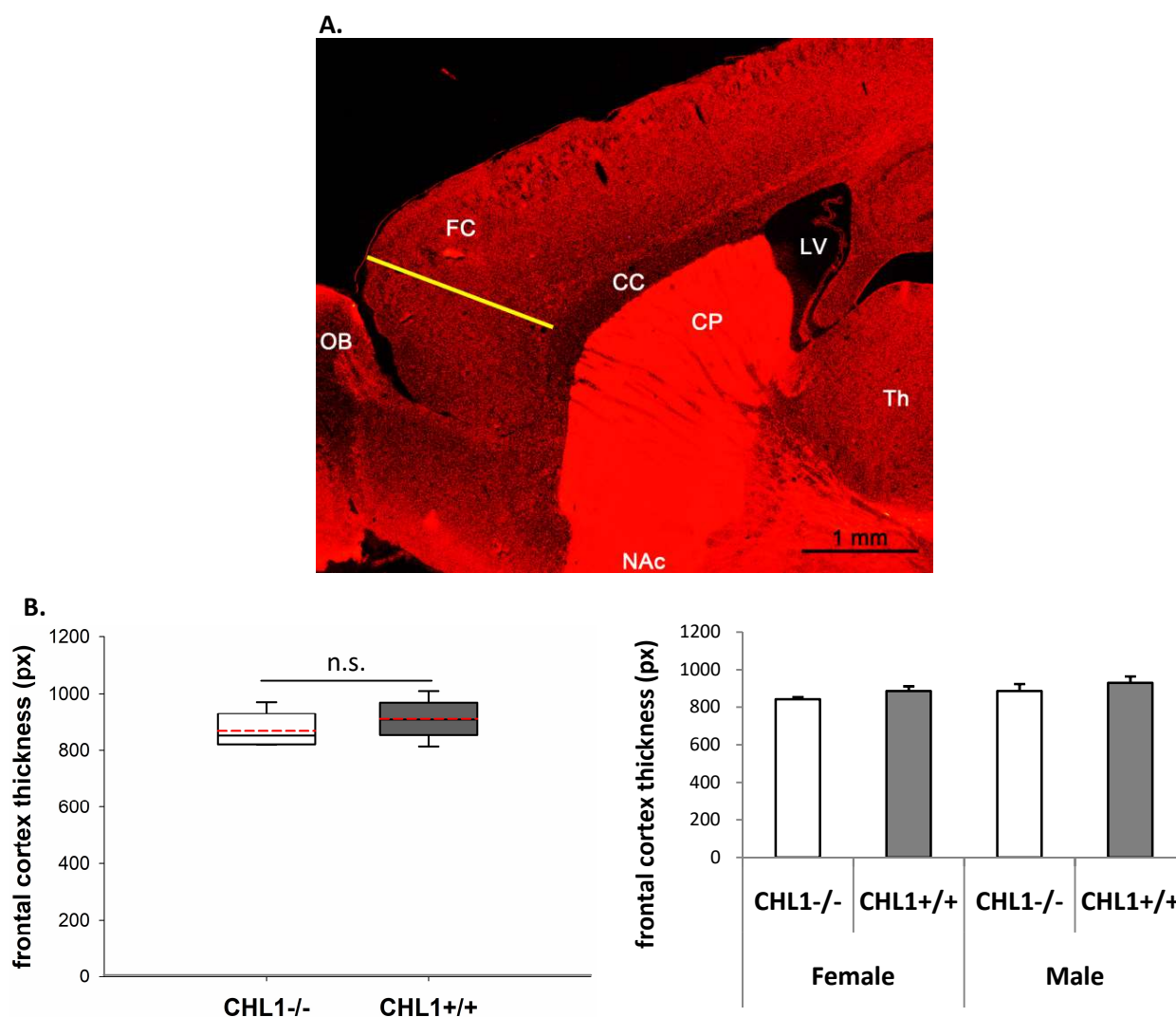


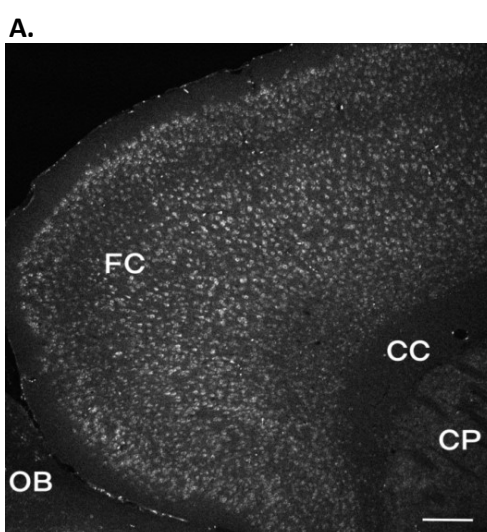
**Figure 46:**

**Thickness of the frontal cortex is normal in CHL1<sup>-/-</sup> mice.** **A)** Presentation of the method used for determination of the frontal cortex thickness in brains of 3-4.5 months old CHL1<sup>-/-</sup> and CHL1<sup>+/+</sup> mice: 20  $\mu$ m-

thick sagittal sections were stained using primary antibody against TH followed by fluorescently-labeled secondary antibody; in fluorescence microscopic images of the sections a line (yellow line in the image) connecting the corpus callosum with the edge of the frontal cortex was drawn and its length was measured. **B)** Presented are the results of the frontal cortex thickness measurement in the sagittal sections of CHL1<sup>-/-</sup> and CHL1<sup>+/+</sup> mice collected between 1000 and 1800  $\mu\text{m}$  laterally off the intrahemispheric fissure (every tenth section was used which made 4 sections per hemisphere). Box plots represent the frontal cortex thickness of 7-9 mice per group of mixed genders; red dotted line represents the mean. Bar graphs present means  $\pm$ SEM from 3-5 mice per group of single gender. Result of two-tailed Student's *t*-test performed to compare two groups or one-way ANOVA performed to compare more than two groups:  $p > 0.05$ . Abbreviations: CC – corpus callosum, CHL1<sup>-/-</sup> – mice knock-out for close homolog of L1, CHL1<sup>+/+</sup> – wild-type mice, CP – caudate and putamen, FC – frontal cortex, OB – olfactory bulb, LV – lateral ventricle, NAC – nucleus accumbens, n.s. – not significant, px – pixels, Th – thalamus.

#### 8.4.3. Expression of DRD2 in the frontal cortex is normal in CHL1<sup>-/-</sup> mice

To investigate if adult CHL1<sup>-/-</sup> mice express more DRD2 in their frontal cortex compared to CHL1<sup>+/+</sup> mice, sagittal sections of the adult mouse brains were collected and stained using a primary antibody against DRD2 followed by fluorescently-labeled secondary antibody (**Figure 47.A**). Images of the frontal cortex were taken at the confocal microscope; then the intensity of fluorescence of the immunolabeled DRD2 was measured in ImageJ and calculated as described by McCloy et al. (2014): integrated density of the area of interest was reduced by background mean grey value measured on the DRD2-negative corpus callosum. Statistical comparison of the DRD2 expression in the frontal cortex showed no significant difference between CHL1<sup>-/-</sup> and CHL1<sup>+/+</sup> mice when both genders were analyzed together as well as between CHL1<sup>-/-</sup> and CHL1<sup>+/+</sup> males and females analyzed separately (**Figure 47.B**). This result shows that CHL1<sup>-/-</sup> mice do not have increased DRD2 expression in the frontal cortex and thus do not present this brain feature related to schizophrenia.



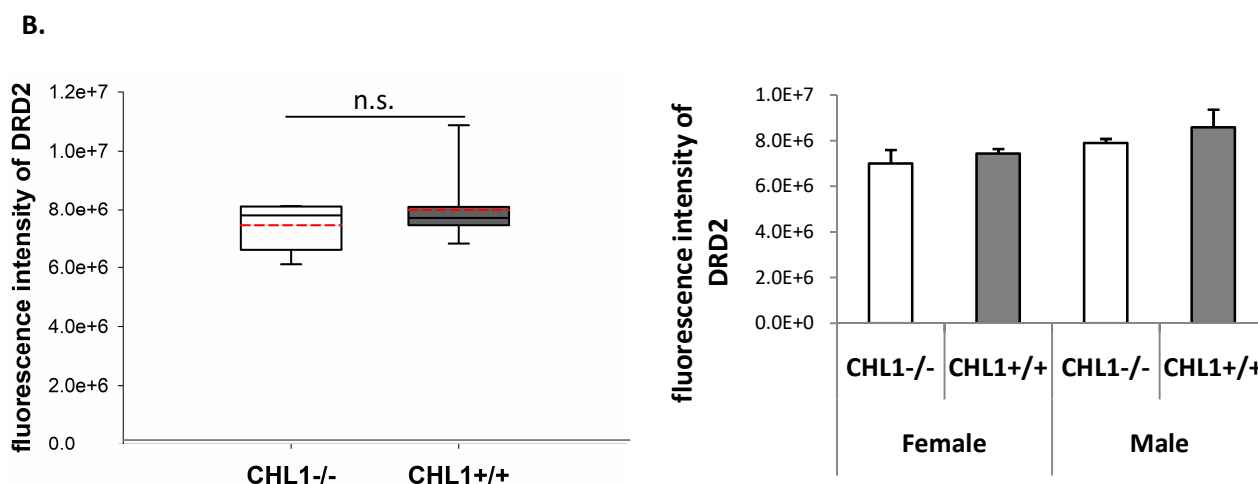


**Figure 47:**

**DRD2 expression in the frontal cortex of CHL1<sup>-/-</sup> mice is similar to that in CHL1<sup>+/+</sup> mice.** **A)** Presented is a representative confocal image of a portion of the anti-DRD2 immunofluorescently stained 20  $\mu\text{m}$ -thick sagittal section of a 3-4.5 months old CHL1<sup>+/+</sup> mouse. The staining against DRD2 (labeled in the picture in white) allowed to visualize the inner border of the frontal cortex – corpus callosum. Scale bar: 250  $\mu\text{m}$ . **B)** Analysis of the DRD2 expression in the frontal cortex of 3-4.5 months old CHL1<sup>-/-</sup> and CHL1<sup>+/+</sup> mice was performed measuring the integrated density of DRD2 fluorescence in the frontal cortex and reducing it by the mean grey value of background fluorescence measured on the corpus callosum. For the analysis every tenth section collected between 1000  $\mu\text{m}$  and 1800  $\mu\text{m}$  laterally off the intrahemispheric fissure (4 sections per hemisphere) was used. Box plots represent the result of the DRD2 expression measurement in the frontal cortex of CHL1<sup>-/-</sup> and CHL1<sup>+/+</sup> mice (6-8 per group) of both genders; red dotted line represents the mean. Bar graphs present means +SEM for 3-4 mice per group of single gender. Result of Mann-Whitney U-test performed to compare 2 groups or one-way ANOVA performed to compare more than two groups:  $p > 0.05$ . Abbreviations: CC – corpus callosum, CHL1<sup>-/-</sup> – mice knock-out for close homolog of L1, CHL1<sup>+/+</sup> – wild-type mice, CP – caudate and putamen, FC – frontal cortex, n.s. – not significant, OB – olfactory bulb.

#### 8.4.4. CHL1<sup>-/-</sup> mice have enlarged lateral ventricles compared to CHL1<sup>+/+</sup> mice

To analyze if the lateral ventricles of CHL1<sup>-/-</sup> mice are larger than the lateral ventricles of CHL1<sup>+/+</sup> mice, sagittal sections of adult CHL1<sup>-/-</sup> and CHL1<sup>+/+</sup> mouse brains were stained using DAPI. Then pictures of the whole sections were taken at a fluorescence microscope. The staining, which labels only the DNA (cell nuclei), was sufficient to clearly visualize the lateral ventricles, which turned out to be visibly larger in CHL1<sup>-/-</sup> mice than in CHL1<sup>+/+</sup> mice (**Figure 48**). With this result a morphological brain feature related with schizophrenia – the enlargement of lateral ventricles, was shown to exist in the brains of adult CHL1<sup>-/-</sup> mice.

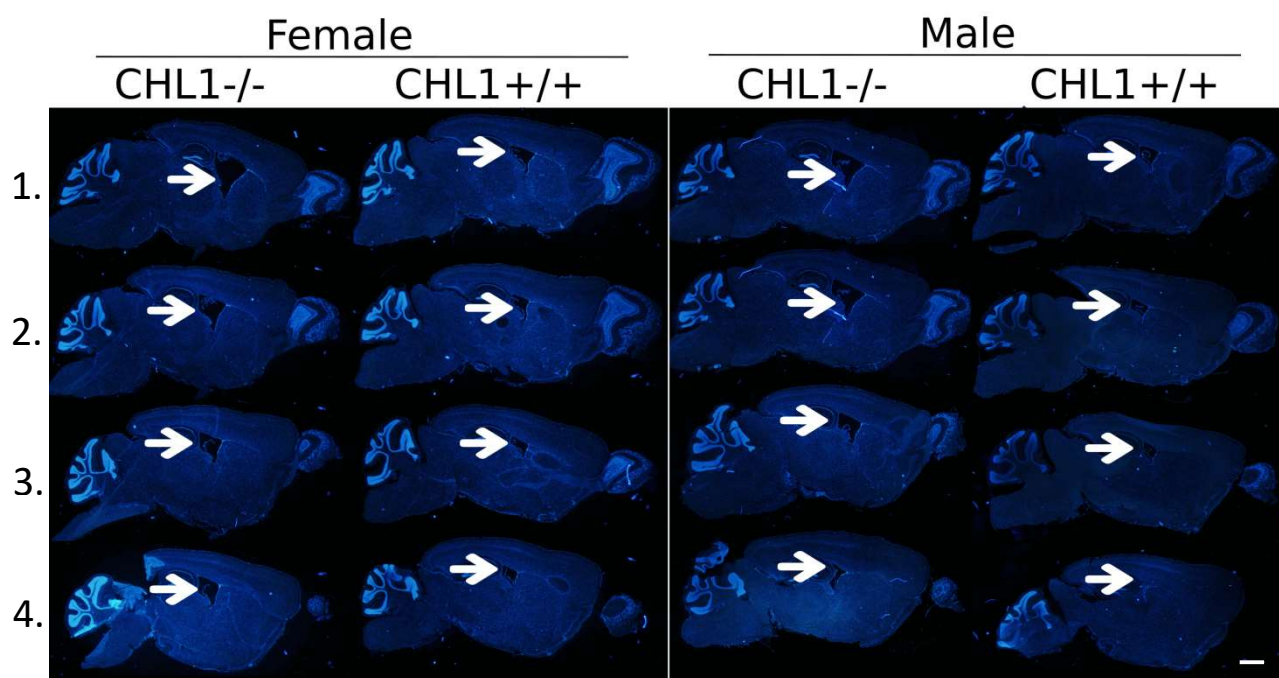


**Figure 48:**

**CHL1<sup>-/-</sup> mice have enlarged lateral ventricles compared to CHL1<sup>+/+</sup> mice.** Representative fluorescence microscope images of DAPI-stained 20  $\mu\text{m}$ -thick sagittal sections of brains of 3-4.5 months old male and female CHL1<sup>-/-</sup> and CHL1<sup>+/+</sup> mice are shown. The sections were collected between 1000  $\mu\text{m}$  and 1800  $\mu\text{m}$  laterally off the intrahemispheric fissure and every tenth section was used for the analysis. The presented sections are separated by 200  $\mu\text{m}$  and organized in order 1-4, where 1. is the most medial and 4. the most lateral section. Arrows point at the lateral ventricles. Scale bar: 1 mm. 2-3 mice per group of mixed genders were analyzed in the experiment. Abbreviations: CHL1<sup>-/-</sup> – mice knock-out for close homolog of L1, CHL1<sup>+/+</sup> – wild-type mice.

## 9. Discussion

### 9.1. CHL1 interacts with DRD2S and DRD2L

Through experiments performed with the aim to verify the direct interaction between CHL1 and DRD2 I showed that CHL1 co-localizes with DRD2 in the mouse striatum and in transfected HEK293 cells predominantly at the surface of cells, and that CHL1 binds directly to the first extracellular loop of DRD2 through its extracellular domain. In addition, I found that the interaction between DRD2 and CHL1 may occur in *trans*-orientation.

With immunofluorescent staining and PLA I showed that DRD2 and CHL1 co-localize closely in the mouse striatum, indicating the possible binding between the two proteins in this brain structure. In the striatum, dopaminergic neurons running from the ventral midbrain make synapses on the striatal MSNs (Money & Stanwood, 2013). In these synapses, DRD2 is expressed both pre- and post-synaptically. The two DRD2 forms, DRD2S and DRD2L, existing due to alternative splicing, were shown, by e.g. Khan et al. (1998) and Lindgren et al. (2003), to be functionally either pre- (DRD2S) or post-synaptic (DRD2L). Pre-synaptic functions of DRD2L and post-synaptic functions of DRD2S were found to be negligible, for instance, in the studies using DRD2L knock-out mice, which presented unaffected pre-synaptic DRD2 signaling and impaired post-synaptic DRD2 signaling (Lindgren et al., 2003). As the main reason for DRD2S functioning mostly pre- and DRD2L functioning mostly post-synaptically differential expression of the two DRD2 forms in the dopaminergic neurons and the MSNs was proposed: DRD2S is supposed to be expressed mostly by the dopaminergic neurons and DRD2L mostly by the MSNs (Khan et al., 1998). By PLA experiments performed on HEK293 cells transfected to express DRD2S alone, DRD2L alone, DRD2S with CHL1 and DRD2L with CHL1 I showed that both the pre-synaptic DRD2S and the post-synaptic DRD2L co-localize closely with CHL1. However, I found more co-localization of CHL1 with the pre-synaptic DRD2S than with the post-synaptic DRD2L. Considering that the co-localization of DRD2S and DRD2L with CHL1 was seen mostly at the surface of the transfected HEK293 cells, I hypothesize that expression of DRD2S and DRD2L at the cell surface affects the amount of the receptor interaction with CHL1. In fact, differential expression of DRD2S and DRD2L at the cell surface was reported (Khan et al., 1998). Using electron microscopic images, Khan et al. (1998) observed that DRD2S is located predominantly at the surface of cells whereas DRD2L is located predominantly intracellularly. Considering that the differential expression of DRD2S and DRD2L at the cell surface reported by Khan et al. (1998) was analyzed only in the dopaminergic neurons, the hypothesis presented here should be verified analyzing the DRD2S and DRD2L expression at the surface of mouse dopaminergic neurons and mouse MSNs. Altogether, I show that both DRD2 forms co-localize with CHL1 mostly at the cell surface, but DRD2S co-localizes with CHL1 to a higher extent than DRD2L. I propose that the different level of co-localization of CHL1 with DRD2S and DRD2L is a consequence of reduced expression of DRD2L at the cell surface compared to the cell surface expression of DRD2S.

In an initial experiment, I showed a potential binding between CHL1 and DRD2 by co-immunoprecipitation experiments performed on CHL1<sup>-/-</sup> and CHL1<sup>+/+</sup> mouse brains homogenates, revealing that DRD2 and CHL1 are in a complex and might bind to each other. Next, by ELISA, I found a direct binding between the first extracellular loop of DRD2 and the extracellular domain of CHL1. The first extracellular loop of DRD2 may function as a regulator of ligand binding and of ligand-induced receptor response due to being directly linked to and affecting the third transmembrane domain, which forms, together with other transmembrane domains of DRD2, the ligand binding site (Grundbeck et al., 2011; Wheatley et al., 2012). The conformation of DRD2, especially of its ligand binding pocket (formed by transmembrane domains 3, 5, 6 and 7), of its second extracellular loop and of its G protein-binding third intracellular loop (Kling et al., 2014) is differentially affected by different DRD2 ligands such as an inverse agonist risperidone (Wang et al., 2018) and partial agonists aripiprazole and FAUC350 (Kling et al., 2014). Also, different substances classified as the same type of DRD2 ligand, for instance aripiprazole and FAUC350, lead to different conformations of the receptor (Kling et al., 2014). The first extracellular loop is not mentioned as often as the second extracellular loop with regard to the ligand-induced conformational changes of the receptor, however, it was shown that a single Gly residue in the first extracellular loop determines the selectivity of certain ligands for the DRD3 versus the DRD2 receptors (for instance in case of R-PG 648, which is a DRD3 antagonist) (Keck et al., 2014) suggesting a role for the first extracellular loop in adaptation of a specific ligand-induced receptor conformations resulting in a cellular response to the ligand. This role of the first extracellular loop of DRD2 was recently confirmed by Wang et al. (2018), who showed that risperidone-bound DRD2 rearranges its binding pocket exposing Trp100 of the first extracellular loop to interact with Ile184 of the second extracellular loop and with Leu94 to form a hydrophobic patch to which risperidone binds. Therefore, it is possible that binding of CHL1 to the first extracellular loop of DRD2 may affect the formation of a ligand-induced conformation of the receptor and thus may have an impact on the response of the receptor to its ligands.

Considering that CHL1 and DRD2 interact through their extracellular domains, both *cis*- and *trans*-interactions between these molecules are possible. The interaction in *cis*-orientation occurs when both molecules that interact are expressed by the same cell, and interaction in *trans*-orientation occurs when the two interacting molecules are expressed by different cells (Held & Mariuzza, 2011). I showed the *trans*-interaction between CHL1 and DRD2 forms by binding of CHL1-Fc, containing only the extracellular domain of CHL1, to DRD2S- and DRD2L-expressing HEK293 cells. This result indicates that the pre-synaptic CHL1 may interact with and regulate the post-synaptic DRD2L, which is important considering that only the pre- (Andreyeva et al., 2010) and not the post-synaptic expression of CHL1 was found so far.

## 9.2. CHL1 regulates agonist-induced internalization of DRD2, but not DRD2 degradation, ligand binding to DRD2 and DRD2-regulated intracellular signaling cascades

Using transfected HEK293 cells I showed that CHL1 reduces agonist-induced internalization of DRD2S. I could not find the impact of CHL1 on agonist-induced DRD2 degradation, binding of agonist to DRD2 and activation of intracellular signaling cascades triggered by stimulation of DRD2.

By “antibody feeding” experiments and cell surface biotinylation performed on transfected HEK293 cells I found that, in absence of CHL1, the internalization of DRD2S in response to stimulation with quinpirole is enhanced in comparison to the presence of CHL1. Internalization of receptors upon agonist binding functions to protect cells from over-stimulation (Del’guidice et al., 2011). The internalization is mediated via the intracellular signaling cascades which are activated upon DRD2 stimulation: receptors become phosphorylated by GRKs leading to recruitment of  $\beta$ -arrestins desensitizing receptors and recruiting a clathrin adaptor protein adaptin and clathrin, which results in the internalization of receptors (Del’guidice et al., 2011). As CHL1 was found to participate in the uncoating of clathrin-coated vesicles during exocytosis processes at the pre-synaptic membrane (Leshchyns’ka et al., 2006), one explanation for the CHL1-dependent inhibition of DRD2S internalization is that CHL1 regulates the clathrin-mediated receptor endocytosis. CHL1 could potentially inhibit the clathrin-mediated endocytosis by interfering with recruitment, binding or functioning of proteins participating in this process. The possible role of CHL1 in clathrin-dependent endocytosis should be investigated in future experiments.

In addition, CHL1 may influence the DRD2S internalization by affecting the response of the receptor to its agonist. CHL1 could regulate the receptor’s response to agonists by affecting the agonist binding affinity state of the receptor. It was shown that DRD2 may exist in two inter-convertible states: DRD2<sup>high</sup> which has a high agonist binding affinity due to being coupled with the G-protein, and DRD2<sup>low</sup> which is G-protein uncoupled and thus has a low agonist-binding affinity (Graff-Guerrero et al, 2009). Different proteins may have impact on the agonist binding affinity state of DRD2, for instance Ferre et al. (1991) showed that stimulation of adenosine receptor A<sub>2a</sub> reduces DRD2 agonist binding affinity in cell membranes prepared from rat striatum, and Seeman et al. (1989) found that treatment of DRD1 with an antagonist reduced the amount of DRD2<sup>high</sup> receptors in canine striatal preparations. Interestingly, adenosine receptor A<sub>2a</sub> and DRD1 were identified as binding partners of DRD2 (Perreault et al., 2014). Therefore, CHL1 as a binding partner of DRD2 could influence its agonist binding affinity state leading to a larger amount of low-affinity DRD2S (DRD2S<sup>low</sup>) and thereby reducing the DRD2S response to quinpirole. Interestingly, although not confirmed by experiments, it is suggested that in a psychosis a higher proportion of DRD2<sup>high</sup> to DRD2<sup>low</sup> exists (Graff-Guerrero et al., 2009; Kubota et al., 2017). If more DRD2<sup>high</sup> exists in psychosis, which exists in schizophrenia (Cannon, 2015) – a disorder in which mutated version of CHL1 plays a role (Sakurai et al., 2002; Chen et al., 2005; Shaltout et al., 2013) – and more DRD2S are internalized by quinpirole-stimulated HEK293 cells in

absence of CHL1, then it is tempting to speculate that the mutation in CHL1, similarly as the absence of CHL1, affects the agonist binding affinity state of DRD2S leading to a higher amount of high affinity DRD2S (DRD2S<sup>high</sup>). This further supports the notion that CHL1 could influence the internalization of DRD2S by regulating its agonist binding affinity state.

I found that CHL1 has no impact on DRD2 degradation upon stimulation with quinpirole as well as has no effect on binding of a ligand to DRD2 and on activation of intracellular signaling pathways in transfected HEK293 cells. The explanation for these results may be that CHL1 simply does not play a role in the mentioned processes, which is possible considering that in all but one of the experiments (measurement of TH phosphorylation) stimulations of cells co-expressing DRD2 forms and CHL1 gave expected results. However, HEK293 cells are not neurons and do not normally express DRD2 and CHL1, therefore it is conceivable that some factors necessary for DRD2 to function properly (like special G-proteins or elements of signaling cascades) or for CHL1 to exert its function related to regulation of DRD2 are missing in these cells. In order to confirm that CHL1 does not have an effect on agonist-induced degradation of DRD2, DnsylD1 binding to DRD2 and phosphorylation of TH, DARPP32 and ERK upon stimulation of DRD2, these experiments should be repeated in future studies using neuronal cell lines or, preferably, primary cultures of dopaminergic neurons and MSNs.

It is established that, upon stimulation with an agonist, DRD2 is internalized in  $\beta$ -arrestin- and clathrin-dependent manner (Del'guidice et al., 2011) and destined for degradation (Bartlett et al., 2005). My results on the impact of CHL1 on quinpirole-induced degradation of DRD2S and DRD2L showed clearly that the quinpirole-induced DRD2 degradation occurs in presence and absence of CHL1 and is associated with the degradation of CHL1, but CHL1 does not have an impact on DRD2 degradation. These results imply that CHL1 has no role in the degradation of DRD2, but the stimulation of cells with the DRD2 agonist or the subsequent DRD2 degradation might influence the degradation of CHL1. Considering that the aim of the study was to investigate the role of CHL1 in the functioning of the receptor, the impact of the receptor on CHL1 degradation was not further investigated. Nevertheless, as CHL1 is relevant for the proper functioning of many proteins other than DRD2, it would be important to know how the DRD2 level affects the level of CHL1. Certain impact on the degradation of proteins in this experiment could also be attributed to treatment of cells with cycloheximide, which was added to cells before stimulation with quinpirole in order to inhibit protein synthesis. Cycloheximide was not removed from the cells afterwards and was present in the culture media over the whole time of quinpirole stimulation. In the future, the possibility that cycloheximide influences the degradation of the measured proteins should be excluded performing a control experiment in which degradation of DRD2 and CHL1 in response to cycloheximide would be measured.

In the experiment measuring binding of a fluorescent dopamine analog DnsylD1 to DRD2 I expected to find an impact of CHL1 on the ligand binding by DRD2S and DRD2L, because the interaction of CHL1 with the

DRD2 is mediated by the first extracellular loop of the DRD2 and a possible function of this DRD2 loop is the regulation of the ligand-binding site of the receptor (Grundbeck et al., 2011; Wheatley et al., 2012). I propose that the impact of CHL1 on the DnsylD1 binding could not be shown, because the DRD2 agonist used in my experiment does not induce changes in the conformation of DRD2 that involve the change of the conformation of the CHL1-bound first extracellular loop. Moreover, conformations of DRD2 bound to many ligands were not yet described, and changes in the first extracellular loop of DRD2 were so far characterized only regarding the binding of one inverse agonist (Wang et al., 2018), thus it is unknown how dopamine analogs affect the DRD2 conformation. Of note, DRD2 may adopt different conformations upon binding of different substances classified as the same type of DRD2 ligand (Kling et al., 2014). Further studies should elucidate how different DRD2 agonists influence its conformation and if the CHL1-bound first extracellular loop of DRD2 participates in the conformational changes.

In addition, CHL1 had no effect on the phosphorylation of the elements of the DRD2-mediated intracellular signaling pathways: TH, ERK and DARPP32. The experiments measuring the activation of the intracellular signaling pathways upon quinpirole stimulations were performed on HEK293 cells co-transfected with plasmid constructs carrying DARPP32 and DRD2L with and without CHL1 as a model of post-synaptic cells, and with plasmid constructs carrying TH and DRD2S with and without CHL1 in case of a pre-synaptic model. Binding of agonists to DRD2 leads to an exchange of a guanosine diphosphate (GDP) to a guanosine triphosphate (GTP) at the  $\alpha$  subunit of the heterotrimeric  $G_i$  protein, dissociation of the  $\alpha$  subunit and inhibition of the ACy by the GTP- $\alpha$  subunit complex (Beaulieu & Gainetdinov, 2011). The inhibition of ACy leads to reduction of the active PKA (Beaulieu & Gainetdinov, 2011), which is an enzyme phosphorylating TH (Dunkley et al., 2004; Chen et al., 2012) and DARPP32 (Beaulieu & Gainetdinov, 2011). ERK, in turn, is phosphorylated mostly in the RAF / MEK / ERK pathway activated upon  $\beta$ -arrestin recruitment and receptor internalization (Chen et al., 2012). In my experiments the expected increase in ERK phosphorylation upon DRD2S and DRD2L stimulation (Luessen et al., 2016), as well as the expected reduction in DARPP32 phosphorylation at Thr34 upon DRD2L stimulation (Lindskog et al., 1999) were observed. Interestingly, no response of TH upon the DRD2S stimulation was detected. Lack of any effect of the DRD2S stimulation on the TH phosphorylation at Ser40 could be explained by the use of non-neuronal cell line HEK293 as experimental model. HEK293 cells do not endogenously express DRD2, CHL1 and TH and, possibly, lack certain mechanisms relevant for at least some aspects of the functioning of these proteins or part of the signaling cascades that are present in dopaminergic neurons. Moreover, HEK293 cells are tumor cells having abnormal signaling cascades and proliferating constantly in contrast to post-mitotic neurons. Therefore, the experiment in which TH phosphorylation is measured upon DRD2S stimulation with quinpirole should be repeated using primary cultures of dopaminergic neurons from CHL1<sup>-/-</sup> and CHL1<sup>+/+</sup> mice.

Although transfection of cells simultaneously with two plasmid constructs is a common technique successfully used by other research groups (Xie et al., 2011; Abbah et al., 2016), an explanation for the lack of effect of quinpirole stimulation on TH phosphorylation could also be that the co-transfection of cells was not successful and resulted in a co-expression of TH with DRD2S by only small fractions of cells.

### **9.3. CHL1 regulates the level of proteins related to DRD2 signaling in the dorsal and the ventral striatum of adult mice**

The measurement of levels of proteins involved in dopaminergic signaling in the striatum of CHL1<sup>-/-</sup> mice showed that these mice express lower levels of DRD2 and pTH in the dorsal striatum, whereas in the ventral striatum they express less pDARPP32 and more DARPP32 compared to CHL1<sup>+/+</sup> mice. Furthermore, in the dorsal versus the ventral striatum of CHL1<sup>+/+</sup> mice different levels of all analyzed proteins were observed, whereas the dorsal and the ventral striatum of mice not expressing CHL1 differed only in the amount of TH.

Binding of agonists to DRD2S and DRD2L leads to inhibition of TH phosphorylation (Dunkley et al., 2004; Chen et al., 2012) and DARPP32 phosphorylation (Beaulieu & Gainetdinov, 2011), respectively. The obtained result showing reduced amounts of DRD2 and pTH but normal amount of pDARPP32 in the dorsal striatum of mice lacking CHL1 compared to wild-type mice suggests that the activation of the pre-synaptic DRD2S, but not the post-synaptic DRD2L may be affected in the dorsal striatum of CHL1<sup>-/-</sup> mice. Phosphorylation (activation) of TH is inhibited by dopamine in a negative feedback loop, meaning that dopamine released from the pre-synaptic neuron activates DRD2S autoreceptors which results in pTH reduction (Ford, 2014). The found reduced level of DRD2 may seem to be contrary to the found reduced pTH level; however, increased cell surface availability of DRD2S or a higher proportion of DRD2S<sup>high</sup> might explain this changes. More receptor located at the cell surface would mean that more receptor is available for dopamine binding, leading to increased activation of the signaling pathways and inhibition of TH phosphorylation. On the other hand, a theory about a higher proportion of DRD2S<sup>high</sup> in absence of CHL1 and a lower proportion of DRD2S<sup>high</sup> in presence of CHL1 could not only explain the found reduction in the pTH level in CHL1<sup>-/-</sup> mice, but is also in line with my results on DRD2S internalization which showed that CHL1 reduces quinpirole-induced internalization of DRD2S possibly due to increased proportion of DRD2S<sup>low</sup> to DRD2S<sup>high</sup> receptors. Therefore, I suggest that CHL1 promotes the low agonist binding affinity state of DRD2S, meaning that in absence of CHL1 a higher proportion of DRD2S<sup>high</sup> would be present at the cell surface. Another factor leading to pTH reduction could be an elevation in dopamine levels in the dorsal striatum, however, no change in the amount of the post-synaptic pDARPP32 suggests presence of normal dopamine levels in CHL1<sup>-/-</sup> mice. The reduction of pDARPP32 associated with an unaltered DRD2 amount in the ventral striatum of CHL1<sup>-/-</sup> mice indicates that the change in pDARPP32 level could be caused by changes in other dopamine

receptors, such as downregulation of DRD1, the activation of which leads to increased DARPP32 phosphorylation (Bateup et al., 2008). However, similarly as in case of DRD2S and pTH in the dorsal striatum, the distribution of DRD2L in the ventral striatal MSNs with more receptor distributed at the cell surface, or higher proportion of a high-affinity state DRD2L in the ventral striatum of CHL1<sup>-/-</sup> compared to CHL1<sup>+/+</sup> mice also could result in pDARPP32 reduction. Based on these findings, I hypothesize that the reduced levels of pTH in the dorsal striatum and pDARPP32 in the ventral striatum of mice lacking CHL1 are caused by a higher proportion of DRD2S<sup>high</sup> and DRD2L<sup>high</sup> in the dorsal and the ventral striatum of these mice, respectively, or the cell surface levels of DRD2S in the dorsal striatum and DRD2L in the ventral striatum of CHL1<sup>-/-</sup> mice are higher than in CHL1<sup>+/+</sup> mice.

In the experiment in which I measured protein levels in the dorsal and the ventral striatum of CHL1<sup>-/-</sup> and CHL1<sup>+/+</sup> mice I found also that the dorsal and the ventral striatum of CHL1<sup>-/-</sup> mice have similar levels of DRD2, pTH, pDARPP32 and DARPP32, but not TH, whereas the dorsal and the ventral striatum of CHL1<sup>+/+</sup> mice differ regarding expression of all these proteins. This finding implies that lack of CHL1 affects protein expression and physiology of the striatum. Considering that proper functioning of the striatum is relevant, for instance, for the development of speech (Takahashi et al., 2003; De Diego-Balaguer et al., 2008), the observed striatal protein expression abnormalities in CHL1<sup>-/-</sup> mice may suggest that the delayed speech development, found so far in all reported cases of deletions and duplications of the CHL1 gene in humans (Pohjola et al., 2010; Cuoco et al., 2011; Shoukier et al., 2013; Tassano et al., 2014; Palumbo et al., 2015; Li et al., 2016; Bertini et al., 2017), could be the consequence of striatal abnormalities. Further studies characterizing the impact of CHL1 on striatal morphology and expression of proteins, for instance on expression of Forkhead box protein P2 (Foxp2) that is one of the proteins most relevant for the speech development (Takahashi et al., 2003) should be performed.

#### **9.4. CHL1 affects the number of dopaminergic fibers in the mesolimbic dopaminergic pathway of mice**

I found that CHL1<sup>-/-</sup> mice exhibit more dopaminergic fibers running to the ventral striatum but normal dopaminergic fibers density in the ventral striatum compared to CHL1<sup>+/+</sup> mice. Dopaminergic fibers running towards the dorsal striatum and the dopaminergic fibers density in the dorsal striatum of CHL1<sup>-/-</sup> mice were unaffected.

The analysis of the dopaminergic fibers running from the ventral midbrain to the striatum in sections of adult CHL1<sup>-/-</sup> and CHL1<sup>+/+</sup> mouse brains showed that CHL1<sup>-/-</sup> mice have stronger TH-fluorescence intensity of the fibers running to the ventral striatum compared to CHL1<sup>+/+</sup> mice, and that the fibers running to the ventral striatum in CHL1<sup>-/-</sup> mice cover a larger area than in CHL1<sup>+/+</sup> mice, indicating that CHL1<sup>-/-</sup> mice may have more dopaminergic fibers running to the ventral striatum. These results were similar for male and female

mice. With the qualitative results obtained from the analysis of the anti-TH- and anti-pTH-stained sections of CHL1<sup>-/-</sup> and CHL1<sup>+/+</sup> mice brains I showed that CHL1<sup>-/-</sup> mice have more dopaminergic fibers running in the ventral portion of the brain and towards the ventral striatum. Additionally, the quantification of TH-positive dopaminergic fibers entering the striatum showed that the relative area of dopaminergic fibers entering the ventral striatum in CHL1<sup>-/-</sup> mice is larger than in CHL1<sup>+/+</sup> mice, further suggesting that CHL1<sup>-/-</sup> mice have more dopaminergic fibers running to the ventral striatum. Based on these results I conclude that CHL1<sup>-/-</sup> mice may have more dopaminergic fibers running to the ventral striatum than CHL1<sup>+/+</sup> mice, meaning that CHL1<sup>-/-</sup> mice may have more dopaminergic fibers in the mesolimbic dopaminergic pathway that runs from the VTA to the ventral striatum. The analyses showed that the dopaminergic fibers of the nigrostriatal pathway (running from the SN to the dorsal striatum) are not changed, meaning that CHL1 affects only the dopaminergic fibers of the mesolimbic pathway. Although the dopaminergic fibers running to the striatum were not counted, the indirect measures used here to assess their amount indicate a higher number of dopaminergic fibers running to the ventral striatum in CHL1<sup>-/-</sup> compared to CHL1<sup>+/+</sup> mice.

The observed abnormal number of dopaminergic fibers in the mesolimbic pathway of CHL1<sup>-/-</sup> mice could be caused by several factors. One cause could be the increased number of midbrain dopaminergic neurons sending their axons to the ventral striatum in CHL1<sup>-/-</sup> mice. The result of the stereological quantification of the dopaminergic neurons in the SN and the VTA showed that CHL1<sup>-/-</sup> mice have normal number of SN dopaminergic neurons but reduced number of VTA dopaminergic neurons compared to CHL1<sup>+/+</sup> mice. Considering that the VTA sends dopaminergic fibers to the ventral striatum, a reduced number of VTA dopaminergic neurons suggests there are less fibers running to the ventral striatum in CHL1<sup>-/-</sup> mice, which is contrary to my finding. Nevertheless, with the result obtained by the quantification of TH-positive cells of the SN and the VTA I still cannot exclude the possibility that more dopaminergic cells project to the striatum in CHL1<sup>-/-</sup> than in CHL1<sup>+/+</sup> mice, because in the quantification different subpopulations of VTA dopaminergic neurons projecting to different brain structures were not analyzed separately. In the VTA at least two such subpopulations of dopaminergic neurons are distinguished based on differential responds to opioids (Margolis et al., 2006; Van den Heuvel & Pasterkamp, 2008; Thomas et al., 2018) – the subpopulation not responding to kappa opioids sends axons to the ventral striatum forming the mesolimbic dopaminergic pathway and the subpopulation responding to kappa opioids sends axons to the frontal cortex forming the mesocortical dopaminergic pathway (Margolis et al., 2006; Van den Heuvel & Pasterkamp, 2008). Therefore, a quantification of the subpopulations of the VTA dopaminergic neurons is necessary to determine which dopaminergic pathway running from the VTA contains less dopaminergic neurons in CHL1<sup>-/-</sup> mice.

Increased number of dopaminergic fibers running to the ventral striatum of CHL1<sup>-/-</sup> mice could potentially be caused by increased arborization of the dopaminergic fibers. However, Alsanie et al. (2017) reported that homophilic CHL1-CHL1 interaction promotes outgrowth and branching of developing dopaminergic axons,

potentially resulting in more dopaminergic fibers in CHL1<sup>+/+</sup> mice compared to CHL1<sup>-/-</sup>, which is opposite to what I found. This discrepancy between my results and the results of Alsanie et al. could be caused by the different age of the analyzed animals as well as by the fact that the Alsanie et al. measured the impact of CHL1 on dopaminergic neurite outgrowth and branching *in vitro*, using cultured dopaminergic precursors, and did not supplement it with an *in vivo* analysis. In fact, in one of their experiments Alsanie et al. (2017) found an impact of CHL1 on differentiation of dopaminergic neurons *in vitro* but could not confirm this result with the *in vivo* analysis. Therefore, I hypothesize that I did not find the increased number of dopaminergic fibers in CHL1<sup>+/+</sup> mice either because the homophilic CHL1 interaction did not affect the branching of dopaminergic fibers in the mouse brains, or because the effect of CHL1 found by Alsanie et al. plays a role and can be detected in the dopaminergic system only during developmental stages or in a specific brain location such as the striatum.

A factor that could affect the number of the dopaminergic fibers running to the striatum is abnormal withdrawal of dopaminergic fibers from the ventral striatum in a process called synaptic pruning. During embryonic development of the dopaminergic system, the ventral and the dorsal striatum receive dopaminergic fibers from both the VTA and the SN, and during late embryonic and early postnatal development the fibers sent by the SN to the ventral striatum and the fibers sent by the VTA to the dorsal striatum are removed (Van den Heuvel & Pasterkamp, 2008). Although the factors regulating the synaptic pruning are unknown, brain-derived neurotrophic factor (BDNF), glial cell line-derived neurotrophic factor (GDNF) and neurotrophins 3, 4 and 5 potentially play a role (Bissonette & Roesch, 2016). Abnormal pruning of the synapses that SN dopaminergic neurons make on ventral striatal neurons of CHL1<sup>-/-</sup> mice could contribute to the increased amount of dopaminergic fibers running to the ventral striatum in these mice. In order to investigate this possibility, anterograde and retrograde tracing experiments should be performed to map the dopaminergic fibers sent from the VTA and the SN.

The analysis of the dopaminergic fibers density in the whole striatum, in the dorsal striatum and in the ventral striatum showed no effect of CHL1, implying that the increased number of dopaminergic fibers entering the ventral striatum of CHL1<sup>-/-</sup> mice does not reflect the density of the dopaminergic fibers in the ventral striatum. The results in this experiment were similar for male and female mice. Outgrowth of dopaminergic axons towards their target structures starts in a rat brain at E14-E15. First, the developing NAc receives the dopaminergic fibers and about 2-3 days later (at E17) the dopaminergic fibers reach the developing CP (Van den Heuvel & Pasterkamp, 2008). The guidance of the dopaminergic fibers is regulated by different cues, which influence this process both negatively (for instance in case of ephrins, DCC, receptor for netrins Unc5, semaphorin-3A and Slit) and positively (like in case of ephrins, DCC and GDNF). Some of these guidance molecules, for instance netrin-1 and DCC, can regulate both the dopaminergic axon outgrowth towards the striatum and the establishment of local circuits within the striatum (Van den Heuvel

& Pasterkamp, 2008). Considering that I found abnormal levels of DRD2, CHL1, pDARPP32, DARPP32 and pTH in the dorsal and ventral striatum of CHL1<sup>-/-</sup> mice, it is possible that the protein composition of the striatum in these mice is different also for other proteins, e.g. for proteins functioning as guidance cues regulating the outgrowth of the dopaminergic fibers in the striatum. Interestingly, the molecules regulating the outgrowth of fibers sometimes may affect also the branching of fibers: CHL1, which is also an axon guidance molecule, induced branching of the dopaminergic fibers in the cultured cells (Alsanie et al., 2017); therefore, although more dopaminergic fibers reach the ventral striatum in CHL1<sup>-/-</sup> mice, the absence of CHL1 could result in less branching of these dopaminergic fibers leading to similar dopaminergic fibers density in the ventral striatum of CHL1<sup>-/-</sup> and CHL1<sup>+/+</sup> mice. Normal striatal dopaminergic fibers density despite reduced number of VTA dopaminergic neurons in mice was reported earlier, by Pham et al. (2010), who studied mice lacking protein deglycase DJ-1 known also as Parkinson's disease protein 7 (PARK7). DJ-1 protein is expressed in the cytoplasm of cells but may translocate to mitochondria, and its main function is to protect cells against oxidative stress (Yokota et al., 2003). Pham et al. (2010) suggested that the unaffected striatal dopaminergic fibers density despite reduced number of VTA dopaminergic neurons is an effect of a presence of some sort of compensatory mechanisms in the brains of DJ-1-deficient (DJ-1<sup>-/-</sup>) mice, for instance, increased sprouting of the dopaminergic fibers. Similarly, such compensatory mechanisms may be present in the brains of CHL1<sup>-/-</sup> mice.

#### **9.5. CHL1<sup>-/-</sup> mice exhibit a lower number of dopaminergic neurons in the VTA compared to CHL1<sup>+/+</sup> mice**

The stereological quantification of SN and VTA dopaminergic neurons in sections of adult CHL1<sup>-/-</sup> and CHL1<sup>+/+</sup> mice, performed by Prof. Moratalla and Dr. Granado (Cajal Institute, Madrid), showed that CHL1<sup>-/-</sup> mice have significantly less dopaminergic neurons in the VTA. CHL1<sup>-/-</sup> mice also have less dopaminergic neurons in the SN compared to CHL1<sup>+/+</sup> mice, though not significantly. The analysis of VTA and SN dopaminergic neurons in males and females showed that both genders have less neurons in the SN and the VTA when they do not express CHL1, but only in case of males the difference in the number of VTA dopaminergic neurons is statistically significant.

The found difference in the number of VTA dopaminergic neurons in CHL1<sup>-/-</sup> and CHL1<sup>+/+</sup> mice is probably not caused by different level of differentiation of dopaminergic progenitors in presence and absence of CHL1 during dopaminergic system development, as Alsanie et al. (2017) showed that CHL1 does not influence the number of differentiating dopaminergic neurons *in vivo*, in brains of developing mice. This observation suggests that events leading to the reduction of VTA dopaminergic neurons in CHL1<sup>-/-</sup> mice occur later during development or in adulthood.

The number of ventral midbrain dopaminergic neurons in mice changes naturally during two events of apoptosis that occur directly after birth and during the second postnatal week (Burke et al., 2003; Oo et al., 2003). Interestingly, mouse cerebellar neurons undergo developmental apoptosis and the impact of CHL1 on this process was studied by Katic et al. (2017). In their studies, Katic et al. found that CHL1 promotes survival of the cerebellar neurons during cerebellar neuron apoptosis due to interaction with Ptc1 and activation of the Ptc1 / smoothed pathway. Considering that both cerebellar neurons and dopaminergic neurons undergo programmed cell death during early postnatal development and that the presence of CHL1 is correlated with the enhanced survival of cerebellar neurons and with the larger number of VTA dopaminergic neurons in adult mice, it is possible that the reduction of VTA dopaminergic neurons in mice lacking CHL1 is a consequence of abnormal apoptosis during early postnatal development and that the apoptosis in both the cerebellum and the VTA are regulated by the same or similar mechanisms. The impact of the interaction of CHL1 with Ptc1 on the survival of VTA dopaminergic neurons should be investigated in future studies.

So far, factors regulating dopaminergic neurons apoptosis during dopaminergic system development are largely unknown, but it was suggested that this process may be regulated by signals coming from the target structures of the dopaminergic projections. This conclusion was based on the observations that damages induced in the striatum or a disrupted connection of the dopaminergic neurons with the striatum resulted in increased cell death of ventral midbrain dopaminergic neurons (Marti et al., 1997; Burke et al., 2003). Moreover, intrastriatal administration of GDNF suppressed natural cell death of SN dopaminergic neurons in P1 rats (Oo et al., 2003). Of note, in the experiment in which I analyzed the levels of proteins (DRD2, pTH, TH, pDARPP32, DARPP32 and CHL1) in dorsal and ventral striatum of adult CHL1<sup>-/-</sup> and CHL1<sup>+/+</sup> mice, different expression of most of the analyzed proteins was found in dorsal and ventral striatum of CHL1<sup>-/-</sup> compared to CHL1<sup>+/+</sup> mice, which suggests abnormalities in the functioning of the striatal cells and, possibly, in the morphology of the striatum in these mice. This result indicates that there is a possibility that CHL1 affects apoptosis of ventral midbrain dopaminergic neurons by regulating expression of proteins in the target structures of the dopaminergic projections, such as the striatum. The structure with the reduced number of dopaminergic neurons in CHL1<sup>-/-</sup> mice, the VTA, projects mainly to the ventral striatum and to the frontal cortex, but small portions of VTA cells project also to other structures such as the hippocampus (Nobili et al., 2017). Thus, the frontal cortex or the hippocampus as target structures of the projection may, just like the striatum, regulate the amount of VTA neurons. In fact, some structural changes in the cortex and the hippocampus were reported in CHL1<sup>-/-</sup> mice (Montag-Sallaz et al., 2002; Demyanenko et al., 2004). In order to determine whether the dopaminergic neurons projecting to the ventral striatum or those projecting to the frontal cortex or the hippocampus are eliminated, stereological quantification of the subpopulations of VTA dopaminergic neurons and anterograde/retrograde tracing experiments should be performed. The information about the specific subpopulation of the dopaminergic neurons affected by lack of CHL1 is

necessary in order to establish the mechanisms through which CHL1 could regulate the dopaminergic neurons apoptosis.

In schizophrenia, a disorder associated with CHL1 (Sakurai et al., 2002; Chen et al., 2005; Shaltout et al., 2013), abnormal signaling in the dopaminergic pathways running from the VTA is observed. Interestingly, no change in the number of the VTA dopaminergic neurons was found in schizophrenic patients (Rice et al., 2016). However, TH level was found to be significantly reduced in the VTA and the SN (Rice et al., 2016) and the amount of neuromelanin, which is a byproduct of dopamine synthesis, was reduced in the VTA of schizophrenics compared to healthy people (Yamashita et al., 2016). These reports suggest that the VTA activity related to dopamine production but not the number of VTA dopaminergic neurons is affected in schizophrenia.

A factor that was shown to contribute to a reduction of the number of VTA dopaminergic neurons is loss of DJ-1 protein (Pham et al., 2010). Abnormal functioning of DJ-1 is associated with Parkinson's disease, but, interestingly, at all ages DJ-1<sup>-/-</sup> mice do not present the hallmark of Parkinson's disease which is a reduced number of dopaminergic neurons in the SN, indicating that DJ-1 possibly contributes to the non-motor symptoms of the disease such as cognitive problems and loss of motivation (Pham et al., 2010). The reduced number of VTA dopaminergic neurons in DJ-1<sup>-/-</sup> mice does not affect the number of the dopaminergic fibers in the striatum, suggesting that the remaining VTA dopaminergic cells compensate with increased sprouting of the fibers (Pham et al., 2010). With the reduced level of VTA dopaminergic neurons but normal dopaminergic fibers density in the striatum, CHL1<sup>-/-</sup> mice resemble the DJ-1<sup>-/-</sup> mice, which means that CHL1 and DJ-1 may be functionally associated. Experiments verifying a potential interaction between DJ-1 and CHL1 as well as experiments analyzing the impact of CHL1 on DJ-1 functioning are recommended.

I show that the number of VTA dopaminergic neurons is reduced in both male and female CHL1<sup>-/-</sup> compared to CHL1<sup>+/+</sup> mice, but the reduction is statistically significant only in males. Although no statistically significant difference was observed when males and females were compared, the found effect of CHL1 only in males suggests that certain gender-related factors play a role in the reduction of VTA cell number in CHL1-deficient mice. In fact, gender-related differences in VTA morphology, physiology and functions were reported (Gillies et al., 2014 and references therein). Some of the reported gender-related morphological differences in the VTA include enlarged volume and increased number of dopaminergic cells in females (McArthur et al., 2007), the latter of which was not observed in my study. Dopamine release into the striatum is equal in males and females at rest, however, females present a higher density of DAT and a higher rate of dopamine synthesis compared to males, whereas males have a higher DRD2 expression (Pohjalainen et al., 1998; Gillies et al., 2014). Additionally, disorders associated with abnormal functioning of the dopaminergic system often affect one gender more than the other: ADHD is more prevalent in men (Ougrin et al., 2010) whereas depression and anxiety disorders occur in women more often than in men

(Seeman, 1997). Moreover, it was shown that women are more sensitive to the rewarding aspect of drugs compared to men, which is related to differential activation of the NAc to which the VTA projects (Carroll, 2004; Lynch, 2006). The differences between female and male brains are caused in part by the production of different hormones in males (testosterone) and females (estrogens and progesterone) (Gillies et al., 2014). The role of hormones different in males and females was concluded based on observations that the gender-related differences in VTA-dependent functions such as cognitive functions, mood and motivation are regulated by these gender-related hormones (Brinton, 2009; Gillies et al., 2014). The other cause for differences between males and females is the expression of genes located at the Y chromosome in males (Milsted et al., 2004; Czech et al., 2012; Gillies et al., 2014). Sex-determining region Y (SRY), a transcription factor expressed from the Y chromosome, is detected in the VTA and the SN and its presence positively regulates expression of enzymes participating in dopamine synthesis (Milsted et al., 2004; Czech et al., 2012). It is unknown what makes males more susceptible than females to the reduction of VTA dopaminergic neurons caused by the absence of CHL1. Nevertheless, based on the finding presented in this thesis, one can speculate that CHL1 regulates the activity of certain gonadal steroids or proteins relevant for the VTA dopaminergic cells. Further studies should identify the specific population of VTA dopaminergic cells that becomes absent in males lacking CHL1 and elucidate the role of CHL1 in these cells.

#### **9.6. CHL1<sup>-/-</sup> mice do not present some of the features related to schizophrenia**

In the study I found that only one of the four analyzed schizophrenia-related features – the enlargement of brain ventricles – can be found in the brains of CHL1<sup>-/-</sup> mice. The enlarged lateral ventricles in CHL1<sup>-/-</sup> mice were already reported by Montag-Sallaz et al. (2002). The three other features that are related to schizophrenia – thinning of the frontal cortex, reduction of thalamus size and increased DRD2 expression in the frontal cortex – could not be observed in the brains of CHL1<sup>-/-</sup> mice.

In schizophrenia, enlargement of the brain ventricles is likely a consequence of reduction of the size of other brain structures – thalamus, temporal cortex and striatum (Gaser et al., 2004). Abnormal size of the brain structures in schizophrenia is considered to be the outcome of abnormal neurodevelopment and different organization of cells and their connections (Brickman et al., 2004; Salgado-Pineda et al., 2007). In brains of schizophrenia patients changes of the volumes of different structures are thought to be interconnected and the affected structures are often elements of the impaired subcortico-cortical circuitry: for instance, thalamic reduction, considered to be related to the attention deficits and sensory-perceptual impairment in schizophrenia, correlates with reduced volume of either the frontal or the temporal grey matter depending on the part of the thalamus that is most affected (Brickman et al., 2004). The reduced thickness of the frontal cortex, which is an often reported feature of the pathomorphology of schizophrenia (Goldman et al., 2009),

is likely involved in information processing deficits, prioritizing deficits and in impaired response to information (Salgado-Pineda et al., 2007). Apart from presenting the morphological abnormalities, it was reported that people suffering from schizophrenia express more DRD2 in the frontal cortex. Talerico et al. (2001) showed that the increased expression of DRD2 forms in schizophrenia exists in non-medicated patients, which indicates that the receptor may be involved in the disorder or its increased amount is due to, for instance, elevated dopamine levels, rather than due to administration of antipsychotic medication (Abi-Dargham et al., 2000).

My results suggest that CHL1 does not have a strong influence on the development of schizophrenia-related brain morphology and protein expression. However, it is important to note that the SNP (Leu17Phe) correlated with schizophrenia in the studies of Sakurai et al. (2002), Chen et al. (2005) and Shaltout et al. (2013) does not necessarily lead to production of a non-functional CHL1 protein and thus the mice not expressing CHL1 protein may not be a good model to study the role of CHL1 in schizophrenia. The Leu17Phe SNP of CHL1 was never studied and it is unknown how it affects the structure, trafficking and functions of CHL1. In order to investigate how CHL1 contributes to schizophrenia, the Leu17Phe missense polymorphism in the CHL1 gene should be studied and my experiments should be repeated using transgenic mice homozygous for the mutated version of the CHL1 gene. The second possible explanation for the discrepancy between my results and reports of research groups studying the morphological changes in the brains of people suffering from schizophrenia is the different method used for the analysis of the size of brain structures. The methods used by other research groups (for instance the structural magnetic resonance imaging) allow to determine volumes of the analyzed structures, whereas my analysis was performed on tissue sections and, although from each animal several sections from different positions on the Z-axis were analyzed, instead of the volumes the areas of the analyzed structures were measured. It is therefore recommended to repeat the analysis of the size of the thalamus, the frontal cortex and the brain ventricles using a method determining the volumes of these structures.

### **9.7. General conclusions**

In the present study I performed experiments to determine the interaction between CHL1 and DRD2 and to find the impact of this interaction on functions of DRD2. Moreover, I analyzed the morphology of dopaminergic pathways running from the ventral midbrain to the striatum of CHL1<sup>-/-</sup> mice and studied the morphological features and DRD2 expression related to schizophrenia in brains of CHL1<sup>-/-</sup> mice.

I propose here that CHL1 interacts with DRD2 mostly at the cell surface due to the fact that both, CHL1 and DRD2 molecules, are expressed at the cell surface in large amounts. A direct interaction between CHL1 and DRD2, mediated through the extracellular domain of CHL1 and the first extracellular loop of DRD2, may

affect conformations that the receptor takes in response to different ligands. The found effect of CHL1 on DRD2S internalization could be a result of CHL1 affecting an agonist binding affinity state of the receptor. Moreover, CHL1 influences DRD2-regulated intracellular signaling cascades in the dorsal and the ventral striatum of mice, which also could be explained with CHL1 affecting the agonist binding affinity state of DRD2 or with an abnormal cell surface distribution of DRD2 in the absence of CHL1.

The found abnormal protein levels in the dorsal and the ventral striatum of CHL1<sup>-/-</sup> mice suggest that functions of the striatum may be affected by the lack of CHL1 in these mice. Of note, striatal abnormalities are one of the reasons for problems with language development in humans, and delayed language development is a symptom of known cases of duplications and deletions of the CHL1 gene in humans.

Apart from affecting the agonist-induced internalization of DRD2 in transfected cells, no impact of CHL1 on the receptor degradation, ligand binding and activation of intracellular signaling cascades in transfected HEK293 cells could be shown. In order to confirm the lack of impact of CHL1 on these processes, experiments should be repeated using dopaminergic neurons and MSNs.

Based on the information given in the scientific literature, e.g. by Katic et al. (2017), it is tempting to speculate that the found reduced number of VTA dopaminergic neurons in CHL1<sup>-/-</sup> mice may be due to CHL1 promoting dopaminergic neurons survival during dopaminergic system development. Although CHL1<sup>-/-</sup> mice have reduced number of VTA dopaminergic neurons, they have more dopaminergic fibers running towards the ventral striatum and normal dopaminergic fibers density in the ventral striatum, which may be caused by mechanisms compensating for the reduced number of dopaminergic cells; for instance, the remaining dopaminergic cells may increase fiber arborization, or more dopaminergic cells may project to the ventral striatum in CHL1<sup>-/-</sup> mice due to, for instance, abnormal pruning of dopaminergic fibers sent by the SN. Of note, the phenotype of CHL1<sup>-/-</sup> mice, with reduced number of VTA neurons and normal striatal dopaminergic fibers density, resembles the phenotype of mice lacking DJ-1, which suggests that CHL1 and DJ-1 may be functionally related.

I propose here that the lack of CHL1 in mice does not lead to the development of schizophrenia-related abnormalities in the frontal cortex and the thalamus because the mutation in CALL that correlates with schizophrenia does not lead to the production of a non-functional CHL1 protein. Future studies should characterize an impact of the mutation in the CHL1 gene on the structure and functions of the CHL1 protein.

The results presented in this thesis indicate potential roles for CHL1 in the regulation of the agonist binding affinity state of DRD2, cell surface distribution of DRD2, ligand-induced conformational changes of DRD2 as well as in the survival of dopaminergic neurons during the development, regulation of functions of DJ-1 and the development of speech.

My results show that CHL1 is an important player in the functioning of the dopaminergic system as it not only regulates its physiological processes but also affects its morphology. The provided results contribute to the understanding of the dopaminergic system functioning and indicate new potential roles for CHL1.

## 10. List of figures

Figure 1: Schematic presentation of the CHL1 molecule. 15

Figure 2: CHL1 is a member of the IgSF-CAMs and L1 family of CAMs. 16

Figure 3: CAMs of the L1 family. 17

Figure 4: Localization of the human CHL1 gene (CALL) at the 3p26-pter (pter = terminus of the p arm). 21

Figure 5: Types of dopamine receptors. 27

Figure 6: Forms of DRD2. 28

Figure 7: Dopamine receptor trafficking. 29

Figure 8: Targets of DRD2S and DRD2L signaling. 31

Figure 9: Brain dopaminergic pathways. 32

Figure 10: Synaptic pruning in the developing dopaminergic pathways. 34

Figure 11: CHL1 and DRD2 co-localize in the adult mouse striatum. 70

Figure 12: CHL1 and DRD2 are in a close proximity in the adult mouse striatum. 71

Figure 13: Cloned plasmid constructs carrying DRD2S or DRD2L in presence and absence of CHL1. 72

Figure 14: CHL1 co-localizes closely with DRD2S and DRD2L in transfected HEK293 cells and the co-localization of DRD2S with CHL1 is more pronounced than the co-localization of DRD2L with CHL1. 74

Figure 15: Similar expression of DRD2S and DRD2L in transfected HEK293 cells. 75

Figure 16: DRD2 is co-precipitated with CHL1. 76

Figure 17: The extracellular domain of CHL1 binds directly to the first extracellular loop of DRD2. 77

Figure 18: CHL1 co-localizes closely with DRD2S and DRD2L predominantly at the surface of transfected HEK293 cells. 78

Figure 19: CHL1 interacts with DRD2S and DRD2L in trans-orientation via its extracellular domain. 79

Figure 20: CHL1 affects internalization of DRD2S upon stimulation with the DRD2 agonist quinpirole. 81

Figure 21: CHL1 affects the cell surface amount of DRD2S upon receptor stimulation with its agonist quinpirole. 82

Figure 22: CHL1 does not influence DRD2S degradation upon receptor stimulation with quinpirole. 84

Figure 23: CHL1 does not influence DRD2L degradation upon receptor stimulation with quinpirole. 85

Figure 24: Degradation of CHL1 induced by DRD2 agonist quinpirole is similar in cells expressing DRD2S and DRD2L. 86

Figure 25: CHL1 does not influence dopamine analog binding to DRD2S and DRD2L. 87

- Figure 26: CHL1 does not affect DARPP32 phosphorylation upon DRD2L stimulation with quinpirole. 89**
- Figure 27: CHL1 does not affect the level of phosphorylated ERK upon DRD2L stimulation with quinpirole. 90**
- Figure 28: CHL1 does not affect TH and ERK phosphorylation upon DRD2S stimulation with quinpirole. 91**
- Figure 29: CHL1 affects the level of pDARPP32 and DARPP32 in the ventral striatum of adult mice. 93**
- Figure 30: CHL1 influences pTH level in the dorsal striatum of adult mice. 94**
- Figure 31: Mice lacking CHL1 present reduced level of DRD2 in the dorsal striatum. 95**
- Figure 32: Method for the collection of sagittal sections for the analysis of the dopaminergic fibers running from the ventral midbrain to the striatum. 96**
- Figure 33: Separation of the dopaminergic fibers running from the ventral midbrain to the striatum into two portions. 98**
- Figure 34: Dopaminergic fibers running to the ventral striatum in CHL1<sup>-/-</sup> mice show stronger fluorescence intensity. 100**
- Figure 35: Dopaminergic fibers running from the ventral midbrain to the striatum have similar fluorescence intensity in male and female mice. 101**
- Figure 36: Dopaminergic fibers running to the ventral striatum in CHL1<sup>-/-</sup> mice cover a larger area. 102**
- Figure 37: Dopaminergic fibers running from the ventral midbrain to the striatum cover a similar area in male and female mice. 103**
- Figure 38: CHL1<sup>-/-</sup> mice have more dopaminergic fibers running to the ventral portion of the striatum than CHL1<sup>+/+</sup> mice. 104**
- Figure 39: CHL1<sup>-/-</sup> mice have more pTH-expressing dopaminergic fibers running to the ventral striatum than CHL1<sup>+/+</sup> mice. 106**
- Figure 40: More dopaminergic fibers enter the ventral striatum in CHL1<sup>-/-</sup> mice. 107**
- Figure 41: Lack of CHL1 does not affect the dopaminergic fibers density in the dorsal striatum. 109**
- Figure 42: Lack of CHL1 does not affect the dopaminergic fibers density in the ventral striatum. 110**
- Figure 43: Lack of CHL1 does not affect the dopaminergic fibers density in the whole striatum. 111**
- Figure 44: Adult CHL1<sup>-/-</sup> mice have less dopaminergic neurons in the VTA compared to CHL1<sup>+/+</sup> mice. 112**
- Figure 45: Thalamus size is similar in CHL1<sup>-/-</sup> and CHL1<sup>+/+</sup> mice. 115**
- Figure 46: Thickness of the frontal cortex is normal in CHL1<sup>-/-</sup> mice. 116**
- Figure 47: DRD2 expression in the frontal cortex of CHL1<sup>-/-</sup> mice is similar to that in CHL1<sup>+/+</sup> mice. 117**
- Figure 48: CHL1<sup>-/-</sup> mice have enlarged lateral ventricles compared to CHL1<sup>+/+</sup> mice. 119**

## 11. List of tables

**Table 1: Duplications and deletions affecting CALL. 22**

**Table 2: Primary antibodies used in the study. 40**

**Table 3: Secondary antibodies used in the study. 41**

**Table 4: List of buffers, solutions and media used for maintenance and experimental treatment of living HEK293 cells. 45**

**Table 5: List of solutions and media used for bacteria cultures. 47**

**Table 6: Buffers and solutions used for SDS-PAGE and Western Blot analyses. 48**

**Table 7: List of solutions and buffers used for fixation and staining of mouse tissue and HEK293 cells. 50**

**Table 8: List of solutions and buffers used for ELISA. 52**

**Table 9: List of buffers, solutions and chemicals used for agarose gel electrophoresis. 52**

**Table 10: Buffers used for the in-cell Western experiment. 53**

**Table 11: Cycling conditions – Amplification of fragments used for cloning with InFusion Kit (Clontech). 55**

**Table 12: Cycling conditions – genotyping of mice. 68**

## 12. Acknowledgements

I thank Professor Melitta Schachner for giving me the opportunity to study and work in her research group, for helping me to develop my ideas, for correcting me when I was wrong, and for letting me live in her apartment.

I am grateful to Ralf and Gaby for the enormous amount of help with my experiments, presentations, official work and correcting this thesis.

I thank my boyfriend Szymon, my family (especially my parents Daniel and Dorota), my friends, Kitka, Czarus, Maskotek and Czakuś for their support in many ways.

I thank Professor Julia Kehr for being my supervisor and for supporting me.

I am grateful to Professor Meliha Karsak and Professor Thomas Oertner for their mentorship at the ZMNH PhD Program.

I thank Professor Rosario Moratalla and Doctor Noelia Granado from the Cajal Institute in Madrid for cooperating with us regarding some experiments.

I thank Patricia Garcia, Doctor Edgar Kramer, Professor Jeroen Pasterkamp and Doctor Prakash Nidadavolu for the consultations and for their suggestions regarding the project.

I thank Doctor David Lutz for letting me work with him on his projects, teaching me new techniques and for always being there when I needed to talk.

I thank Doctor Eva-Maria Suciu for the administrative assistance.

Last but not least, I thank my colleagues from the Professor Schachner's lab for cooperating with me, for helping me, for exchanging ideas with me and for having lunches with me. In random order, I thank: Jelena, Kristina, Nina, Jelena, Ute, Gaston, Mina, Maria, Patricia, Vlad, Ofi, Viviana and Mujeeb.

### 13. References

Abbah SA, Thomas D, Browne S, O'Brien T, Pandit A, Zeugolis DI. "Co-transfection of decorin and interleukin-10 modulates pro-fibrotic extracellular matrix gene expression in human tenocyte culture." *Sci Rep.* 6, 2016: 20922.

Abi-Dargham A, Rodenhiser J, Printz D, Zea-Ponce Y, Gil R, Kegeles LS, Weiss R, Cooper TB, Mann JJ, Van Heertum RL, Gorman JM, Laruelle M. "Increased baseline occupancy of D2 receptors by dopamine in schizophrenia." *Proc Natl Acad Sci U S A.* 97, 2000: 8104-8109.

Allen Brain Atlas: Mouse Brain Map. Lein ES, Hawrylycz MJ, Ao N, Ayres M, Bensinger A, Bernard A, Boe AF, Boguski MS, Brockway KS, Byrnes EJ, Chen L, Chen L, Chen TM, Chin MC, Chong J, Crook BE, Czaplinska A, Dang CN, Datta S, Dee NR, Desaki AL, et al. "Genome-wide atlas of gene expression in the adult mouse brain." *Nature.* 445, 2007: 168-176.

Alsanie WF, Penna V, Schachner M, Thompson LH, Parish CL. "Homophilic binding of the neural cell adhesion molecule CHL1 regulates development of ventral midbrain dopaminergic pathways." *Sci Rep.* 7, 2017: 9368.

Andreyeva A, Leshchyn'ska I, Knepper M, Betzel C, Redecke L, Sytnyk V, Schachner M. "CHL1 is a selective organizer of the presynaptic machinery chaperoning the SNARE complex." *PLoS One.* 5, 2010: 12018.

Arias-Carrión O, Stamelou M, Murillo-Rodríguez E, Menéndez-González M, Pöppel E. "Dopaminergic reward system: a short integrative review." *Int Arch Med.* 3, 2010: 24.

Bartlett SE, Enquist J, Hopf FW, Lee JH, Gladher F, Kharazia V, Waldhoer M, Mailliard WS, Armstrong R, Bonci A, Whistler JL. "Dopamine responsiveness is regulated by targeted sorting of D2 receptors." *Proc Natl Acad Sci U S A.* 102, 2005: 11521-11526.

Bateup HS, Svenningsson P, Kuroiwa M, Gong S, Nishi A, Heintz N, Greengard P. "Cell type-specific regulation of DARPP-32 phosphorylation by psychostimulant and antipsychotic drugs." *Nat Neurosci.* 11, 2008: 932-939.

Beaulieu JM, Gainetdinov RR. "The physiology, signaling, and pharmacology of dopamine receptors." *Pharmacol Rev.* 63, 2011: 182-217.

Beitz JM. "Parkinson's disease: a review." *Front Biosci (Schol Ed).* 6, 2014: 65-74.

Bell C. "Summary of Conference Proceedings - Endogenous DA." In *Peripheral Actions of Dopamine*, by McGrath B. Bell C, 219-225. The Macmillan Press Ltd, 1988.

Belujon P, Grace AA. "Dopamine System Dysregulation in Major Depressive Disorders." *Int J Neuropsychopharmacol.* 20, 2017: 1036-1046.

Bertini V, Azzarà A, Toschi B, Gana S, Valetto A. "3p26.3 terminal deletions: a challenge for prenatal genetic counseling." *Prenat Diagn.* 37, 2017: 197-200.

Bissonette GB, Roesch MR. "Development and function of the midbrain dopamine system: what we know and what we need to." *Genes Brain Behav.* 15, 2016: 62-73.

Brickman AM, Buchsbaum MS, Shihabuddin L, Byne W, Newmark RE, Brand J, Ahmed S, Mitelman SA, Hazlett EA. "Thalamus size and outcome in schizophrenia." *Schizophr Res.* 71, 2004: 473-484.

- Brinton RD. "Estrogen-induced plasticity from cells to circuits: predictions for cognitive function." *Trends Pharmacol Sci.* 30, 2009: 212-222.
- Buhusi M, Midkiff BR, Gates AM, Richter M, Schachner M, Maness PF. "Close homolog of L1 is an enhancer of integrin-mediated cell migration." *J Biol Chem.* 278, 2003: 25024-25031.
- Burke RE. "Postnatal developmental programmed cell death in dopamine neurons." *Ann N Y Acad Sci.* 991, 2003: 69-79.
- Bye CR, Jönsson ME, Björklund A, Parish CL, Thompson LH. "Transcriptome analysis reveals transmembrane targets on transplantable midbrain dopamine progenitors." *Proc Natl Acad Sci U S A.* 112, 2015: 1946-1955.
- Cannon TD. "How Schizophrenia Develops: Cognitive and Brain Mechanisms Underlying Onset of Psychosis." *Trends Cogn Sci.* 19, 2015: 744-756.
- Carroll ME, Lynch WJ, Roth ME, Morgan AD, Cosgrove KP. "Sex and estrogen influence drug abuse." *Trends Pharmacol Sci.* 25, 2004: 273-279.
- Chen HT, Ruan NY, Chen JC, Lin TY. "Dopamine D2 receptor-mediated Akt/PKB signalling: initiation by the D2S receptor and role in quinpirole-induced behavioural activation." *ASN Neuro.* 4, 2012: 371-382.
- Chen QY, Chen Q, Feng GY, Lindpaintner K, Chen Y, Sun X, Chen Z, Gao Z, Tang J, He L. "Case-control association study of the close homologue of L1 (CHL1) gene and schizophrenia in the Chinese population." *Schizophr Res.* 73, 2005: 269-274.
- Chinta SJ, Andersen JK. "Dopaminergic neurons." *Int J Biochem Cell Biol.* 37, 2005: 942-946.
- Cuoco C, Ronchetto P, Gimelli S, Béna F, Divizia MT, Lerone M, Mirabelli-Badenier M, Mascaretti M, Gimelli G. "Microarray based analysis of an inherited terminal 3p26.3 deletion, containing only the CHL1 gene, from a normal father to his two affected children." *Orphanet J Rare Dis.* 6, 2011: 12.
- Czech DP, Lee J, Sim H, Parish CL, Vilain E, Harley VR. "The human testis-determining factor SRY localizes in midbrain dopamine neurons and regulates multiple components of catecholamine synthesis and metabolism." *J Neurochem.* 122, 2012: 260-271.
- Daubner SC, Le T, Wang S. "Tyrosine hydroxylase and regulation of dopamine synthesis." *Arch Biochem Biophys.* 508, 2011: 1-12.
- De Diego-Balaguer R, Couette M, Dolbeau G, Dürr A, Youssov K, Bachoud-Lévi AC. "Striatal degeneration impairs language learning: evidence from Huntington's disease." *Brain.* 131, 2008: 2870-2881.
- Del'guidice T, Lemasson M, Beaulieu JM. "Role of Beta-arrestin 2 downstream of dopamine receptors in the Basal Ganglia." *Front Neuroanat.* 5, 2011: 58.
- Demyanenko GP, Schachner M, Anton E, Schmid R, Feng G, Sanes J, Maness PF. "Close homolog of L1 modulates area-specific neuronal positioning and dendrite orientation in the cerebral cortex." *Neuron.* 44, 2004: 423-437.
- Drozak J, Bryła J. "Dopamine: not just a neurotransmitter." *Postepy Hig Med Dosw (Online).* 59, 2005: 405-420.

- Dunkley PR, Bobrovskaya L, Graham ME, von Nagy-Felsobuki EI, Dickson PW. "Tyrosine hydroxylase phosphorylation: regulation and consequences." *J Neurochem.* 91, 2004: 1025-1043.
- Egerton A, Howes OD, Houle S, McKenzie K, Valmaggia LR, Bagby MR, Tseng HH, Bloomfield MA, Kenk M, Bhattacharyya S, Suridjan I, Chaddock CA, Winton-Brown TT, Allen P, Rusjan P, Remington G, Meyer-Lindenberg A, McGuire PK, Mizrahi R. "Elevated Striatal Dopamine Function in Immigrants and Their Children: A Risk Mechanism for Psychosis." *Schizophr Bull.* 43, 2017: 293-301.
- Ellenbroek BA, Budde S, Cools AR. "Prepulse inhibition and latent inhibition: the role of dopamine in the medial prefrontal cortex." *Neuroscience.* 75, 1996: 535-542.
- Ferre S, von Euler G, Johansson B, Fredholm BB, Fuxe K. "Stimulation of high-affinity adenosine A2 receptors decreases the affinity of dopamine D2 receptors in rat striatal membranes." *Proc Natl Acad Sci U S A.* 88, 1991: 7238-7241.
- Flanigan M, LeClair K. "Shared Motivational Functions of Ventral Striatum D1 and D2 Medium Spiny Neurons." *J Neurosci.* 37, 2017: 6177-6179.
- Ford CP. "The role of D2-autoreceptors in regulating dopamine neuron activity and transmission." *Neuroscience.* 282, 2014: 13-22.
- Frints SG, Marynen P, Hartmann D, Fryns JP, Steyaert J, Schachner M, Rolf B, Craessaerts K, Snellinx A, Hollanders K, D'Hooge R, De Deyn PP, Froyen G. "CALL interrupted in a patient with non-specific mental retardation: gene dosage-dependent alteration of murine brain development and behavior." *Hum Mol Genet.* 12, 2003: 1463-1474.
- Gaser C, Nenadic I, Buchsbaum BR, Hazlett EA, Buchsbaum MS. "Ventricular enlargement in schizophrenia related to volume reduction of the thalamus, striatum, and superior temporal cortex." *Am J Psychiatry.* 161, 2004: 154-156.
- Gillies GE, Virdee K, McArthur S, Dalley JW. "Sex-dependent diversity in ventral tegmental dopaminergic neurons and developmental programming: A molecular, cellular and behavioral analysis." *Neuroscience.* 282, 2014: 69-85.
- Goldman AL, Pezawas L, Mattay VS, Fischl B, Verchinski BA, Chen Q, Weinberger DR, Meyer-Lindenberg A. "Widespread reductions of cortical thickness in schizophrenia and spectrum disorders and evidence of heritability." *Arch Gen Psychiatry.* 66, 2009: 467-477.
- Goodman A. "Neurobiology of addiction. An integrative review." *Biochem Pharmacol* 75, 2008: 266-322.
- Graff-Guerrero A, Mizrahi R, Agid O, Marcon H, Barsoum P, Rusjan P, Wilson AA, Zipursky R, Kapur S. "The dopamine D2 receptors in high-affinity state and D3 receptors in schizophrenia: a clinical [11C]-(+)-PHNO PET study." *Neuropsychopharmacology.* 34, 2009: 1078-1086.
- Granado N, Ares-Santos S, Oliva I, O'Shea E, Martin ED, Colado MI, Moratalla R. "Dopamine D2-receptor knockout mice are protected against dopaminergic neurotoxicity induced by methamphetamine or MDMA." *Neurobiol Dis.* 42, 2011a: 391-403.
- Granado N, Lastres-Becker I, Ares-Santos S, Oliva I, Martin E, Cuadrado A, Moratalla R. "Nrf2 deficiency potentiates methamphetamine-induced dopaminergic axonal damage and gliosis in the striatum." *Glia.* 59, 2011: 1850-1863.

- Granado N, O'Shea E, Bove J, Vila M, Colado MI, Moratalla R. "Persistent MDMA-induced dopaminergic neurotoxicity in the striatum and substantia nigra of mice." *J Neurochem.* 107, 2008: 1102-1112.
- Grunbeck A, Huber T, Sachdev P, Sakmar TP. "Mapping the ligand-binding site on a G protein-coupled receptor (GPCR) using genetically encoded photocrosslinkers." *Biochemistry.* 50, 2011: 3411-3413.
- Guo N, Guo W, Kralikova M, Jiang M, Schieren I, Narendran R, Slifstein M, Abi-Dargham A, Laruelle M, Javitch JA, Rayport S. "Impact of D2 receptor internalization on binding affinity of neuroimaging radiotracers." *Neuropsychopharmacology.* 35, 2010: 806-817.
- Guseva D, Jakovcevski I, Irintchev A, Leshchyn'ska I, Sytnyk V, Ponimaskin E, Schachner M. "Cell Adhesion Molecule Close Homolog of L1 (CHL1) Guides the Regrowth of Regenerating Motor Axons and Regulates Synaptic Coverage of Motor Neurons." *Front Mol Neurosci.* 11, 2018: 174.
- Hall W, Degenhardt L. "Cannabis use and the risk of developing a psychotic disorder." *World Psychiatry.* 7, 2008: 68-71.
- Held W, Mariuzza RA. "Cis-trans interactions of cell surface receptors: biological roles and structural basis." *Cell Mol Life Sci.* 68, 2011: 3469-3478.
- Herron LR, Hill M, Davey F, Gunn-Moore FJ. "The intracellular interactions of the L1 family of cell adhesion molecules." *Biochem J.* 419, 2009: 519-531.
- Hillenbrand R, Molthagen M, Montag D, Schachner M. "The close homologue of the neural adhesion molecule L1 (CHL1): patterns of expression and promotion of neurite outgrowth by heterophilic interactions." *Eur J Neurosci.* 11, 1999: 813-826.
- Holm J, Hillenbrand R, Steuber V, Bartsch U, Moos M, Lübbert H, Montag D, Schachner M. "Structural features of a close homologue of L1 (CHL1) in the mouse: a new member of the L1 family of neural recognition molecules." *Eur J Neurosci.* 8, 1996: 1613-1629.
- Horstkorte R & Fuss B. "9. Cell Adhesion Molecules." In *Basic Neurochemistry - Principles of Molecular, Cellular, and Medical Neurobiology. Eighth edition.*, by Siegel GJ, Albers RW, Price DL, Brady ST, 165-179. Elsevier Academic Press, 2012.
- Human Protein Atlas available from [www.proteinatlas.org](http://www.proteinatlas.org). Uhlén M, Fagerberg L, Hallström BM, Lindskog C, Oksvold P, Mardinoglu A, Sivertsson Å, Kampf C, Sjöstedt E, Asplund A, Olsson I, Edlund K, Lundberg E, Navani S, Szgyarto CA, Edqvist PH, et al. "Proteomics. Tissue-based map of the human proteome." *Science.* 347, 2015: 1260419.
- Irintchev A, Koch M, Needham LK, Maness P, Schachner M. "Impairment of sensorimotor gating in mice deficient in the cell adhesion molecule L1 or its close homologue, CHL1." *Brain Res.* 1029, 2004: 131-134.
- Iwaki A, Kawano Y, Miura S, Shibata H, Matsuse D, Li W, Furuya H, Ohayagi Y, Taniwaki T, Kira J, Fukumaki Y. "Heterozygous deletion of ITPR1, but not SUMF1, in spinocerebellar ataxia type 16." *J Med Genet.* 45, 2008: 32-35.
- Jakovcevski I, Wu J, Karl N, Leshchyn'ska I, Sytnyk V, Chen J, Irintchev A, Schachner M. "Glial scar expression of CHL1, the close homolog of the adhesion molecule L1, limits recovery after spinal cord injury." *J Neurosci.* 27, 2007: 7222-7233.

- Katic J, Loers G, Kleene R, Karl N, Schmidt C, Buck F, Zmijewski JW, Jakovcevski I, Preissner KT, Schachner M. "Interaction of the cell adhesion molecule CHL1 with vitronectin, integrins, and the plasminogen activator inhibitor-2 promotes CHL1-induced neurite outgrowth and neuronal migration." *J Neurosci.* 34, 2014: 14606-14623.
- Katic J, Loers G, Tomic J, Schachner M, Kleene R. "The cell adhesion molecule CHL1 interacts with patched-1 to regulate apoptosis during postnatal cerebellar development." *J Cell Sci.* 130, 2017: 2606-2619.
- Keck TM, Burzynski C, Shi L, Newman AH. "Beyond small-molecule SAR: using the dopamine D3 receptor crystal structure to guide drug design." *Adv Pharmacol.* 69, 2014: 267-300.
- Khan ZU, Mrzljak L, Gutierrez A, de la Calle A, Goldman-Rakic PS. "Prominence of the dopamine D2 short isoform in dopaminergic pathways." *Proc Natl Acad Sci U S A.* 95, 1998: 7731-7736.
- Kleene R, Chaudhary H, Karl N, Katic J, Kotarska A, Guitart K, Loers G, Schachner M. "Interaction between CHL1 and serotonin receptor 2c regulates signal transduction and behavior in mice." *J Cell Sci.* 128, 2015: 4642-4652.
- Kling RC, Tschammer N, Lanig H, Clark T, Gmeiner P. "Active-state model of a dopamine D2 receptor-Gai complex stabilized by aripiprazole-type partial agonists." *PLoS One.* 9, 2014: e100069.
- Kolata S, Wu J, Light K, Schachner M, Matzel LD. "Impaired working memory duration but normal learning abilities found in mice that are conditionally deficient in the close homolog of L1." *J Neurosci.* 28, 2008: 13505-13510.
- Kubota M, Nagashima T, Takano H, Kodaka F, Fujiwara H, Takahata K, Moriguchi S, Kimura Y, Higuchi M, Okubo Y, Takahashi H, Ito H, Suhara T. "Affinity States of Striatal Dopamine D2 Receptors in Antipsychotic-Free Patients with Schizophrenia." *Int J Neuropsychopharmacol.* 20, 2017: 928-935.
- Leshchyns'ka I, Sytnyk V, Richter M, Andreyeva A, Puchkov D, Schachner M. "The adhesion molecule CHL1 regulates uncoating of clathrin-coated synaptic vesicles." *Neuron.* 52, 2006: 1011-1025.
- Li C, Liu C, Zhou B, Hu C, Xu X. "Novel microduplication of CHL1 gene in a patient with autism spectrum disorder: a case report and a brief literature review." *Mol Cytogenet.* 9, 2016: 51.
- Lindgren N, Usiello A, Goiny M, Haycock J, Erbs E, Greengard P, Hokfelt T, Borrelli E, Fisone G. "Distinct roles of dopamine D2L and D2S receptor isoforms in the regulation of protein phosphorylation at presynaptic and postsynaptic sites." *Proc Natl Acad Sci U S A.* 100, 2003: 4305-4309.
- Lindskog M, Svenningsson P, Fredholm BB, Greengard P, Fisone G. "Activation of dopamine D2 receptors decreases DARPP-32 phosphorylation in striatonigral and striatopallidal projection neurons via different mechanisms." *Neuroscience.* 88, 1999: 1005-1008.
- Lodish H, Berk A, Zipursky SL, Matsudaira P, Baltimore D, James Darnell J. „Section 21.4: Neurotransmitters, Synapses, and Impulse Transmission.” In *Molecular Cell Biology (4th edition)*. New York: Freeman & Co., 2000.
- Luessen DJ, Hinshaw TP, Sun H, Howlett AC, Marrs G, McCool BA, Chen R. "RGS2 modulates the activity and internalization of dopamine D2 receptors in neuroblastoma N2A cells." *Neuropharmacology.* 110, 2016: 297-307.

- Luo SX, Huang EJ. "Dopaminergic Neurons and Brain Reward Pathways: From Neurogenesis to Circuit Assembly." *Am J Pathol.* 186, 2016: 478-488.
- Lynch WJ. "Sex differences in vulnerability to drug self-administration." *Exp Clin Psychopharmacol.* 14, 2006: 34-41.
- Lyons DJ, Hellysaz A, Broberger C. "Prolactin regulates tuberoinfundibular dopamine neuron discharge pattern: novel feedback control mechanisms in the lactotrophic axis." *J Neurosci.* 32, 2012: 8074-8083.
- Maness PF, Schachner M. "Neural recognition molecules of the immunoglobulin superfamily: signaling transducers of axon guidance and neuronal migration." *Nat Neurosci.* 10, 2007: 19-26.
- Margolis EB, Lock H, Chefer VI, Shippenberg TS, Hjelmstad GO, Fields HL. "Kappa opioids selectively control dopaminergic neurons projecting to the prefrontal cortex." *Proc Natl Acad Sci U S A.* 103, 2006: 2938-2942.
- Marti MJ, James CJ, Oo TF, Kelly WJ, Burke RE. "Early developmental destruction of terminals in the striatal target induces apoptosis in dopamine neurons of the substantia nigra." *J Neurosci.* 17, 1997: 2030-2039.
- McArthur S, McHale E, Gillies GE. "The size and distribution of midbrain dopaminergic populations are permanently altered by perinatal glucocorticoid exposure in a sex- region- and time-specific manner." *Neuropsychopharmacology.* 32, 2007: 1462-1476.
- McCloy RA, Rogers S, Caldon CE, Lorca T, Castro A, Burgess A. "Partial inhibition of Cdk1 in G 2 phase overrides the SAC and decouples mitotic events." *Cell Cycle.* 13, 2014: 1400-1412.
- McColgan P, Tabrizi SJ. "Huntington's disease: a clinical review." *Eur J Neurol.* 25, 2018: 24-34.
- Meiser J, Weindl D, Hiller K. "Complexity of dopamine metabolism." *Cell Commun Signal.* 11, 2013: 34.
- Milsted A, Serova L, Sabban EL, Dunphy G, Turner ME, Ely DL. "Regulation of tyrosine hydroxylase gene transcription by Sry." *Neurosci Lett.* 369, 2004: 203-207.
- Mohan V, Wade SD, Sullivan CS, Kasten MR, Sweetman C, Stewart R, Truong Y, Schachner M, Manis PB, Maness PF. "Close Homolog of L1 Regulates Dendritic Spine Density in the Mouse Cerebral Cortex through Semaphorin 3B." *J Neurosci.*, 2019: 2984-18.
- Money KM, Stanwood GD. "Developmental origins of brain disorders: roles for dopamine." *Front Cell Neurosci.* 7, 2013: 260.
- Montag-Sallaz M, Schachner M, Montag D. "Misguided axonal projections, neural cell adhesion molecule 180 mRNA upregulation, and altered behavior in mice deficient for the close homolog of L1." *Mol Cell Biol.* 22, 2002: 7967-7981.
- Morellini F, Lepsveridze E, Kähler B, Dityatev A, Schachner M. "Reduced reactivity to novelty, impaired social behavior, and enhanced basal synaptic excitatory activity in perforant path projections to the dentate gyrus in young adult mice deficient in the neural cell adhesion molecule CHL1." *Mol Cell Neurosci.* 34, 2007: 121-136.
- Naus S, Richter M, Wildeboer D, Moss M, Schachner M, Bartsch JW. "Ectodomain shedding of the neural recognition molecule CHL1 by the metalloprotease-disintegrin ADAM8 promotes neurite outgrowth and suppresses neuronal cell death." *J Biol Chem.* 279, 2004: 16083-16090.

- Nikonenko AG, Sun M, Lepsveridze E, Apostolova I, Petrova I, Irintchev A, Dityatev A, Schachner M. "Enhanced perisomatic inhibition and impaired long-term potentiation in the CA1 region of juvenile CHL1-deficient mice." *Eur J Neurosci.* 23, 2006: 1839-1852.
- Nobili A, Latagliata EC, Viscomi MT, Cavallucci V, Cutuli D, Giacobazzo G, Krashia P, Rizzo FR, Marino R, Federici M, De Bartolo P, Aversa D, Dell'Acqua MC, Cordella A, Sancandi M, Keller F, Petrosini L, Puglisi-Allegra S, Mercuri NB, et al. "Dopamine neuronal loss contributes to memory and reward dysfunction in a model of Alzheimer's disease." *Nat Commun.* 8, 2017: 14727.
- Oo TF, Kholodilov N, Burke RE. "Regulation of natural cell death in dopaminergic neurons of the substantia nigra by striatal glial cell line-derived neurotrophic factor in vivo." *J Neurosci.* 23, 2003: 5141-5148.
- Ougrin D, Chatterton S, Banarsee R. "Attention deficit hyperactivity disorder (ADHD): review for primary care clinicians." *London J Prim Care (Abingdon).* 3, 2010: 45-51.
- Palmiter RD. "Dopamine signaling in the dorsal striatum is essential for motivated behaviors: lessons from dopamine-deficient mice." *Ann N Y Acad Sci.* 1129, 2008: 35-46.
- Palumbo O, Fischetto R, Palumbo P, Nicastro F, Papadia F, Zelante L, Carella M. "De novo microduplication of CHL1 in a patient with non-syndromic developmental phenotypes." *Mol Cytogenet.* 8, 2015: 66.
- Patel KR, Cherian J, Gohil K, Atkinson D. "Schizophrenia: overview and treatment options." *P T.* 39, 2014: 638-645.
- Perreault ML, Hasbi A, O'Dowd BF, George SR. "Heteromeric dopamine receptor signaling complexes: emerging neurobiology and disease relevance." *Neuropsychopharmacology.* 39, 2014: 156-168.
- Pham TT, Giesert F, Röthig A, Floss T, Kallnik M, Weindl K, Hölter SM, Ahting U, Prokisch H, Becker L, Klopstock T, Hrabé de Angelis M, Beyer K, Görner K, Kahle PJ, Vogt Weisenhorn DM, Wurst W. "DJ-1-deficient mice show less TH-positive neurons in the ventral tegmental area and exhibit non-motoric behavioural impairments." *Genes Brain Behav.* 9, 2010: 305-317.
- Pohjalainen T, Rinne JO, Någren K, Syvälahti E, Hietala J. "Sex differences in the striatal dopamine D2 receptor binding characteristics in vivo." *Am J Psychiatry.* 155, 1998: 768-773.
- Pohjola P, de Leeuw N, Penttinen M, Kääriäinen H. "Terminal 3p deletions in two families--correlation between molecular karyotype and phenotype." *Am J Med Genet A.* 152A, 2010: 441-446.
- Poltorak M, Khoja I, Hemperly JJ, Williams JR, el-Mallakh R, Freed WJ. "Disturbances in cell recognition molecules (N-CAM and L1 antigen) in the CSF of patients with schizophrenia." *Exp Neurol.* 131, 1995: 266-272.
- Probst-Schendzielorz K, Scholl C, Efimkina O, Ersfeld E, Viviani R, Serretti A, Fabbri C, Gurwitz D, Lucae S, Ising M, Paul AM, Lehmann ML, Steffens M, Crisafulli C, Calabrò M, Holsboer F, Stingl J. "CHL1, ITGB3 and SLC6A4 gene expression and antidepressant drug response: results from the Munich Antidepressant Response Signature (MARS) study." *Pharmacogenomics.* 16, 2015: 689-701.
- Ren J, Zhao T, Xu Y, Ye H. "Interaction between DISC1 and CHL1 in regulation of neurite outgrowth." *Brain Res.* 1648, 2016: 290-297.

- Rice MW, Roberts RC, Melendez-Ferro M, Perez-Costas E. "Mapping dopaminergic deficiencies in the substantia nigra/ventral tegmental area in schizophrenia." *Brain Struct Funct.* 221, 2016: 185-201.
- Sakurai K, Migita O, Toru M, Arinami T. "An association between a missense polymorphism in the close homologue of L1 (CHL1, CALL) gene and schizophrenia." *Mol Psychiatry.* 7, 2002: 412-415.
- Salgado-Pineda P, Caclin A, Baeza I, Junqué C, Bernardo M, Blin O, Fonlupt P. "Schizophrenia and frontal cortex: where does it fail?" *Schizophr Res.* 91, 2007: 73-81.
- Sanders-Bush E, Hazelwood L. "Chapter 13: 5-Hydroxytryptamine (Serotonin) and Dopamine." In *Goodman & Gilman's: The Pharmacological Basis of Therapeutics, 12th edition*, by Chabner BA, Knollmann BC Brunton LL. McGraw-Hill Education / Medical, 2011.
- Schmalbach B, Lepsveridze E, Djogo N, Papashvili G, Kuang F, Leshchyns'ka I, Sytnyk V, Nikonenko AG, Dityatev A, Jakovcevski I, Schachner M. "Age-dependent loss of parvalbumin-expressing hippocampal interneurons in mice deficient in CHL1, a mental retardation and schizophrenia susceptibility gene." *J Neurochem.* 135, 2015: 830-844.
- Schultz SH, North SW, Shields CG. "Schizophrenia: a review." *Am Fam Physician.* 75, 2007: 1821-1829.
- Seeman MV. "Psychopathology in women and men: focus on female hormones." *Am J Psychiatry.* 154, 1997: 1641-1647.
- Seeman P, Niznik HB, Guan HC, Booth G, Ulpian C. "Link between D1 and D2 dopamine receptors is reduced in schizophrenia and Huntington diseased brain." *Proc Natl Acad Sci U S A.* 86, 1989: 10156-10160.
- Shaltout TE, Alali KA, Bushra S, Alkaseri AM, Jose ED, Al-Khainji M, Saleh R, Salama Dahir A, Shaltout H, Al-Abdullah M, Rizk NM. "Significant association of close homologue of L1 gene polymorphism rs2272522 with schizophrenia in Qatar." *Asia Pac Psychiatry.* 5, 2013: 17-23.
- Shaw SH, Kelly M, Smith AB, Shields G, Hopkins PJ, Loftus J, Laval SH, Vita A, De Hert M, Cardon LR, Crow TJ, Sherrington R, DeLisi LE. "A genome-wide search for schizophrenia susceptibility genes." *Am J Med Genet.* 81, 1998: 364-376.
- Shoukier M, Fuchs S, Schwaibold E, Lingen M, Gärtner J, Brockmann K, Zirn B. "Microduplication of 3p26.3 in nonsyndromic intellectual disability indicates an important role of CHL1 for normal cognitive function." *Neuropediatrics.* 44, 2013: 268-271.
- Smigiel R, Sherman DL, Rydzanicz M, Walczak A, Mikolajkow D, Krolak-Olejnik B, Kosinska J, Gasperowicz P, Biernacka A, Stawinski P, Marciniak M, Andrzejewski W, Boczar M, Krajewski P, Sasiadek MM, Brophy PJ, Ploski R. "Homozygous mutation in the Neurofascin gene affecting the glial isoform of Neurofascin causes severe neurodevelopment disorder with hypotonia, amimia and areflexia." *Hum Mol Genet.* 27, 2018: 3669-3674.
- Takahashi K, Liu FC, Hirokawa K, Takahashi H. "Expression of Foxp2, a gene involved in speech and language, in the developing and adult striatum." *J Neurosci Res.* 73, 2003: 61-72.
- Tallerico T, Novak G, Liu IS, Ulpian C, Seeman P. "Schizophrenia: elevated mRNA for dopamine D2(Longer) receptors in frontal cortex." *Brain Res Mol Brain Res.* 87, 2001: 160-165.

- Tammimäki A, Pietilä K, Raattamaa H, Ahtee L. "Effect of quinpirole on striatal dopamine release and locomotor activity in nicotine-treated mice." *Eur J Pharmacol.* 531, 2006: 118-125.
- Tassano E, Biancheri R, Denegri L, Porta S, Novara F, Zuffardi O, Gimelli G, Cuoco C. "Heterozygous deletion of CHL1 gene: detailed array-CGH and clinical characterization of a new case and review of the literature." *Eur J Med Genet.* 57, 2014: 626-629.
- Thomas TS, Baimel C, Borgland SL. "Opioid and hypocretin neuromodulation of ventral tegmental area neuronal subpopulations." *Br J Pharmacol.* 175, 2018: 2825-2833.
- Tian N. *Dissertation: CHL1 organizes ankyrin-B /  $\beta$ II spectrin based cytoskeleton in developing neurons.* Universität Hamburg, 2009.
- Tian N, Leshchyn'ska I, Welch JH, Diakowski W, Yang H, Schachner M, Sytnyk V. "Lipid raft-dependent endocytosis of close homolog of adhesion molecule L1 (CHL1) promotes neuritogenesis." *J Biol Chem.* 287, 2012: 44447-44463.
- Van den Heuvel DM, Pasterkamp RJ. "Getting connected in the dopamine system." *Prog Neurobiol.* 85, 2008: 75-93.
- van Domburg PH, ten Donkelaar HJ. "The human substantia nigra and ventral tegmental area. A neuroanatomical study with notes on aging and aging diseases." *Adv Anat Embryol Cell Biol.* 121, 1991: 1-132.
- Vaughan RA, Foster JD. "Mechanisms of dopamine transporter regulation in normal and disease states." *Trends Pharmacol Sci.* 34, 2013: 489-496.
- Vita A, De Peri L, Silenzi C, Dieci M. "Brain morphology in first-episode schizophrenia: a meta-analysis of quantitative magnetic resonance imaging studies." *Schizophr Res.* 82, 2006: 75-88.
- Wang S, Che T, Levit A, Shoichet BK, Wacker D, Roth BL. "Structure of the D2 dopamine receptor bound to the atypical antipsychotic drug risperidone." *Nature.* 555, 2018: 269-273.
- Wheatley M, Wootten D, Conner MT, Simms J, Kendrick R, Logan RT, Poyner DR, Barwell J. "Lifting the lid on GPCRs: the role of extracellular loops." *Br J Pharmacol.* 165, 2012: 1688-1703.
- Wittmann BC, Bunzeck N, Dolan RJ, Düzel E. "Anticipation of novelty recruits reward system and hippocampus while promoting recollection." *Neuroimage.* 38, 2007: 194-202.
- Xiao M. *Dissertation: Neural cell adhesion molecule NCAM modulates dopamine-related behavior by regulating dopamine D2 receptor internalization in mice (Mus musculus Linnaeus, 1758).* Universität Hamburg, 2009.
- Xiao MF, Xu JC, Tereshchenko Y, Novak D, Schachner M, Kleene R. "Neural cell adhesion molecule modulates dopaminergic signaling and behavior by regulating dopamine D2 receptor internalization." *J Neurosci.* 29, 2009: 14752-14763.
- Xie ZL, Shao SL, Lv JW, Wang CH, Yuan CZ, Zhang WW, Xu XJ. "Co-transfection and tandem transfection of HEK293A cells for overexpression and RNAi experiments." *Cell Biol Int.* 35, 2011: 187-192.

Yamashita F, Sasaki M, Fukumoto K, Otsuka K, Uwano I, Kameda H, Endoh J, Sakai A. "Detection of changes in the ventral tegmental area of patients with schizophrenia using neuromelanin-sensitive MRI." *Neuroreport*. 27, 2016: 289-294.

Yokota T, Sugawara K, Ito K, Takahashi R, Ariga H, Mizusawa H. "Down regulation of DJ-1 enhances cell death by oxidative stress, ER stress, and proteasome inhibition." *Biochem Biophys Res Commun*. 312, 2003: 1342-1348.

Zecca L, Tampellini D, Gerlach M, Riederer P, Fariello RG, Sulzer D. "Substantia nigra neuromelanin: structure, synthesis, and molecular behaviour." *Mol Pathol*. 54, 2001: 414-418.

Zhou L, Barão S, Laga M, Bockstael K, Borgers M, Gijzen H, Annaert W, Moechars D, Mercken M, Gevaer K, Strooper BD. "The Neural Cell Adhesion Molecules L1 and CHL1 Are Cleaved by BACE1 Protease in Vivo." *J Biol Chem*. 287, 2012: 25927–25940.

Zhou X, Pace J, Filichia E, Lv T, Davis B, Hoffer B, Selman W, Luo Y. "Effect of the sonic hedgehog receptor smoothed on the survival and function of dopaminergic neurons." *Exp Neurol*. 283, 2016: 235-245.

## Eidesstattliche Versicherung

Declaration on oath

**Hiermit erkläre ich an Eides statt, dass ich die vorliegende Dissertationsschrift selbst verfasst und keine anderen als die angegebenen Quellen und Hilfsmittel benutzt habe.**

I hereby declare, on oath, that I have written the present dissertation by my own and have not used other than the acknowledged resources and aids.

Hamburg, den 01.08.2019

Unterschrift

Aguirre Kotsch



Zentrum für Molekulare Neurobiologie Hamburg (ZMNH)  
Institut für Synaptische Physiologie

Universitätsklinikum Hamburg-Eppendorf | ZMNH | Institute für Synaptische Physiologie  
Falkenried 94 | 20251 Hamburg

Dr. Christine Gee  
Institut für Synaptische Physiologie

ZMNH, Falkenried 94  
20251 Hamburg

Telefon: +49 (0) 40 7410-57190

Fax: +49 (0) 40 7410-58364

[christine.gee@zmnh.uni-hamburg.de](mailto:christine.gee@zmnh.uni-hamburg.de)

English Language Thesis Certification – Agnieszka Kotarska

Hamburg, 17.07.2019

As a native english speaker, I can certify that the quality of English in the thesis "Cell adhesion molecule close homolog of L1 regulates internalization of the dopamine receptor D2 and formation of the mesolimbic dopaminergic pathway in mice (*Mus musculus* Linnaeus, 1758)" is of a very high standard and that the thesis is fully understandable.

Sincerely yours,

Christine Gee